ATS 01946

MCR-75-444
Contract NAS1-13377

NASA CR-144892

File with N76-11218

Final Report

November 1975

A Study to Define an In-Flight Dynamics Measurement and Data Applications Program for Space Shuttle Payloads

MARTIN MARIETTA

NASA CR-144892

A STUDY TO DEFINE AN INFLIGHT DYNAMIC MEASUREMENT AND DATA APPLICATIONS PROGRAM FOR SPACE SHUTTLE PAYLOADS

By W. Paul Rader, Stanley Barrett
and Kenneth R. Payne.

Prepared under Contract No. NAS1-13377 by
Martin Marietta Corporation
Denver Division
Denver, Colorado
for
NATIONAL AERONAUTICS AND SPACE ADMINISTRATION

FOREWORD

This document presents the results of a study performed for the Langley Research Center under Contract NAS1-13377. The primary objective of the study was to provide NASA with a definition of measurements and data interpretation techniques needed on the first few shuttle flights such that the dynamic environment is sufficiently well established for use in the design of all future payloads, and to define an environmental test methodology which makes efficient use of these measurements in reducing the cost of environmental testing and the failure potential of payloads.

The authors gratefully acknowledge the cooperation and contributions of Mr. Brantley Hanks and Mr. Larry Pinson of Langley Research Center throughout this study.

Page Intentionally Left Blank

TABLE OF CONTENTS

ILLUSTRATIONS

TABLES

INTRODUCTION

The availability of the reusable space shuttle near the end of this decade will open a new era in the performance of scientific experiments in space. Effective utilization of this new capability depends not only on the basic shuttle launch vehicle but also on the development of cost effective techniques for designing, building and testing the payloads to be flown.

The primary objective of this study is to provide a definition of data measurement and interpretation techniques for application to the first few shuttle flights, so that the dynamic environment can be sufficiently well established to be used to reduce the cost of future payloads through more efficient design and environmental test techniques.

Specifically, the tasks performed under this study are as follows:

1. Survey and definition of current shuttle payloads;

2. Define a current state-of-the-art dynamic environments measurements program for the first several space shuttle flights and identify potential improvements which might be realized if advanced, on-board measurement technology could be developed. The measurement program defined shall consider transient, vibration and acoustic environments and will include consideration of payload-vehicle dynamic interactions which may change with payload configurations;

3. Define a data interpretation program and demonstrate analytical techniques necessary to extrapolate data from the flight measurement program to a broad class of space shuttle payloads and apply them in the advanced environmental test methodology.

4. Define a feasible environmental test methodology which makes efficient use of the flight measurement and data interpretation programs in reducing the cost of environmental testing and the failure potential of payloads;

5. Utilize the results of Tasks 2, 3 and 4 to provide rationale for overall payload cost reduction.

The technical effort in this study addressed the entire spectrum of dynamic environments, broadly classified into low, mid and high frequency regions. In the low frequency (0-50 Hz) region, maximum loads in primary structure are produced by vehicle transients such as engine ignition and shutdown, gust loading, oscillatory shock and landing shock. In the midfrequency region (30-100 Hz), environments such as buffet and vehicle transients excite higher order modes of primary structures and subassemblies. This frequency range represents a "gray" region between the low frequency range where a relatively high degree of confidence exists in analyses, and the high frequency range where the environment is controlled by random response to acoustic excitation. The high frequency (50-20,000 Hz) region includes acoustics, random vibration and pyrotechnic shock.

Section 1.0 presents a summary of information collected on current proposed payload characteristics which indicate the potential range of dynamic problems which may be encountered during shuttle missions. A brief description of current practices and examples from recent programs are presented in Section 2.0 to indicate capabilities and limitations of current technology, and point out areas where improvements are needed. Improved techniques for application to shuttle payloads are discussed in Section 3.0, and include the flight measurement program, data interpretation techniques and test methodology, and how these improved techniques can result in cost reductions for shuttle payloads.

1.0 SURVEY AND DEFINITION OF CURRENT SHUTTLE PAYLOADS

1.1 Initial Flights

Initial efforts during this study were directed towards obtaining information on current proposed payload characteristics including weights, volumes, surface areas, c.g. locations, and structural interfaces with the cargo bay. The information collected is advantageous in formulating flight measurement and data interpretation programs, and in assessing the types of dynamic test programs which may be required for different types of shuttle payloads. Since the payload configurations are constantly changing, the information presented should be regarded as a representative sample for use in this study. The primary source of information was a series of reports published by the NASA/MSFC Shuttle Utilization Planning Office of Program Development, References 1, 2 and 3.

Payload data for the first eleven flights taken from Reference 1, are listed in Table A-1 of Appendix A. Information for only seven payloads is included, since no payloads have been identified for flights 1, 2, 3 and 10. Sketches of these payloads and orbiter mounting provisions are shown in Appendix A, in Figures A-1 through A-13. The payloads range in weight from 2627 Kg (5793 pounds) to 11752 Kg (25914 pounds) and present a variety of configurations including relatively small, pallet mounted experiments and satellites as well as large, self-contained units such as LDEF and Spacelab.

1.2 Future Flights

Additional payloads as described in References 2 and 3 have been broadly categorized as sortie and automated classifications. Sortie payloads, by definition, include all experiments, payload unique support equipment and required consumables carried by the Spacelab or elsewhere in the orbiter for science missions. A sortie mission is a short duration (seven to thirty days) mission which is conducted in low earth orbit using the shuttle orbiter and equipment attached to it for experiments, observations and other space activities. Automated or "free flying" payloads are self-contained payloads which operate in space independent of the shuttle system. Observatories which require revisits by the shuttle to maintain them are included in this classification.

These payloads are listed in Appendix A, in Tables A-2 and A-3, along with their weights, dimensions and number of missions.

2.0 CURRENT PRACTICES

This section is included to present a summary of current test philosophy, describe test techniques used on recent programs, and indicate data interpretation techniques used in criteria development, in order to form a basis for improved, more cost effective techniques for shuttle payloads. Examples are presented from the Viking and Skylab programs.

2.1 Summary of Surveys

Significant differences in test requirements and dynamic test practices for spacecraft exist among the military, NASA and commercial programs. These differences have been described in References 4 and 5, and are briefly summarized here in order to point out the need for a more uniform approach for shuttle payloads. The different approaches are, in general, dictated by program funding and schedules, launch vehicle and launch facility configurations, and number of missions required.

The resources expended in verifying spacecraft design capability for dynamic environments are estimated (References 4 and 5) to vary from 2 to 15 percent of the total program funding. These include the expenditures required for analytical efforts to define dynamic environments and loads applicable for each spacecraft/launch vehicle configuration and for conducting development, qualification, and acceptance test programs.

Examples of the differences in test requirements (excerpted from Reference 4) are as follows.

"Qualification test requirements are generally based on predicted maximum flight or ground test responses, with margins of safety applied to account for variability in hardware strengths and test tolerances. The margins of safety vary with each spacecraft program and the basic design philosophy of the spacecraft customer. An example of the variations in design/criteria philosophies is illustrated below:

- Vibration design and test criteria based on confidence levels of 97.5 percent;
- Maximum expected vibration environment, flight +6 dB when large data samples available; maximum predicted vibration environments derived from 95 percentile with 50 percent confidence based on a one-side tolerance limit as determined through statistical analysis procedures;
- 2-sigma flight vibration environment with 1.5 factor of safety;

- o 3-sigma flight vibration environment with 3-4 dB margin;
- o Qualification test margins for component pyrotechnic shock environment vary from 3-sigma amplitude margins with 1.2-2 factors; one to three repetitive flight shock tests on system test using flight ordnance hardware;
- o Structural test loads represent 3-sigma flight loads with varying margins of safety (1.0-1.5).

Acceptance test requirements are generally based on the maximum expected or 3-sigma flight environments. However, when mission environments fall below a certain threshold, a minimum test level is established. This minimum test level is generally applicable to subsystem or component acceptance tests and their related sinusoidal and random vibration environments. The purpose of establishing minimum acceptance test levels is to provide flight dynamic tests that yield a consistent workmanship quality in the flight hardware."

In addition to the differences in confidence level bases and test factors used, there are differences in where the emphasis is placed in verifying spacecraft design capability. For example, at Goddard Space Flight Center the "general philosophy is to develop a spacecraft that passes the required system level test requirements as modified by flight loads analysis" (Reference 5), whereas the Air Force requires extensive environmental testing at both the component and system level. At the Marshall Space Flight Center, the emphasis is placed on component testing using an early acoustic development test to establish test criteria.

Almost all spacecraft programs require system level tests including some form of sinusoidal excitation and random vibration and/or acoustic tests depending on the size, weight and configuration. For the larger payloads, the trend has been towards acoustic testing rather than random vibration. For the sine tests, input levels are controlled and/or limited such that loads in primary structure do not exceed analytically predicted flight conditions. The validity of the test is, therefore, subject to the accuracy of the analysis, and to the capability of the control system in terms of number of control channels, switching speed, overshoot tolerances, etc. The latter parameters are dependent on the dynamic response characteristics of the test article and test set-up. Broader tolerances are required for specimens with high amplification resonances.

The following section presents examples of current test methodology from recent major test programs.

2.2 Examples of Test Techniques

2.2.1 Skylab

The Skylab vibro-acoustic test program was conducted in two phases: the orbital workshop (OWS) and the payload assembly (PA). The objectives of the tests were to:

1) Verify the dynamic design and test criteria for components and subassemblies;

2) Verify the structural integrity of bracketry and secondary structure;

3) Qualify selected flight hardware components.

For the acoustic tests of each of the assemblies (OWS and payload assembly) the reverberant chamber test levels were determined from the differences between flight and test vibro-acoustic transfer functions. These differences occur because the reverberant noise field is more efficient in producing structural vibration than is the acoustic environment produced in flight. Examples of the transfer functions (in one-third octave bands) are shown in Figure 2-1. The transfer functions were calculated from one-third octave band analyses of the measured acoustic and vibration data. The vibration spectra were defined in terms of dB re 1.0 g rms, and the applicable acoustic levels subtracted from the vibration level to produce the transfer function value in each one-third octave band. These calculations were performed for all flight measurements which were duplicated on the test articles, and the average differences (ΔdB) between the flight and test transfer functions plotted as shown in Figure 2-2. A smooth curve drawn through these points produced the correction factors in each frequency band to apply to the specification levels, resulting in chamber levels which were 3 to 10 dB lower than the flight levels. (See Figure 2-3). The chamber test levels derived by this method were intended to produce vibration levels equivalent to the 97.5% confidence levels of the flight environment.

The orbital workshop and payload assembly were subjected to low frequency sinusoidal vibration to simulate the transients produced during launch, engine cutoff and stage separation. During each of the tests, response limit instrumentation was used to control the input levels such that structural design loads would not be exceeded. An example of the measured test input levels are compared to the test specification (for

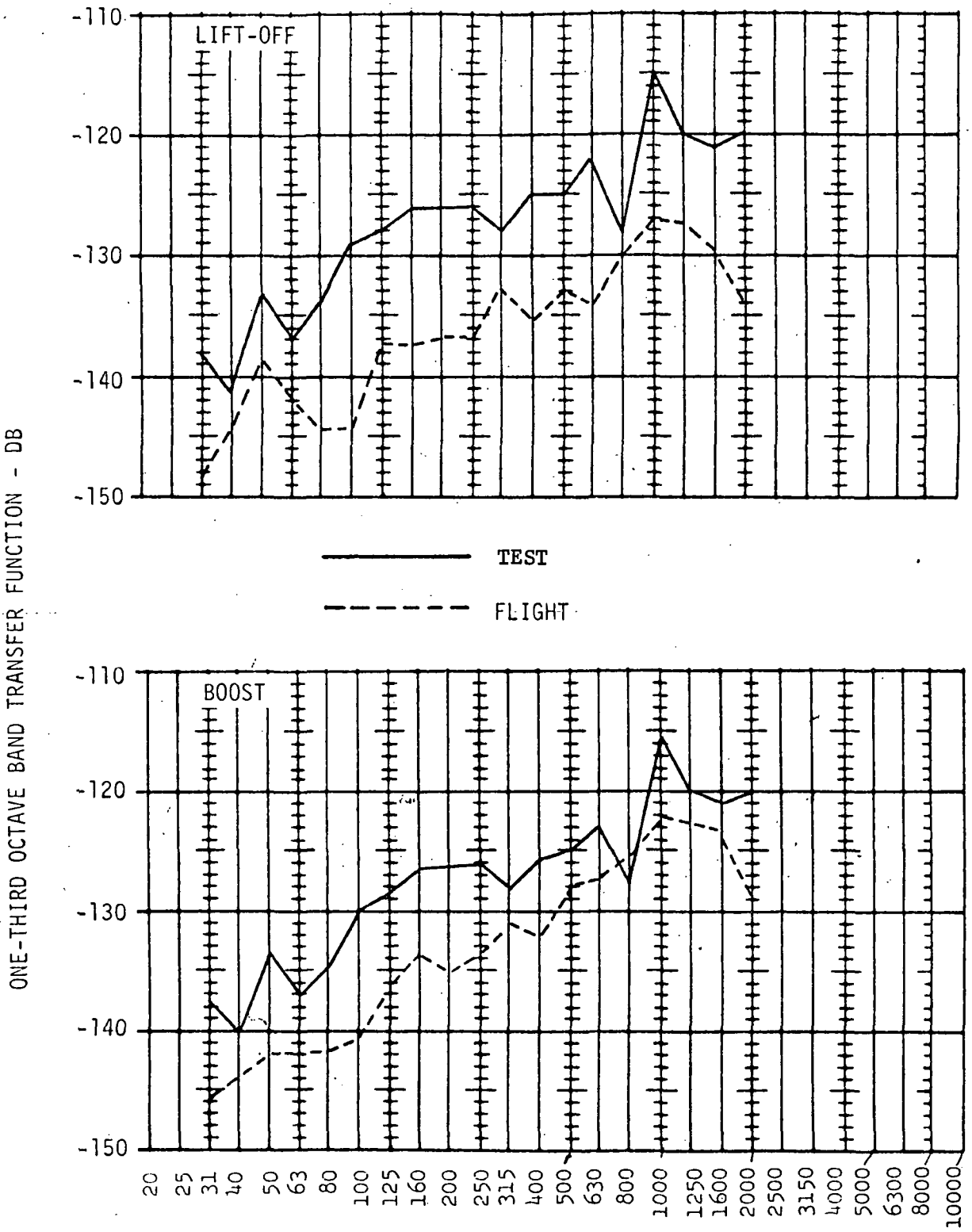

Source: Fig. 5.9 Of Reference 6.

Figure 2-1. Comparison of Test and Flight Transfer Functions

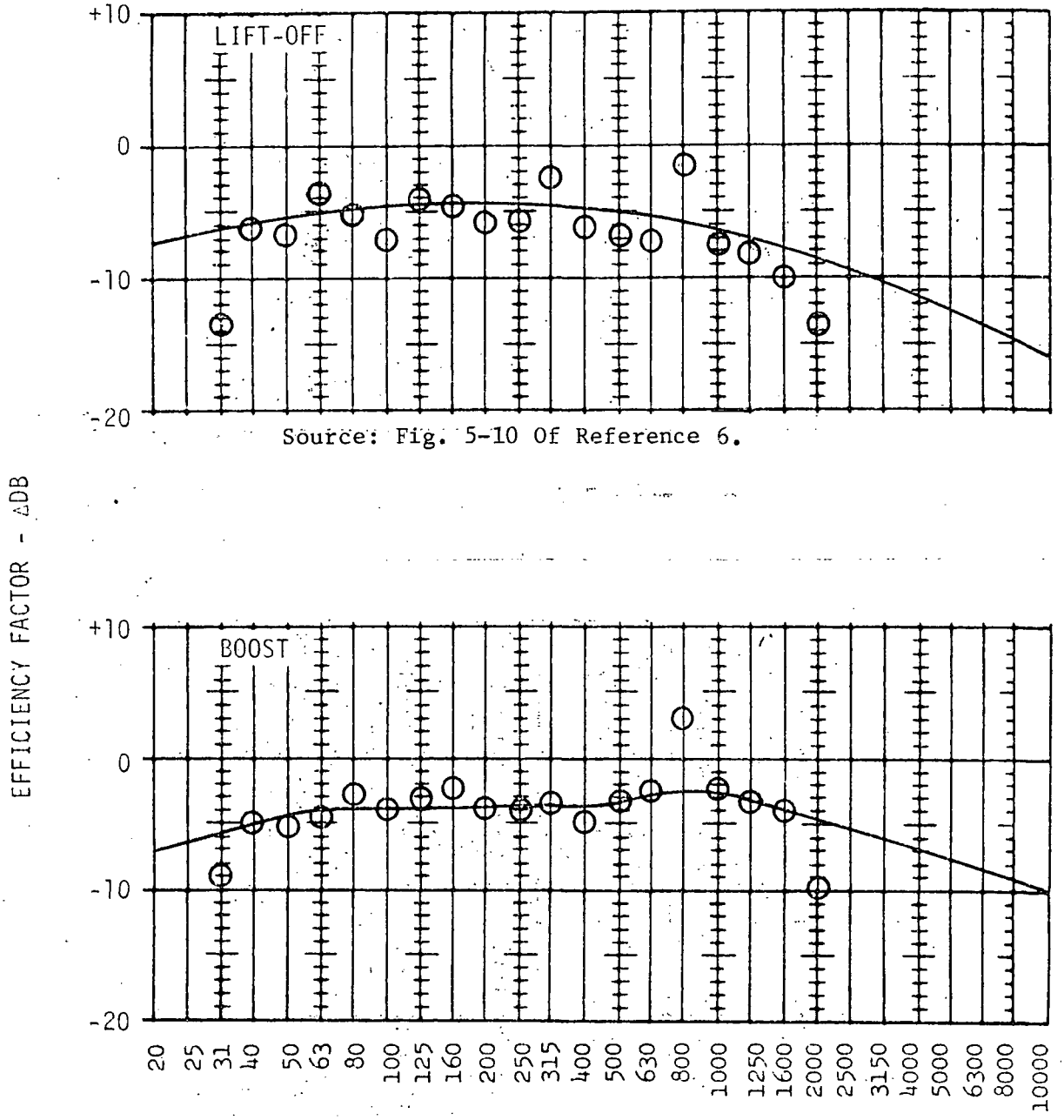

Source: Fig. 5-10 Of Reference 6.

LEGEND:

○ Average ΔdB Difference Between Dynamic Test Article and Flight Transfer Functions.

—— Final Efficiency Factor Used in Test

Figure 2-2. Efficiency Factors for Lift-Off and Boost Flight Conditions

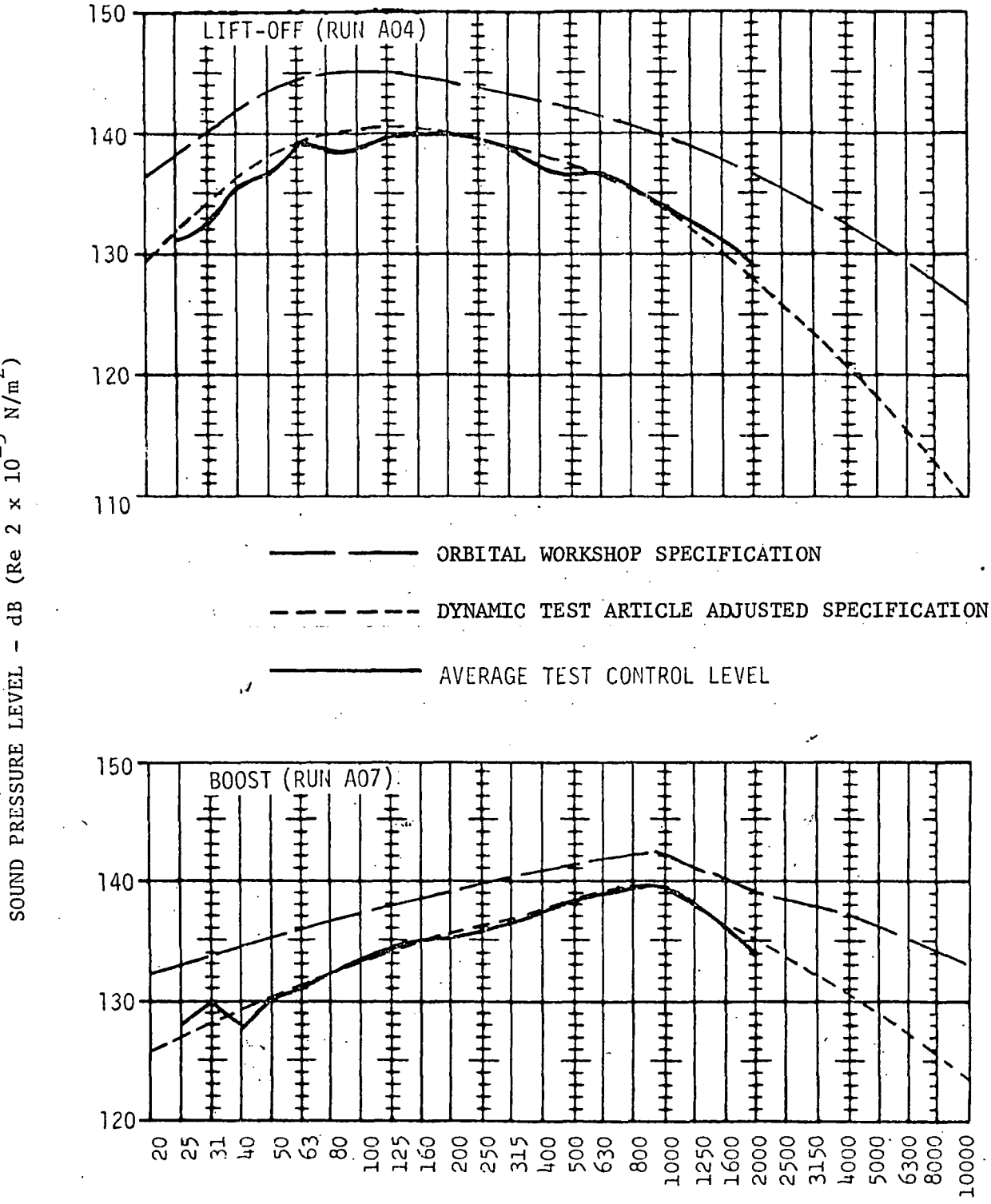

Source: Fig. 5-11 Of Reference 6.

Figure 2-3. Comparison of Orbital Workshop Specification, Dynamic Test Article Adjusted Specification and Computer Average Test Control Level

the orbital workshop longitudinal axis test) is shown in Figure 2-4. Also indicated in the figure are the structural areas which limited the input levels in various frequency ranges.

For the payload assembly tests an attempt was made to conduct sinusoidal tests of the complete spacecraft to levels enveloping the vehicle dynamic transients. The intent was to produce the specification levels at the various subassemblies of the spacecraft while limiting the response in primary structure in other areas . The results of low level sweeps indicated that this was not possible because of the payload assembly dynamic characteristics and the available force/control capabilities. An alternate approach was utilized. Selected decaying sinusoids were applied at the base ring fixture in the longitudinal axis. The transients (amplitudes and frequencies) were selected based on analyses of the launch vehicle.

The objectives of the test program were achieved in that the structural integrity of bracketry and secondary structure was verified, selected flight hardware components were qualified, and sufficient data were obtained to verify or modify the dynamic design and test criteria for components.

The data interpretation program and evaluation of results are described in Paragraph 2.3.

2.2.2 Viking

An extensive test program on both the component and system level was conducted for the Viking spacecraft. For this program, the Langley Research Center is Project Manager for the overall Viking Project, JPL is responsible for the orbiter, and Martin Marietta Corporation is responsible for the lander.

The lander was subjected to a series of dynamic tests including modal surveys of the launch and terminal descent configurations to verify analytical models, acoustic tests to obtain component vibration criteria and verify the integrity of bracketry and secondary structure, and sinusoidal vibration tests simulating vehicle transients. In addition, the orbiter/lander "stacked" configuration (Figure 2.5) was subjected to forced vibration sine tests at the JPL facility (Reference 8).

The objectives of the "stack" test series were to:

(1) Evaluate the effect of lander/orbiter interaction on response at subsystem/component locations;

(2) Evaluate the adequacy of secondary structure;

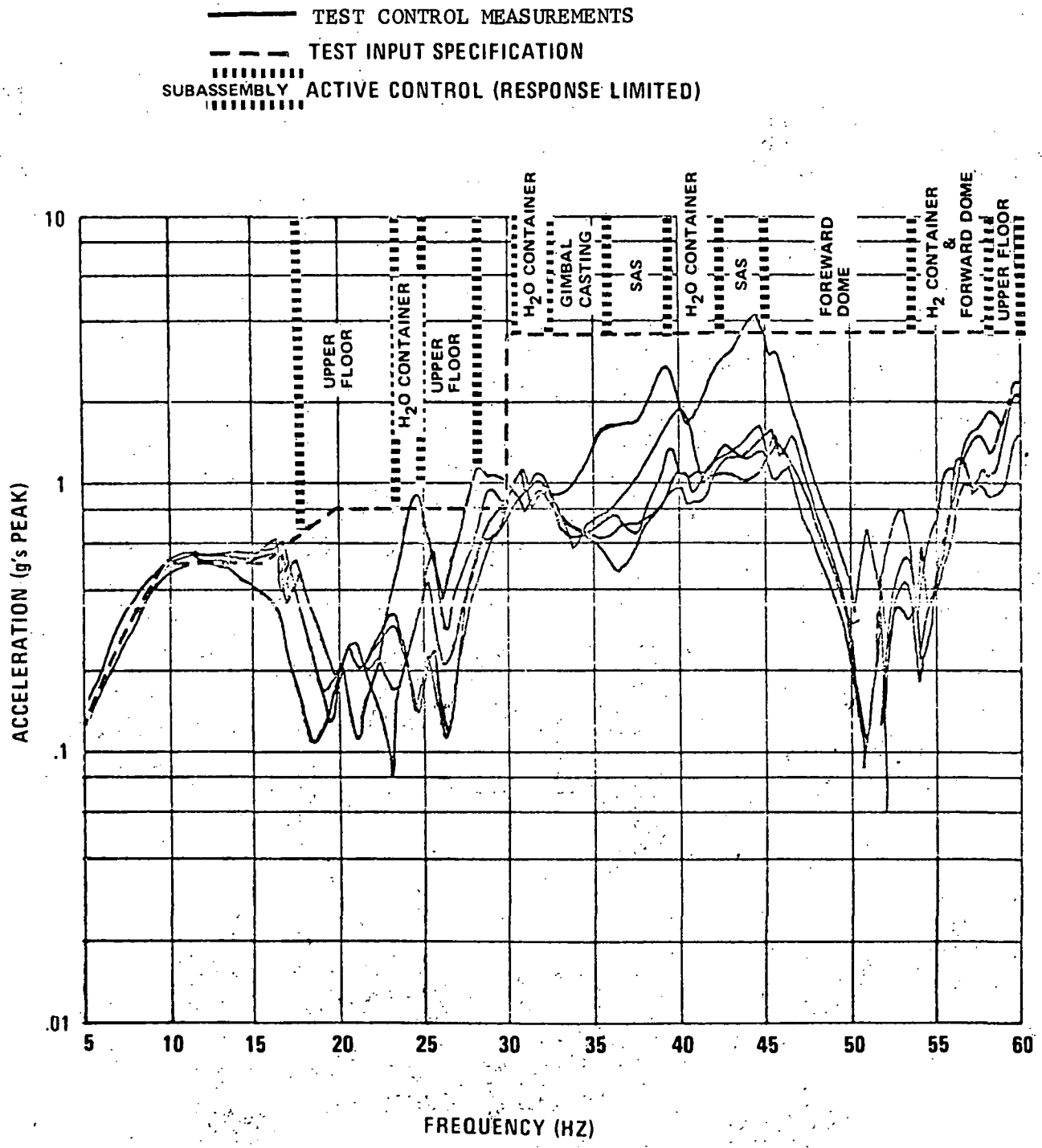

Source: Figure 5-1 of Reference 7.

Figure 2-4. Comparison of Test Specification With Measured Test Input Levels During A-Axis Test (Run V25)

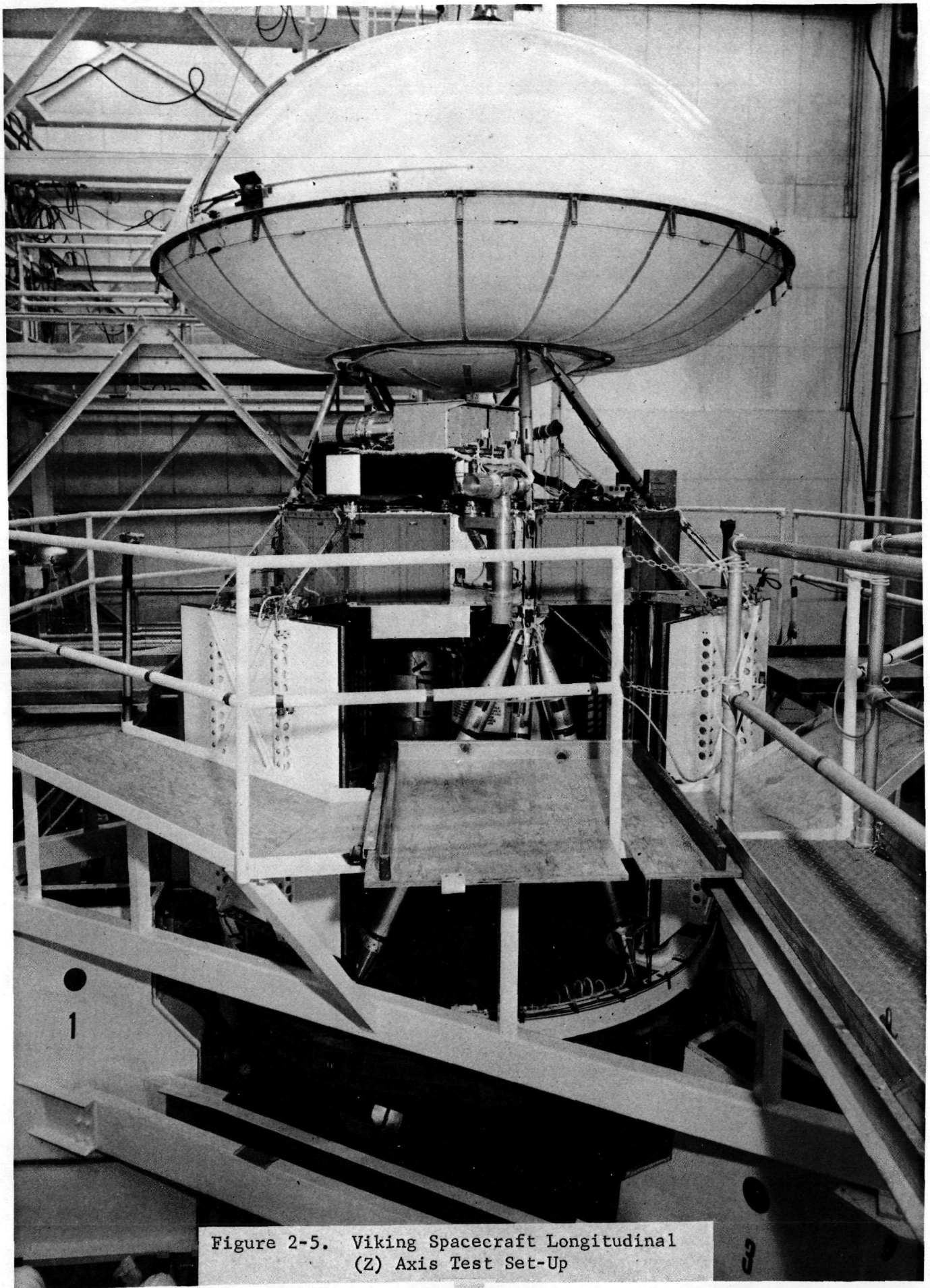

Figure 2-5. Viking Spacecraft Longitudinal (Z) Axis Test Set-Up

(3) Serve as a precursor to the proof test orbiter (PTO) qualification test;

(4) Evaluate component sinusoidal test levels;

(5) Obtain data for comparison with analytical results.

Significant analytical efforts were expended to provide assurance that test peculiar failures of primary structure should not occur, and the vibration input to the test specimen was controlled so that loads in primary structure would not exceed analytically predicted flight loads. To meet this objective, a 36 channel control and 60 channel limit system was utilized. Test input levels were controlled at the orbiter bus hard points except as modified by primary structural response loads. The envelope of levels measured at control accelerometer locations on the orbiter bus is compared to the test specification in Figure 2-6. From the figure, it is evident that the response of primary structure controlled the input level in the frequency range from 10 to 55 Hz. Above 55 Hz, the test level was controlled at the orbiter bus hard points.

The test predictions based on the Viking mathematical model correlated reasonably well with the test data as shown in the examples in Figures 2-7 through 2-10, establishing confidence in the coupled Viking spacecraft mathematical model. In general, measured frequencies were slightly higher than those predicted by the analysis, and amplitudes were lower by approximately that amount established by control system tolerances. The test results were reviewed and compared to component qualification levels. No changes to component sine test requirements were required.

2.3 Data Interpretation and Criteria Development

2.3.1 Skylab

A description of the Skylab vibro-acoustic test program is presented in Paragraph 2.2.1. Tests were conducted on two major hardware assemblies, the orbital workshop (OWS) and the payload assembly (PA). Even though the flight acoustic environment was known with confidence, from data collected on previous Saturn flights, the test programs resulted in a number of changes to the component qualification criteria and cost impacts due to component requalification. Subsequent to each of the test programs, the major hardware contractors in conjunction with NASA, reviewed the random vibration data and compared these data with component qualification levels.

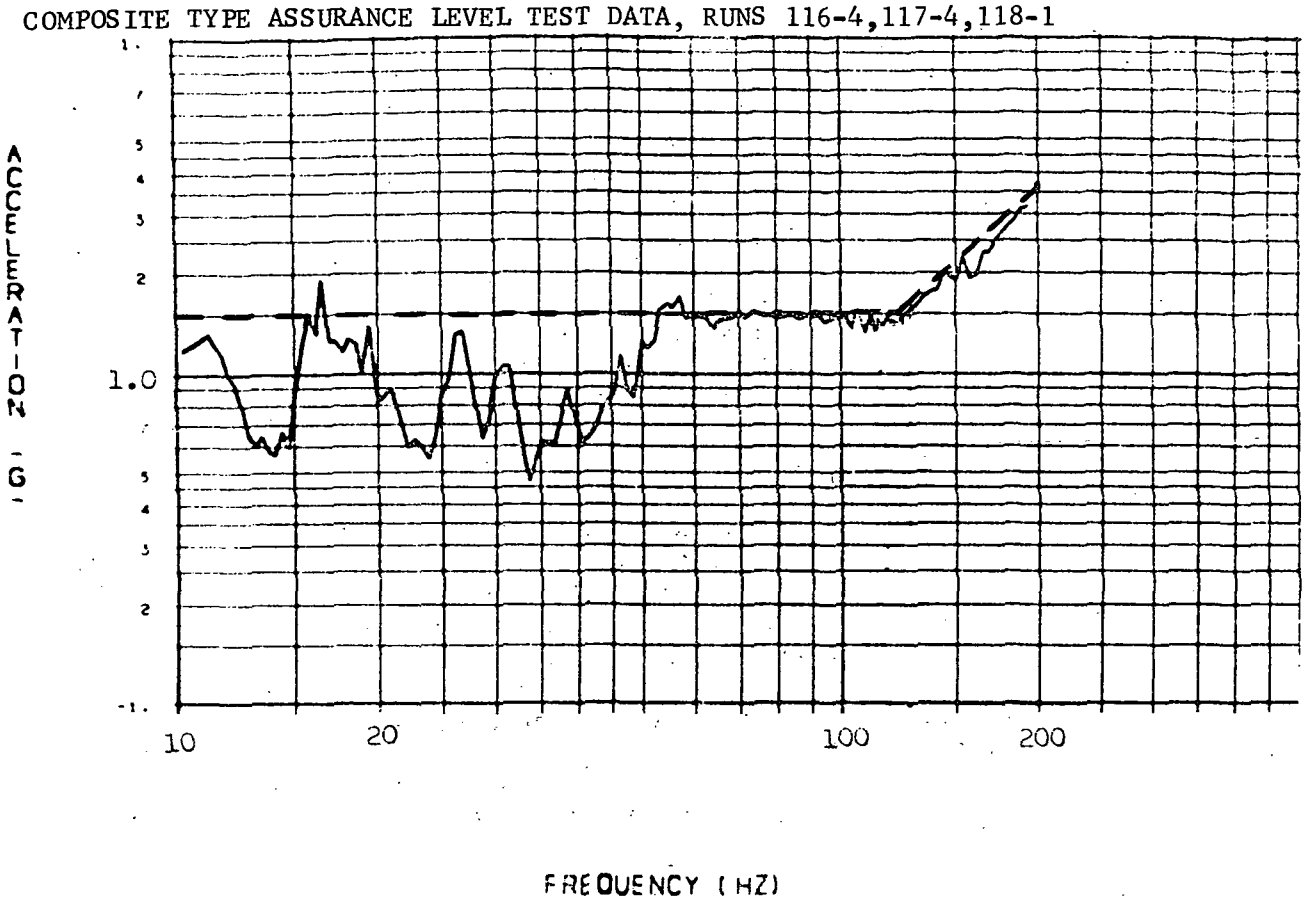

Figure 2-6. Composite Input Levels at Orbiter Bus Hard Points

Source: Figures 14,15,16 and 17 of Reference 8.

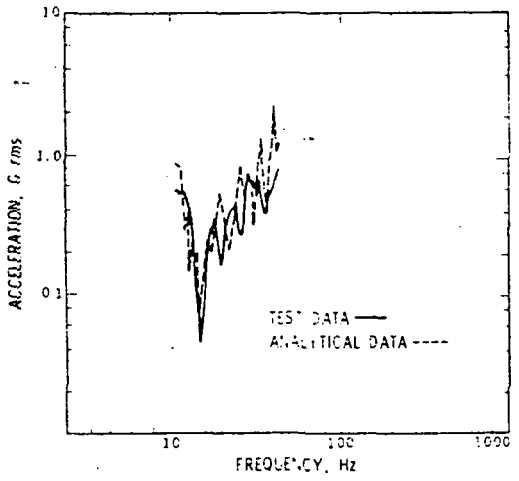

Fig. 2-7. Comparison of Test and Analytical Data at the Viking Transition Adapter

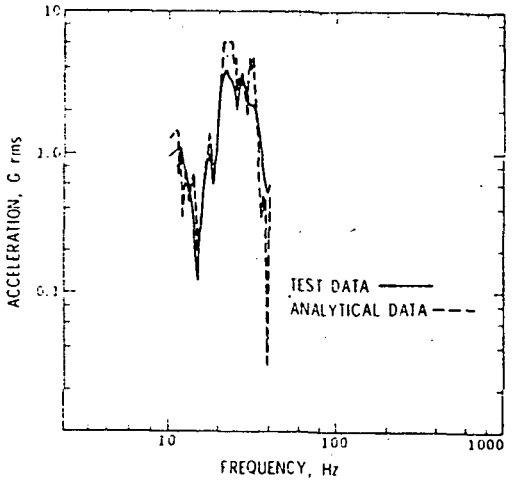

Fig. 2-8. Comparison of Test and Analytical Data on the Equipment Plate

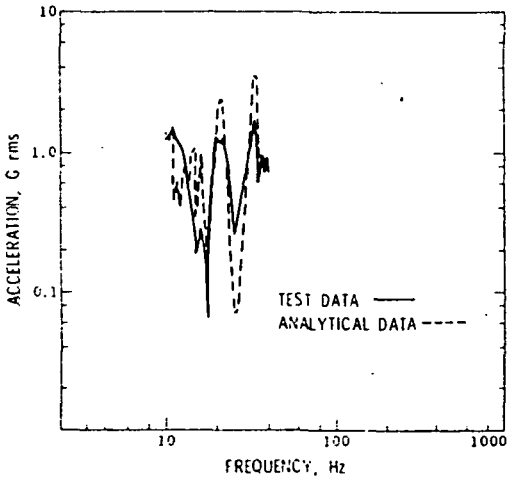

Fig. 2-9. Comparison of Test and Analytical Data on Terminal Descent Engine No. 1

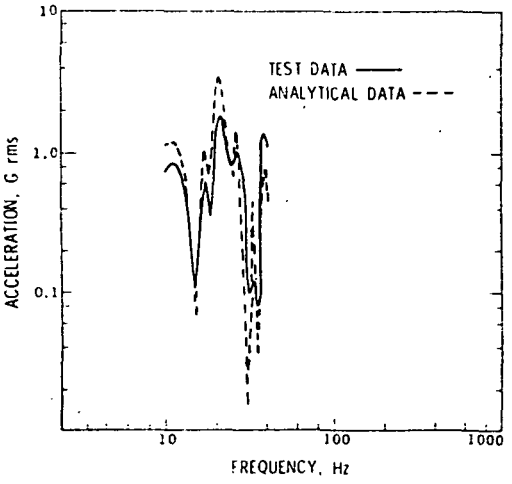

Fig. 2-10. Comparison of Test and Analytical Data on Terminal Descent Engine No. 2

For the orbital workshop, the specification evaluation resulted in raising the criteria in six (11.3%) of the environmental subzones, lowered in 33 (62.3%) of the subzones and unchanged in 14 (26.4%) of the subzones. Forty-seven new subzones were added. Examples of the changes to criteria are shown in Figures 2-11 through 2-13. Examples of both increases and decreases to the original criteria are shown. In some cases an order of magnitude change was required, potentially resulting in a significant impact with regard to number of flight and/or test failures of components. The scheduling of this test phase was such that the criteria changes were made before the start of the qualification test program, therefore, no component requalification was required.

As a result of the payload assembly acoustic tests, criteria were changed in 15 environmental subzones, 12 new subzones were added, and 28 components were recommended for requalification including the flight control computer and the control moment gyro.

2.3.2 Viking

This example is included to show how changes to the predicted flight acoustical environment affected the qualification criteria for Viking Lander Capsule (VLC) components. The discussion and results presented are taken from Reference 9.

The random vibration criteria originally specified for design and testing of the VLC subsystem components were based on analytical predictions of the vibration developed on various VLC structures during the course of the Viking mission. The highest vibration levels on the lander structure were predicted to result from terminal propulsion engine operation. The highest levels on the aeroshell, base cover and bioshield were predicted to result from acoustic noise generated by the launch vehicle's rocket motors during the launch phase of the mission. Vibration data were acquired during the performance of a terminal propulsion system verification test, in which an engine was operated under simulated mission conditions. These data showed the level of the engine vibration applied to the lander structure to be considerably lower than that which originally had been predicted. Conversely, vibration data acquired during the performance of the launch acoustic test of the Lander Development Test Model (LDTM) vehicle showed higher vibration levels than originally predicted on certain parts of the lander structure and also on the aeroshell, base cover/decelerator and bioshield equipment module. Due to these higher vibration levels, the vibration criteria specified for nineteen VLC components were determined to be too low in level.

LIFT-OFF

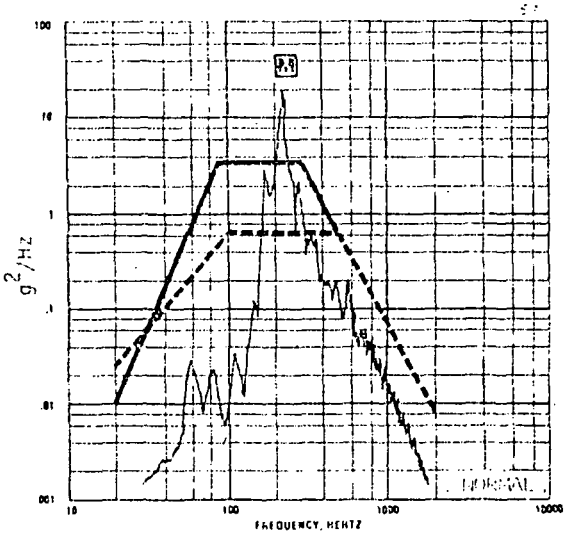

BOOST

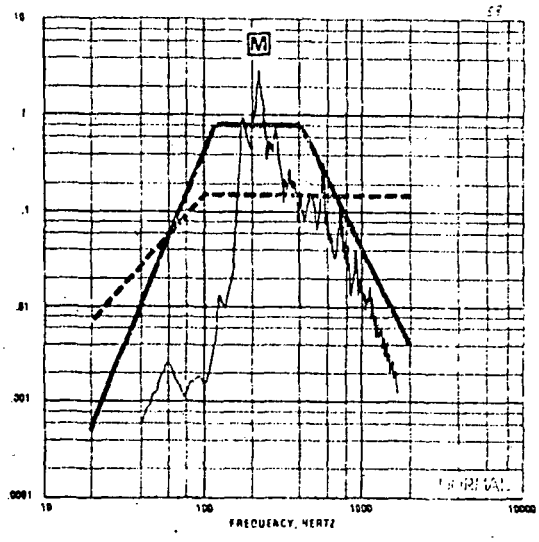

LEGEND: _ _ _ ORIGINAL CRITERIA ____ REVISED CRITERIA

[M] Local effect at accelerometer location - overtest condition would occur if entire test specimen were subjected to these levels

Source: Figure 7-27 Of Reference 6.

Figure 2-11. Comparison of Test Data With Criteria - Lift-Off and Boost. Zone 4-6-A. Forward Dome Mounted Component.

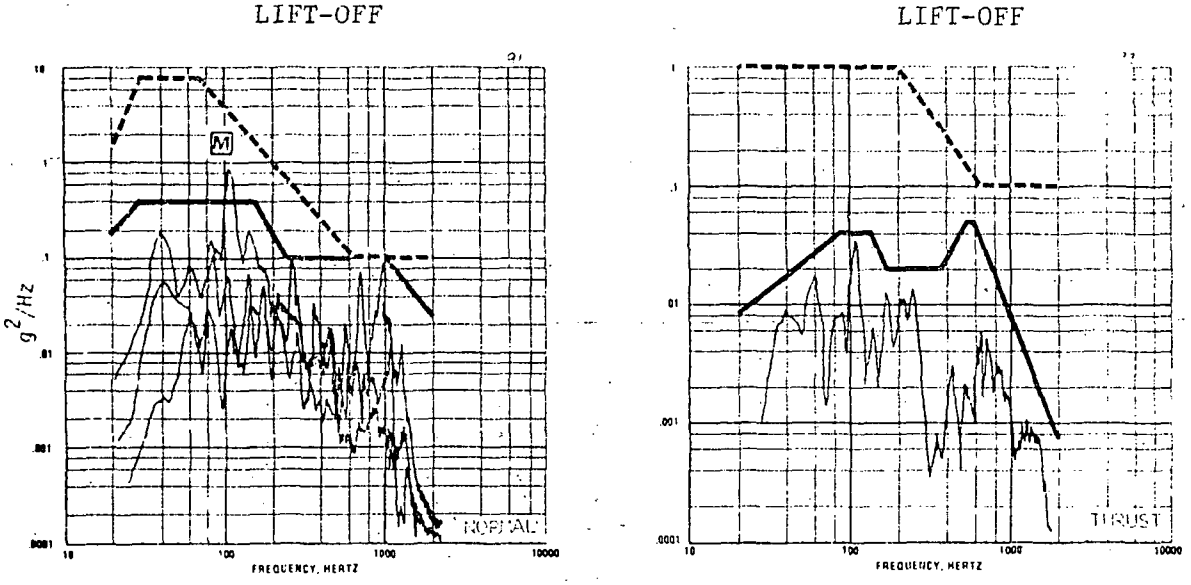

LEGEND: _ _ _ ORIGINAL CRITERIA ____ REVISED CRITERIA

[M] Local effect at accelerometer location - overtest condition would occur if entire test specimen were subjected to these levels

Source: Figure 7-49 of Reference 6.

Figure 2-12. Comparison of Test Data With Criteria - Lift-Off Input to Components Mounted on the Power and Display Console

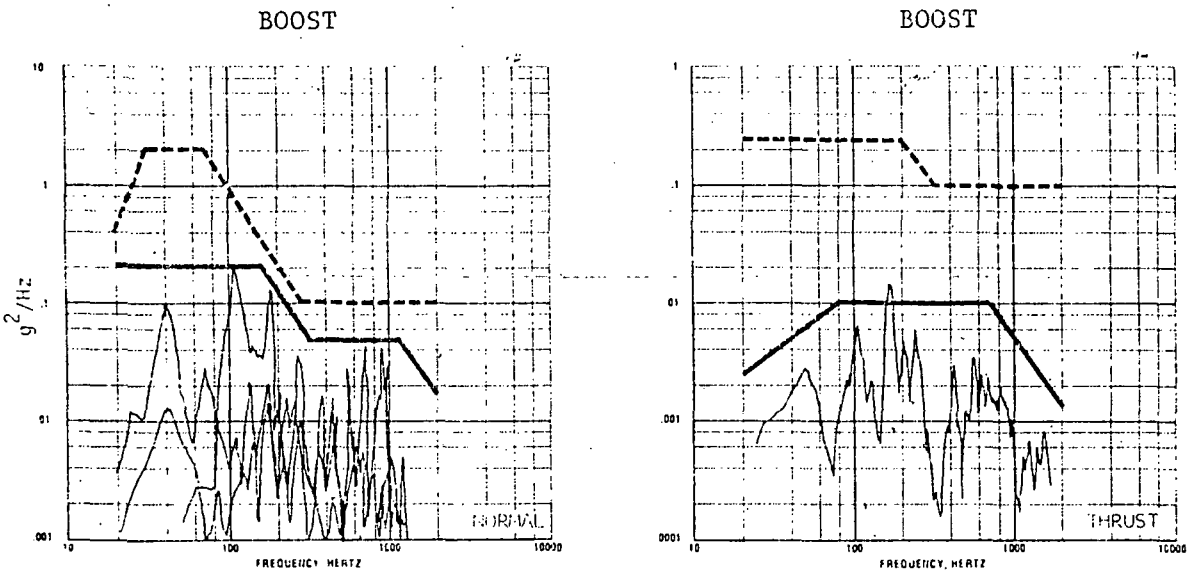

Source: Figure 7-50 of Reference 6.

Figure 2-13. Comparison of Test Data With Criteria - Boost Input to Components Mounted on the Power and Display Console

The vibration data secured from the LDTM launch acoustic test were employed to derive revised random vibration criteria for eleven of the VLC components. Test specification revisions were incorporated for nine of the components.

The proof flight of the Viking Titan/Centaur 1 launch vehicle was conducted in February 1974, subsequent to the time that the VLC component vibration specifications were revised. Acoustic noise measurements recorded in the VLC area of the launch vehicle's nose fairing exhibited overall noise levels much lower than those which had been predicted to occur during the launch phase of the mission. Therefore, a new prediction of the maximum acoustic noise levels to which the VLC would be subjected was derived, based on the data obtained from these measurements.

The revised, launch acoustic noise prediction was employed to derive new predictions of the random vibration environments to which eleven VLC components were subjected. In the case of five of the components, data acquired on the test lander employed for the Proof Test Capsule precursor acoustic test were utilized in deriving the new vibration criteria. This test, conducted to calibrate the acoustic facility in the Acoustic/Vibration Laboratory (AVL), was performed using the revised acoustic noise levels.

The original and revised predictions of the maximum launch acoustic noise levels to which the VLC was exposed are described by the one-third octave band acoustic spectra shown in Figure 2-14. The spectral differences between these two acoustic spectra are shown in Figure 2-15.

Revised vibration criteria were derived from eleven VLC components using the revised launch acoustic noise criteria defined for the VLC and the vibration data acquired from the LDTM launch acoustic test and the Proof Test Capsule precursor acoustic test.

The revised vibration criteria for the VLC components were derived using the following procedures. For the derivations based on LDTM test data, a maximum envelope of the random vibration spectra produced from the applicable LDTM vibration measurements was made for a given component. This spectra envelope then was scaled to account for the differences between the original and the revised launch acoustic noise criteria. These noise criteria differences are shown by the one-third octave band noise spectra difference spectrum shown in Figure 2-15. The modified vibration spectra envelope provided a revised prediction of the component's vibration environment. A smooth-envelope spectrum was drawn over this prediction

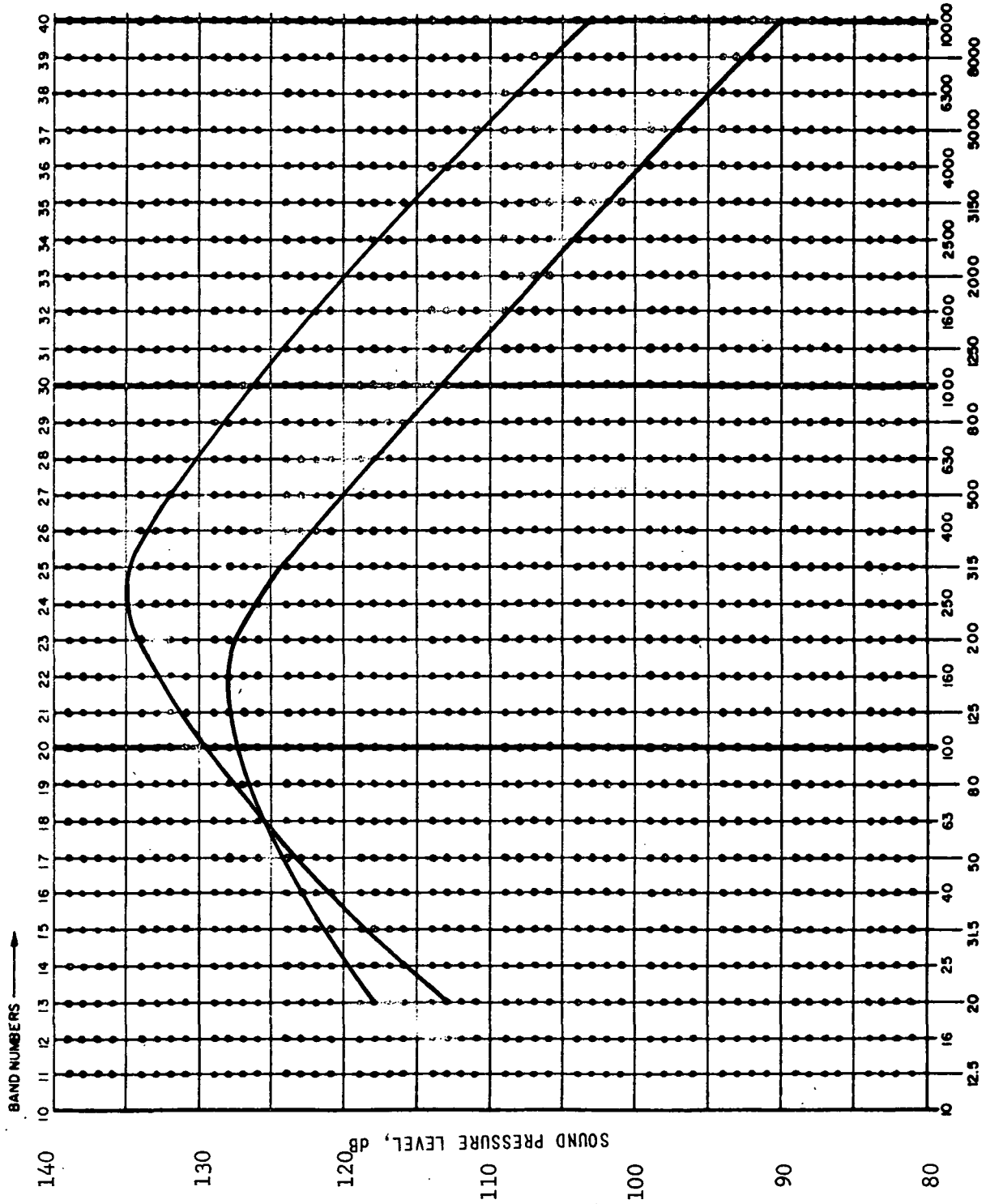

Figure 2-14. Viking Lander Capsule Launch Acoustic Spectra-
Original and Revised Acoustic Criteria

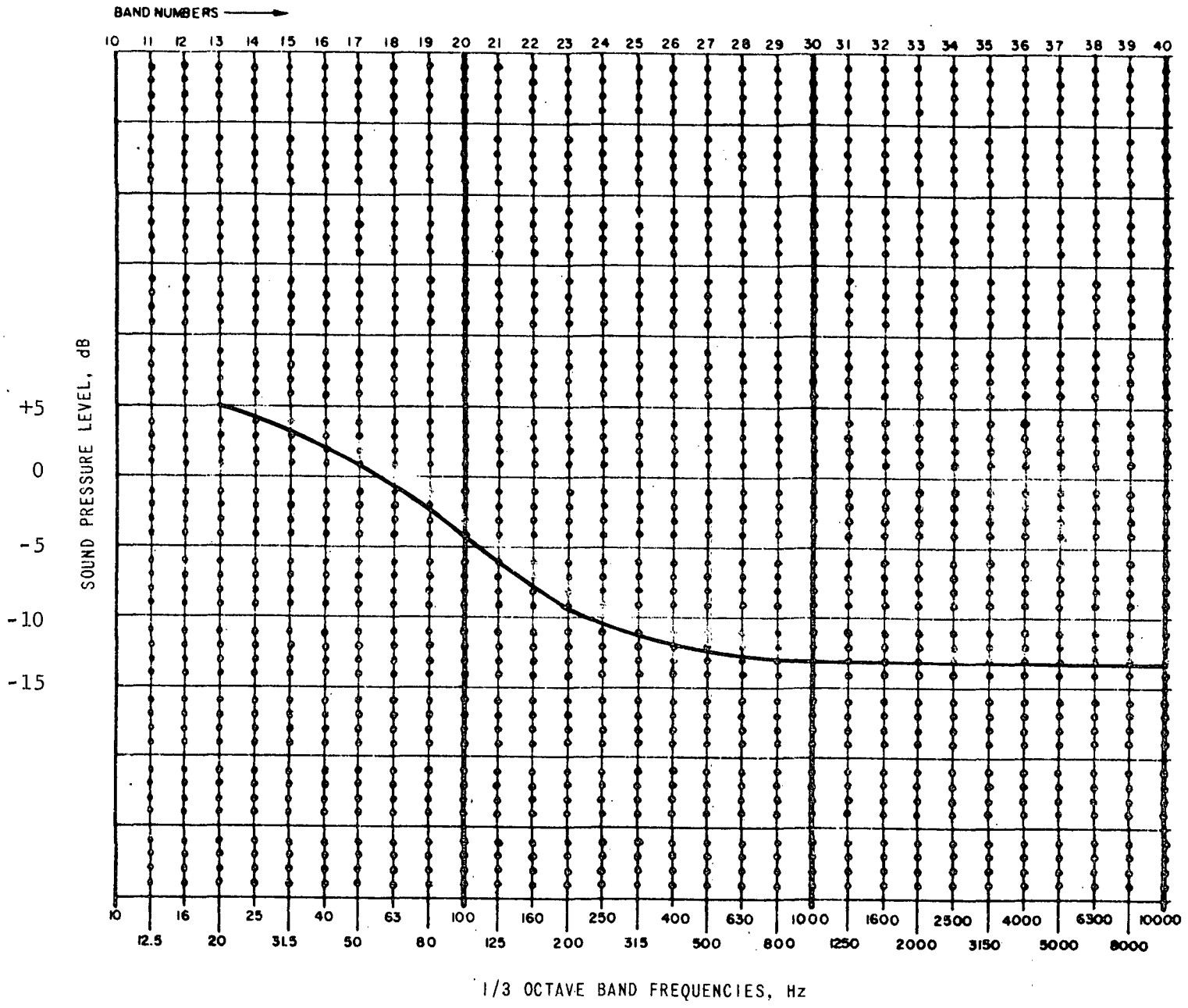

Figure 2-15. Acoustic Spectra Level Differences (Revised Acoustic Criteria Minus Original Criteria)

spectrum to define the revised vibration criteria for the component. For the derivations based on Proof Test Capsule precursor test data, the maximum envelope of the reference vibration spectra for a given component was used directly to derive the revised vibration criteria. No scaling of the maximum envelope was required since this test was performed using the revised acoustic levels.

Examples of the original criteria, test data, and revised criteria are presented in Figures 2-16 through 2-23. Note that in some frequency ranges, order of magnitude changes (both increases and decreases to the original criteria) were required for some components. In other cases, the overall levels did not change appreciably, but significant alterations to the spectrum shapes were required, generally resulting in increases in the low frequency region and reductions in the high frequency energy.

2.3.3 Data Banks

Vibro-acoustic data banks have been developed from acoustic and random vibration measurements obtained from flight and ground test programs. These data, which indicate the vibration level produced by a given sound pressure level acting on a particular structural configuration, are utilized for formulating design and test criteria for components and subsystems.

Two examples of data banks currently in use will be described to illustrate the techniques.

1. NASA TN D-7159. Development of Vibro-Acoustic Structural Data Banks in Predicting Vibration Design and Test Criteria for Rocket Vehicle Structures

This data bank was developed from approximately 1285 vibration and acoustic measurements obtained during static firings and flights of the Saturn vehicles and from the Mobile Acoustic Research Laboratory (MARL) testing program. The data banks were developed for three types of structural configurations:

Ring Frame - This type of structure is not directly susceptible to acoustic forcing functions, but receives motion from adjacent panels;

Skin/Stringer - This type of structure responds to acoustic forcing functions. The stringer response depends directly on the motion of the skin;

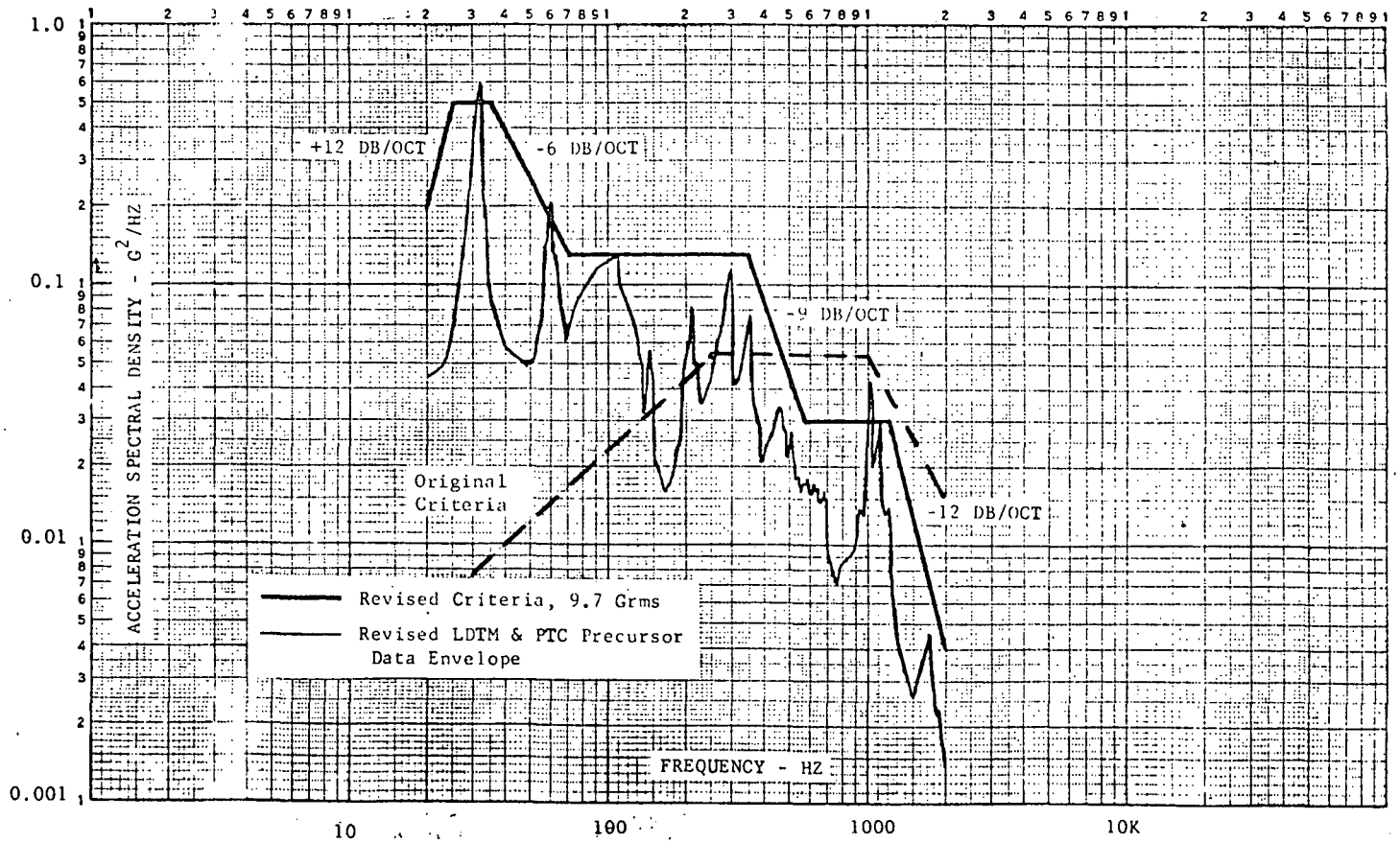

Figure 2-16. Random Vibration Spectra for the Bioshield Power Assembly

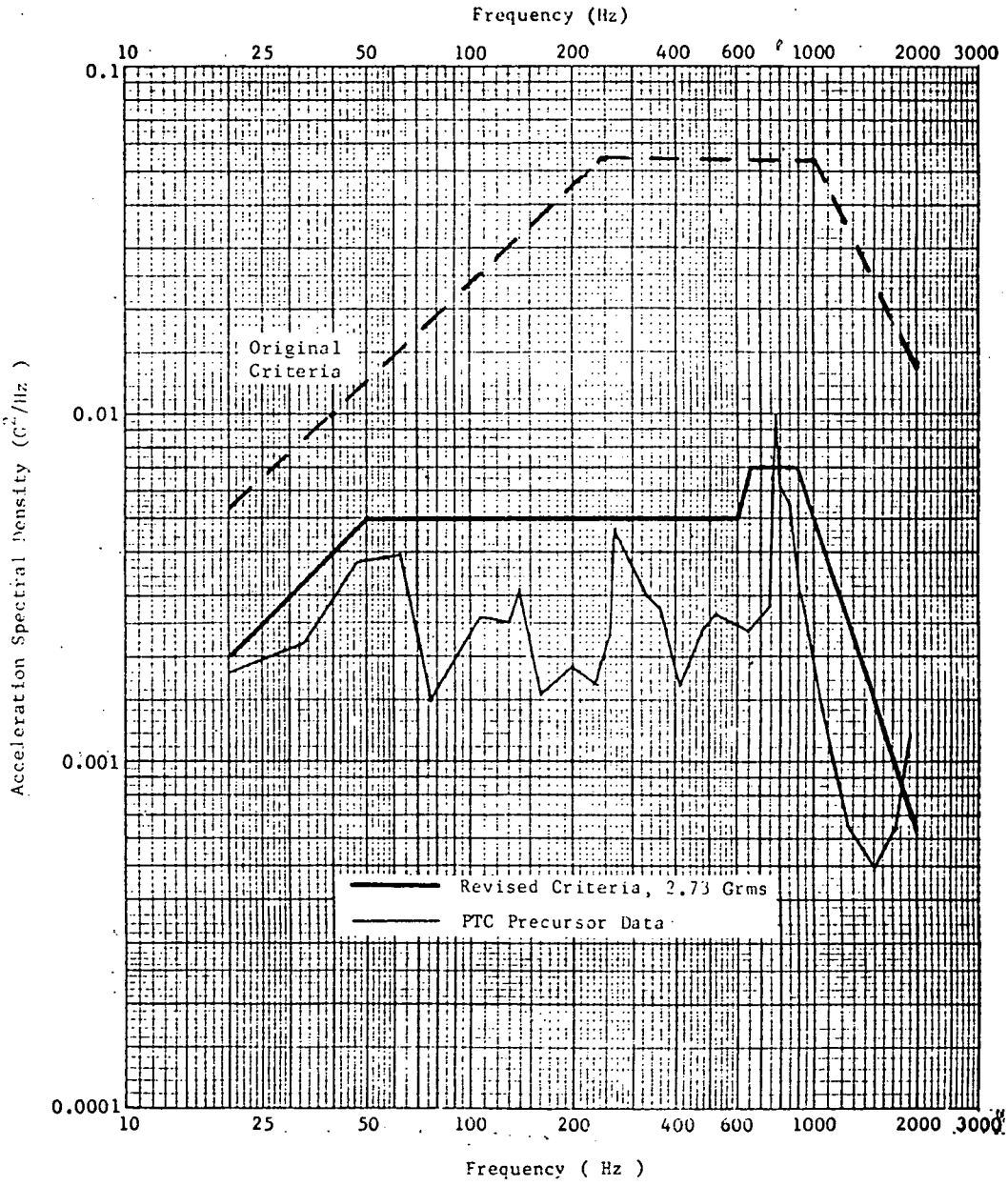

Figure 2-17. Random Vibration Spectra for the UHF Low Gain Antenna/Bracket Assembly

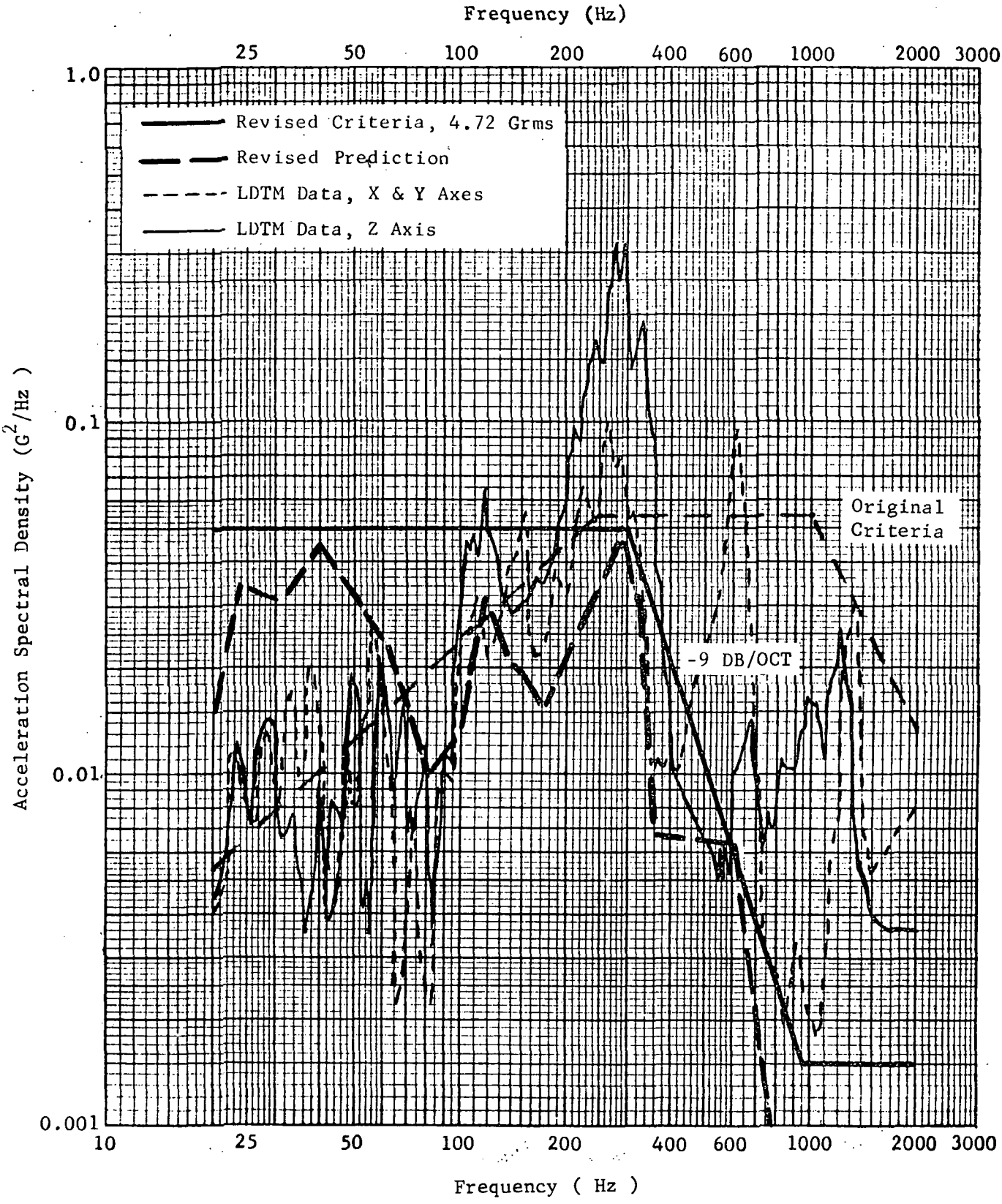

Figure 2-18. Random Vibration Spectra for the DCS S-Band High Gain Antenna

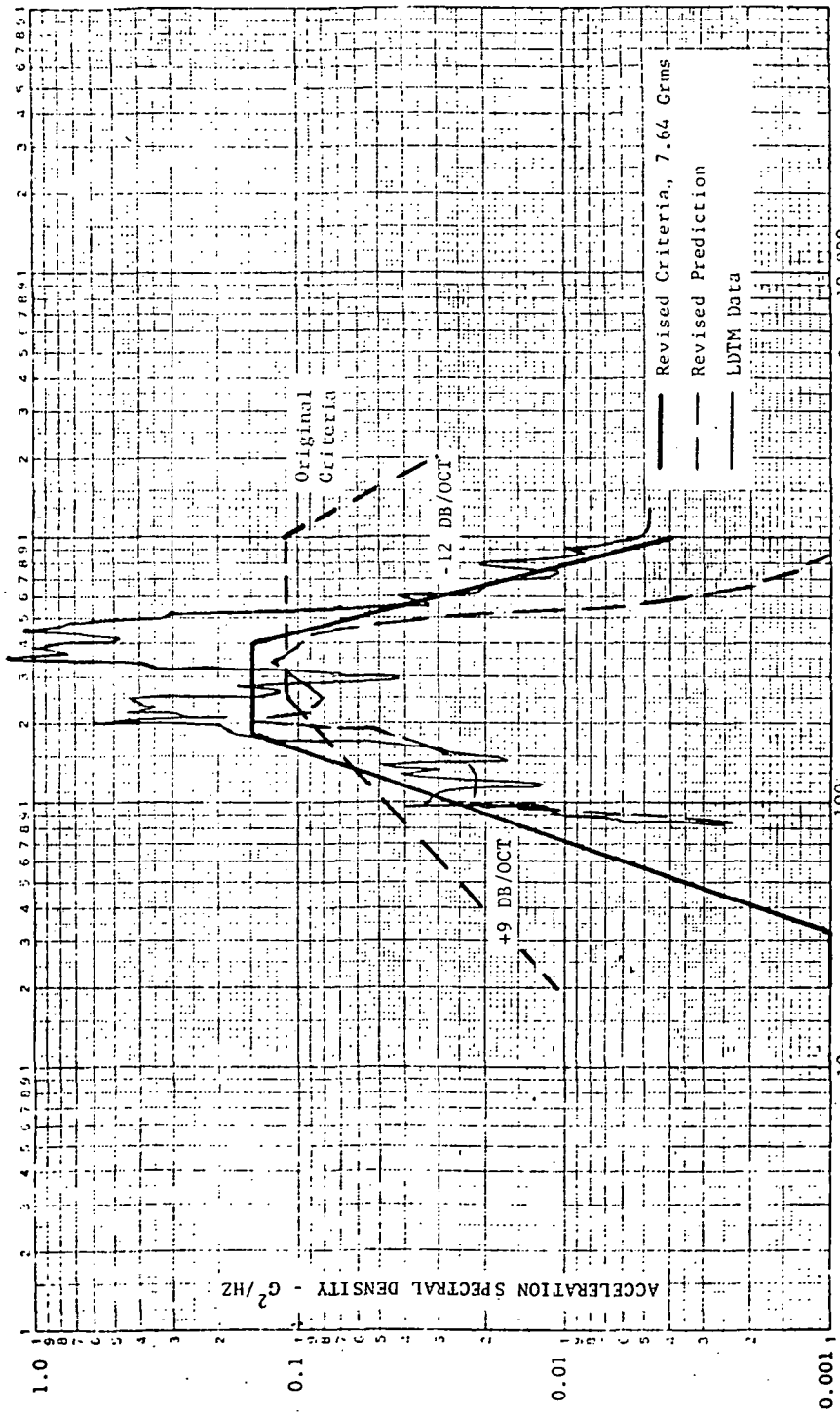

Figure 2-19. Random Vibration Spectra for Tube and Wire Cutters (PD5000010-001)

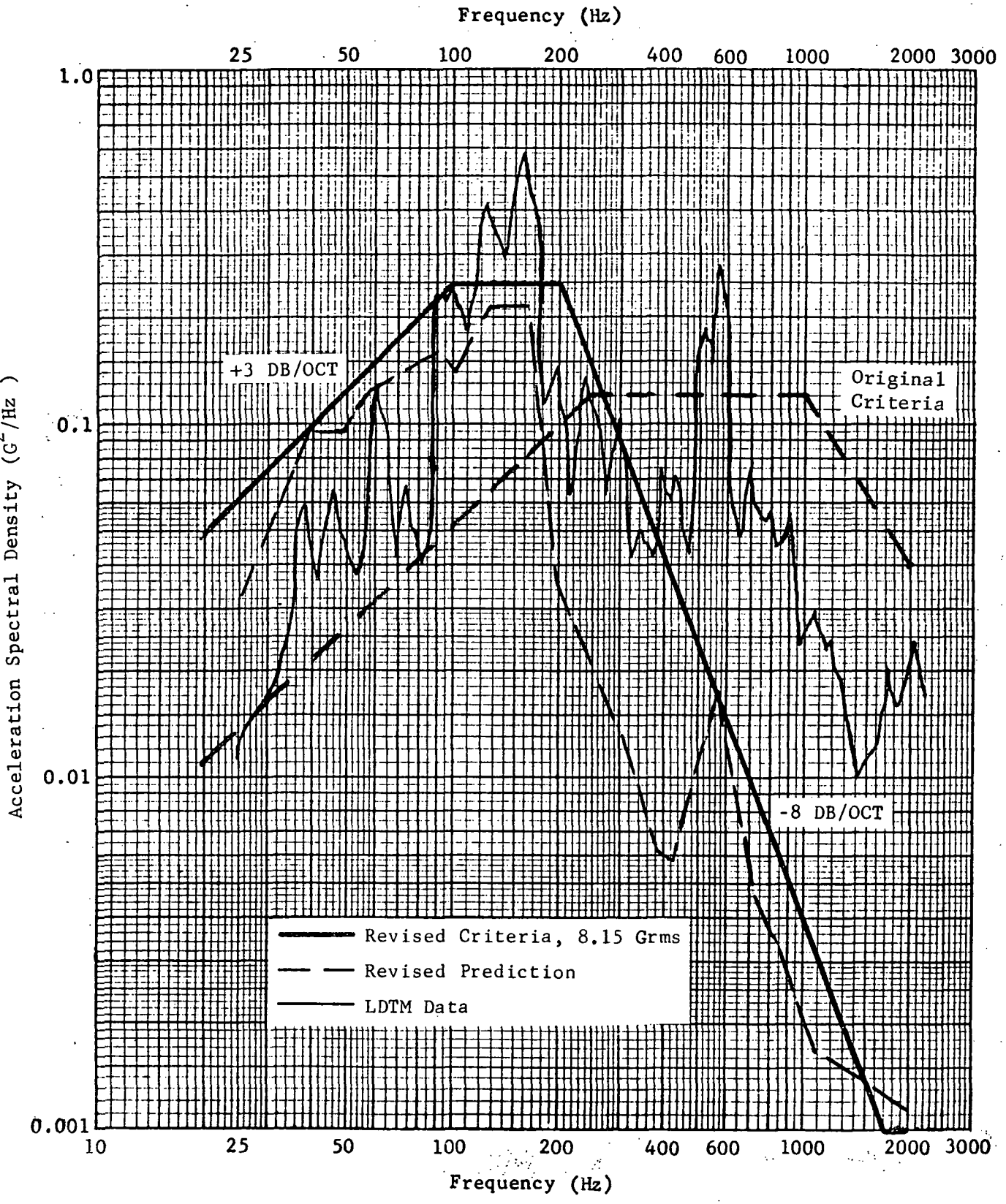

Figure 2-20. Random Vibration Spectra for the Bioshield Filter

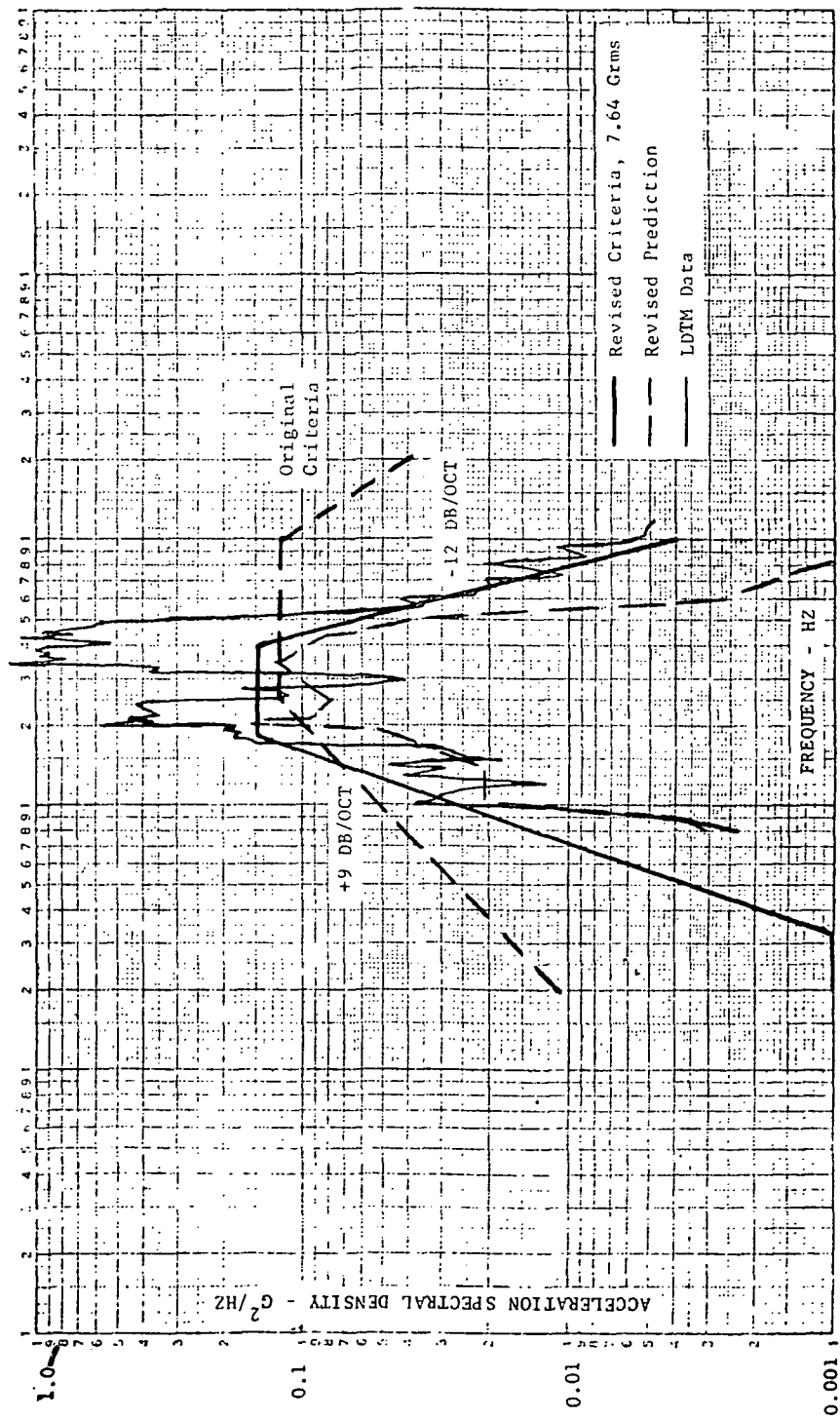

Figure 2-21. Random Vibration Spectra for the 2.5 PSIA Low Absolute Pressure Transducer (PD7400091-020)

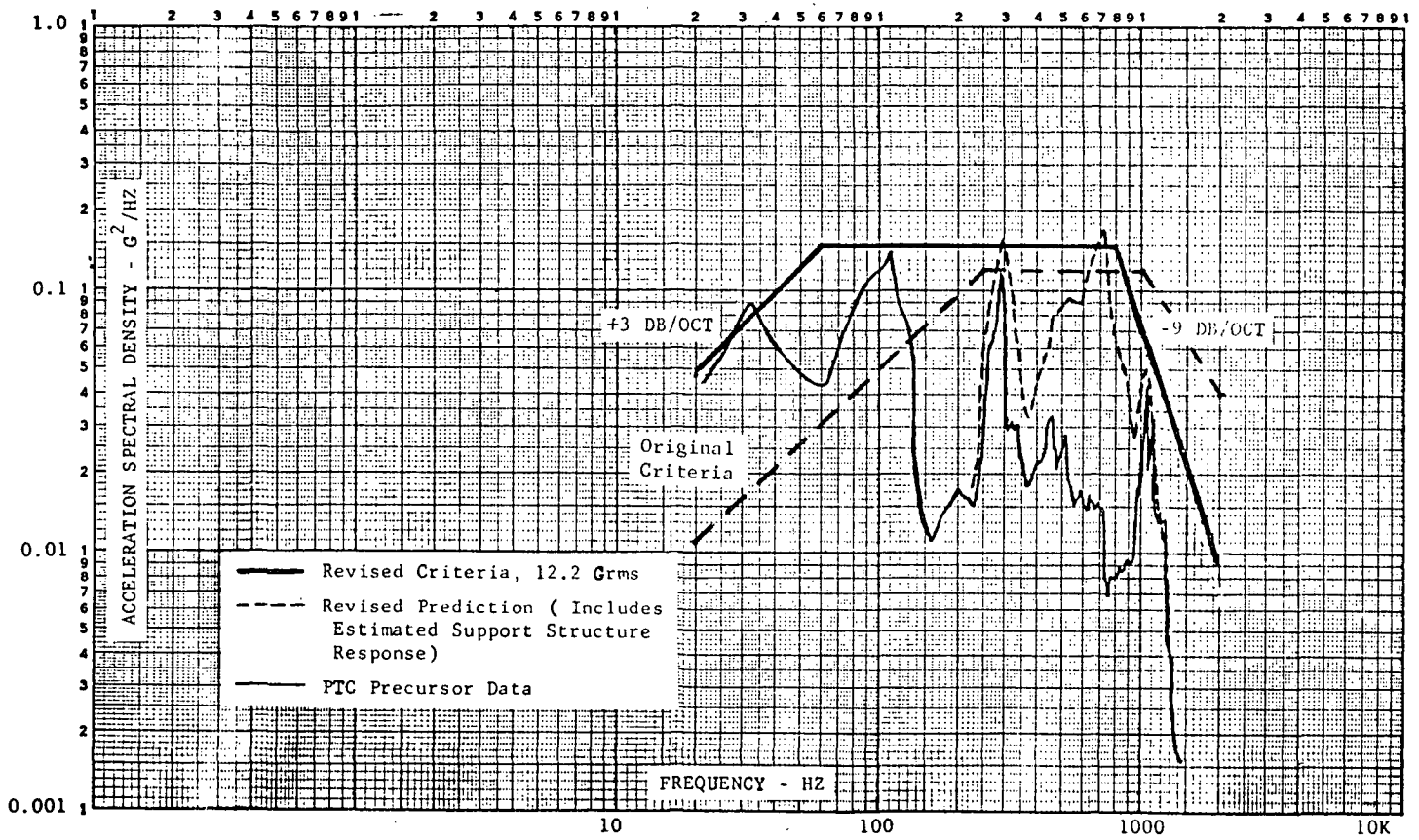

Figure 2-22. Random Vibration Spectra for the 16 PSIA Absolute Pressure Transducer (PD7400091-010)

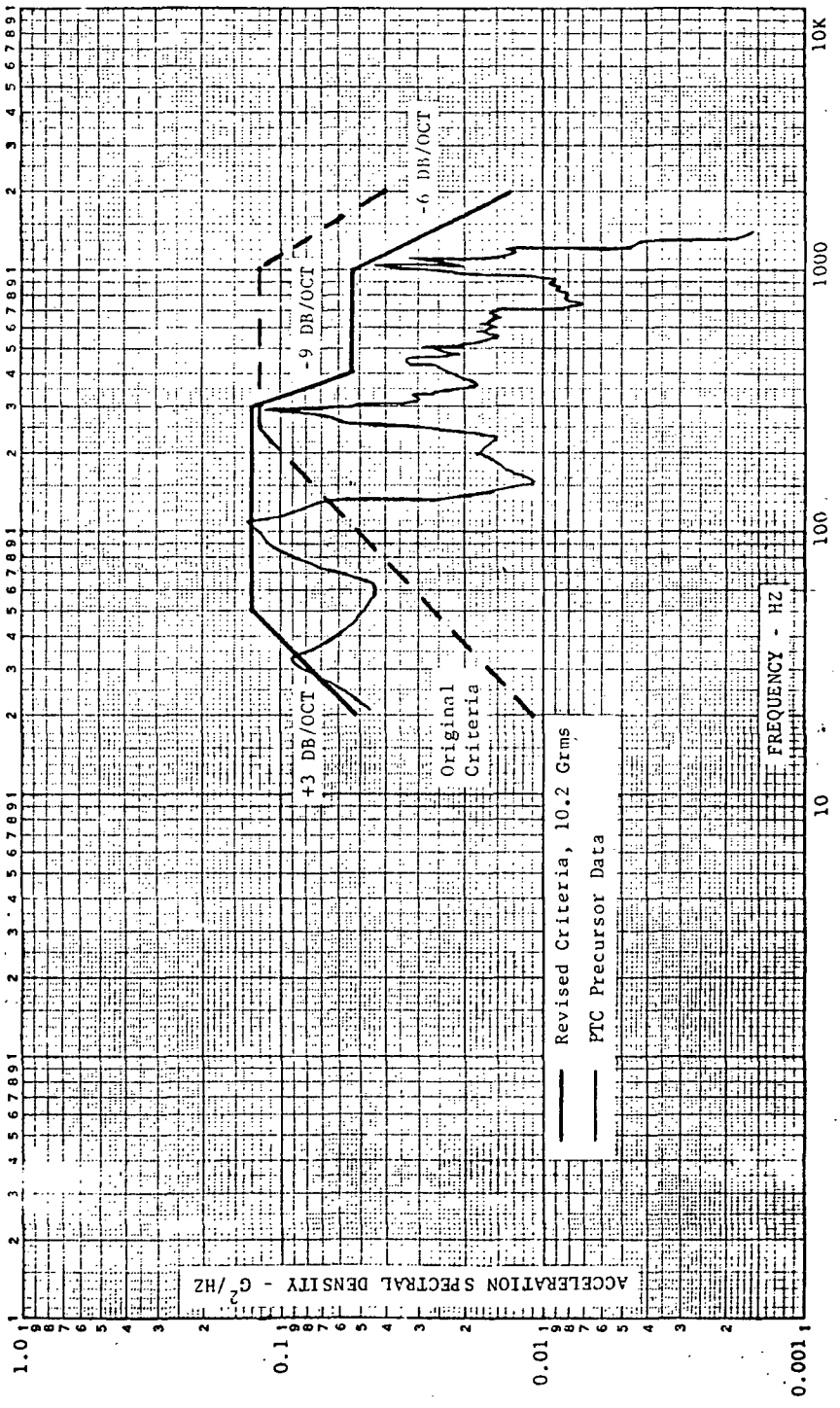

Figure 2-23. Random Vibration Spectra for the 0.6 & 1.0 PSID Differential Pressure Transducers (837F8100110-009 & -010) 0.1 PSIA Low Absolute Pressure Transducer (837F8100100)

Honeycomb - This type of structure is directly excited by acoustic forcing functions.

The vibration and acoustic data were normalized to the reference acoustic spectrum (a typical Saturn liftoff acoustic spectrum) shown in Figure 2-24. The normalization was performed utilizing the following equation.

$$G_L(f) = G_M(f) \left[\frac{P_L(f)}{P_M(f)} \right]^2$$

where

$G_L(f)$ = normalized power spectral density (G^2/Hz) as a function of frequency f,

$P_L(f)$ = reference acoustic pressure (N/m^2_{rms}) as a function of frequency f,

$G_M(f)$ = measured power spectral density (G^2/Hz) as a function of frequency f,

$P_M(f)$ = measured acoustic pressure (N/m^2_{rms}) as a function of frequency f.

Statistical analyses of the normalized vibro-acoustic data were performed and the mean and 97.5% confidence levels of the acceleration density spectra were determined for the different structural configurations. An example is shown in Figure 2-25. These data banks were compiled for unloaded structure, and corrections applied for the effects of component weight.

To utilize the data bank, it is necessary to select the data bank which best represents the new vehicle structure and then apply the necessary mass and sound pressure corrections to determine the vibration criteria for unloaded new vehicle structure using the following formula.

$$G_N(f) = G_R(f) \left[\frac{P_N(f)}{P_R(f)} \right]^2 \cdot \left[\frac{M_R}{M_N} \right]^2$$

where

$G_N(f)$ = new vehicle power spectral density (G^2/Hz) as a function of frequency f,

$G_R(f)$ = data bank power spectral density (G^2/Hz) as a function of frequency f,

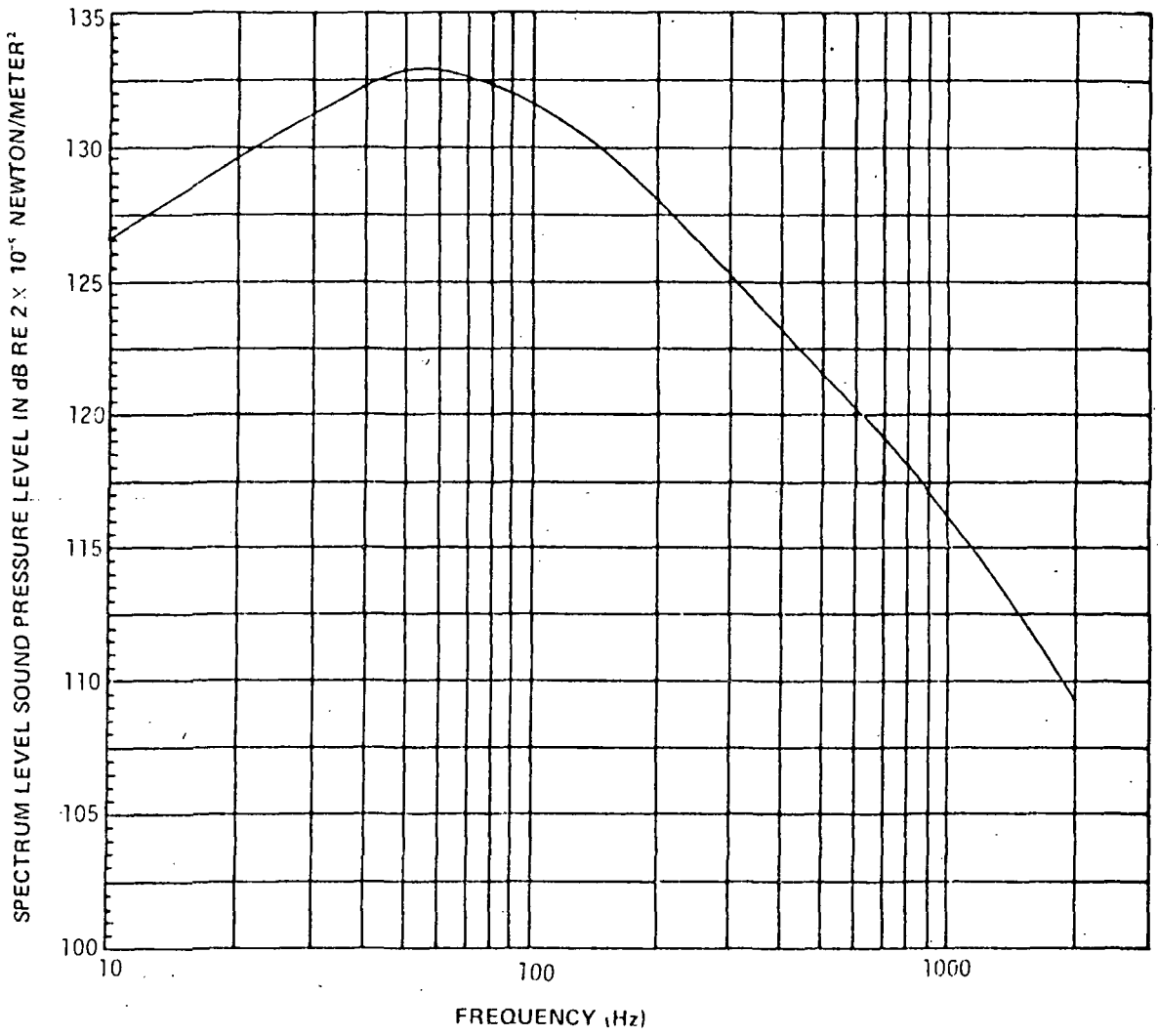

Figure 2-24. Reference Acoustic Spectrum

DIRECTION – RADIAL
SKIN THICKNESS – .10 cm (.040 in.)
RING SEPARATION – N/A
RING WEIGHT – 3.73 kg/m (2.51 lb/ft)
STRINGER SEPARATION – 22 cm (8.63 in.)
STRINGER WEIGHT – 1.06 kg/m (.71 lb/ft)

FLIGHT OR TEST
CONDITION – LIFTOFF
MATERIAL – ALUMINUM
COMPOSITE MEAN – 12.44
COMPOSITE 97.5 – 29.24
VEHICLE DIAMETER – 10.06 m (33 ft)

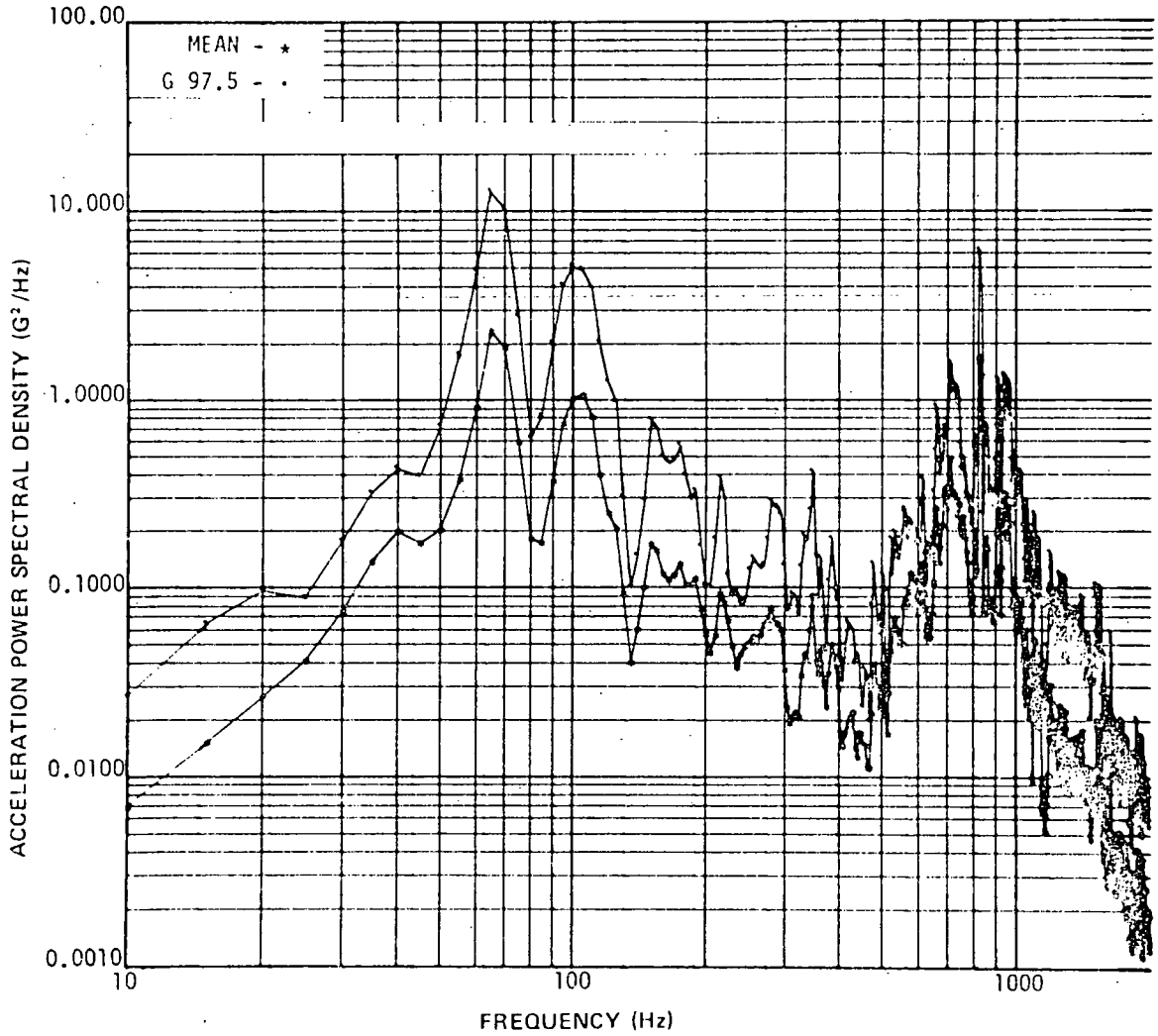

Figure 2-25. Ring Frame Acceleration Power Spectral Density, Radial, Liftoff

$P_N(f)$ = new vehicle measured or predicted acoustic pressure (N/m^2_{rms}) as a function of frequency f,

$P_R(f)$ = reference acoustic pressure (N/m^2_{rms}) as a function of frequency f,

M_N = mass per unit area of new structure,

M_R = mass per unit area of data bank structure.

A similar data bank is currently being compiled for the Titan III vehicles, and will include data from skin/stringer structure, tank domes and trusses.

2. AFFDL-TR-74-74. A Method for Predicting Acoustically Induced Vibration in Transport Aircraft

This study describes a method for predicting acoustically induced vibration in transport aircraft. The results of the study are in the form of a set of nomographs for the prediction of structural vibration, and include methods to account for variations in structural mass and rigidity.

The prediction technique includes a set of SPL-vibration correlation charts for each one-third octave band in the frequency range from 50 to 2500 Hz. Each chart contains the statistically derived confidence level lines of 50%, 80%, 90%, and 97.5% as shown in the example in Figure 2-26. The charts were developed for two basic structural types:

a. shell structure (skin-frame-stringer) typical of fuselages, fairings, etc. (Figure 2-27);

b. box structure (skin-stiffened box-beam) typical of wings and control surfaces (Figure 2-28);

For each type of structure, the mass and rigidity of the structures are calculated by variations of the following formulas:

$$M \propto \left[\frac{A_f \rho_f}{b} + \frac{A_s \rho_s}{a} + h \rho_p \right]$$

where

A_f, A_s = cross-sectional areas (cm^2) of frames and stringers

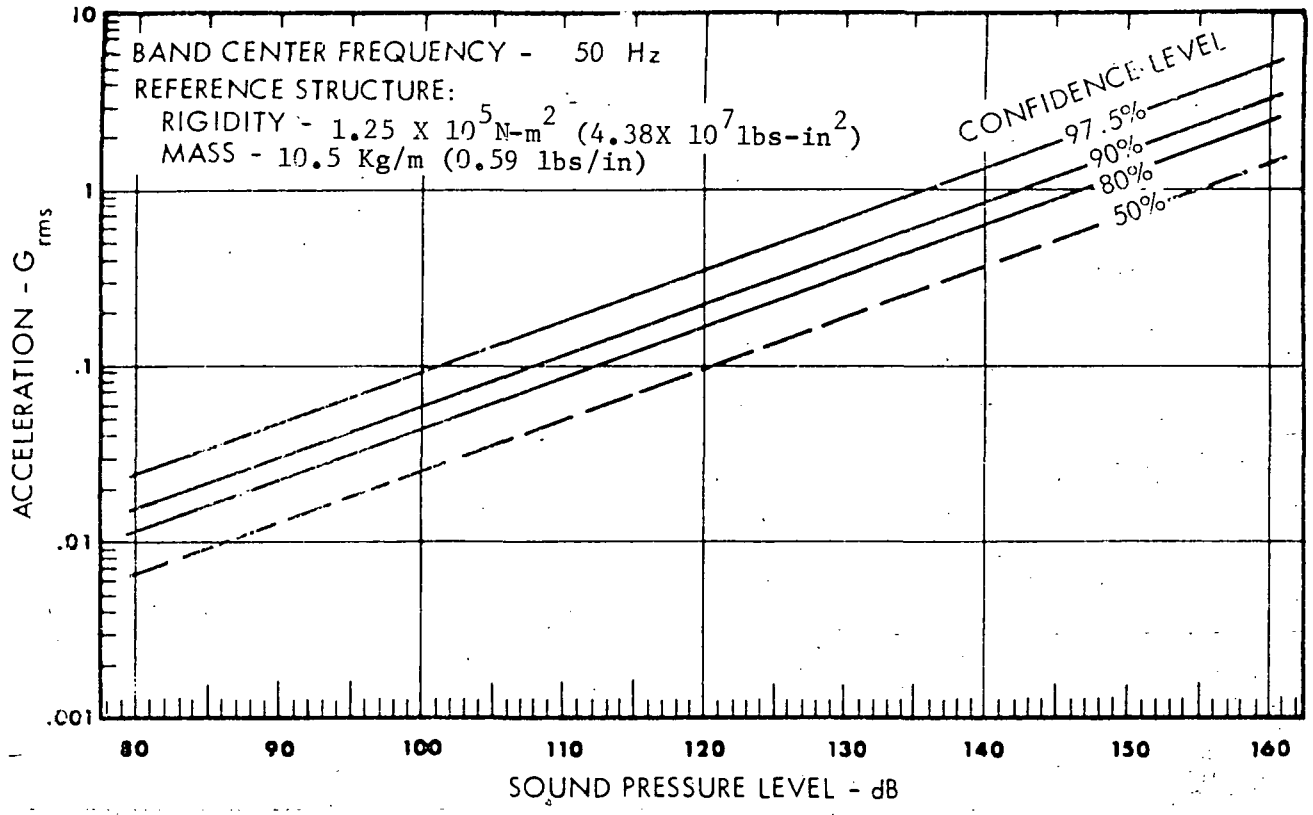

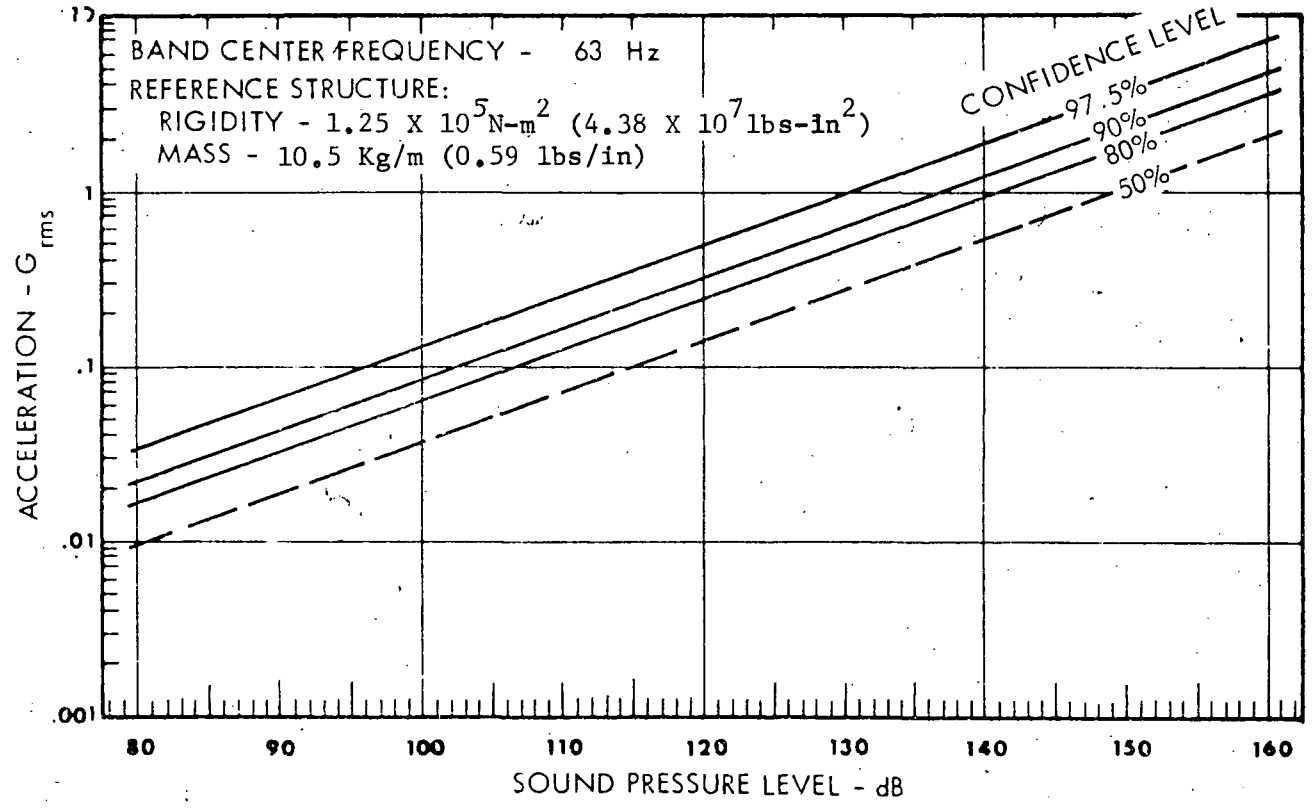

Source: Figure 1 of Reference 10.

Figure 2-26. Third-Octave Band Vibration Prediction Chart for Shell Structure - Normal Direction, Ground Operation

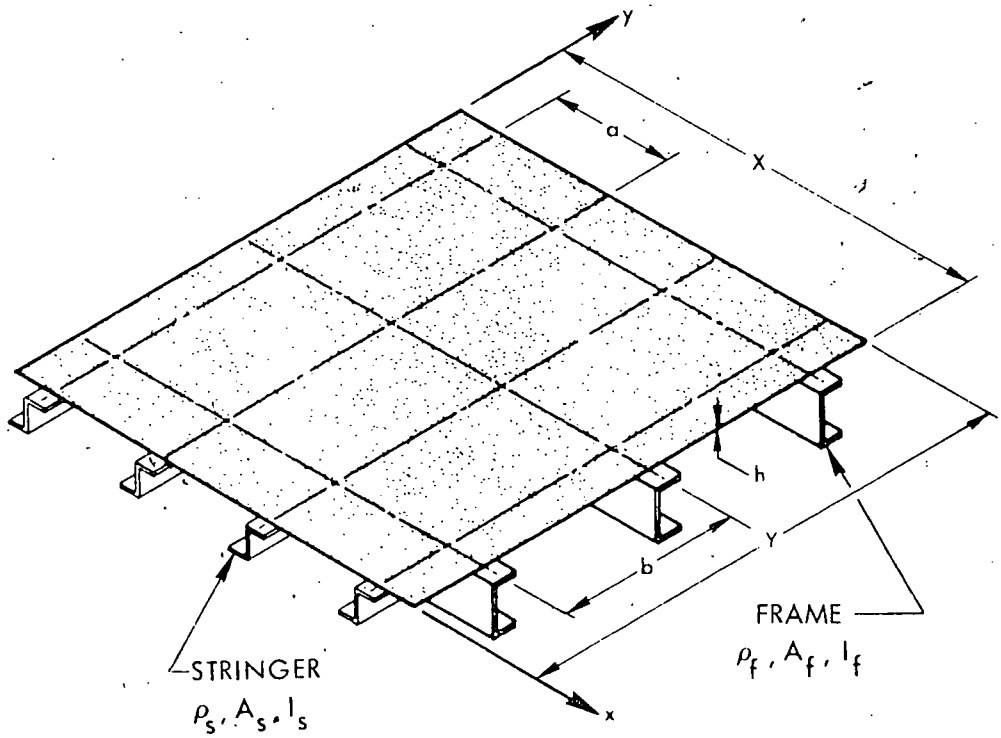

(Figure 23 of Reference 10.)

Figure 2-27. Shell Structure

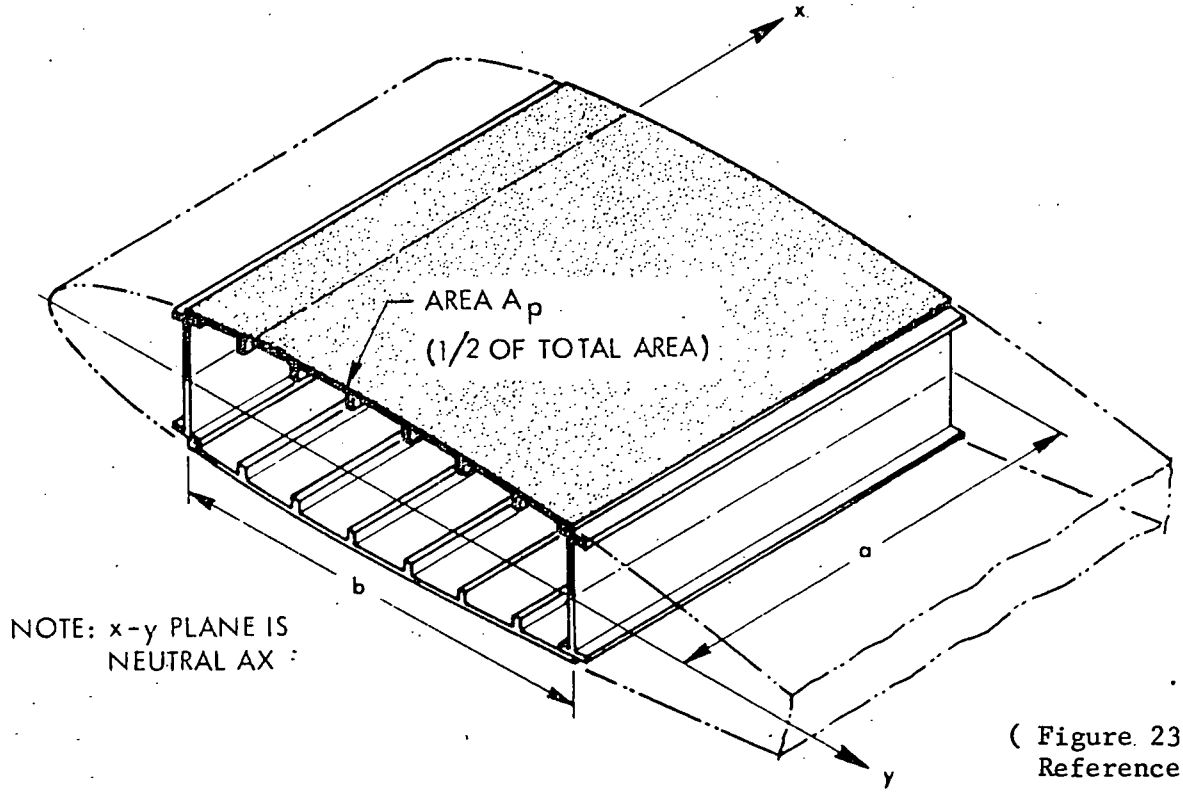

(Figure 23 of Reference 10.)

Figure 2-28. Box Structure

ρ_f, ρ_s, ρ_p = densities of frames, stringers and skin (grams/in^3)

h = skin thickness (cm)

b = frame spacing (cm)

a = stringer spacing (cm)

$$D \propto \left[\frac{E_f I_f}{b}\right] + \left[\frac{E_s I_s}{a}\right]$$

where

D = rigidity factor

E_f, E_s = moduli of elasticity for frames and stringers (dynes/cm^2)

I_f, I_s = area moments of inertia for frames and stringers (cm^4)

a = stringer spacing (cm)

b = frame spacing (cm)

A nomograph (Figure 2-29) was developed for determining the mass/rigidity correction factor.

The examples presented in this section are included to indicate the capabilities and limitations of current methods of random vibration prediction techniques. Even in the case (Skylab) where the flight acoustical environment was known with a relatively high degree of confidence, the configuration differences between Skylab and previous Saturn vehicles resulted in a number of changes to component specifications, and requalification requirements. Similar results were obtained on the Viking program, where the measured data from the proof flight vehicle necessitated changes to the definition of the flight environment, and associated modifications to component criteria.

These examples emphasize the importance of obtaining accurate definition of the shuttle environments as early in the program as possible, and for developing improved methodology for determining random vibration criteria for components, either by the data bank process or by improved analytical techniques. Based on these examples, it appears that development type acoustic tests of initial payloads are warranted in order

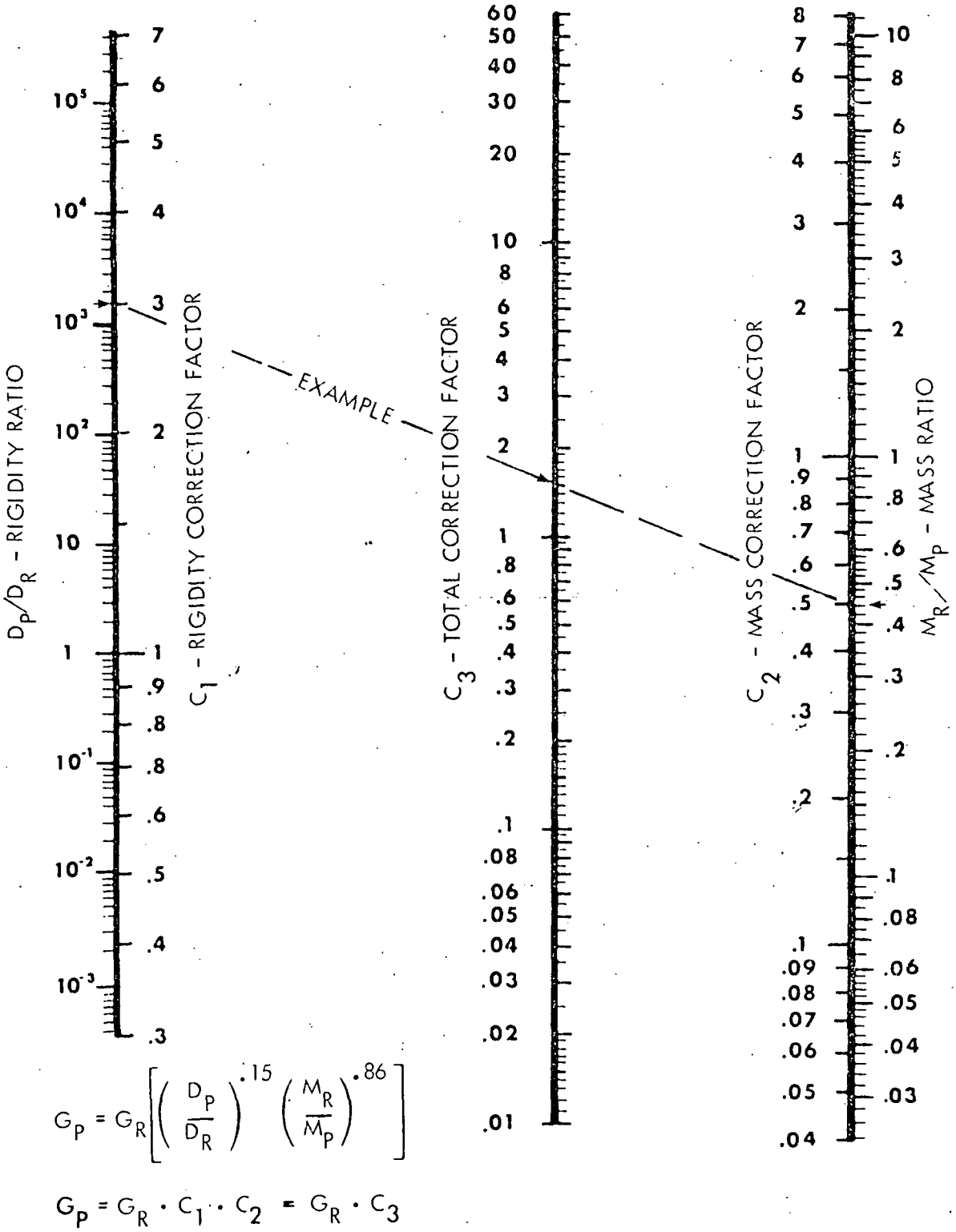

Source: Figure 21 of Reference 10.

Figure 2-29. Mass and Rigidity Correction Nomograph

to define component criteria as accurately as possible and to determine vibro-acoustic transfer functions for as many different types of structure and component loading conditions as possible for application to future payloads.

3.0 IMPROVED TECHNIQUES FOR SHUTTLE

3.1 Flight Measurement Program

3.1.1 Current State-of-the-Art

In a "state-of-the-art" approach, the instrumentation installed on the shuttle payloads for measuring the dynamic environments would be limited to that which is in current use and is well-proven and reliable within its known capability. The exact number, type and locations of the transducers depends upon the specific characteristics and size of each particular payload or experiment. In general, most of the available data channels will be assigned to accelerometers (both high and low frequency), microphones and strain gauges; for special loads-identification purposes, it is desirable to use load-cells at selected Orbiter/payload interface points. In addition, engine pressure transducers are required in order to measure the engine pressure-time histories, to be used to reconstruct the forcing functions which are generating structural loads. The greater part of the measured data will be recorded on-board for later playback and analysis. However, some of the more important data should be telemetered to ground stations to be used for diagnostic purposes in the event of a launch vehicle malfunction.

The frequency range covered by the dynamic instrumentation may be divided, for purposes of this discussion, into a low-frequency band (below 100 Hz or so) and a high frequency band (above 100 Hz). The low-frequency covers the range in which dynamic modeling and analysis can be performed with high confidence and used to calculate structural frequencies and responses to low-frequency flight transients. By using appropriately located instrumentation, the analytical predictions can be correlated with the test data and the dynamic model refined as necessary so that loads resulting from later missions can be predicted with greater accuracy and confidence. Instrumentation pertinent to this frequency range are accelerometers, strain-gauges, load cells and engine pressure transducers.

The high-frequency band covers the frequency range associated with the acoustic environment and the resulting random vibration, and with short-duration transients such as pyrotechnic events. In this range, a relatively low degree of confidence exists in the results of current analytical techniques, and the most reliable current methods are semi-empirical, extrapolating responses measured on previous flights to predict responses in the new situation. The flight measurements used for the high-frequency environments are limited to accelerometers and microphones. The measured data, together with a knowledge of the structural details, will be organized into a data bank of the

type described in Paragraph 3.2.2.3 for future applications. The overall relationship between the instrumentation and the subsequent data usage is summarized in flow-chart form in Figure 3-1.

3.1.1.1 Initial Flights

The term "initial flights" is intended to cover the first ten to twelve missions. Of these, information is currently available on seven payloads, as tabulated in Appendix A. Even this small number of payloads covers a wide range of sizes, going from approximately 2600 kg (5700 lb) to 11,800 kg (26,000 lb) in total weight. In order to specify exact locations of the instrumentation, detailed information on the actual structure would be required. Since this is not yet available for any payload, many assumptions have to be made in order to start planning instrumentation coverage. As an example of a flight measurement plan, the Long Duration Exposure Facility (LDEF) payload, which is planned to be flown on Mission #4, was selected and detailed instrumentation was called out, based upon a number of assumptions, as described in the next paragraph.

3.1.1.2 LDEF Example

The payload for Mission #4 actually consists of the LDEF and three Integrated Real Time Contamination Monitors (IRTCMs). The LDEF is described in Reference 1 as a low-cost simple structure on which many different totally self-contained experiment packages can be mounted for transportation to and from space via the shuttle. The objective of the LDEF is to measure the effect of the space environment on biomedical and material specimens and investigate particulate matter in space. Each IRTCM is a relatively small modularized system weighing approximately 53 kg (120 lbs) and consists of several rather dense modules mounted on a rectangular pallet. Thus, the LDTM/IRTCM provides a good example on which to demonstrate the approach used to define the instrumentation requirements for a large payload.

The detailed flight measurement program, together with a demonstration of the dynamic modeling analysis performed to investigate low-frequency loads is given in Appendix B.

3.1.1.3 Variations for Other Payloads on Initial Flights

Because of the wide variation in payload size in the initial flights (as described in Appendix A), the instrumentation scheme will differ considerably for each payload. The following general approach is recommended for establishing instrumentation requirements for the second and subsequent flights within the group designated "initial flights".

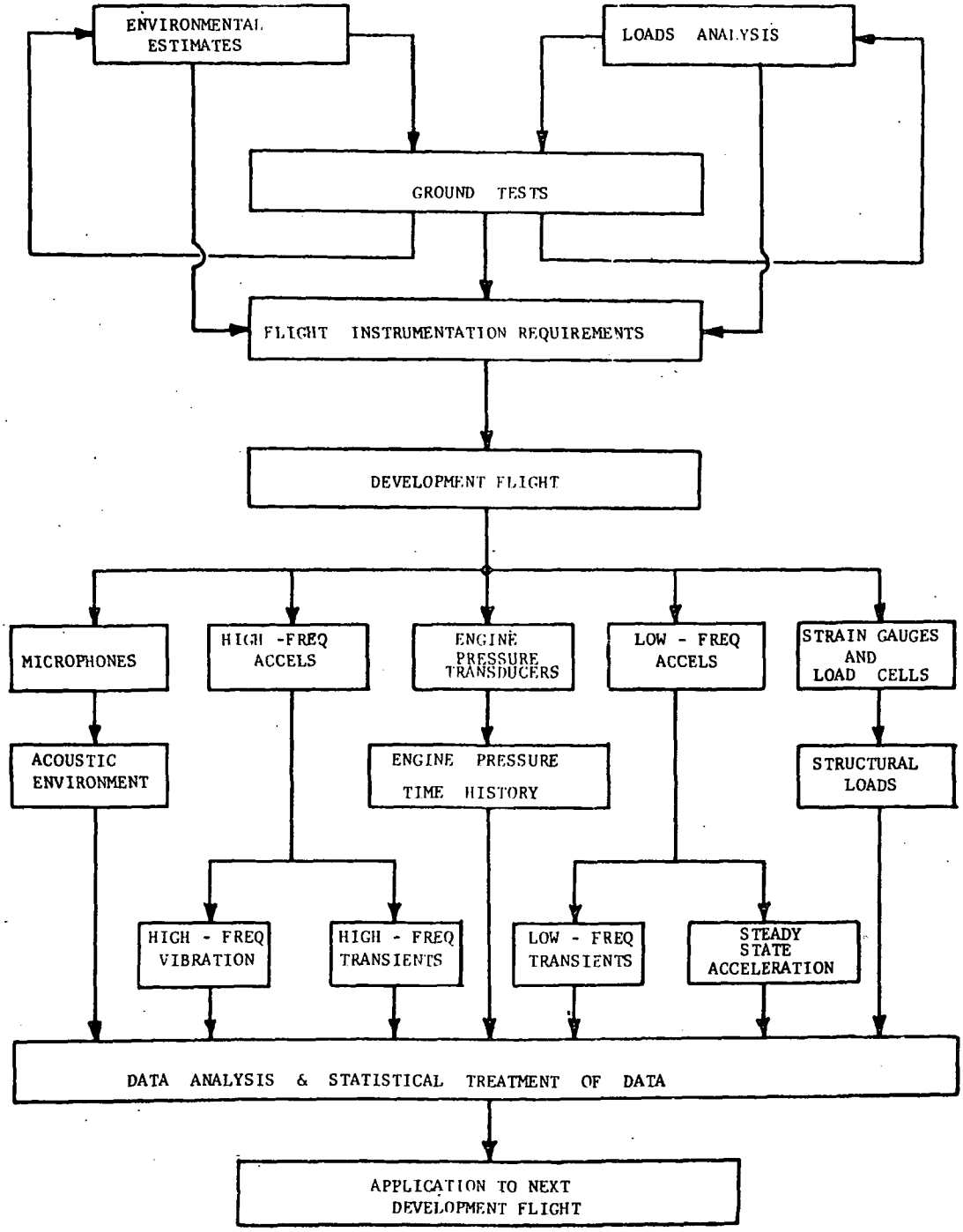

Figure 3-1: Relationship of Instrumention to Data Usage

A. In the treatment of the LDEF payload, it was assumed that as many as 14 channels of data could be telemetered in real time to a ground station. These channels should be maintained on subsequent initial flights for diagnostic purposes in the event of flight failures.

B. Microphone locations will be varied so that a complete mapping of the internal sound field can be achieved. Other microphones will remain at the same locations for all flights in order to gain enough data to allow statistical sampling to be used with confidence, and to enable the effects of changes in payload size on the internal acoustic environment to be evaluated.

C. The distribution and relative quantities of low and high-frequency accelerometers will be adjusted to reflect differences in payload overall density and size. Thus, a payload having large, lightweight surfaces or appendages, such as solar panels, antennae, etc. would be relatively susceptible to acoustics and should have good coverage in terms of high-frequency accelerometers. For a more dense payload, the emphasis will be on low-frequency accelerometers in order to obtain loads information.

   As with the microphones, certain accelerometer locations will be maintained in order to study the effects of payload stiffness and mass on interface loads.

   One important area which will be investigated as sufficient data is acquired is the mass-loading phenomenon, i.e., the effect of variation in component mass on the frequency response of the component/mounting structure. Data for this application will require accelerometers to be mounted at the same locations on the mounting structure for a number of different payload component weights.

D. Strain gauges and load cells are basically installed at the payload/orbiter interface points, so that these will vary with payload as different mounting points are utilized. Calibration levels and dynamic ranges on the instrumentation will need to be adjusted as a function of the weight and stiffness of the payload.

3.1.1.4 Future Payloads

Payloads launched after the initial group of missions will differ from their predecessors in the quantity of instrumentation which will be installed. Information gained from the initial flights will have been used to develop the data banks for the full frequency range applicable to the flight environment, and to update and refine the dynamic models of the Orbiter, coupled with various sizes and types of payload. Instrumentation on the later payloads will thus be limited to that necessary to give diagnostic data in the event of flight anomalies occurring, to fill in gaps in the data banks, and to increase the number of data samples to the point where statistical analysis can be used to calculate associated confidence levels.

In order to provide useful diagnostic data it will be necessary to have each Orbiter/payload interface point instrumented in three axes in order to measure the load and acceleration time histories for use in driving the mathematical model of the payload, so that the dynamic events leading up to the anomaly can be reconstructed. A small number of microphones should also be included so that an unusually high acoustic environment would be detected. It would obviously be desirable to telemeter the diagnostic data.

The data banks will be continuously updated as each flight provides additional measurements. However, when a payload seems likely to fill a gap in the data bank in terms of weight, volume, etc., advantage should be taken of the chance to use that flight to obtain the missing dynamic data, with a comprehensive instrumentation program. In order to assess how evenly the range of payload weights is covered, information on payloads expected to fly on the first twenty flights was reviewed. It was noted that of the thirteen flights for which information has been published, three payloads fall in the range 0 to 5000 Kg; one in the range 5000 to 10,000 Kg, and the remaining nine in the range 10,000 to 15,000 Kg. Thus, a later payload whose total weight was less than 10,000 Kg should be considered as a potential low-frequency data bank entry and instrumented accordingly.

Data defining the overall environment inside the payload bay would need to be updated if revisions to the mission plan caused changes in ascent trajectories or introduced dynamic events which had not previously been encountered. This would be accomplished by installing additional microphones and/or accelerometers in the payload bay, in locations which would be selected on the basis of experience gained in the initial flights.

3.1.2 Improved On-Board Measurement Technology

Current technology for acquiring flight data, using telemetry or on-board recording, has traditionally provided results which suffer from a number of shortcomings in the quantity and quality of data including the following:

a. Insufficient coverage across the structure to provide adequate checks with analysis;

b. Inadequate signal-to-noise ratio;

c. Restricted frequency and dynamic range.

Telemetry systems are invariably quite restricted in the number of channels available for dynamics data on the payload. For example, the Viking Spacecraft had only one microphone, four accelerometers and six strain gauges on-board. Airborne systems have usually had to contend with severe weight and space limitations, limiting the allowable number of transducers and associated signal conditioning equipment.

Since the space shuttle is neither weight or volume critical, at least for the great majority of payloads, the usual restrictions on the size of the on-board system do not apply to the same degree. Thus, it is feasible to provide a sufficient number of instrumentation channels to give good coverage of the entire structure for verification of analysis and spatially detailed definition of the environment.

Recent advances in instrumentation design can be used to advantage in this application. For example, one equipment manufacturer has just introduced a new charge amplifier for use in airborne vibration measurement systems. This unit is approximately one-half of the weight and one-third of the size of the previous smallest available charge amplifier. According to the manufacturer, it is also more reliable than its predecessors because of its relative simplicity, and has variable gain up to a gain range of 100 to 1. Another manufacturer also produces a lightweight airborne charge amplifier with a variable gain setting which can be adjusted in flight to virtually any desired gain range ratio. This is available with multiple outputs for a common input. Each output section can have its own gain and filter characteristics. Thus, a single accelerometer used in conjunction with this charge amplifier could operate in several frequency and dynamic ranges at different periods in the mission.

Because of the many missions to be flown by the orbiter, some of its structural components such as the payload support points and loading pallets will be exposed repeatedly to the

dynamic environments. The probability of eventually developing fatigue failures is therefore quite high and considerable analytical effort will probably be expended in this area. Unfortunately the state of the technology in fatigue analysis is still fraught with uncertainties for practical structures. Special strain gauges are available which facilitate the measurement of fatigue damage (References 11, 12). Unlike conventional strain gauges, these devices do not require continuous monitoring, but can be inspected after every flight. The gauge develops an irreversible resistance change which is directly correlated to fatigue damage when it is subjected to cyclic strains. It appears that the use of these gauges at strategic locations would provide valuable information on the fatigue problem and would represent a distinct improvement over conventional instrumentation.

The use of impedance or admittance measurements to study the interaction effects between the Orbiter and the various payloads is desirable. However, there are several problems which must be accounted for in making such measurements. The stiffness of the force transducer must be great enough to carry structural loads but allows sufficient sensitivity to accurately measure dynamic force. The mass of the transducer and attachments must somehow be accounted for in the analysis of impedance data to obtain the true force relationships between the structures of interest. In ground tests, this is usually accounted for by use of a feedback signal, a technique which may not be practical for flight measurement.

The use and validity of mechanical impedance/admittance techniques for predicting system responses has been studied recently by Kana and Vargas (Reference 13). It was found that an approach using admittance matrices gave satisfactory results for a simplified model of the Orbiter with simulated payloads. This approach could be applied to various Orbiter/payload combinations in order to identify the effects at the interface loading points caused by different payloads. In order to develop confidence in the technique, it is necessary to obtain flight data at these points on the actual payloads.

There are potential benefits to using on-board analog-to-digital data conversion and digital recording. Data storage density can be increased, so that a greater quantity of data can be stored on a single recorder. Post-flight data reduction and analysis time will be decreased if the data storage format is selected to be readily converted to the format used by the data reduction computers. Digital tape recorders are now available with great versatility in terms of tape speed and recording performance. One recently developed recorder is a six-speed, 42-track recorder which can be equipped with 1000 bits/inch/track digital record amplifiers. Tape speeds vary from 1-7/8 ips to 60 ips, giving a data-packing capability up to 60,000 bits/sec, with an

upper frequency limitation which can be as high as 10 KHz. The unit weighs 26 Kg (57 lbs) including tape, and is qualified to MIL-E-5400 dynamic environmental specifications.

It is obviously desirable to have maximum commonality and standardization between equipment being specified for data collection purposes throughout the orbiter. To this end, it should be noted that a Standard Tape Recorder (digital) is being developed under NASA contract, monitored by the NASA Inter-Center Tape Recorder Panel, as discussed in Reference 14. It is stated in the reference that this instrument is being considered for use on the orbiter, so that it would seem worthwhile to thoroughly review the capabilities of the design to handle the dynamic data recording task.

3.2 Data Interpretation Techniques

3.2.1 Current Methods

This section is a general discussion of the approach which would be used to reduce and analyze the data acquired on the early shuttle flights, using conventional methods. For convenience, the frequency range over which the data is acquired is broken down into low, mid and high frequency regions.

3.2.1.1 Low Frequency Region

The low frequency region corresponds to the range 0 to 50 Hz. From the viewpoint of the structural loads analyst, this is the most critical frequency range in which maximum loads are induced in the primary structure by vehicle transients, such as staging events, engine ignition and shutdown, gust loading and landing shock. Analytical methods exist which can be used to calculate the dynamic behavior and associated loads in the structure with a high degree of confidence.

The purpose of the data interpretation program is to analyze the flight-measured data and compile the resulting information for the use of subsequent payloads. To this end, the maximum amount of information should be extracted from the data to obtain a complete definition of the payload environment, total vehicle external loads, and dynamic properties of the structures involved. Possible changes in the vehicle external loads from flight-to-flight, and errors and/or changes in the predicted dynamic characteristics of the structures must be evaluated from the early shuttle flights for their impact upon the environments of the shuttle payloads.

To meet the goal of maximum information, locations of transducers for the low frequency region (accelerometers and/or strain gauges) and the recording procedures must be carefully preselected.

Exact locations for strain gauges to insure complete definition of payload interface loads must be considered. One very important consideration is the time-phasing of all recorded data. Data from the external loads (e.g., engine shutdowns) must be time-phased with the data recorded at the payload interface. This not only assists in diagnosing chronological events on the payload and shuttle, but also provides data for evaluating the total system transfer functions.

The payload interface data should be reduced in the form of time-history plots (g vs sec, or kg vs sec), Fourier spectra (g vs Hz or kg vs Hz), and/or power spectral density (g^2/Hz vs Hz). With the data in this form, complete assessments of the frequency content and amplitude can be made for each boost event. If need be, payload response from the low frequency events can be reconstructed using the time histories of the payload interface loads and "base driving" the payload model.

A complete spectral analysis of the external forcing function will also be necessary. This can be accomplished also with Fourier spectra, and/or power spectral density data. Spectral analysis will aid in determining the changes in frequency content of the staging events from flight-to-flight. Time history data should also be retained in the event that a loads analysis of the total integrated payload/orbiter structure becomes necessary.

The system transfer properties (e.g., from the orbiter engines to the payload interface) are important in evaluating the integrated payload/orbiter system. Once the orbiter and payload data are time-correlated, amplitude and phase information of the transfer characteristics can be extracted. With this data available, the orbiter structural properties can be assessed properly for predictions of subsequent payload environments.

3.2.1.2 Mid Frequency Region

The mid frequency region is assumed to encompass the frequency range from 30 to 100 Hz. This is the range in which higher order modes of primary structure and subassemblies are excited by aerodynamic buffeting and vehicle transients, but generally below the range in which random vibration response to acoustics controls the loads. The accuracy of analytical models becomes questionable toward the upper end of the mid frequency region. Thus, data interpretation techniques applicable to both the low frequency and high frequency regions are utilized and overlapped to cover the mid frequency region.

Data from strain gauges, low frequency accelerometers and impedance transducers provide the primary coverage in this region. The initial data reduction process will play back time histories of all of the significant events, with strong emphasis on maintaining accurate time-phase relationships. Shock spectra, power spectral density plots, acceleration spectra and impedance plots will be produced next and used to generate loads data for comparison with analytical load estimates, as well as environmental data on which to base test requirements for subsequent payloads. Transfer functions between payload interface points and subsystem/component mounting points will be calculated.

3.2.1.3 High Frequency Region

The high frequency region covers a very wide frequency range from 80 Hz or so up to 10,000 Hz. The primary form of excitation is acoustic, with some contribution from transient events and pyrotechnic shock, so that the high frequency data will basically come from microphones and high frequency accelerometers. As in the case of mid frequency data, time histories will be required from selected transducers and special care should again be taken to preserve accurate time synchronization between all of the data channels.

Current methods of predicting high frequency random vibration response to acoustics are mostly empirical based on taking data measured on earlier similar vehicles and then deriving suitable normalizing and scaling factors with which to adapt the data to a new vehicle. The accuracy of these methods is very dependent on the degree of similarity between the baseline vehicle and the new vehicle. Since in the present application the baseline and new vehicle are identical, the accuracy of the prediction process should be quite good when sufficient data has been accumulated. The data reduction and interpretation program should be designed to allow maximum utilization of the data in such techniques.

Acoustic data will be reduced and plotted in the form of sound pressure level spectra (dB versus Hz) and pressure spectral density plots ($(N/m^2)^2$ versus Hz). Vibration response data will be reduced to acceleration spectral density plots and for selected channels, auto-correlation function plots (g^2 versus sec). Other more complex analyses can be performed to facilitate running statistical checks on the data, but are not customarily included in the current methods of data interpretation. These are discussed in Paragraph 3.2.2.

The effect of payload configurations on the internal acoustic levels should be determined from data obtained on initial flights. To obtain this evaluation, the acoustical characteristics of the empty payload bay should be determined from

reverberation time and noise reduction measurements of the orbiter. Preliminary analyses were conducted for the LDEF, Spacelab and Large Space Telescope (LST) to determine the reduction in overall sound pressure level, relative to the OASPL in the empty payload bay, for these three payloads. Since the absorption characteristics are not known, these preliminary analyses were based on relative volumes and surface areas only, using reverberant sound field theory. The results indicate that LDEF and Spacelab cause a reduction of 1.8 dB, and LST would reduce the empty bay acoustic levels by 2.6 dB. These reductions would lower random vibration criteria by 20 to 35%.

3.2.2 Potential Improvements

A number of areas requiring improvement can be identified in the current methods for analyzing and interpreting data. One such area is the verification of some of the basic statistical characteristics of the data to ensure that the assumptions underlying the analysis methods being used are justified. A second area relates to the errors involved in the estimates of loads and environments. These errors should be identified and evaluated, and used in the derivation of test and design factors. Finally, accumulated data showing input environments and the resulting responses need to be organized in data banks to be readily applicable to later missions.

Essentially all of the conventional analytical treatment applied to flight data is based on the assumption that the data is purely random and stationary and has an approximate Gaussian probability distribution of amplitude. It is considered highly desirable to perform the necessary checks on the data to verify or disprove the validity of these assumptions.

Valuable information can be extracted from the data using recently developed statistical analysis techniques. For example, the method of coherence functions is receiving current attention. This is an approach which can be used for identifying multiple inputs to a system and characterizing (in terms of magnitude and frequency content) their relative contributions to the response of the system, taking account of the degree of correlation between the multiple inputs. Although this technique has been available for some time, its usage is not common in the aerospace industry.

The properties of the coherence function and its application to practical problems are discussed in the next section, along with a brief review of the errors associated with statistical treatment of data.

3.2.2.1 Discussion of Coherence Functions

Coherence functions can be used in a situation where it is required to monitor the noise or vibration generated within a mechanical system in order to identify the sources of vibration and determine their relative severity. Other applications are to assess the validity of frequency response functions calculated from measured data and to detect system nonlinearities. Particular emphasis will be placed in this discussion on the first application. The problem is to determine how much of the vibration measured on the payload during launch is caused by acoustics and how much is mechanically induced. This information is needed to help estimate the potential benefits of reducing internal acoustic levels and to determine the need for running various kinds of tests at the system and component levels.

The coherence function (CF) for two time histories x(t) and y(t) is defined as

$$\gamma_{xy}^2(f) = \frac{|G_{xy}(f)|^2}{G_x(f)\ G_y(f)}$$

where

$$0 \leq \gamma^2_{xy}(f) \leq 1$$

$G_{xy}(f)$ is the cross-PSD for the two time histories and $G_x(f)$ and $G_y(f)$ are the respective auto-PSD's.

If $\gamma_{xy}^2(f) = 0$ at a particular frequency, x(t) and y(t) are said to be incoherent; if $\gamma_{xy}^2(f) = 1$ for all frequencies, x(t) and y(t) are said to be fully coherent. If $\gamma_{xy}^2(f)$ has a value between zero and unity, any of three situations may exist:

a) The data contains noise,

b) The physical system relating x(t) and y(t) includes nonlinearities,

c) Multiple inputs $x_i(t)$ are causing output y(t).

A practical application of the coherence function is described in Reference 15, in which it was required to determine what components of the noise measured by a microphone was caused

by an adjacent mechanical system and how much was due to external sources. This was solved by mounting an accelerometer on the mechanical system then calculating the coherence between the microphone signal and the accelerometer signal. The plot of the coherence function showed the frequencies at which the accelerometer output was coherent with the microphone data, so that the noise radiating from the mechanical system could be identified.

In order to explore the use of coherence functions using actual flight data, a calculation was performed on measurements taken on the Viking Proof Test Flight, in which a dynamic simulator of the spacecraft was launched on a Titan III/Centaur. The instrumentation is described in Reference 16.

Data available included the following:

a. Time histories of strain measured on all six members of the Proof Flight Lander Adapter (PFLA) - See Figure 3-2;

b. Time history of a high frequency accelerometer on the Viking Orbiter Dynamic Simulator (VODS) Bus;

c. Time history of the acoustic environment in the region of the VODS Bus.

The response on the VODS bus measured by the accelerometer results from a number of inputs, including acoustics, loads applied through the trusses and feedback from the VODS sprung mass which hangs from the bus.

The objective of the calculation was to determine how much of the response measured by the high frequency accelerometer on the bus was caused by loads feeding back through the PFLA, and how much was due to acoustics.

For simplicity, it was assumed that only loads from the truss member which terminates on the bus at a point close to the accelerometer would contribute to the response measured by the accelerometer. Since this is not true, the contributions from the other members will be analogous to external noise on the measured signal and will detract from the accuracy of the estimate. It was also assumed that no correlation exists between the strain measurement and the acoustic time history.

Under these assumptions the two coherence functions relating the three signals will be

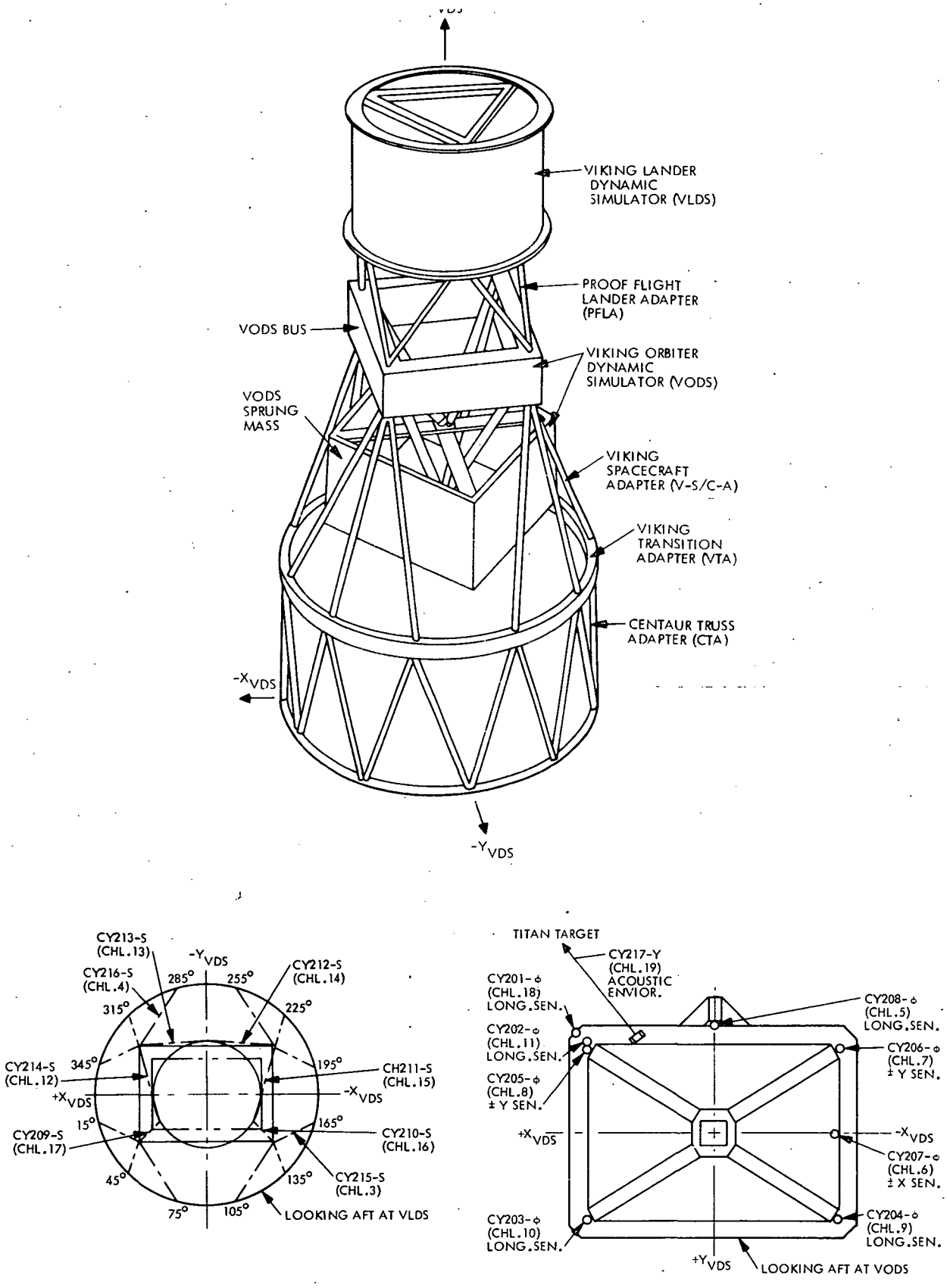

Figure 3-2: Viking Dynamic Simulator Configuration, Showing Instrumentation Locations

$$\gamma_{1,3}^{2}(f) = \frac{|G_{1,3}(f)|^{2}}{G_1(f) \times G_3(f)}$$

$$\gamma_{2,3}^{2}(f) = \frac{|G_{2,3}(f)|^{2}}{G_2(f) \times G_3(f)}$$

where subscript 1 refers to acoustics measurement (CY217-Y in Figure 3-2)

2 refers to strain measurement (CY214-S)

and 3 refers to the acceleration measurement (CY201-Ø)

$G_i(f)$ and $G_{i,j}(f)$ are auto-PSD and cross-PSD functions, respectively.

Note that $\gamma_{1,3}^{2}(f)$ will have units of $\frac{(N/m^2\text{-}g/Hz)^2}{(N/m^2)^2/Hz \cdot g^2/Hz}$

while $\gamma_{2,3}^{2}(f)$ will have units of $\frac{(m/m - g/Hz)^2}{(m/m)^2/Hz \cdot g^2/Hz}$

- that is, the coherence functions are non-dimensional.

The total record length available was approximately 9 seconds of data. It is obviously unlikely that the data would be stationary for this length of time, so tests for stationarity were applied. It was found that the full record did exhibit non-stationary behavior, but if the record is broken into two 4.5 second parts, it can be shown to be acceptably piecewise stationary, at a 5% level of significance. This defines the longest record which can be used in the subsequent analysis.

In order to obtain a realistic estimate of the coherence function, it is necessary to use smoothed auto-PSD's and cross-PSD's, obtained by calculating these spectra for a number of consecutive samples of the time histories and then averaging over the resulting spectra. To achieve this, the available data must be divided into shorter record lengths and used to calculate the average spectra.

Figure 3-3 shows the various steps in the analysis, including some of the preconditioning performed on the data to minimize statistical errors. Samples of the filtered time history plots are given in Figures 3-4, 3-5 and 3-6. The averaged auto-PSD's are plotted in Figures 3-7 through 3-9 and the two averaged

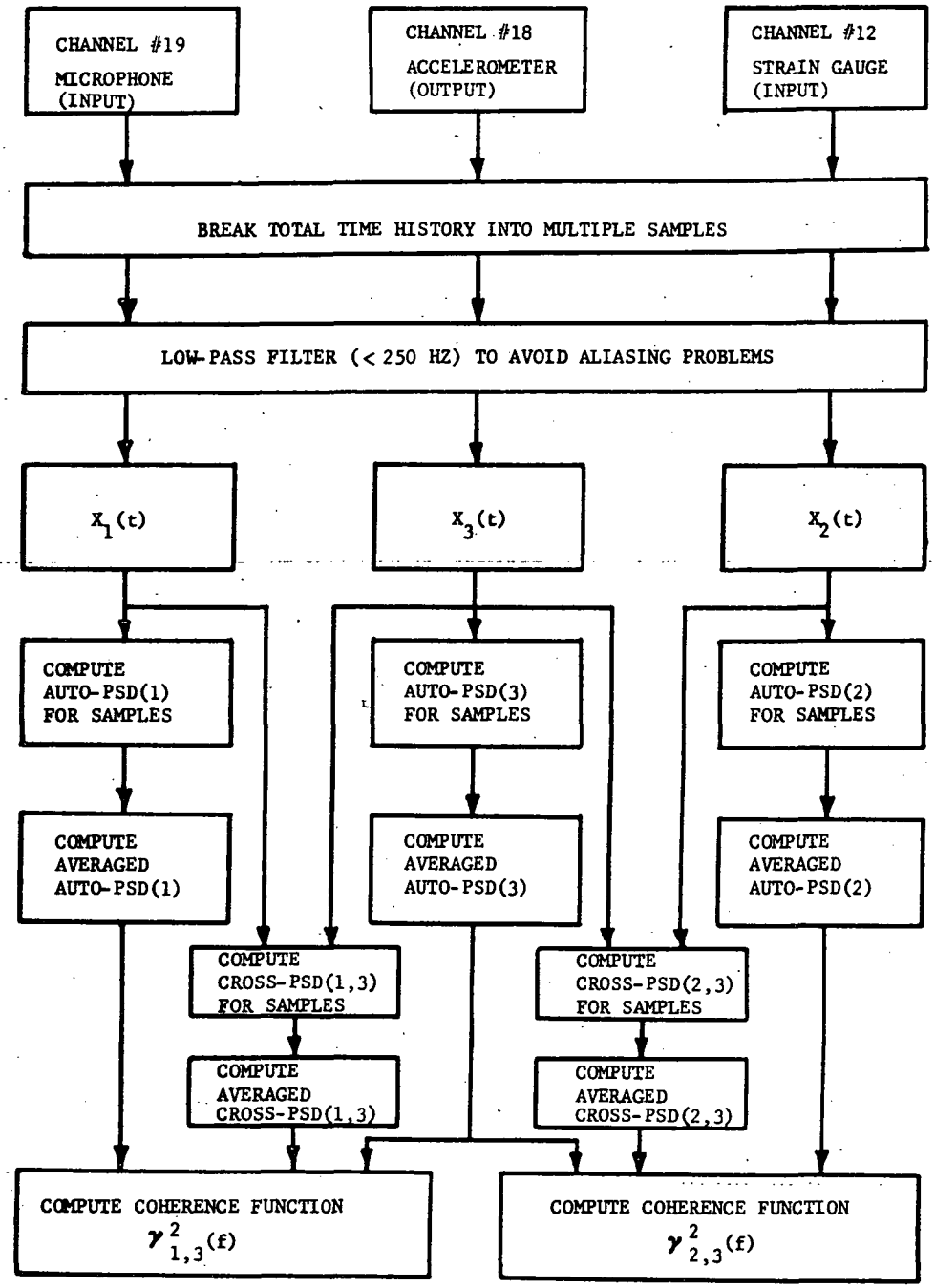

Figure 3-3: Flow Chart for Calculating Coherence Function

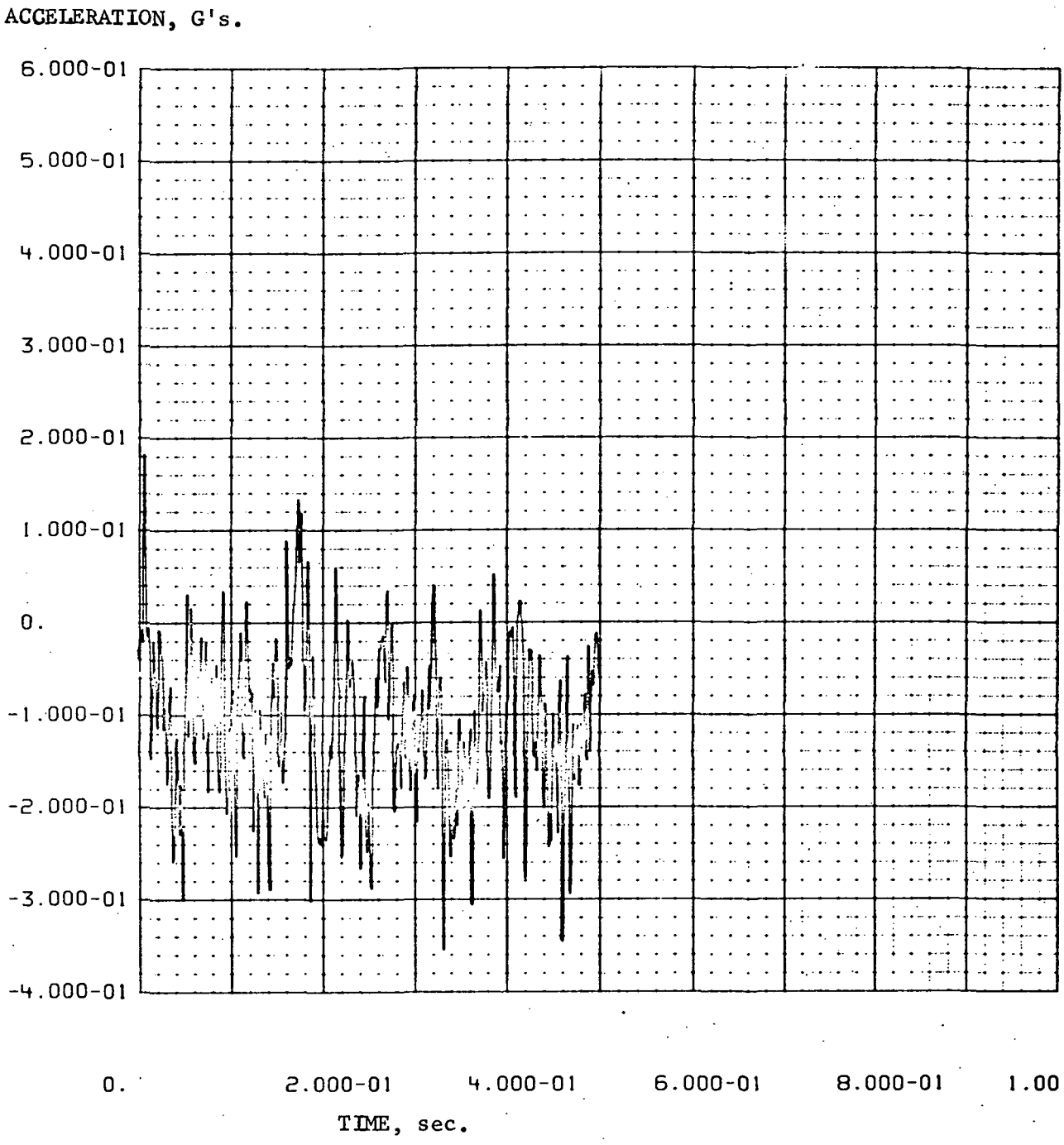

Figure 3-4: Filtered Time History for Accelerometer

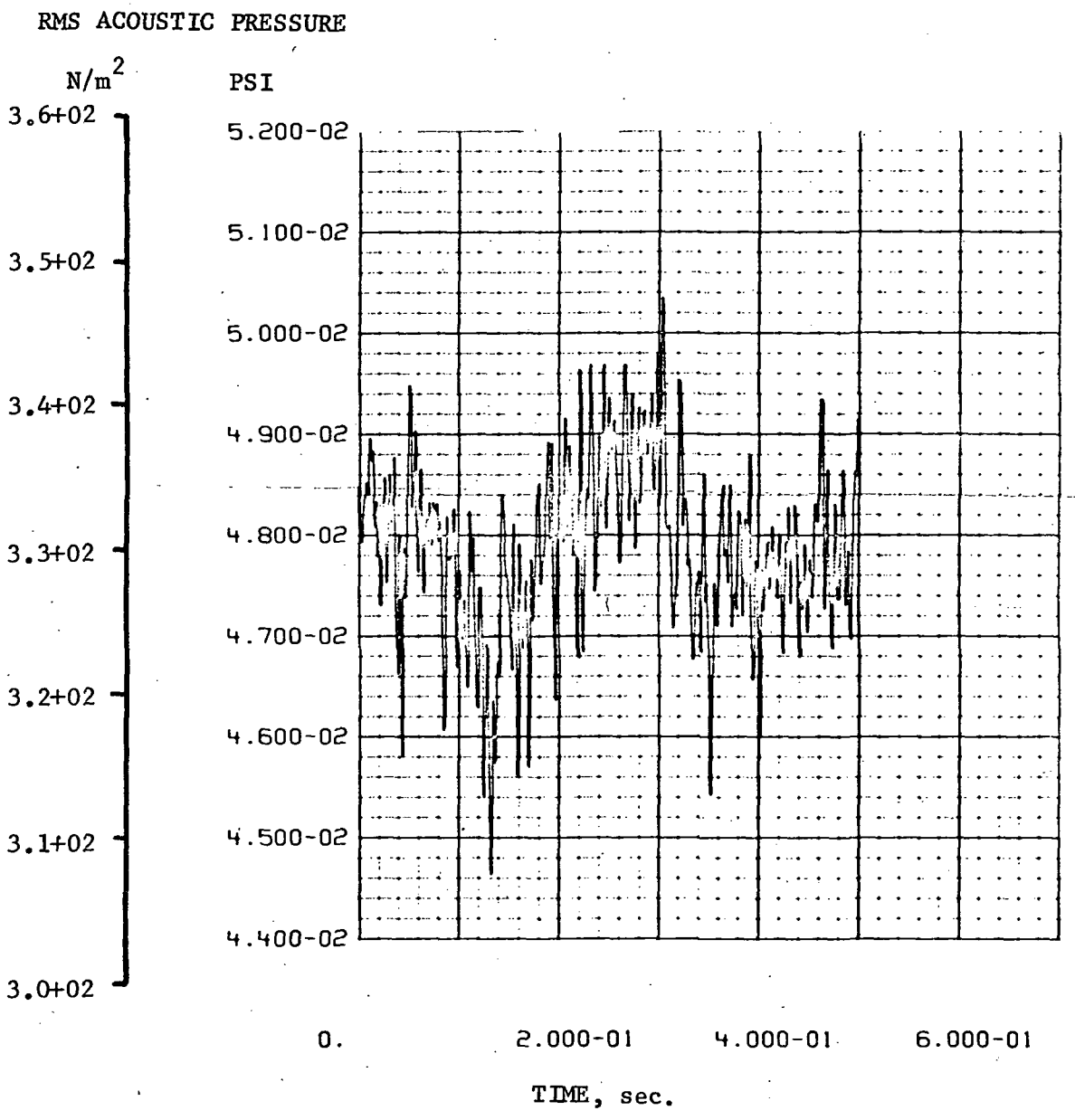

Figure 3-5: Filtered Time History for Microphone

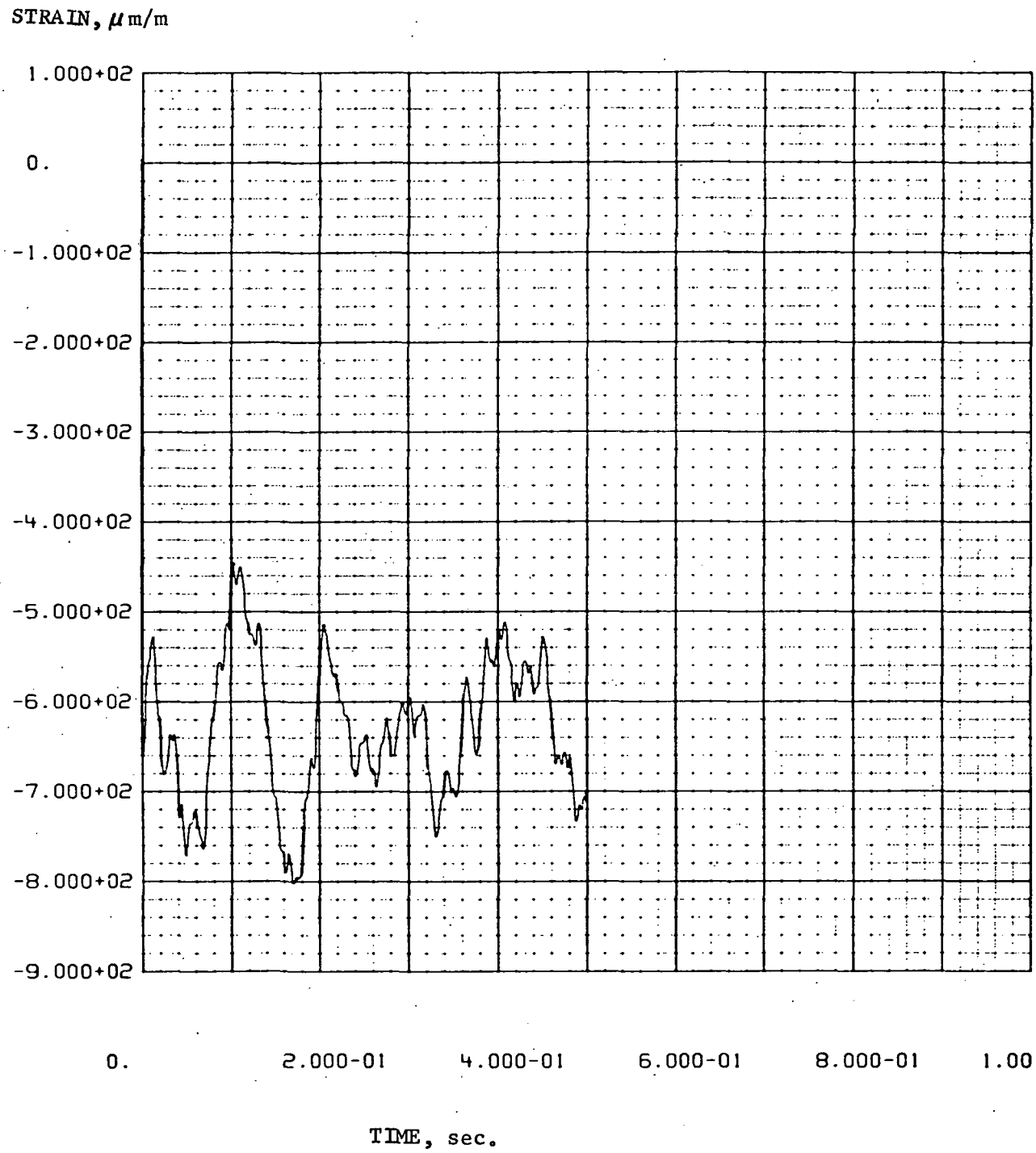

Figure 3-6: Filtered Time History for Strain Gauge

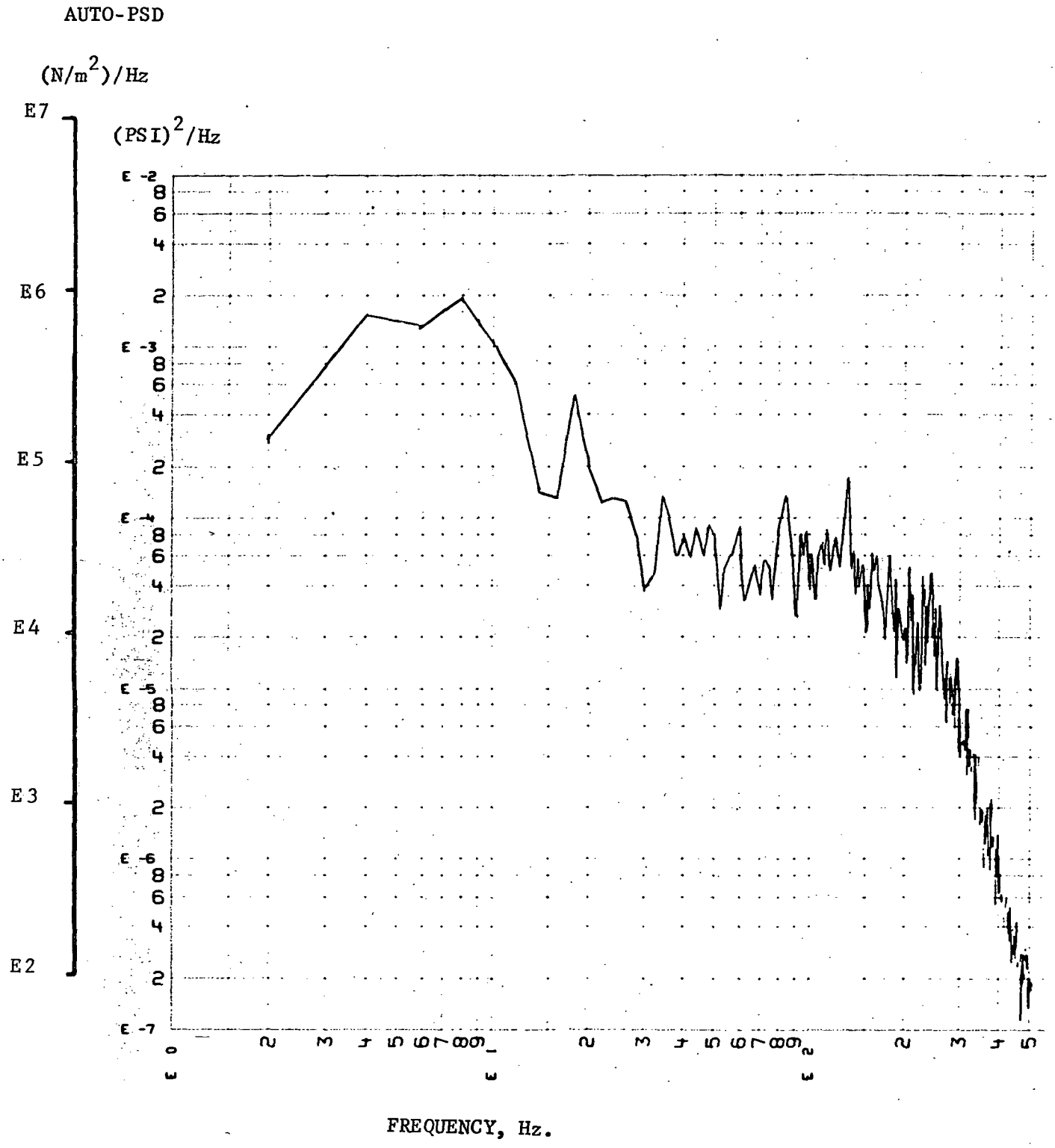

Figure 3-7: Averaged Auto-PSD for Microphone

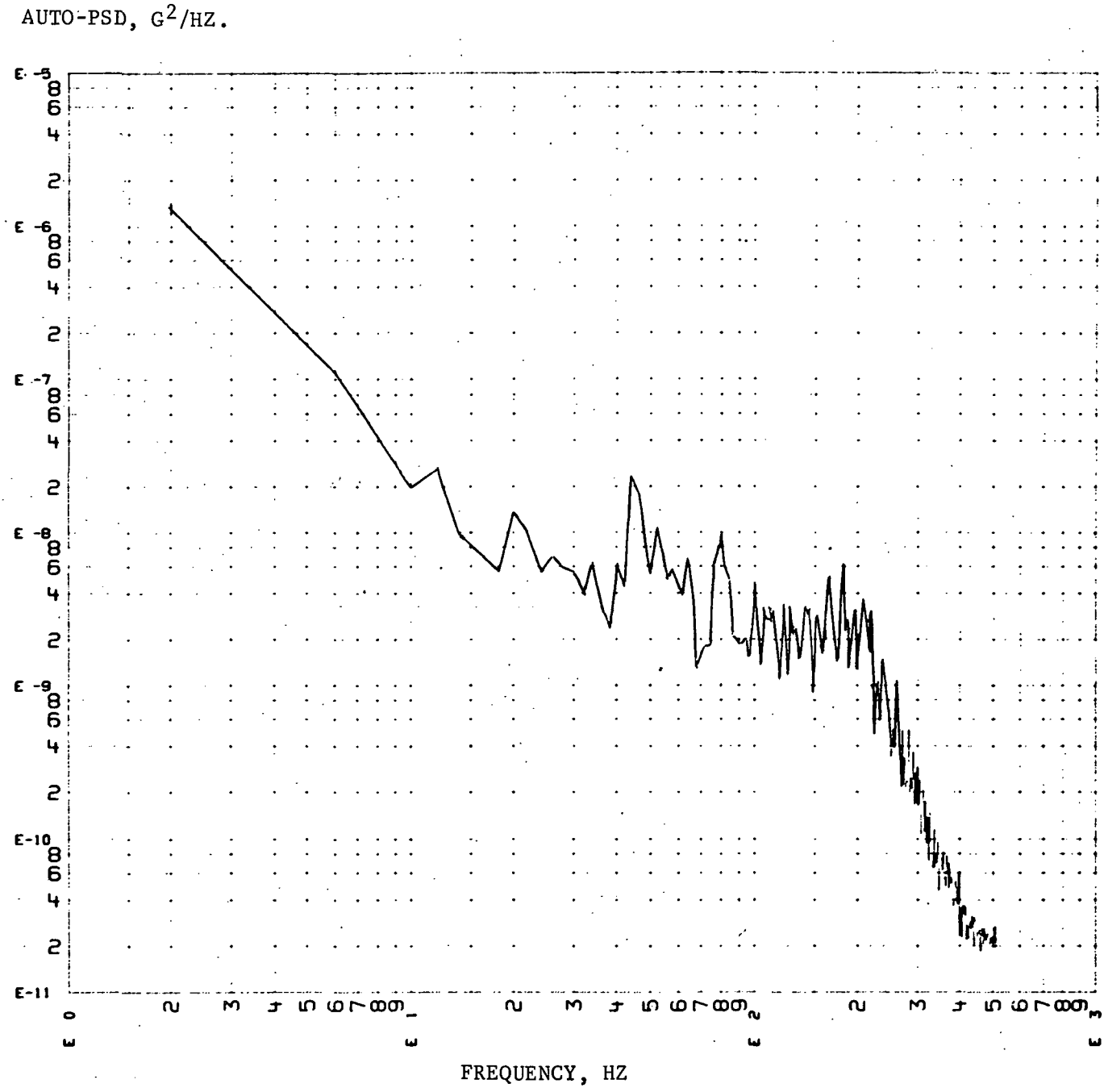

Figure 3-8: Averaged auto-PSD for accelerometer

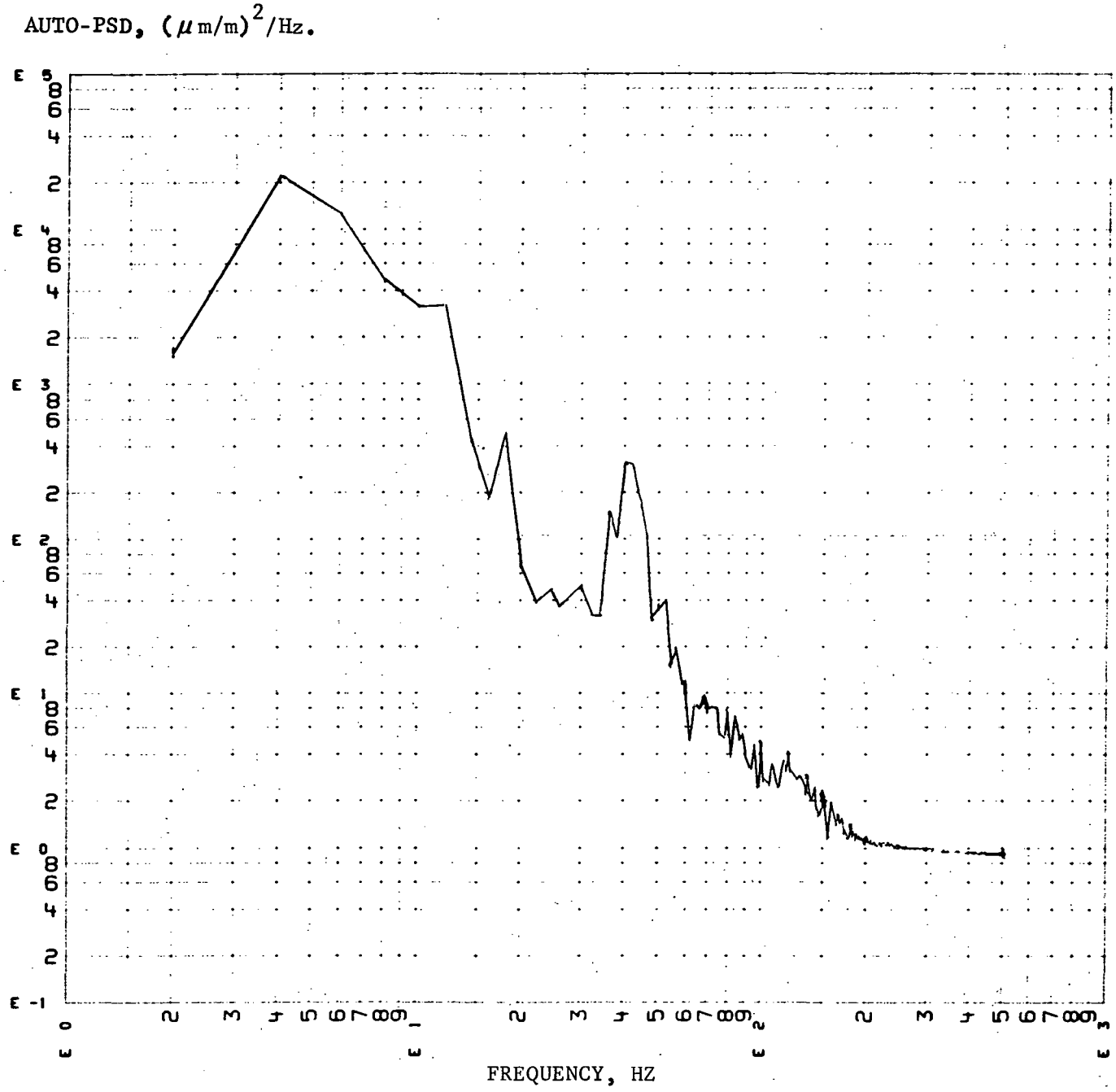

Figure 3-9: Averaged auto-PSD for strain gauge

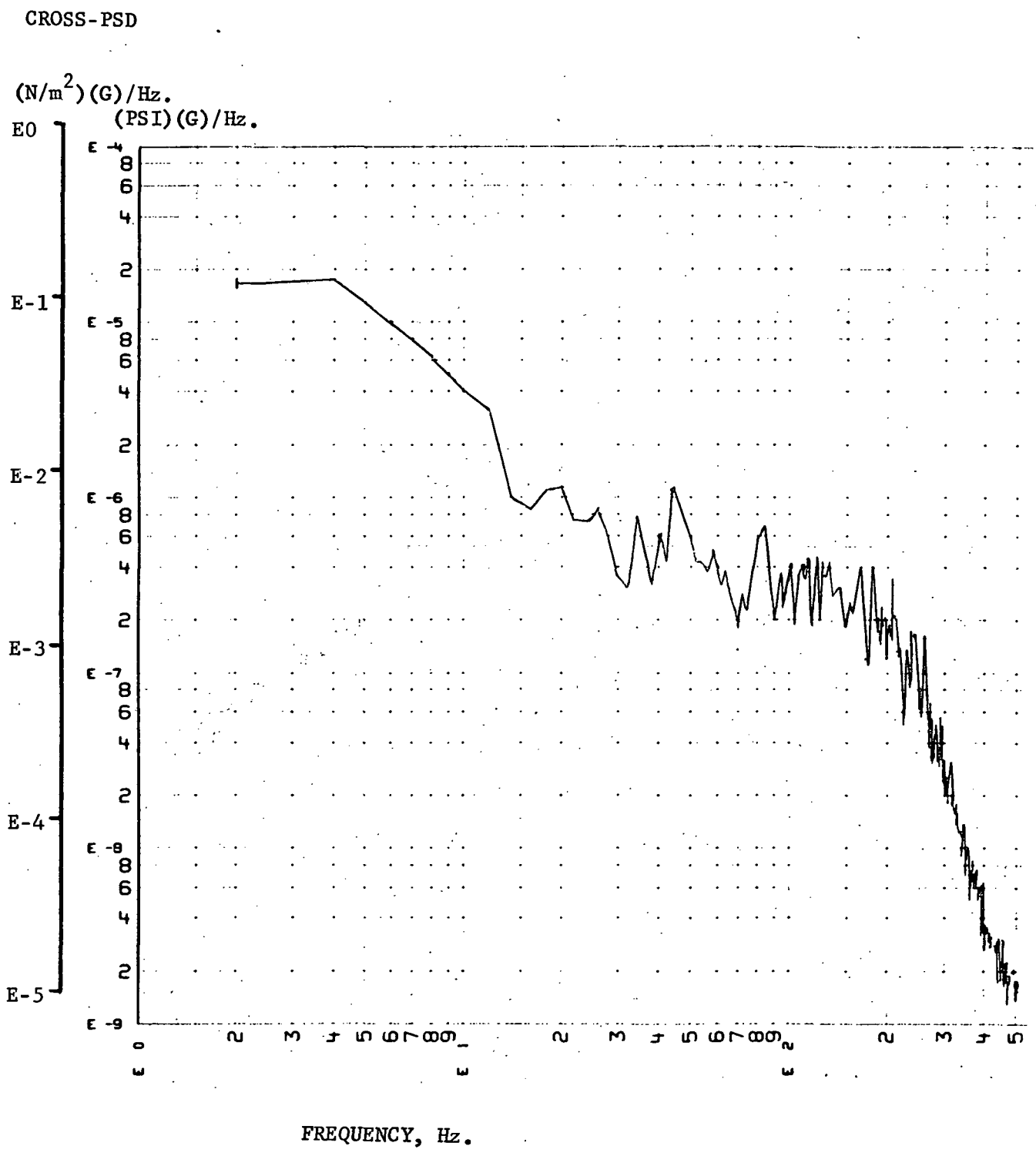

Figure 3-10: Averaged Cross-PSD, Microphone with Accelerometer

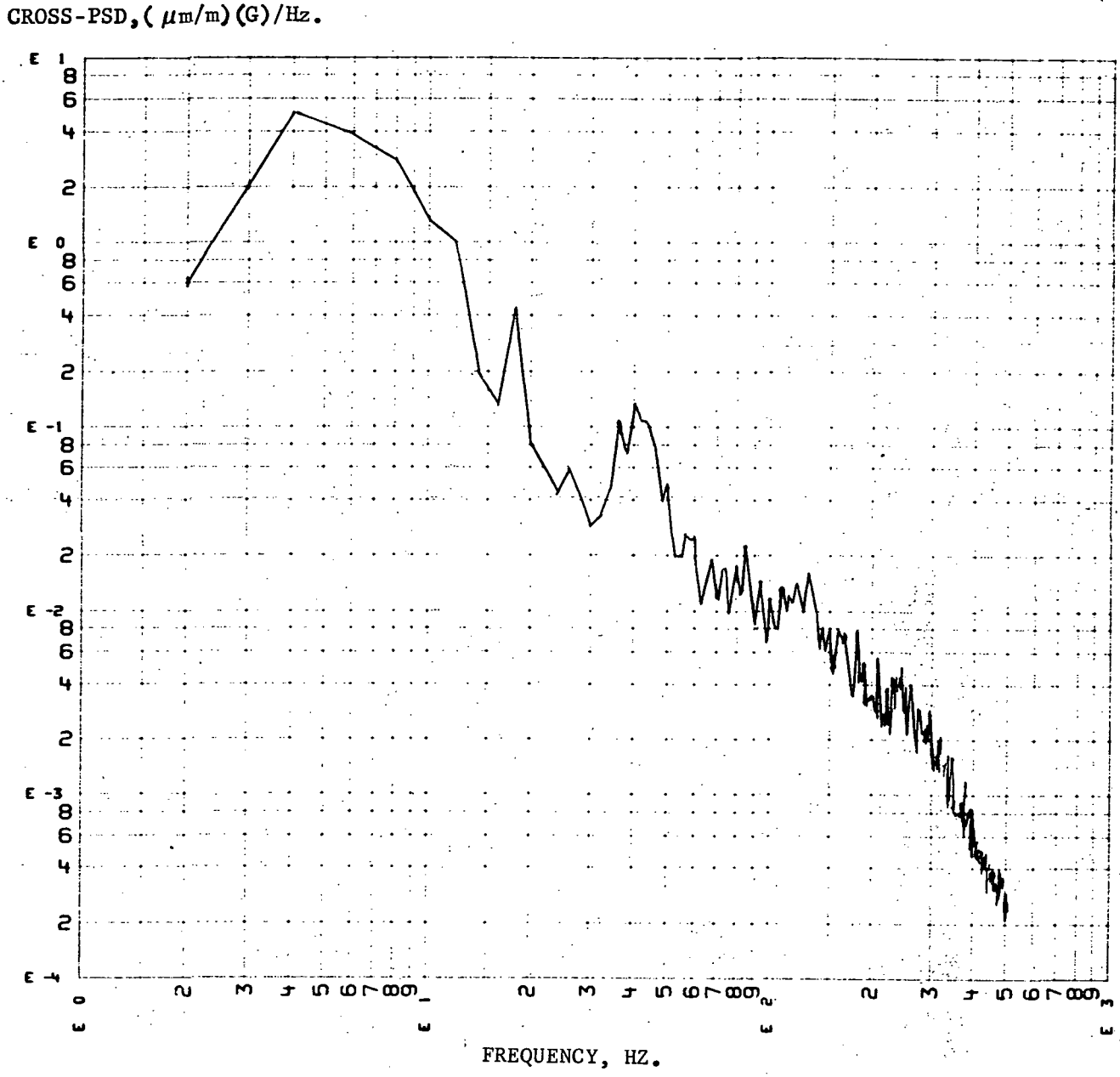

Figure 3-11: Averaged cross-PSD, strain gauge with accelerometer

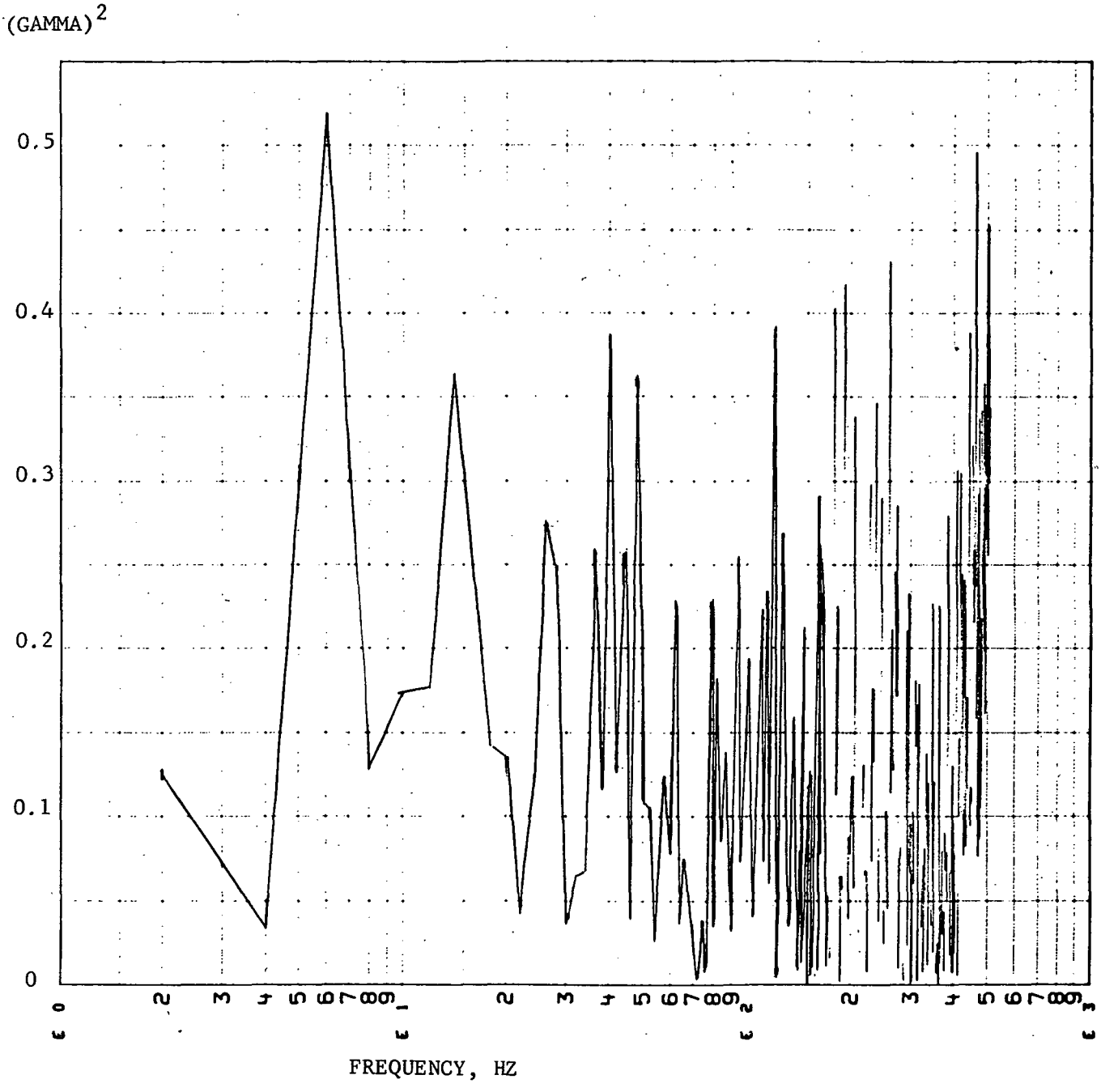

Figure 3-12: Coherence Function, Microphone with Accelerometer

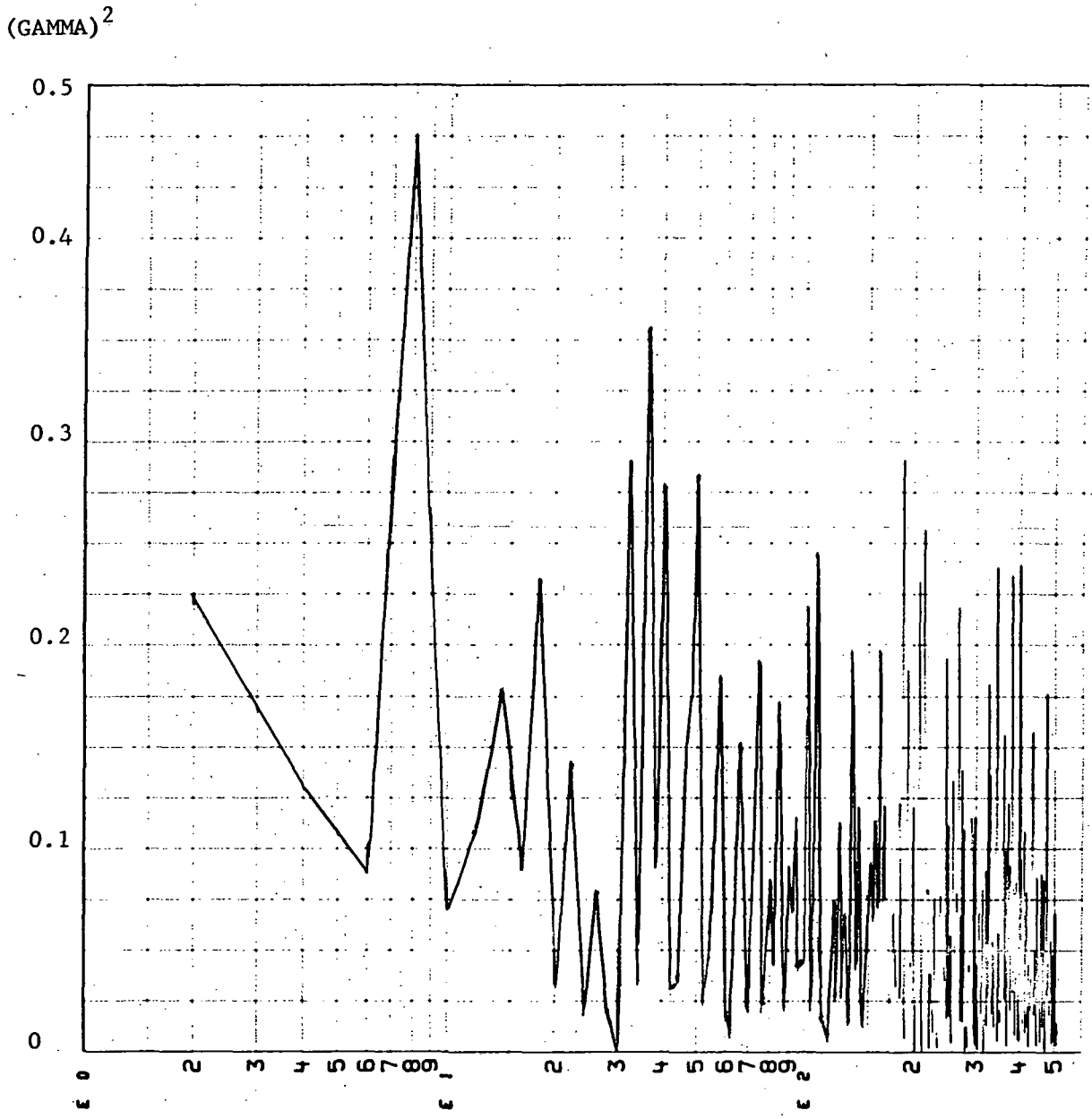

Figure 3-13: Coherence Function, Strain Gauge with Accelerometer

cross-PSD's in Figures 3-10 and 3-11. Finally, the computed coherence functions are presented in Figures 3-12 and 3-13.

It is evident from the time history plots that significant low frequency (< 5 Hz) energy exists in the data. This can be seen more clearly in the auto-PSD and cross-PSD plots. The low frequency content in the microphone signal is unexpected and may be spurious, possibly resulting from motion of the structure at the microphone mounting point. If the strain gauge and the microphone had been monitoring the only two sources of input causing the accelerometer output, the sum of the coherence functions plotted in Figures 3-12 and 3-13 should be close to unity across the frequency range analyzed. This result is not obtained, indicating that the other truss members are contributing significantly to the environment sensed by the accelerometers.

A comparison of Figures 3-12 and 3-13 shows that the coherence function between accelerometer and microphone is higher in magnitude than that for accelerometer and strain gauge for frequencies above 150 Hz or so. This demonstrates that the mid/high frequency environment is more strongly affected by acoustics than by vehicle transients. However, because of the limitations of the available data it is not possible to draw more quantitative conclusions. A more refined analysis would require much more comprehensive instrumentation than was available on the Proof Test Flight.

The approach may be extended to the situation with multiple inputs. These inputs may be correlated, as would be the case with the mechanical interface points on the orbiter.

Consider a set of multiple inputs $x_i(t)$, $i = 1, 2, 3 \ldots q$ with a single output $y(t)$ as shown below:

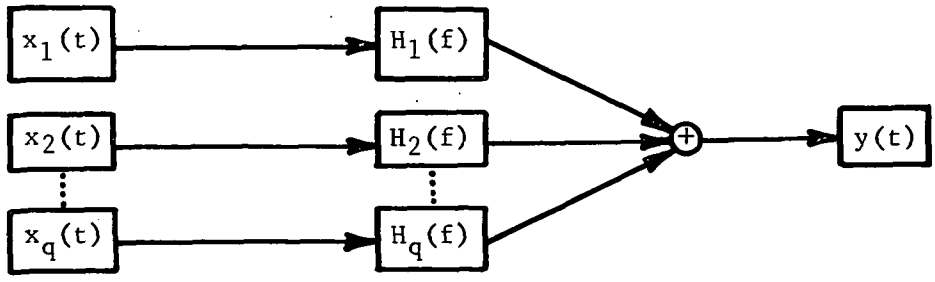

Figure 3-14: Multiple Input/Single Output Model

In the application we are concerned with, one of the inputs (say $x_1(t)$ would be the acoustic excitation adjacent to a point of interest on the shuttle payload, while the remaining inputs ($x_n(t)$, n = 2, 3, . . . q) would be the vibration inputs at the orbiter/payload interface points. The output y(t) would be the response measured at the point of interest on the payload. It is required to determine the relative contribution of each individual input to the output in such a way that the effects of all other inputs are removed. Since the degree of correlation existing between the various inputs is unknown, it is necessary to work in terms of the <u>partial</u> or <u>residual</u> coherence function rather than the ordinary coherence function. The difference is that whereas ordinary coherence function relates the actual input/output signals through their auto- and cross-PSD's, the partial coherence function operates on the "residual" signals, which have been preconditioned to have the effects of correlation between the inputs removed, and uses the residual auto-PSD and residual cross-PSD. The following development is based on material taken from Reference 17.

We first define an augmented spectral matrix

$$G_{yxx} = \left[\begin{array}{c|ccc} G_{yy} & G_{y1} & G_{y2} \cdots G_{yq} \\ G_{1y} & G_{11} & G_{11} \cdots G_{1q} \\ \hline G_{2y} & G_{21} & G_{22} \cdots G_{2q} \\ G_{qy} & G_{q1} & G_{q2} \cdots G_{qq} \end{array}\right]$$

$$= \left[\begin{array}{c|c} A & B \\ \hline B^* & C \end{array}\right]$$

in which the notation G_{ij} is used for brevity to represent $G_{x_i x_j}(f)$, and G_{yi} represents $G_{yx_i}(f)$ etc. (Note that $G_{iy} = G_{yi}^*$, the complex conjugate).

The residual spectral matrix between input x_1 and output y, with the effects of inputs x_2, $x_3 \ldots x_q$ removed (indicated by the subscript 2.....q), is given in terms of the submatrices of G_{yxx}:

$$\tilde{G}_{1y(2.....q)} = \left[A\right] - \left[B\right]\left[C\right]^{-1}\left[B^*\right]$$

$$= \begin{bmatrix} G_{yy(2.....q)} & G_{y1(2.....q)} \\ G_{1y(2.....q)} & G_{11(2.....q)} \end{bmatrix}$$

The partial coherence function between x_1 and y is then given in terms of the elements of this matrix:

$$\gamma^2_{1y(2.....q)} = \frac{\left|G_{1y(2.....q)}\right|^2}{G_{yy(2.....q)}\ G_{11(2.....q)}}$$

Corresponding expressions relating x_2, x_3 ... x_q and y can be written simply by interchanging indices.

Care must be taken to ensure that the PSD's used are of proper statistical variability; this means that the total length of the data samples used must be large enough to contain an adequate number of degrees of freedom, n. This quantity is defined by Enochson and Otnes (Reference 18) as twice the number of observations that appear within the analysis bandwidth for that data, i.e. ;

n = 2 x Bandwidth (Hz) x Sample Length (sec)

= $2 B_e T$ in the usual notation.

If n is too small, a value of $\gamma^2 = 1$ is obtained across the frequency band. The minimum usable value for n depends on the confidence limits established for the analysis; n = 10 appears to be a working minimum, but this needs further investigation for the shuttle payloads application.

3.2.2.2 Error Analysis

During the development of the system-level sine test for Viking, it was recognized that a number of sources of error existed and it was necessary to attempt to evaluate the degree of uncertainty and establish a margin to cover it. This evaluation process, which is described in detail in Reference 19,

was performed by a team of analysts representing NASA/LRC, JPL and MMC. The approach used was to consider separately the uncertainties associated with analytical data (damping, boundary conditions, modeling accuracy, etc.) and with flight data (spatial variations, flight to flight variations, instrumentation tolerances, etc.). Margins were assigned to each potential source of error and the overall uncertainty obtained by calculating the RSS of the individual random, independent uncertainties. The resulting factor was applied as a margin on the initially predicted flight environment to derive a final "working-level" prediction.

This approach is very subjective, since each individual uncertainty was assigned a value which seemed to the team to be reasonable. More objective methods are available, however, and should be used on the shuttle program to estimate the potential errors and thereby give a rational basis for establishing design and test margins. In order to do this properly, consideration must be given to error analysis during the early planning stages of the instrumentation/data analysis program.

Errors may be reduced by proper averaging techniques, and by running equivalence tests on data before adding it to a data bank. In short, the subject of error analysis is complex but very important, since it can be used to increase the efficiency of an instrumentation system and to establish confidence levels on the resulting data, which in turn affect the selection of test and design margins.

It is believed that these types of errors are largely ignored by industry in the statistical treatment of flight measurements used in deriving test criteria, although they may well be accounted for indirectly by the application of test factors. For example, in deriving a random vibration qualification test requirement for a lift-off event, the usual practice is to produce a composite plot of measured power spectral densities and either envelope the data or perform statistical analyses to establish the criteria on a specified confidence level without regard for the analysis bandwidths and record lengths used. If, for example, a set of lift-off flight measurements were analyzed with a 5 Hz bandwidth for 2.0 seconds record length, the normalized standard error would be

$$\epsilon = \frac{1}{\sqrt{BT}} = \frac{1}{\sqrt{5 \times 2}} = 0.316$$

which is significantly large. Thus, if the sample time is short (which may be necessary to ensure that the data is"piecewise stationary") the filter bandwidth must be increased to

minimize the error. However, better resolution is obtained with a narrow filter. These conflicting requirements must be addressed if meaningful test and design factors are to be derived from the data. Some aspects of this problem are treated in Reference 20.

Individual sources of error will now be considered.

The errors associated with the collection, analysis and interpretation of random data stem from three main sources:

a) Statistical error,

b) Instrument error, and

c) Usage error.

Statistical error is the uncertainty in an estimated quantity due to limitations in the quality and quantity of data gathered, the underlying probabilistic nature of the data and the methods used to derive the desired estimate. Instrument error is introduced by inaccuracies in calibration of the system, tolerances on the individual components, noise (both internal and from extraneous sources) and drift in the instrumentation. These errors may be present in both measuring and analysis systems. Usage error, also called personnel error, includes all forms of error which can be caused by imperfect performance on the part of the people involved in the operation. Since instrument error and usage error are obviously dependent in their magnitude on the particular instruments and personnel employed in the data collection/analysis process they are difficult to quantify on a general level, so that emphasis in this discussion will be placed on statistical error.

Consider a sample time history $x_1(t)$, measured over a finite interval T. Let ϕ be the true value of some parameter of the random process of which $x_1(t)$ is a sample, and let $\tilde{\phi}_1$ be the estimated value of ϕ, calculated from $x_1(t)$. A second sample time history $x_2(t)$ would yield a different estimate $\tilde{\phi}_2$ of the parameter ϕ, and so on. The problem is to determine how closely a particular estimate $\tilde{\phi}_i$ will represent the true value. The error involved in the estimate consists of two parts, called the bias (or systematic) error and the variance (or variability) error. In general terms, the bias error arises from using a non-infinitesmal analysis bandwidth and the variance error from using a finite record length.

The expected value (expectation) of the set of estimates $\tilde{\phi}$ should ideally equal the true value, so that $E[\tilde{\phi}] = \phi$; if this is true the estimate is said to be <u>unbiased</u>. In general this is not true and a bias error may be defined:

$$b\left[\tilde{\phi}\right] = E\left[\tilde{\phi}\right] - \phi$$

$$= E\left[\tilde{\phi}\right] - E\left[\phi\right] \quad \text{(since } \phi \text{ is a constant)}$$

$$= E\left[\tilde{\phi} - \phi\right]$$

The variance of the estimate is derived from the relationship

$$V\left[\tilde{\phi}\right] = E\left[\left(\tilde{\phi} - E\left[\tilde{\phi}\right]\right)^2 \right]$$

The two parts are combined by calculating the mean square error, MSE. In terms of expectation this is given by

$$MSE = E\left[\left(\tilde{\phi} - \phi\right)^2 \right]$$

By substituting in terms of the expressions for $b\left[\tilde{\phi}\right]$ and $V\left[\tilde{\phi}\right]$ it can be shown that

$$E\left[\left(\tilde{\phi} - \phi\right)^2 \right] = V\left[\tilde{\phi}\right] + b^2\left[\phi\right]$$

i.e., mean square error = variance + (bias)^2

When the mean square error is divided by the square of the true value of the parameter we obtain the normalized mean square error, ϵ^2:

$$\epsilon^2 = \frac{MSE}{\phi^2}$$

The square root of this quantity, ϵ, is the normalized standard error of the estimate.

Reference 17 derives the normalized standard error for a number of common statistical parameters for bandwidth limited white noise. These are summarized in the following table:

Parameter Estimated	Normalized Standard Error, ϵ
Mean value	$\frac{\sigma_x}{\mu_x} \sqrt{\frac{1}{2BT}}$
Mean square value ($\mu_x = 0$)	$\sqrt{\frac{1}{BT}}$
Power spectral density	$\sqrt{\frac{1}{BT}}$
Autocorrelation function ($\mu_x = 0$)	$\left\{ \frac{1}{2BT} \left[1 + \frac{R_x(0)}{R_x(\tau)} \right] \right\}^{1/2}$

These relationships can be used to find the value of the product BT (analysis bandwidth in Hz multipled by record length in seconds) after an acceptable error has been selected. The minimum sample record length can then be calculated, since the bandwidth requirement is established by the analysis technique being used and frequency resolution criteria. In this context B is defined as the bandwidth of a hypothetical rectangular filter for a white noise input. (Other definitions of bandwidth are discussed in Reference 17).

Other potential sources of error during the data analysis process are aliasing error, which can be introduced during analog-to-digital conversion if the sampling rate is too low, and quantization error which occurs during the actual conversion of observed values to numerical form and depends on the coarseness of the numerical scale being used.

The expression "aliasing" denotes a distortion of the signal, after analysis, due to improper sampling. Suppose the time history containing components at frequency f_1 Hz is sampled at a rate f_s samples/sec. The digitized signal will contain, among others, components at the following frequencies:

$$f_1,\ f_s \pm f_1,\ 2f_s \pm f_1,\ 3f_s \pm f_1,\ \ldots\ \text{etc.}$$

When $f_s - f_1$ falls within the frequency range of the analysis, aliasing occurs. To avoid this it is necessary to use a sampling rate higher by some factor than the highest frequency of concern. In theory, a factor of two is adequate but in practice this does not eliminate aliasing completely and a higher factor is desirable. Since too high a sample frequency would cause data storage problems, a compromise must be made, and a factor of three to five is regarded as a good working range.

Quantization errors occur when an analog signal is being converted to digital form. At each value a choice between two consecutive values must be made, so that, in effect, a "round-off" decision is necessary. If a very fine scale is used the error will be correspondingly small, but some error will always be present.

In Reference 17 it is shown that, if it is assumed that the quantization errors follow a uniform probability distribution over one scale unit then the errors will have a mean value of zero and a standard deviation of $\sqrt{1/12} \simeq 0.289$ units. This is the RMS value of the quantization error, which may be regarded as noise. Thus, if the full range of the signal is quantized at 1024 scale unit the RMS noise-to-signal ratio would be $0.289/1024 = 2.8 \times 10^{-4}$. Providing the full range is 256 units or more the RMS error will not exceed 0.1 percent, and should be negligible.

Finally, errors can occur which are philosophical rather than numerical, during the process of hypothesis testing to examine the statistical properties (stationarity, normality, etc.) of the data. If a hypothesis is rejected when in fact it is true, a Type I error has been incurred. Alternatively, a hypothesis might be accepted when in fact it is false; this is called a Type II error. The effect of these kinds of errors depends on the specific case being tested. Serious consequences could possibly result, for example, by incorrectly concluding that a sample time history was stationary and basing subsequent analysis on this wrong conclusion.

3.2.2.3 Low Frequency Environment Prediction Techniques

Defining the low frequency environment and loads for any given payload based on inflight measurements from previous payloads presents a unique problem. The frequency content and magnitude of the environment depends directly on the dynamic characteristics of the combined payload/launch vehicle structure. Since the structural interface loads for any payload are dependent on its dynamic characteristics and the frequency at which the interface loads are applied, flight measured loads from a previous dissimilar payload cannot be used directly to force another payload.

An example of the currently practiced techniques to minimize this problem can be seen in the analytical treatment of Titan payloads. For each Titan payload a new math model of the coupled payload/launch vehicle is generated. This coupled model is then forced by the engine time histories for the major boost events of previous Titan launches. In order to minimize the errors in calculating the payload responses due to differences in payloads and engine transients from one flight to another, a wide range of launches must be considered.

The engine time histories have been recorded from the transient events from a number of Titan launches. These N time histories are then used to force the all-up coupled models of each individual payload/booster combination for N sets of responses. (The techniques utilized are described in more detail in Appendix B). To obtain a high level of confidence for the payload survivability, the N sets of response are then treated statistically to obtain a "mean plus three sigma value" for such calculations as primary structure loads. This technique was used on the Viking project for a Titan/Centaur/payload configuration. Statistical treatment of responses was utilized for determining the Viking payload loads and the Centaur internal loads. For liftoff, 21 cases were generated; and for Stage I burnout, 20 cases for "oxidizer depletion", and 27 cases for "oxidizer plus fuel depletion" were generated. One of the reasons for the

confidence in this technique is the small change in the dynamic characteristics of the external forcing function (engine transients) when one payload is exchanged for another.

However, this method is costly. For instance, if 20 internal loads were desired for a given payload and 30 different transient forcing functions were available for a given event, then the 20 responses would have to be calculated 30 times. These 30 sets of responses could then be handled statistically. In addition, for each payload a new coupled payload/launch vehicle model must be generated.

There are a number of potential solutions to this problem. One approach is to analytically remove the dynamic effects of the previous payload from the interface loads in order to normalize the flight data for the remaining shuttle payloads. There are a number of possibilities as to the actual technique that could be used.

An attractive approach for evaluating the dynamic response behavior of a wide range of payloads that are candidate sub-elements of a baseline shuttle launch vehicle system is to utilize the interface response of the system without a payload in conjunction with the modal properties of a subject payload to establish the desired vehicle/payload coupled response. Such a "base motion" type of analysis was successfully utilized on the complex Skylab configuration in an "open loop" sense in that no dynamical feedback was permitted between the new payload and basic vehicle. The present approach will account for all dynamic interaction between launch vehicle and payload. The salient features of this approach lie in the fact that the basic booster responses need only be evaluated once for a given event. It is anticipated that the proposed methodology will work very nicely when used in conjunction with modal coupling methods. An overview of the methodology is identified in the following paragraphs.

With reference to Figure 3-15 and for purposes of discussion, let us consider a basic launch vehicle, V, (e.g., the shuttle launch vehicle without payload) and a typical payload, P, (e. g., a typical payload within the orbital cargo bay). The support system, V, has interface accelerations $\ddot{x}_{IF}$ due to the imposed force/torque vector, F, as a function of time. It is desired to evaluate the payload response behavior due to the external environment, F(t) .

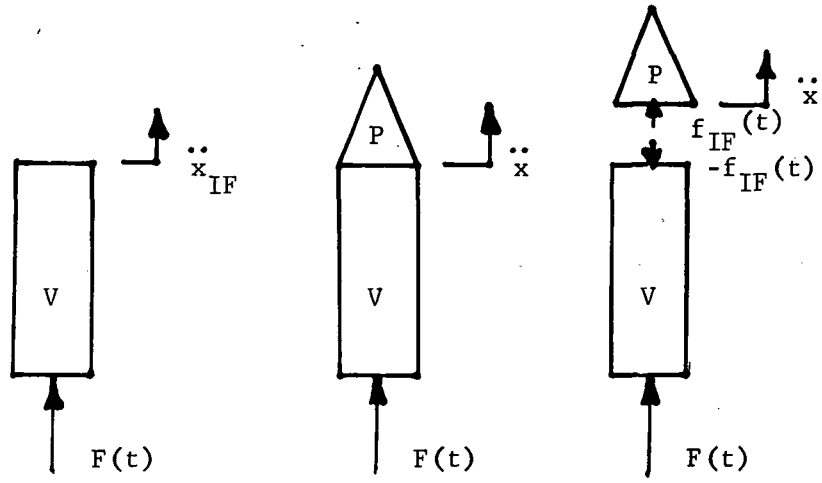

Figure 3-15: Launch Vehicle/Payload Interaction

The assumed available information consists of the following:

1. Response of the interfaces, $\ddot{x}_{IF}$ due to $F(t)$;
2. Launch vehicle mass matrix, $[M_v]$;
3. Support system modal properties, $[\phi_v]$ and $\{\omega_v^2\}$;
4. Payload mass matrix, $[M_p]$;
5. Payload modal properties (constrained at attached points) $[\phi_p]$ and $\{\omega^2{}_p\}$
6. Branch stiffness reduction transformation to interface attach points, $[\beta]$, and/or branch interface inertially relieved loads transformation, $[\sigma]$.

The following block diagram depicts the physical phenomenon under consideration.

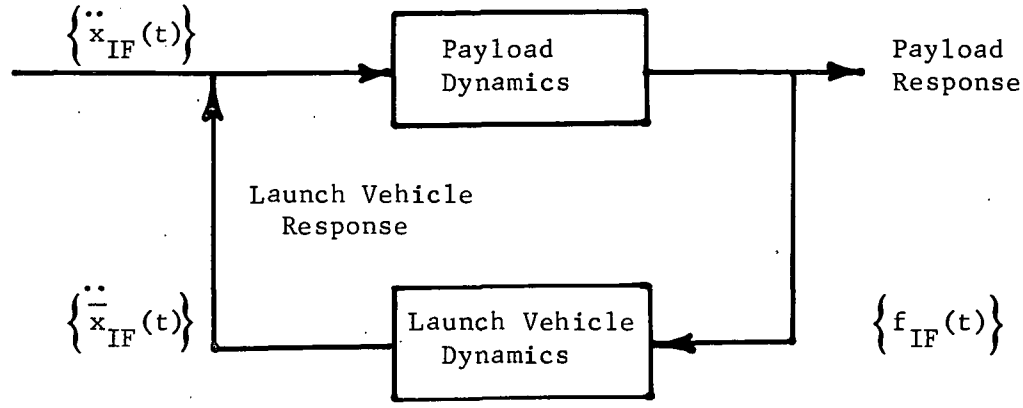

where

$\{\ddot{x}_{IF}(t)\}$ = Interface accelerations as a function of time due to the external forces F(t)

$\{\ddot{\bar{x}}_{IF}(t)\}$ = Interface accelerations as a function of time due to the interface forces

$\{f_{IF}(t)\}$ = Interface forces as a function of time

It is the proper description of the closed loop coupling that permits the total system coupled responses to be evaluated, whereby the dynamical coupling between support system and branch is accommodated.

With reference to the block diagram, it is noted that via superposition, the net interface response $\{\ddot{x}(t)\}$ is given by

$$\{\ddot{x}(t)\} = \{\ddot{x}_{IF}(t)\} + \{\ddot{\bar{x}}_{IF}(t)\} \quad (1)$$

It is assumed that all the following equations are functions of time and the (t) will be omitted. Now, the interface responses, $\ddot{\bar{x}}_{2F}$ due to the interface loads, can be solved for by the differential equation in the modal domain

$$\{\ddot{\xi}_v\} + [2\,\zeta\,\omega_v]\{\dot{\xi}_v\} + [\omega_v^2]\{\xi_v\} = [\phi_v]^T\{f_{IF}\} \quad (2)$$

where

$\{\ddot{\xi}_v\}$, $\{\dot{\xi}_v\}$ & $\{\xi_v\}$ = motions in the modal domain for the vehicle

The payload modal response due to $\left\{\ddot{x}\right\}$ can be computed from

$$\left\{\ddot{\xi}_p\right\} + \left[2\zeta\omega_p\right]\left\{\dot{\xi}_p\right\} + \left[\omega^2_p\right]\left\{\xi_p\right\} = \left[\phi_p\right]^T\left(-\left[M_p\right]\left[\beta\right]\left\{\ddot{x}\right\}\right) \tag{3}$$

where

$\left\{\xi_p\right\}$, $\left\{\xi_p\right\}$ & $\left\{\xi_p\right\}$ = modal responses of payload

$\left[\beta\right]$ = transformation of internal motions to payload interface. (Reduces to rigid body transformation if the interface is statically determinate).

The interface forces as computed from the payload side are simply

$$\left\{f_{IF}\right\} = -\left[\sigma\right]\left[M_p\right]\left\{\ddot{q}_p\right\} \tag{4}$$

where

$\left\{\ddot{q}_p\right\}$ = absolute response of the payload

Also,

$$\left\{\ddot{q}_p\right\} = \left[\beta\right]\left\{\ddot{x}\right\} + \left\{\ddot{\bar{q}}_p\right\} \tag{5}$$

where

$\left\{\ddot{\bar{q}}_p\right\}$ = relative response of payload to the interface (constrained)

Combining (1), (4) and (5) results in the following expression for the interface loads

$$\left\{f_{IF}\right\} = -\left[\sigma\right]\left[M_p\right] \cdot \left[\left[\beta\right]\left(\left\{\ddot{x}_{IF}\right\} + \left[\phi_v\right]\left\{\ddot{\xi}_v\right\}\right) + \left[\phi_p\right]\left\{\ddot{\xi}_p\right\}\right] \tag{6}$$

Finally, after some manipulation and substitution, the coupled response of the total system can be concisely stated in matrix form as

$$\left[\begin{array}{c|c} [I] & [\phi_p]^T [M_p] [\beta] [\phi_v] \\ \hline [\phi_v]^T [\sigma] [M_p] [\phi_p] & [I] + [\phi_v]^T [\sigma] [M_p] [\beta] [\phi_v] \end{array}\right] \left\{\begin{array}{c} \ddot{\xi}_p \\ \ddot{\xi}_v \end{array}\right\}$$

$$+ \left[\begin{array}{c|c} 2\zeta_v \omega_p & \\ \hline & 2\zeta_v \omega_v \end{array}\right] \left\{\begin{array}{c} \dot{\xi}_p \\ \dot{\xi}_v \end{array}\right\} + \left[\begin{array}{c|c} \omega_p^2 & \\ \hline & \omega_v^2 \end{array}\right] \left\{\begin{array}{c} \xi_p \\ \xi_v \end{array}\right\}$$

$$= \left[\begin{array}{c} -[\phi_p]^T [M_p] [\beta] \\ \hline -[\phi_v]^T [\sigma] [M_p] [\beta] \end{array}\right] \left\{\ddot{x}_{IF}\right\} \qquad (7)$$

The coupling in the generalized modal mass matrix in (7) is further recognized as being of the modal inertial coupling form. In fact, an eigensolution with this modal mass matrix and the diagonal modal stiffness matrix will yield the total system modal frequencies and modal mode shapes. It should be pointed out that (7) does not calculate the total response of the vehicle; only the response to the interface forces. When the support system response contains a branch member, the previous methodology can be implemented in "reverse" fashion to remove contribution of the branch from the system response such that the support system interface response resulting only from f(t) can be identified and the desired branch attached.

Different approaches which account for the impedance characteristics of the launch vehicle and payload could be utilized. One technique, Reference 21, utilizes the shock spectra of the interface accelerations of the payload/booster interface. An envelope of the shock spectra from the previous flights is generated to be used in calculating the payload responses for the following flight. Furthermore, the analysis is adjusted by a "Reduction Factor" to account for the tuning of payload and launch vehicle modes and the relative impedance between the two. This technique makes the following assumptions:

1. Adequate linear models for the payload and launch vehicle are available;

2. Shock spectra of the interface accelerations from the previous flights are available;

3. Shock spectra of the interface accelerations from an "unloaded" interface are available. If not, it is assumed that the shock spectra of the "loaded" flights envelope it;

4. The frequency distribution of the exciting force is flat compared to the interface response.

The advantage of this technique is its relatively low cost in analysis because of its small scope. It also has the advantage of being somewhat conservative in that it takes worst case by tuning the payload and launch vehicle modes and yet accounts for the frequency content of the spectra.

There are other impedance techniques that as of yet are untried. One of these is derived below. Referring to Figure 3-16 below, the accelerations for a combined launch vehicle and payload, P_1, can be written in the following fashion:

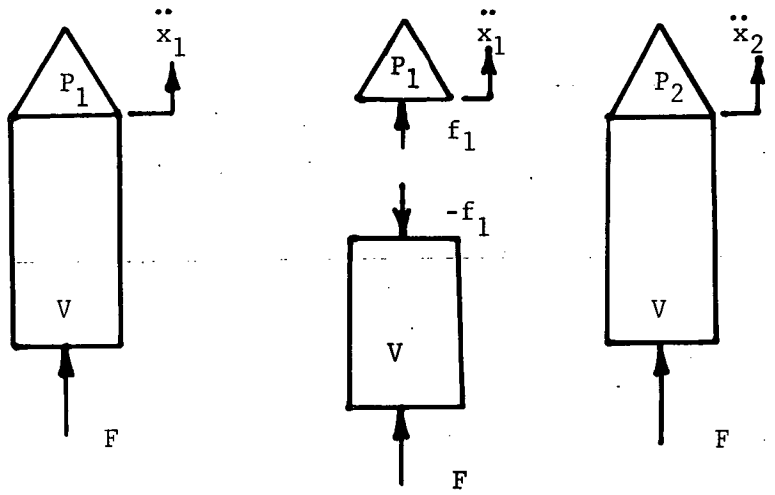

V = vehicle

P_1 = payload 1

P_2 = payload 2

Figure 3-16: Free Body Diagrams

$$\left[Z(\Omega)\right]_{VP_1} \quad \left\{\ddot{x}_1\ (\Omega)\right\} = \left\{F\ (\Omega)\right\} \tag{8}$$

where

$\left[Z\ (\Omega)\right]_{VP_1}$ = Impedance from external loads to payload interface,

$\left\{\ddot{x}_1\ (\Omega)\right\}$ = Interface accelerations for P_1 as function of frequency (Ω),

$\{F(\Omega)\}$ = External loads for structure as a function of frequency (Ω).

The equations to follow are written in the frequency domain and the Ω will be omitted. From the free body diagram in Figure 3-16, there also exists this relationship:

$$[Z]_{P_1} \{\ddot{x}_1\} = \{f_1\} \tag{9}$$

where

$[Z]_{P_1}$ = Impedance of payload no. 1 to the interface loads,

$\{f_1\}$ = Interface loads.

Considering the free body diagram of the launch vehicle separately, $\{\ddot{x}_1\}$ can be written as follows:

$$\{\ddot{x}_1\} = [M]_v \{F\} + [M]_{vI} \{-f_1\} \tag{10}$$

where

$[M]_v = [Z]_v^{-1}$ = Mobility of the vehicle alone due to $\{F\}$,

$[M]_{vI}$ = Mobility of the vehicle at the payload interface due to the interface loads.

From (9),

$$\{f_1\} = [Z]_{P_1} \{\ddot{x}_1\} \tag{11}$$

Substituting into (10) yields

$$\{\ddot{x}_1\} = [M]_v \{F\} - [M]_{vI} [Z]_{P_1} \{\ddot{x}_1\} \tag{12}$$

or,

$$\left([M]_{vI} [Z]_{P_1} + [I]\right) \{\ddot{x}_1\} = [M]_v \{F\} \tag{13}$$

where

$[I]$ = "unity" matrix

It can be seen that a similar equation can be written for the combined structure of the launch vehicle and payload no. 2.

$$\left(\left[M \right]_{vI} \left[Z \right]_{P_2} + \left[I \right] \right) \left\{ \ddot{x}_2 \right\} = \left[M \right]_v \left\{ F \right\} \qquad (14)$$

where

$\left[Z \right]_{P_2}$ = Impedance of payload no. 2 to the interface loads,

$\left\{ \ddot{x}_2 \right\}$ = Interface accelerations for payload no. 2.

Now, if the assumption is made that the dynamic characteristics of the launch vehicle and the external forcing function do not change, the right sides of equations (13) and (14) are equal. Then (13) and (14) can be combined.

$$\left\{ \ddot{x}_2 \right\} = \left(\left[M \right]_{vI} \left[Z \right]_{P_2} + \left[I \right] \right)^{-1} \left(\left[M \right]_{vI} \left[Z \right]_{P_1} + \left[I \right] \right) \left\{ \ddot{x}_1 \right\} \qquad (15)$$

By knowing the impedance characteristics of the payloads and the launch vehicle, the inflight measured environment from one flight, $\left\{ \ddot{x}_1 \right\}$, can be normalized with equation (15) to obtain the predicted environments for the subsequent payloads.

However, there are some limitations to this technique, as in all techniques discussed, due to variations in the forcing functions from flight to flight. It is for this reason that the maximum possible amount of environmental and system structural characteristics information be obtained on the initial shuttle flights and used to form a data bank for the low frequency regime. It is obvious that detailed information for only the payloads would be insufficient. Time phased data from the shuttle vehicle itself will also be vital. This is evident in the analytical techniques discussed above. Each relies to varying degrees on the structural characteristics of the launch vehicle and information of the total vehicle external loads.

The objective of this data bank is to compile the necessary data in the low frequency region from the initial shuttle flights in order to reduce costs for future payloads. This cost reduction impacts two major areas: payload ground testing and analytical efforts.

The philosophy for the reduction of ground testing is straightforward: by gaining more knowledge of the low frequency environment, less ground testing will be necessary to insure payload survivability.

Payload ground testing and analysis are closely related in this respect. Increased verification and greater reliance on the math models to predict structural loads could not only mean a smaller scope in analytical effort, but a reduction in necessary ground tests as well.

With these objectives in mind, the low frequency data bank has two discrete objectives: gather data necessary to define the complete low frequency environment for any payload; gather structural dynamic data to correlate with math models. Once the required data has been compiled, a "user's guide" for payload designers can be created showing design areas (e.g., frequencies of major orbiter modes) to be avoided. For payloads already designed, the payload designers can evaluate the need for extensive ground testing and/or redesign.

The following types of data must be compiled:

1. Dynamic characteristics of the launch vehicle in the form of modal data, transfer functions, and impedance/mobility data;

2. Complete data on the external loads applied to the launch vehicle;

3. Dynamic characteristics of the payloads themselves;

4. Interface loads data in the form of loads and accelerations.

The data bank information should be broken down into a number of categories. For example, payload weight should be a prime consideration. The heavier and more complex the payload, the more complex the analytical effort. These payloads can be grouped together in one category.

Payload/orbiter interface is another consideration. The shuttle is designed to accept a number of interface configurations. Each configuration could classify the low frequency environment that each payload sees. For instance, where the payload is located in the payload bay and its interface configuration could determine the magnitude of the interface loads during transient events.

Finally, the low frequency environment should be broken down into events. Not all payloads will be subjected to the landing environment. Thus, each payload should be able to refer to the data bank in only the areas of its concern.

In summary, the low frequency data bank could be broken down into the following categories:

1. Payload classification: 500 to 1000 Kg, etc.,

2. Payload interfaces: 3 point statically determinate, etc.,

3. Shuttle environment: liftoff, gust, engine shutdown, landing, etc.

3.2.2.4 Random Vibration Criteria

In Section 2.0, two current techniques of utilizing vibro-acoustic data banks were described. These data banks are useful tools for predicting random vibration criteria for new vehicles provided that reasonable structural similarity exists. Improved accuracy in vibration prediction could be achieved if the following improvements could be made:

1. Develop frequency dependent mass and rigidity correction factors so that the effect on spectrum shape can be accounted for;

2. Develop frequency dependent correction factors to properly adjust the spectrum for component loading. Generally, current practice allows adjustment for amplitude only as shown in the example in Figure 3-17, taken from Reference 22. Data from Titan and Skylab vehicles suggest that the high frequencies are attenuated as component weight increases. If the proper empirical correction factors can be derived for this effect, than more realistic, less conservation specifications (perhaps of the form shown in Figure 3-18) could be derived.

3.3 Test Methodology

3.3.1 Impedance Techniques

In the past decade, many investigators (References 13, 23 through 26) have experimented with mechanical impedance, admittance, mobility, or apparent weight concepts as methods to improve vibration testing technology. Special equipment has been developed and manufactured to measure and analyze these parameters. Rather surprisingly, even though the techniques have been known for a number of years, they have seen very limited application on spacecraft programs, and have been used primarily in research and scale model programs. As pointed out in Reference 23, the parameters are difficult to measure accurately in the laboratory,

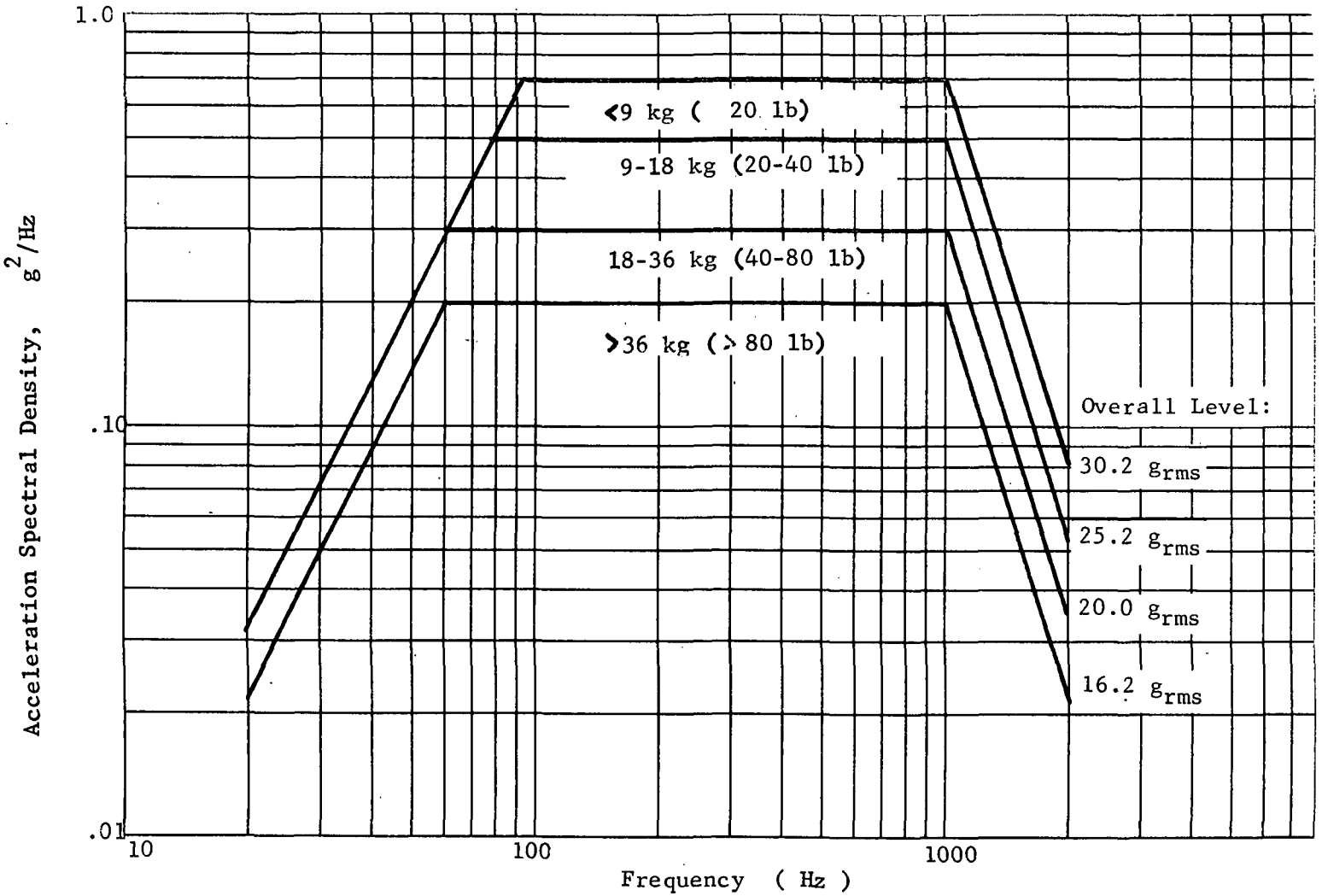

Figure 3-17: Example of Current Vibration Specification for Various Component Weights (Skylab program, Ref. 22)

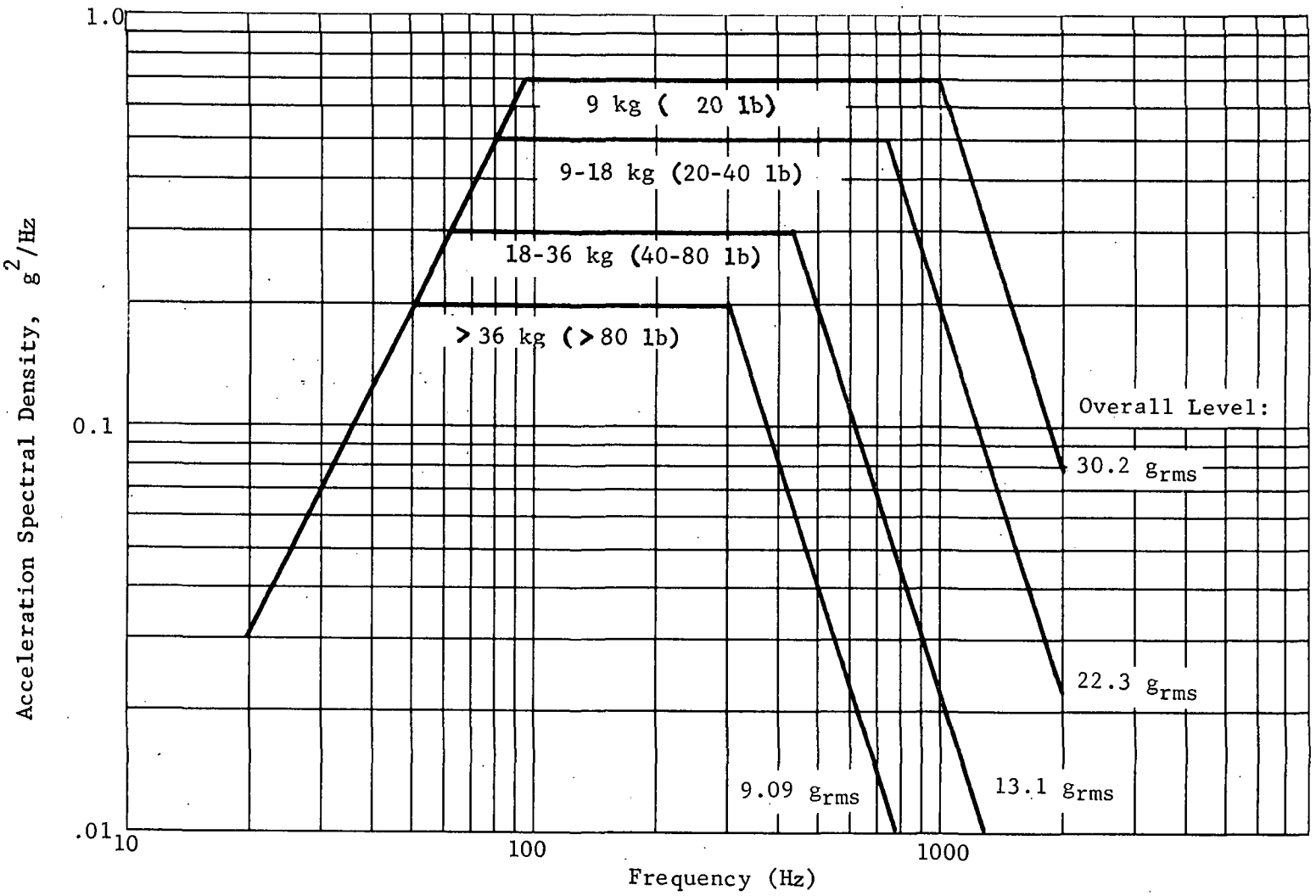

Figure 3-18: Possible Improved Format for Vibration Specification for Various Component Weights

let alone in flight. The dynamic range of impedance can far exceed the useful range of amplifiers, tracking filters, log converters, etc. Since complex ratios are involved, accurate phase measurements are required. In addition, system nonlinearities can significantly affect the apparent impedance characteristics of a particular structure. The measurement and analysis problems, coupled with the problems of duplication in vibration exciter/control systems are probably the reason the techniques have not seen more wide-spread application.

3.3.2 Universal Test Facility

The concept of a universal payload test facility is attractive when the proposed large number of shuttle payloads is considered. Appreciable cost savings may be realizable through standardization of test techniques, instrumentation, data reduction and format. Such cost savings could rapidly amortize the high initial cost of such a facility. However, the logistics problem and costs associated with transporting payloads, equipment, and personnel to and from such a facility must be considered.

These logistics problems can be significant, especially for ground transportation of large payloads. For example, to move the Viking lander from Denver to the JPL facility at Pasadena for the stack test required special permits from the various states, specific escort provisions and speed limitations. The convoy was allowed to move only in certain daylight hours.

A sketch of a universal payload dynamic test facility is shown in Figure 3-19. An acoustic shroud could be constructed to provide good simulation of the acoustic modes and sound field distribution within the payload bay. The vibration facility depicted implies a complex hardware installation to simulate the dynamic characteristics of the orbiter payload bay, high-force shaker systems, and an extensive control/abort instrumentation system to insure protection for the payload. In addition, there still remains the problem that the launch vehicle and test fixture impedances are different.

We feel that this simulation could best be accomplished by providing an electrical simulation of the vehicle/vibration exciter characteristics and utilizing a much simpler fixture (Figure 3-20) which would still provide the proper attachment points but minimize the weight and associated force/power requirements for the shaker systems. The intent of the concept is to provide realistic simulation of vehicle transients including the effects of payload/orbiter interactions, thus minimizing test peculiar unrealistic failures associated with current sine sweep techniques. Initially, analyses of both the flight and test configurations as shown in the flow chart in Figure

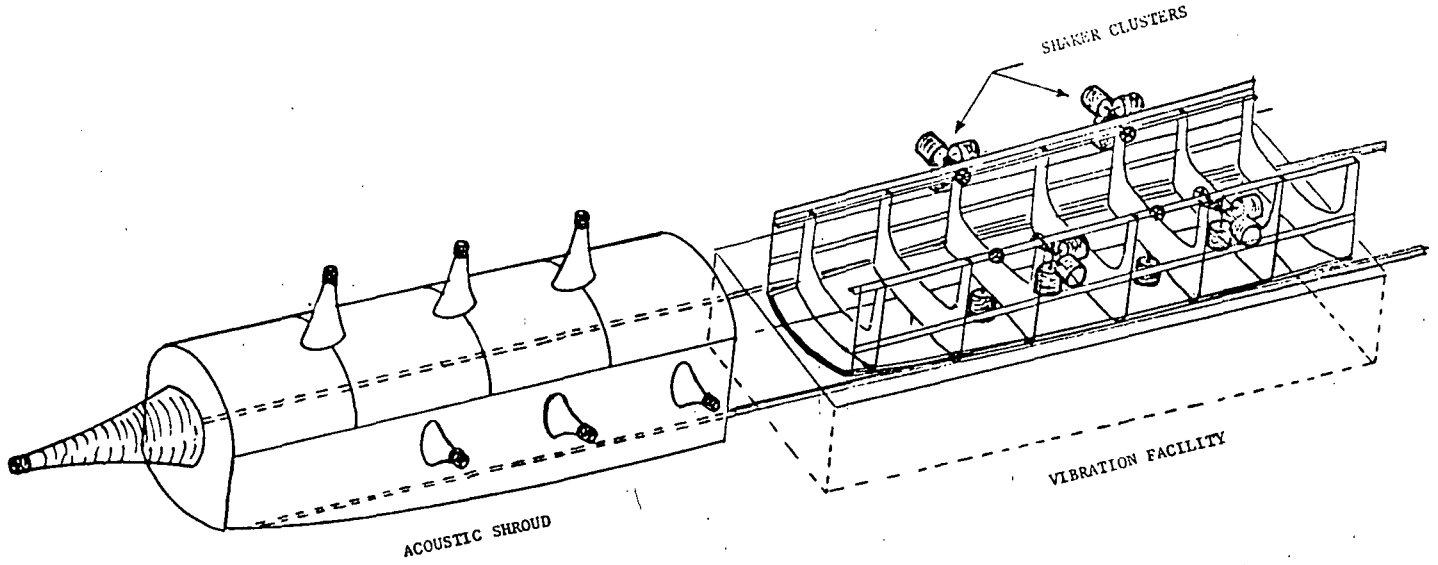

Figure 3-19: Shuttle Payload Dynamic Test Facility Concept

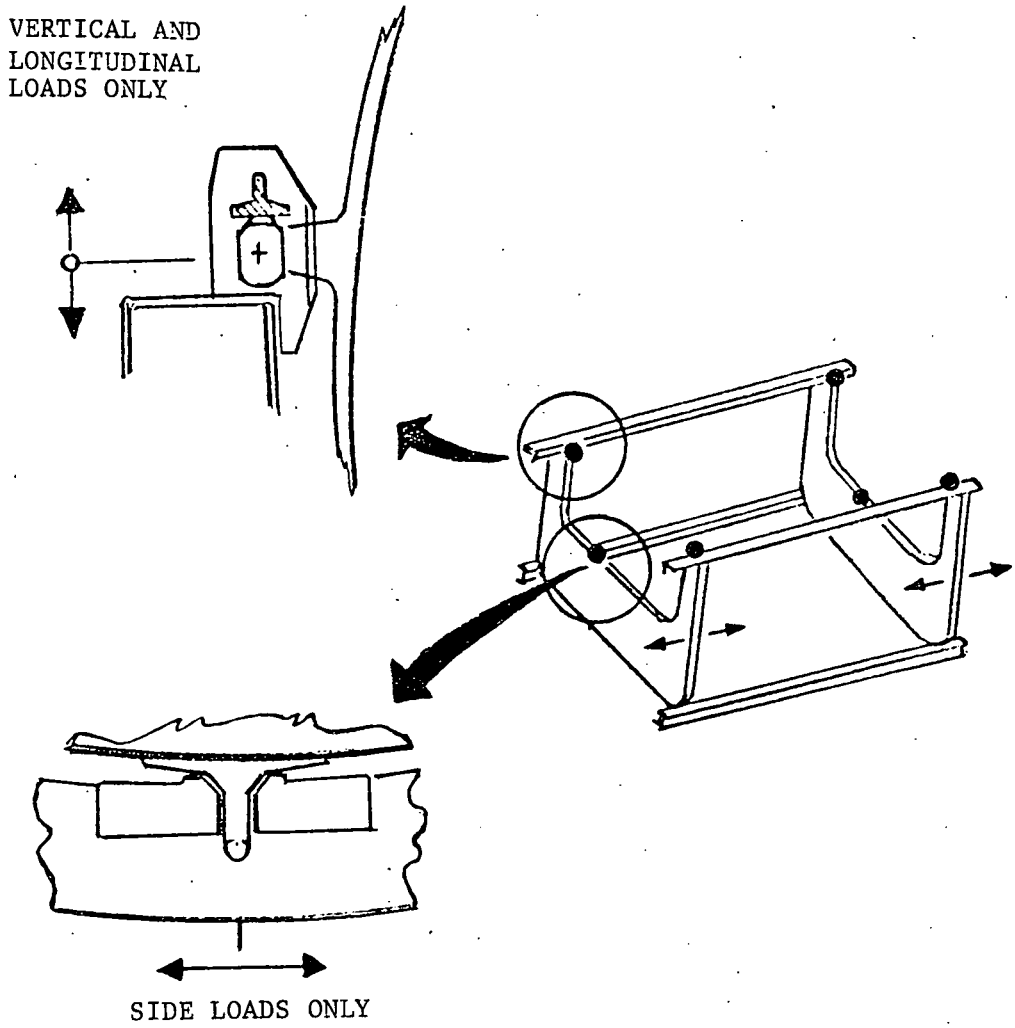

Figure 3-20: Simplified Payload Vibration Fixture

3-21 would be required. The primary problem lies in developing the capability of determining the transfer functions including cross-coupling compensation between the shakers and maintaining phase relationships. The concept involves a significant advance in the state-of-the-art in vibration control techniques; however, previous work by Favour and LeBrun (Reference 27) and recent advancements in digital control systems indicate that the system is realizable.

3.3.3 Transient Control Feasibility Test

A simplified test program was conducted to determine the feasibility of producing realistic simulation of vehicle transients which requires independent control of multiple shakers, accounting for the transfer function of the dynamic system including the vibration exciters. Implementation of the test was complicated by the limitation of having only a single channel digital control system available. Consequently, it was necessary to synchronize the computer with a magnetic tape system utilizing a trigger pulse recorded on tape. Software modifications to the control system program were made to accomplish this synchronization, which allowed phase coherent pulse storage.

The test configuration is shown in Figure 3-22. Two electrodynamic shakers were attached to the mounting points of a Titan instrumentation truss which was supported by a wooden beam and rubber pad assembly. A force gauge and accelerometer were attached to the truss at each shaker input point as shown in Figure 3-23. A block diagram of the control and data acquisition systems is shown in Figure 3-24.

Arbitrary transients (Figures 3-25 and 3-28) were produced to represent the test criteria and a sequence of steps performed to attempt to reproduce these transients at each of the shaker input points, while compensating for the transfer function and cross coupling of the shaker systems.

Test Series 1

1. Parallel inputs were applied to shakers 1 and 2 from the TD 1923 which was used to control shaker 1. The input pulse to shaker 1 was recorded on tape recorder 1 which contained a trigger pulse. The trigger pulse, input pulses, and transducer output signals were recorded on tape system 2.

2. The control system was switched to shaker 2 and simultaneous inputs were applied to both shakers with shaker 1 driven from the previously recorded pulse.

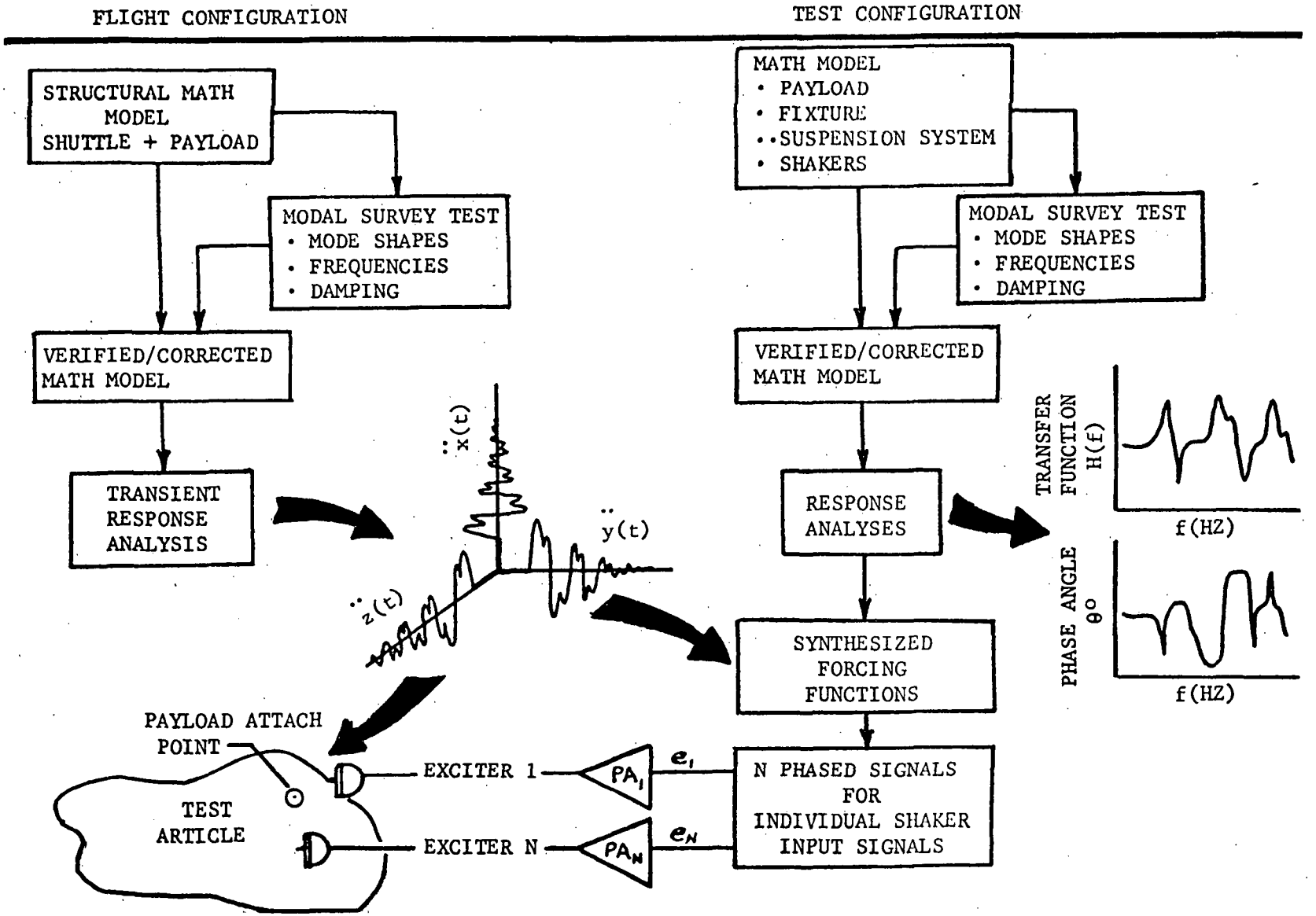

Figure 3-21: Flow Chart of Analysis/Test Correlation

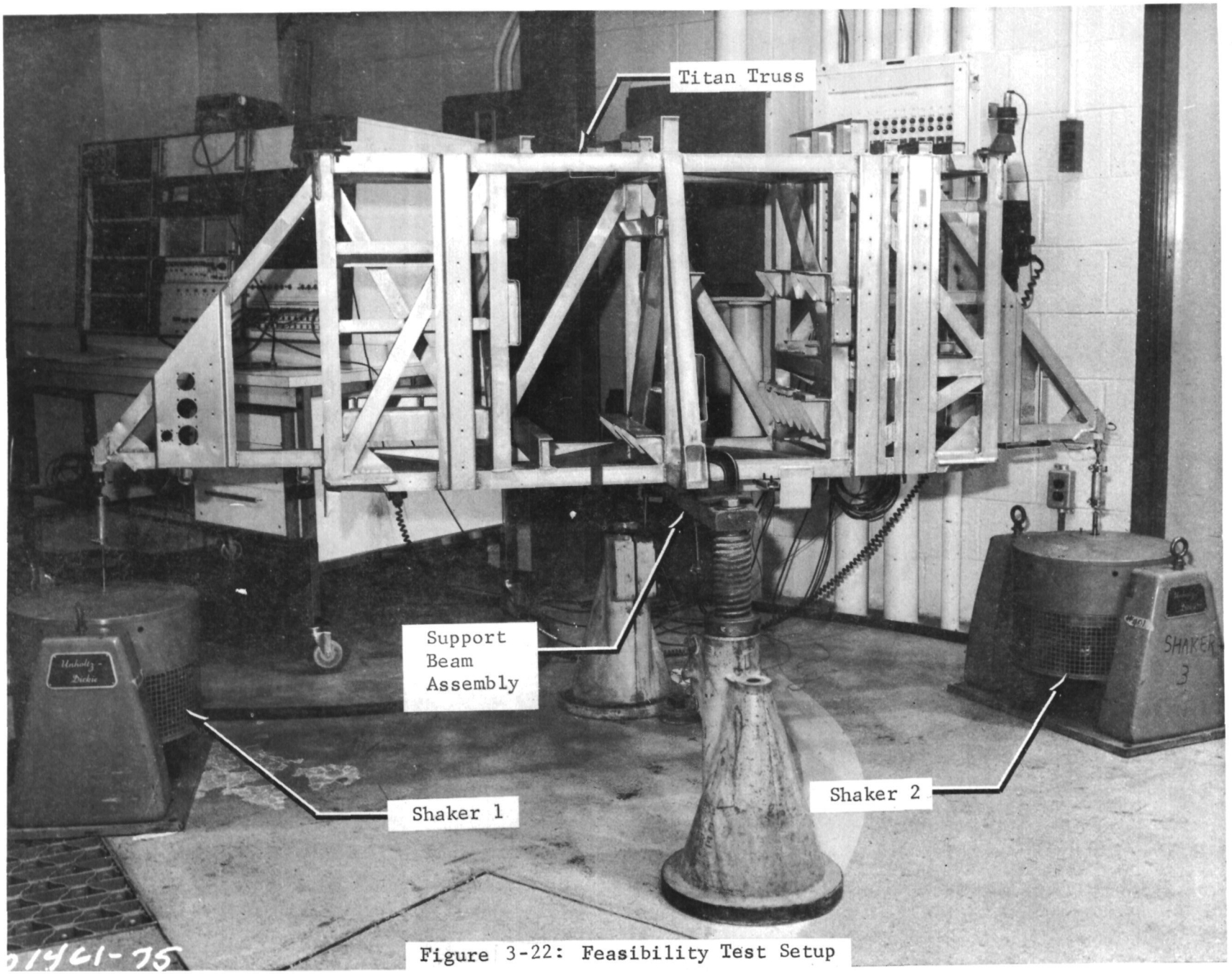

Figure 3-22: Feasibility Test Setup

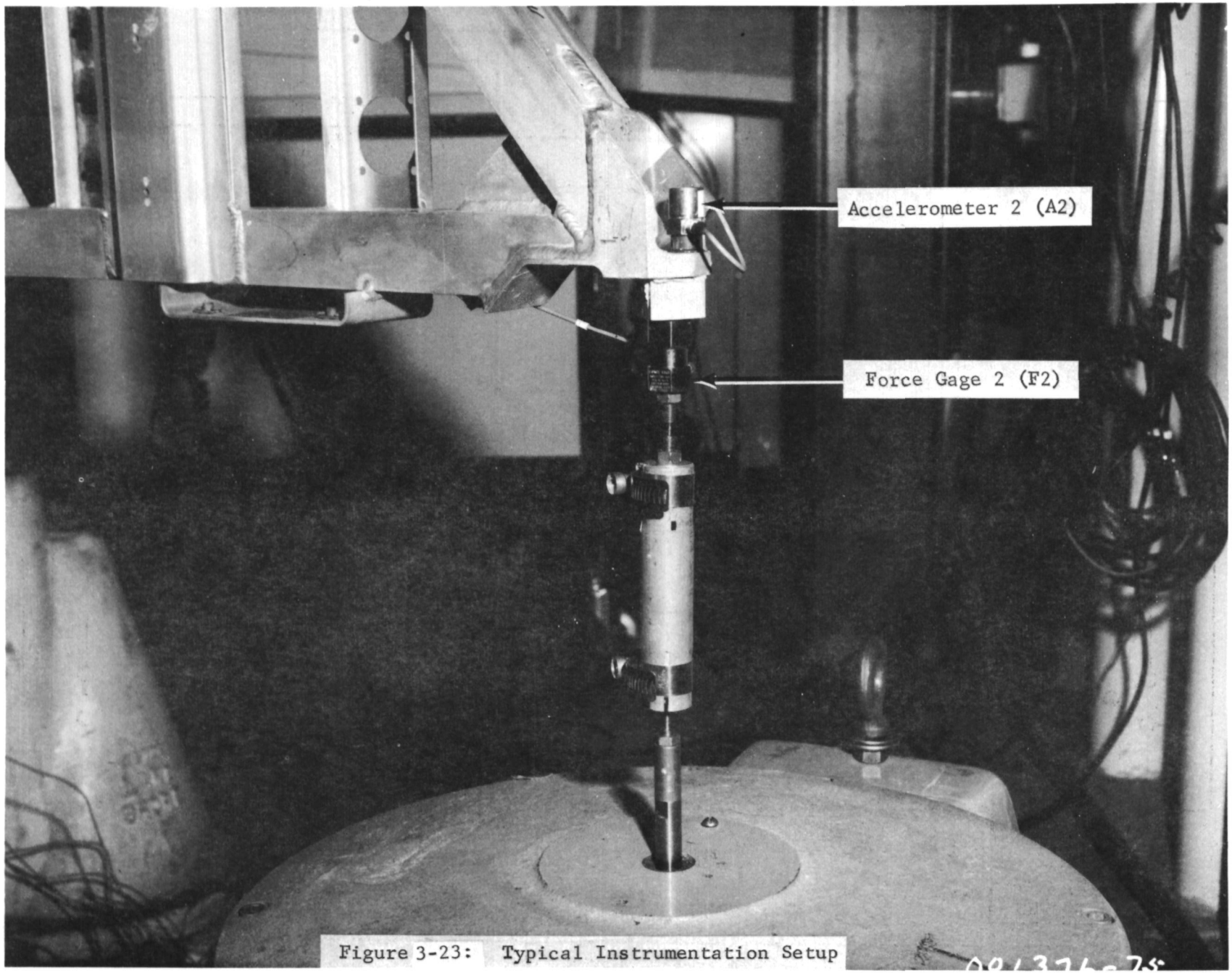

Figure 3-23: Typical Instrumentation Setup

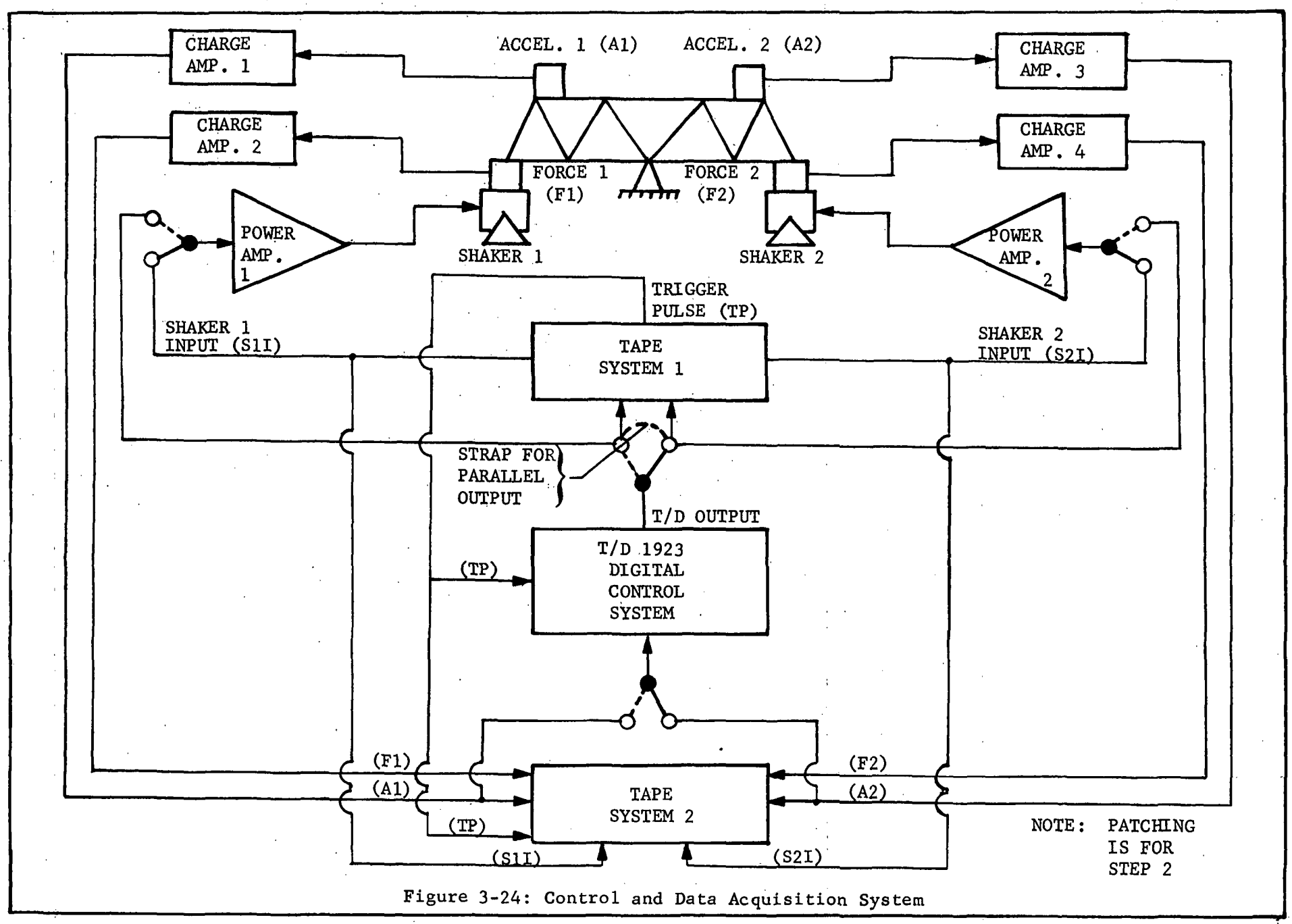

Figure 3-24: Control and Data Acquisition System

3. The process was repeated, switching computer control between shakers 1 and 2, recomputing the transfer function and storing the computed input waveform on magnetic tape.

4. The final step involved applying simultaneous inputs to the 2 shakers from the previously recorded input pulses. The TD 1923 was not in the loop for this operation. Responses at the two input points are shown in Figures 3-26 and 3-27.

Comparison of the responses at the input points with the desired waveform (Figure 3-25) indicates that acceptable control was not achieved for this test sequence.

Test Series 2

Additional testing was conducted in accordance with the following sequence of steps.

1. Parallel inputs were applied to shakers 1 and 2 as specified by Figure 3-28. The input pulses were recorded on tape system 1. The trigger pulse, input pulses, and transducer output signals were recorded on oscillograph. Accelerometer 1 output was input to the TD 1923 for shaker 1 control.

2. A pulse modified by the system transfer function was input to shaker 1. The pulse used in step 1 was simultaneously input to shaker 2.

3. The process was repeated with the TD 1923 controlling shaker 2 and by monitoring A2. The input pulses to the shakers were those generated and recorded in the preceding step where the initial pulse was modified by the system transfer function.

The test criteria pulse for this test series is shown in Figure 3-28 and again in Figure 3-29 where it is plotted along with the test response data at shakers 1 and 2. A comparison of the pulses shows that they are relatively equal in amplitude which establishes the degree of amplitude control achieved and demonstrates that some control was being accomplished, however, the pulse waveforms are not directly comparable. The suspected limiting factor was the frequency resolution of the control system software in computing the transfer function and synthesizing the input waveform. The ultimate objective of this test feasibility study is to control a pulse in both amplitude and waveform at a structural test point using the

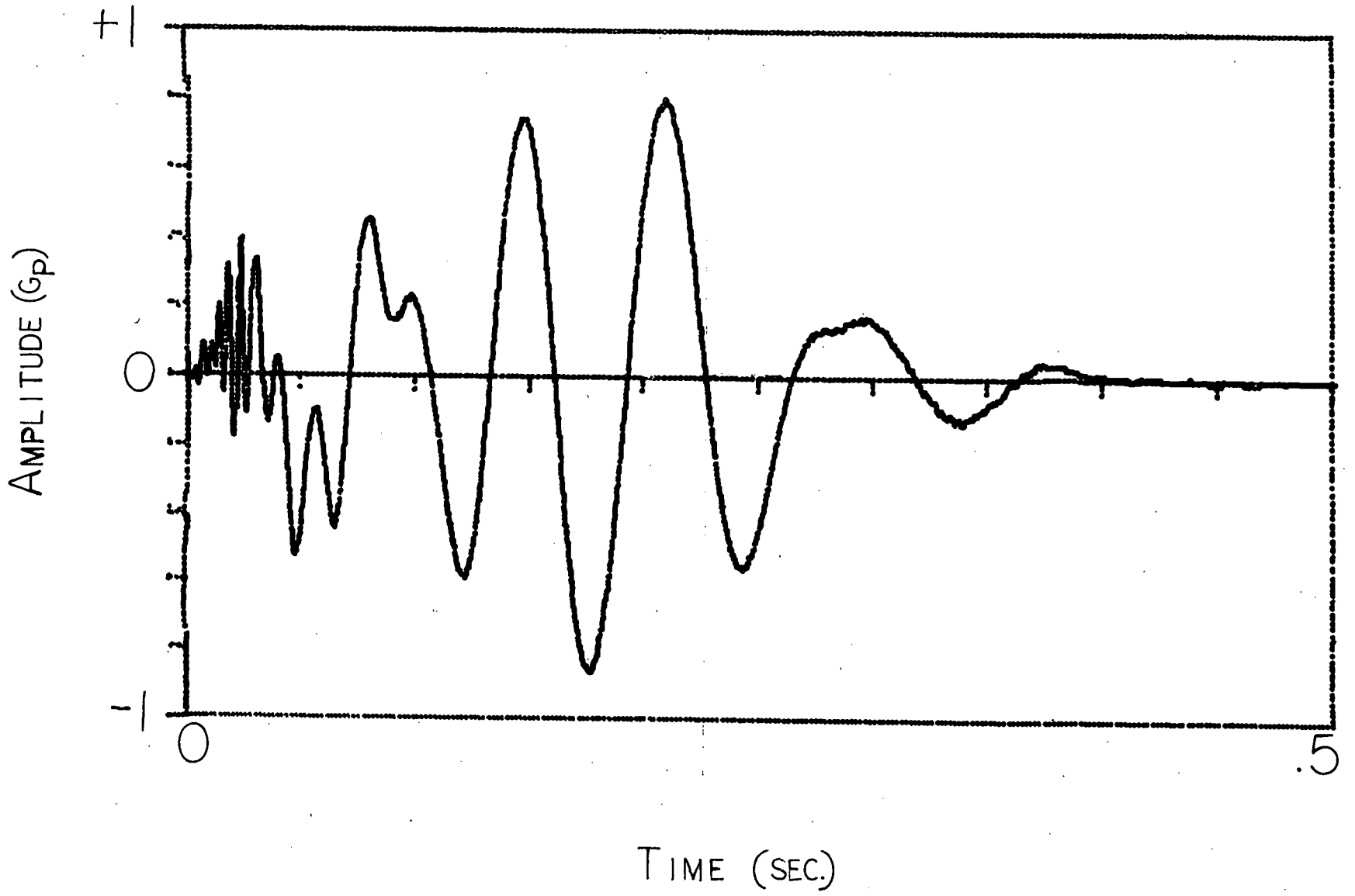

Figure 3-25: Test Criteria - Test Series 1

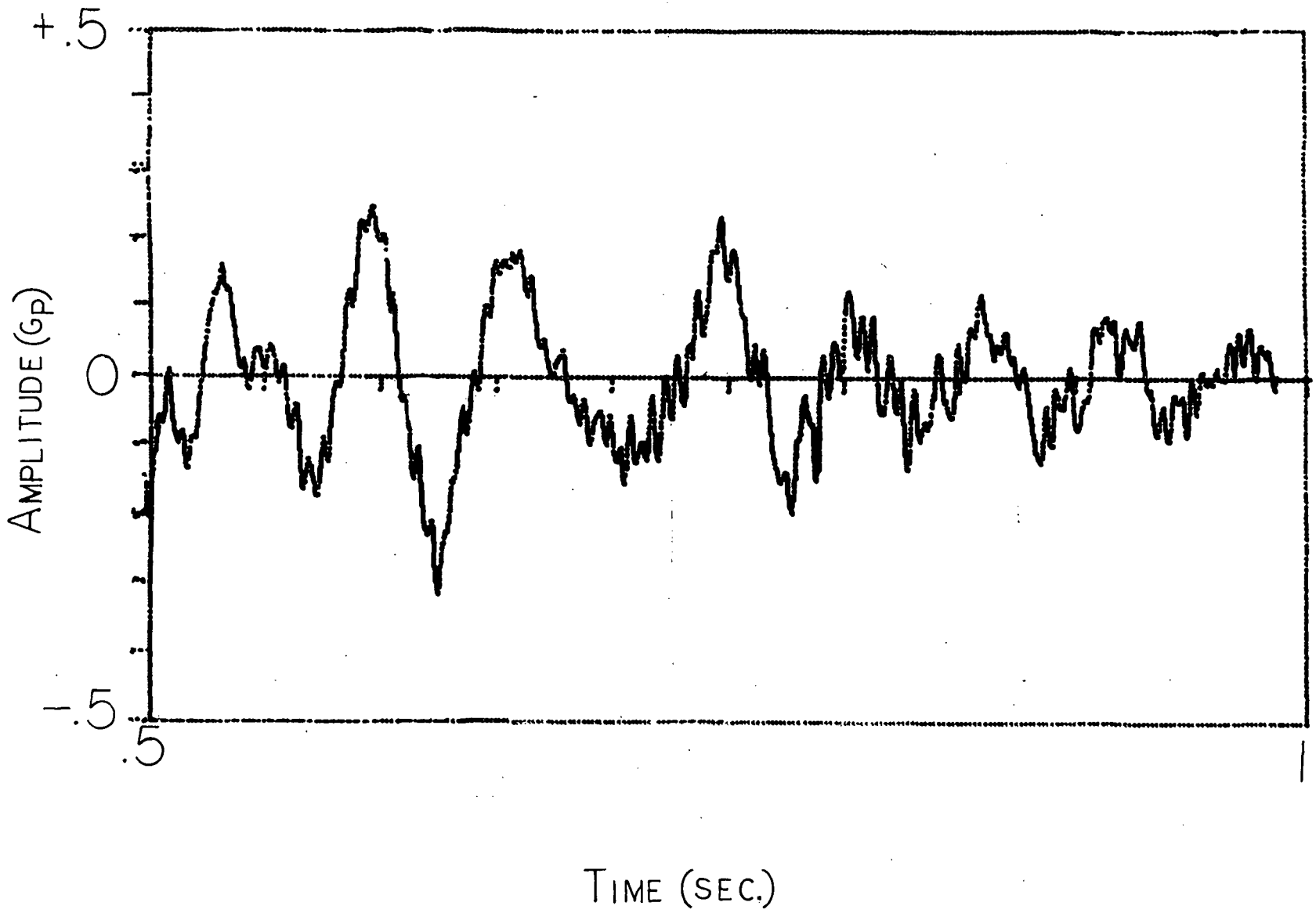

Figure 3-26: Accelerometer 1 Data - Test Series 1

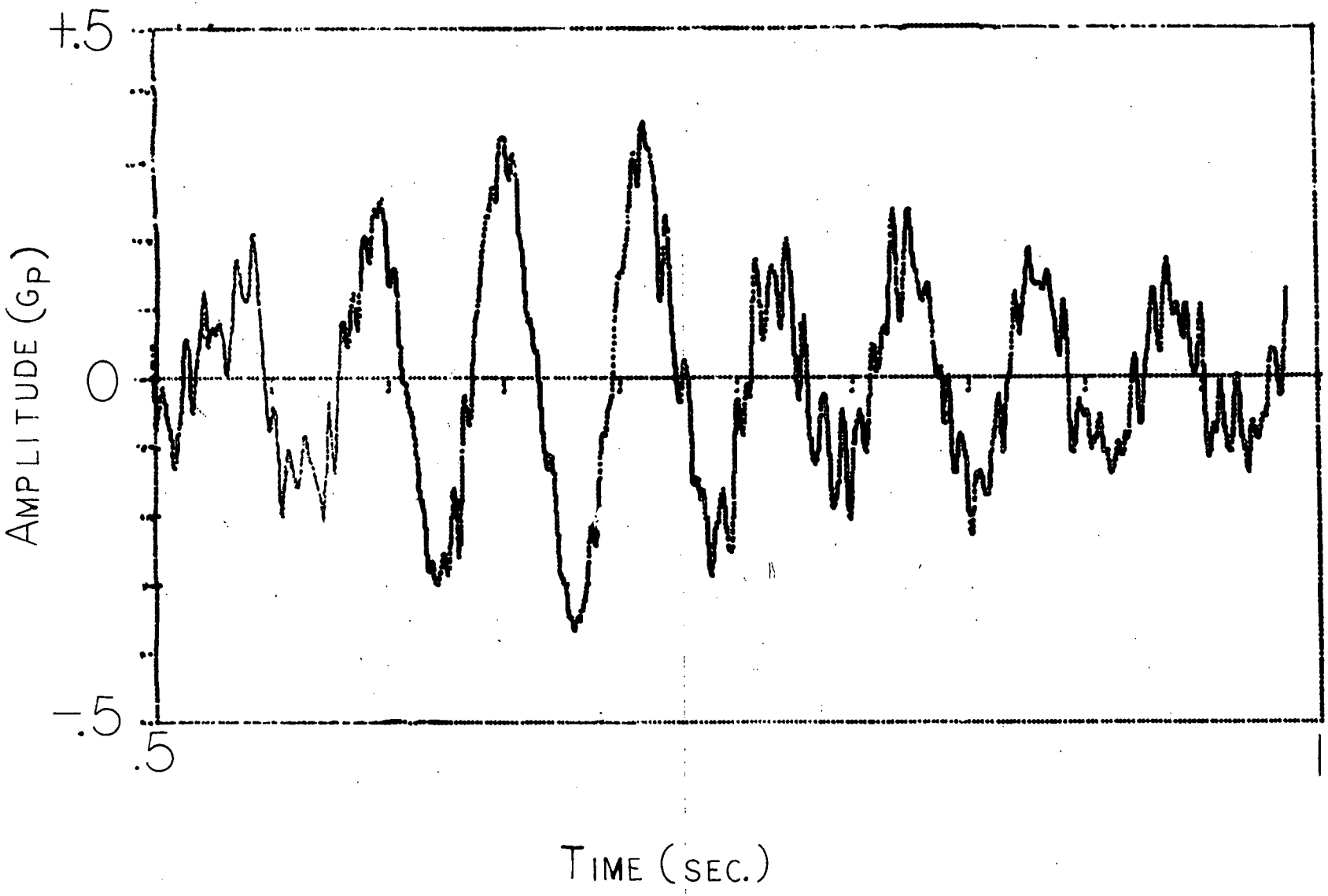

Figure 3-27: Accelerometer 2 Data - Test Series 1

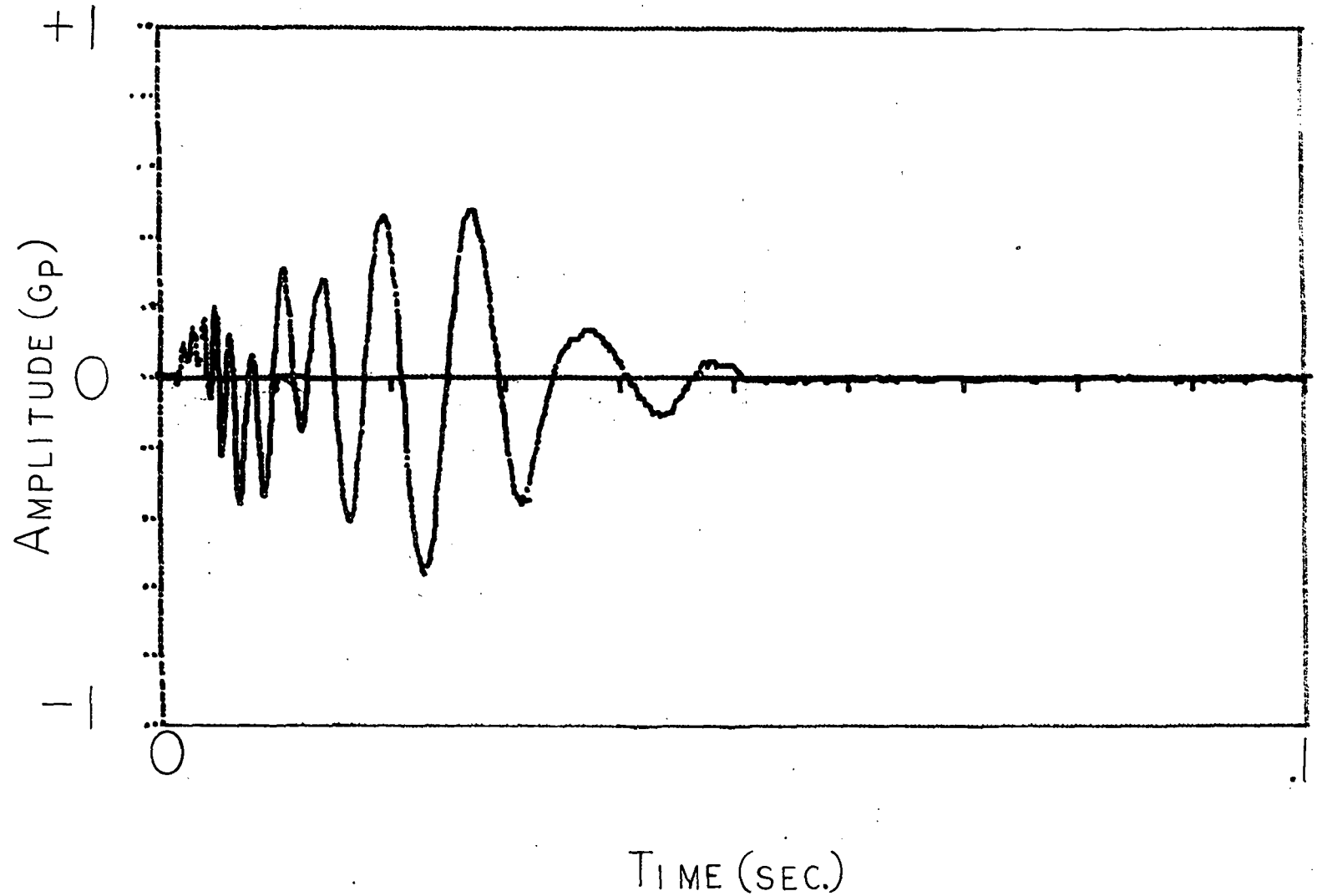

Figure 3-28: Test Criteria - Test Series 2

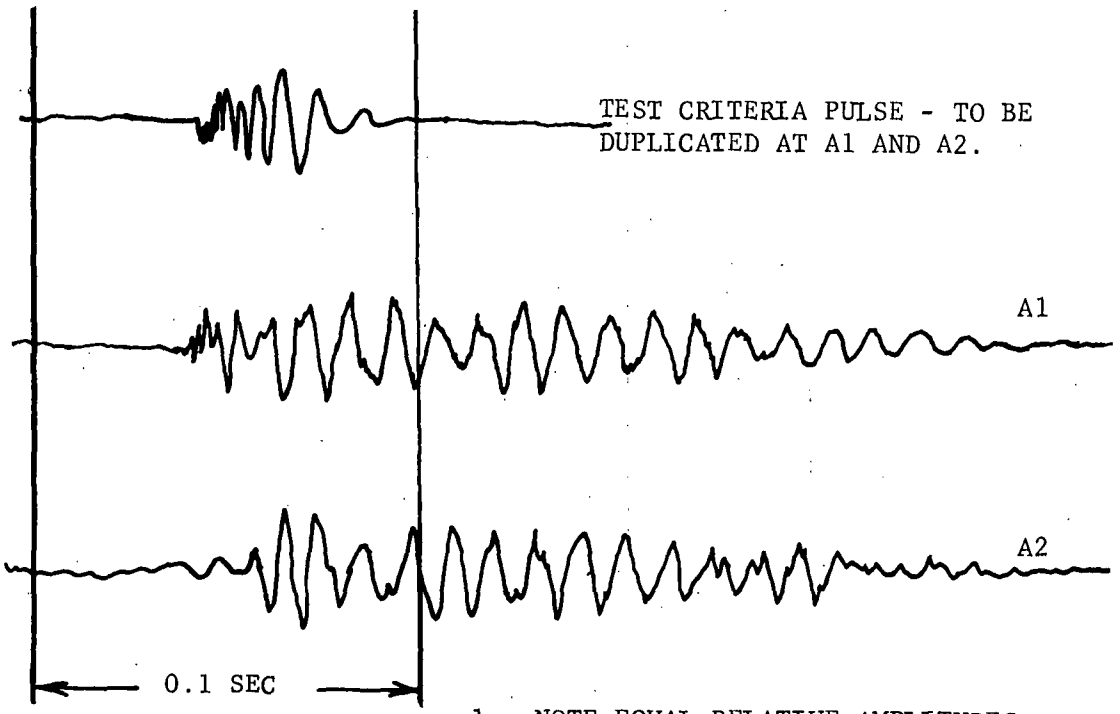

Figure 3-29: Test Data - Test Series 2

maximum resolution available. Additional testing will be required with improved frequency resolution to demonstrate that this method is practical.

3.4 Improved Test/Design Philosophy For Payload Cost Reduction

3.4.1 Improved Design and Test Criteria

Significant cost savings should be achievable by reducing the uncertainty factors associated with design and test criteria for payload components. This can be accomplished to some degree by using the data banks which will be developed and continuously updated as more flight data is collected and statistical confidence is obtained. Excessive conservatism in design and test requirements should, therefore, be eliminated.

Some margin on design and test levels will always be necessary, of course; however, the margin on a particular payload should be tailored to the objectives and characteristics of that payload. For example, a single-mission planetary probe satellite may well require an extensive test program consisting of component, subsystem and system level tests in order to achieve the high reliability required for this type of mission. On the other hand, a significantly lower reliability requirement may be assigned to a multi-mission earth orbit satellite which can be retrieved, repaired and reflown, if necessary, so that a minimum test program based on a relatively low confidence level would be accepted.

For example, a high reliability payload might require a 97.5% confidence level, whereas an 80% confidence level might be adequate for the multi-mission earth orbit satellite. Examination of Figure 3-30 shows that the difference between the 97.5% and 80% confidence levels could result in approximately a factor of 2 decrease in random vibration level for a given sound pressure level, for this example. One might expect a 10% to 15% reduction in the number of qualification test failures, if, for example, the equipment qualification test level could be reduced from 15 g_{rms} to 7.5 g_{rms} as shown in Figure 3-31.

A number of approaches have been proposed for investigating the optimization of test levels. A study by Piersol and Maurer (Reference 28) utilized a cost model based on the ratio of the cost of test failure to cost of flight failure to define an optimal test level as a percentile of the environmental level as shown in Figure 3-32. Young (Reference 29) extended this case to determine an optimum test factor to apply in the protoflight case. His results indicate that the test factor ranges from approximately 1.1 to 1.4 for the most likely range of cost ratio as shown in Figure 3-33. Obviously, as the

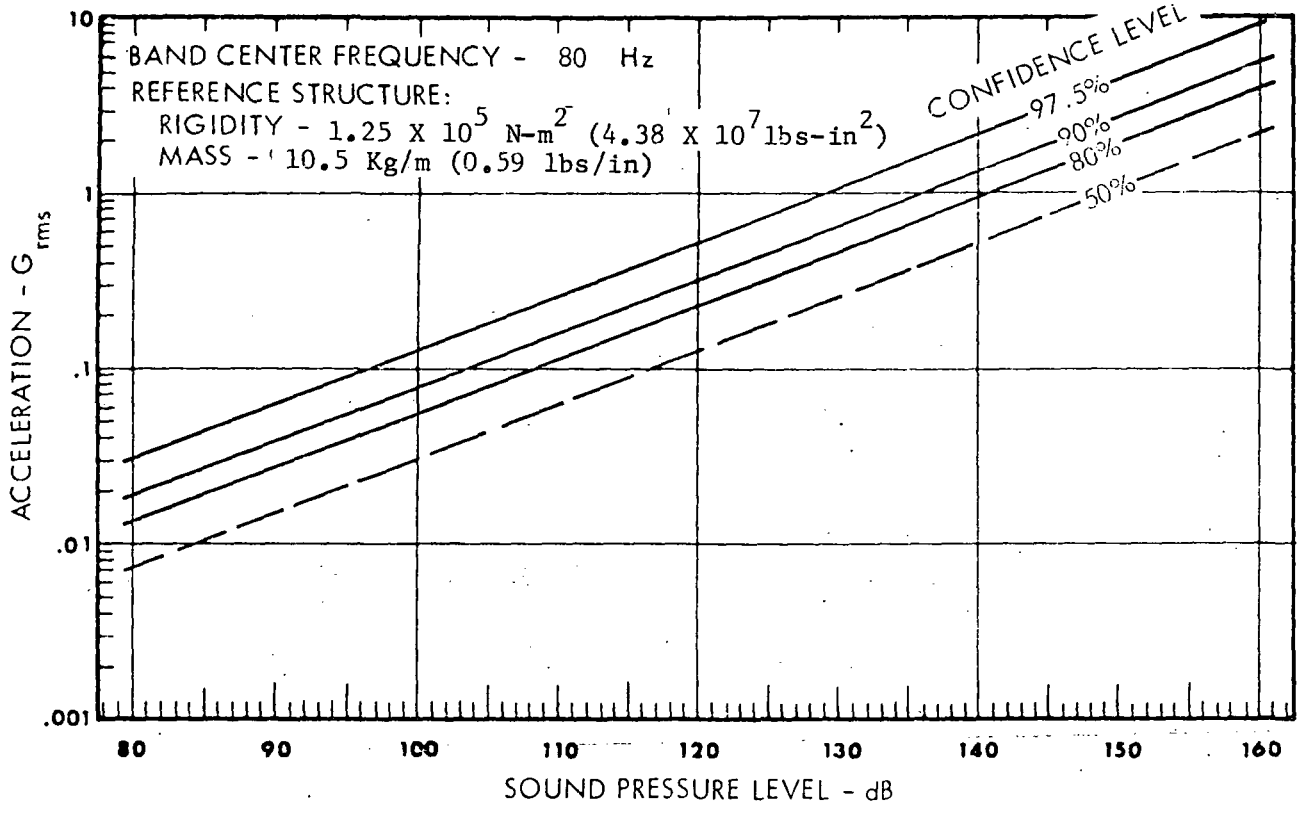

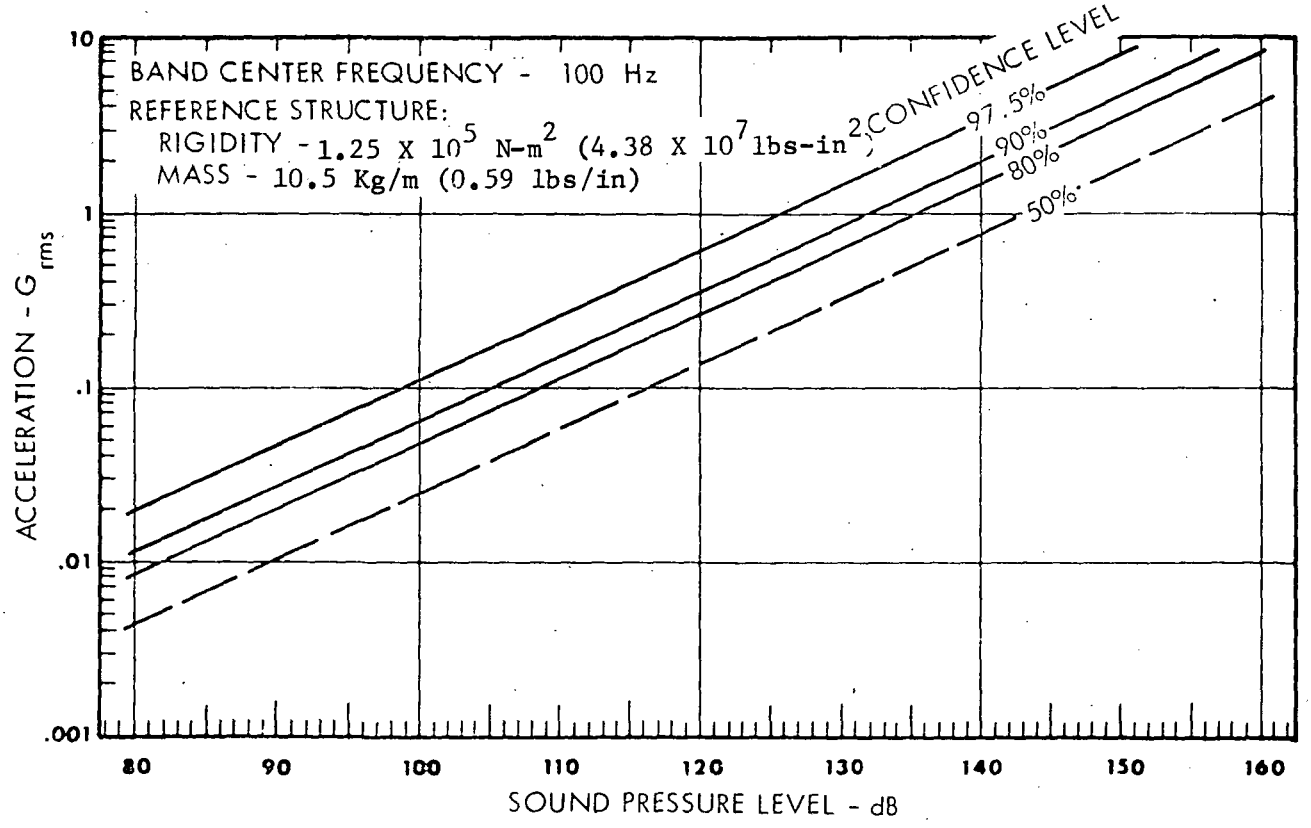

Figure 3-30: Random Vibration As a Function of Sound Pressure Level

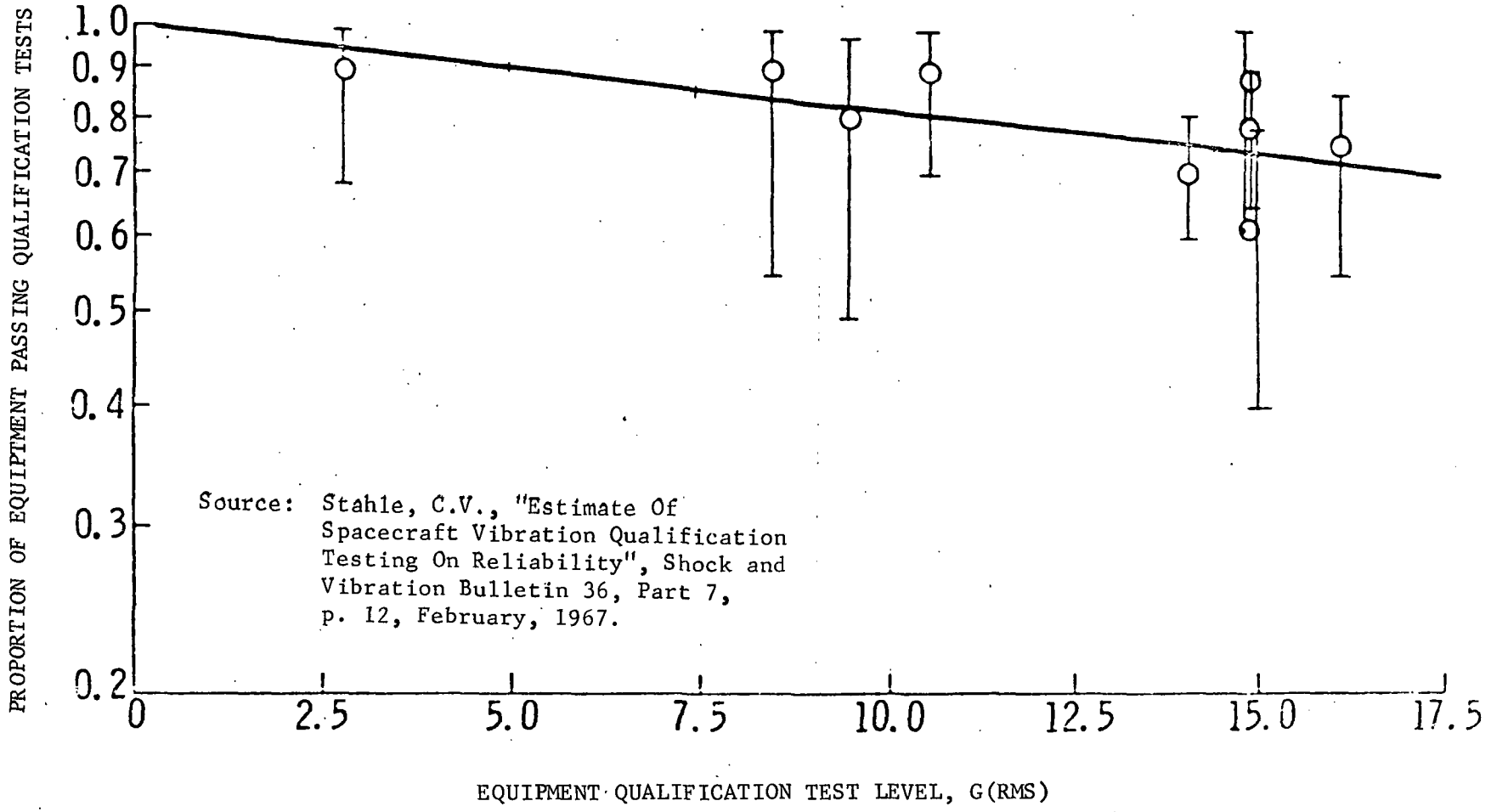

Figure 3-31: Variation of Equipment Test Failures with Qualification Test Level, Showing 95% Confidence Limits for Individual Spacecraft Samples.

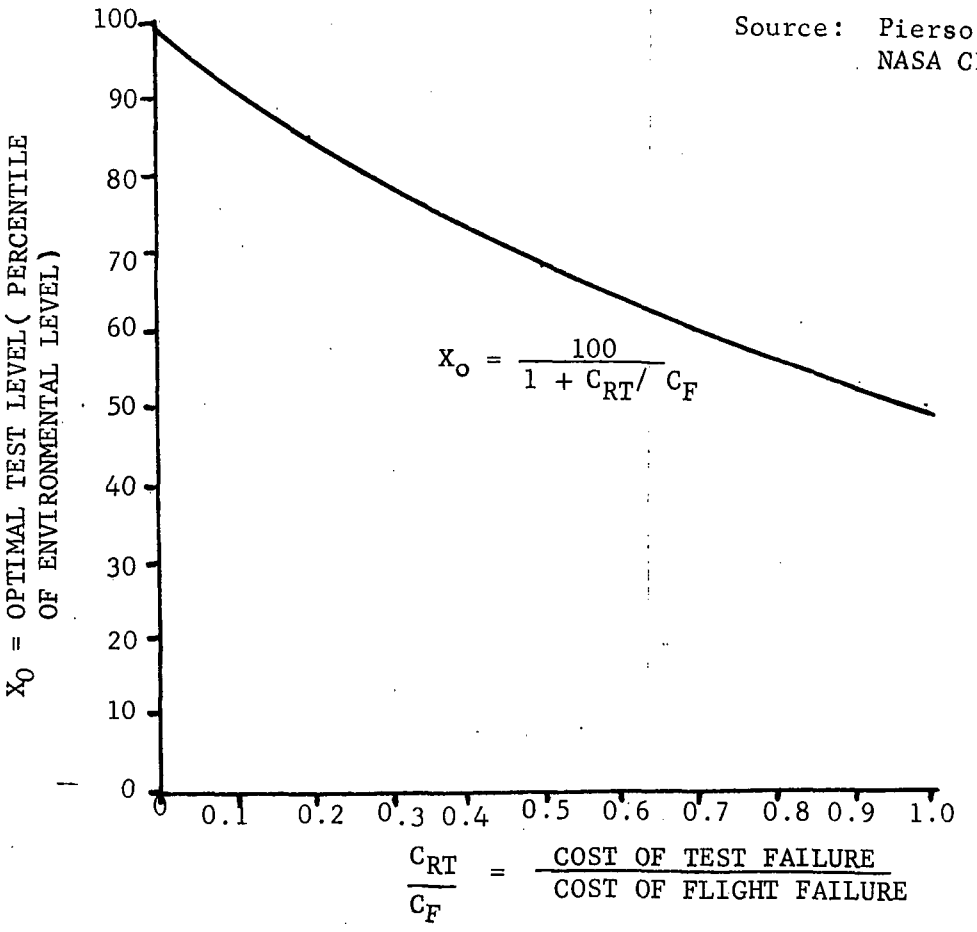

Source: Piersol and Maurer, NASA CR-115778, May, 1971

Figure 3-32: Optimal Test Level versus Cost Ratio

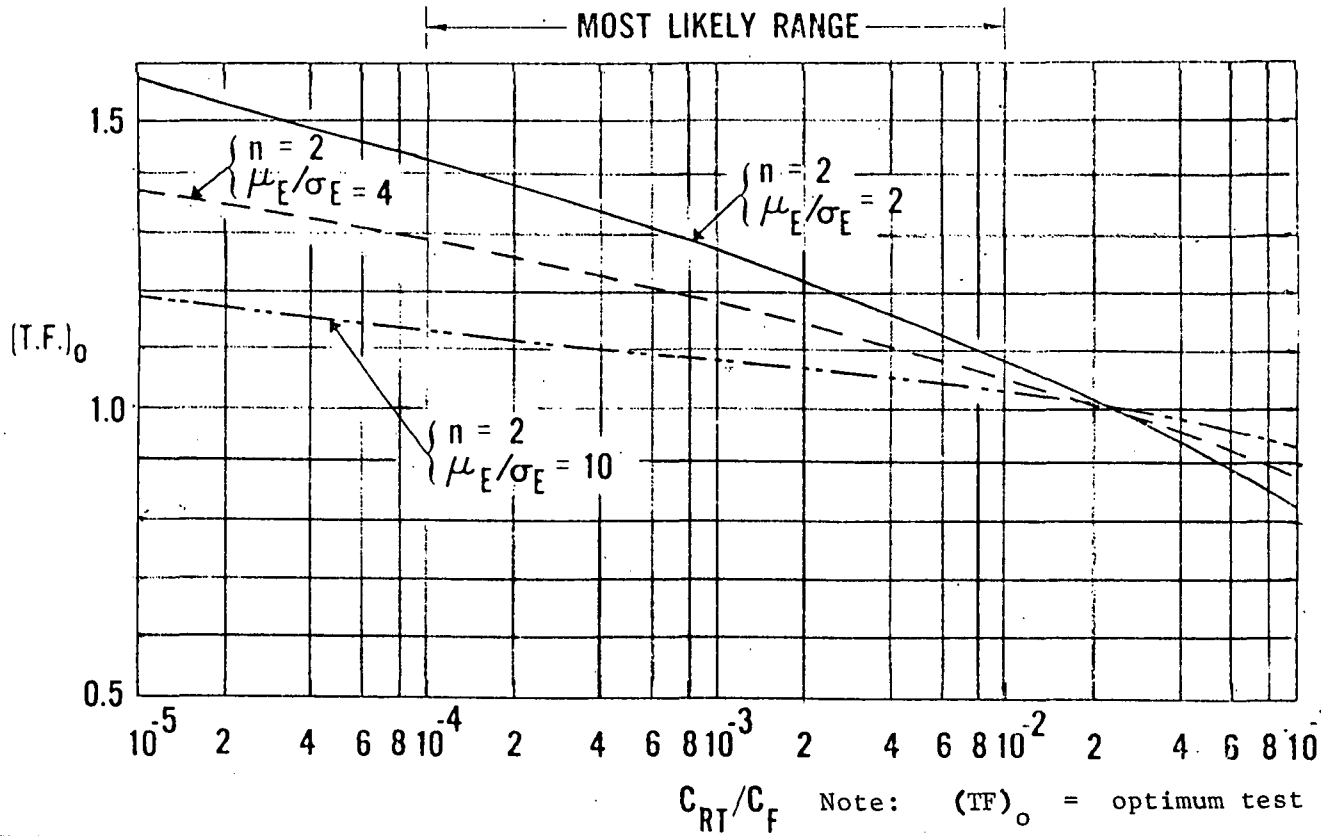

APPLICABLE TO PROTOFLIGHT CASE
Source: Young, J.P.,"Cost Optimization of Spacecraft Test Levels", Proceedings of the IES, 1974

Note: $(TF)_o$ = optimum test factor

μ_E = service environment mean

σ_E = service environment standard deviation

n = factor that establishes the flight loads probability level

Figure 3-33: Test Factor as a Function of Cost Ratio

statistical certainty in the knowledge of the environment increases; i.e., as the standard deviation (σ_E) decreases, the lower the test factor can be made.

The greatest limitation with these approaches is the difficulty in determining actual costs of test and flight failures, especially as related specifically to dynamic environments.

3.4.2 Previous Program Experience

3.4.2.1 Viking Criteria Development

Significant cost savings could have been realized on the Viking program if an adequate data bank had been available for use in establishing component design and qualification test criteria. The procedure actually used was the following:

a. Component environments were calculated using the method of R. E. Barrett (Reference 30), which is based on a limited data bank developed from Saturn flight data;

b. The resulting vibration spectrum shapes were adjusted to take account of the difference between the Saturn acoustic spectrum and the anticipated Titan acoustic spectrum (based on a relatively small amount of measured data);

c. Component qualification test requirements were published using the adjusted predicted vibration environments, and the component test program started;

d. A system-level acoustic test was performed on the Lander Dynamic Test Model (LDTM) and acceleration responses measured adjacent to simulated components;

e. Component qualification spectra were modified as necessary to reflect changes indicated by the LDTM test. Some retesting of components was required;

f. New acoustics data was obtained from the first flight of the Titan III/Centaur launch vehicle, which carried a dynamic simulator of the Viking Spacecraft, enclosed by an actual Viking shroud. This showed the acoustic spectrum to be considerably different in frequency content and overall sound pressure level to the spectrum derived from earlier Titan flights;

g. The qualification test levels were once again changed to account for the revised acoustic environment, and a few components had to be requalified;

h. The final system-level acoustic test was performed on the Proof Test Capsule (PTC), using the updated acoustics, and responses measured adjacent to components. In general, the measured responses confirmed that the final iteration of the qualification test criteria was satisfactory.

These steps are summarized in the flow chart shown in Figure 3-34.

In retrospect, it can be seen that the process which was used was very effective in establishing accurate test requirements for the components, but was also relatively costly and time-consuming. If a comprehensive data bank had been available to provide reliable environmental estimates, the LDTM test could have been eliminated and the number of changes to the component test program drastically reduced.

3.4.2.2 Skylab Component Requalification

As described in Section 3.0, requalification of 28 components was required as a result of the vibro-acoustic test of the payload assembly. If this test could have been conducted earlier in the program such that component criteria could be defined prior to qualification tests (as was the case for the orbital workshop vibro-acoustic test), a cost savings of approximately $300,000 could have been realized.

3.4.2.3 Titan Programs

The average unit cost of qualification testing of components has been estimated at approximately $30,000. This cost includes the test planning and documentation in addition to the actual testing. The test program involves thermal vacuum, humidity, and other environments as well as vibration and shock. The failure rate during qualification testing is greater than 75%, indicating that the test program has been effective in eliminating flight failures, none of which are known to be attributable to vibration. Although this is a desirable goal for the Titan program because of the costs associated with single missions, it may very well be an overly conservative approach for multi-mission payloads for shuttle.

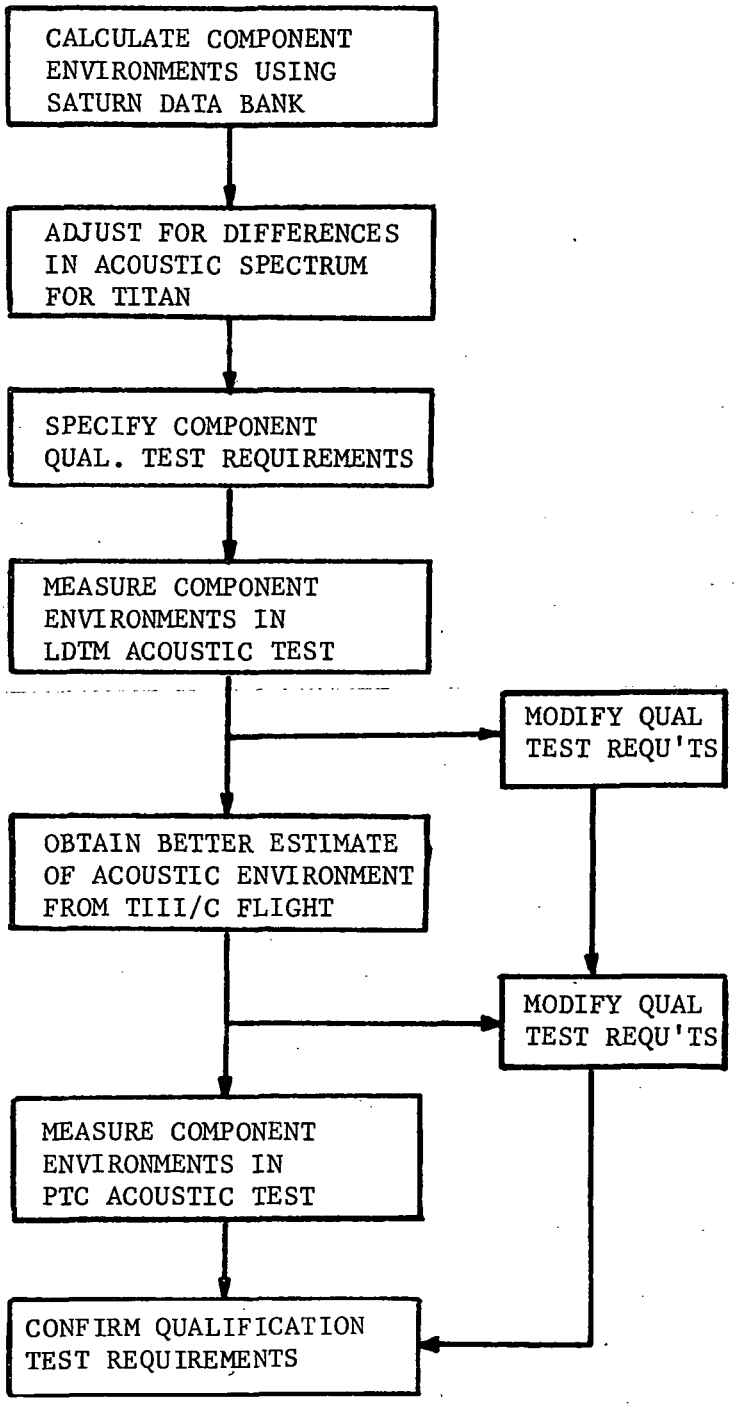

Figure 3-34: Development of Random Vibration Test Requirements for Viking Lander Components

All mission critical components for the Titans are subjected to flight acceptance tests, and a 10% failure rate has been experienced during vibration.

3.4.2.4 Apollo Program

As a result of an acoustic test conducted on the Apollo service module, it was necessary to raise the vibration criteria and retest 52 components, one of which failed during retest.

Considering this program, and the Viking and Skylab experience, there were a total of 89 components which had to be requalified as a result of criteria revisions. If the $30,000 average unit cost experienced on Titan programs is applicable for all programs, and further assuming that 50% of the figure is applicable to vibration, then a cost savings of approximately 89 x $15,000, or $1,335,000, could have been realized on these three programs if changes to the criteria had not been necessary.

3.4.3 Improved Test Methodology

Improved methods of simulating the quasi-sinusoidal motion resulting from vehicle transients has received particular attention in recent years. In general, dynamicists throughout the industry feel that sine sweep testing produces costly, unrealistic failures, and requires a significant expenditure of time and money in analyses and control system hardware to protect the test article from such failures. A number of approaches, including impedance techniques, shock synthesis, and pulse application, have been attempted, but none of these has been developed and utilized successfully on large payloads.

An ideal solution would be the development of a vibration excitation and control system in which the dynamic characteristics of the launch vehicle could be reproduced electrically, such that actual flight transients could be realistically duplicated at specified control points as discussed in Paragraph 3.3.2. This capability would eliminate the basic problem inherent in sine sweep testing; i.e., applying energy to the test article at frequencies to which it will never be exposed in service, for unrealistically long durations.

Similar rationale applies to testing in the high frequency random vibration domain. The current, conservative practice of enveloping flight data in formulating vibration criteria often results in applying energy in frequency bands which the test item would never experience during a mission. This practice was influenced in the past by limitations in equalization/control systems for vibration exciters. As greater confidence

is gained in the definition of environments, and with recent advances in equalization capabilities, the formulation and duplication of test criteria should become more representative of the actual environment as illustrated in Figure 3-35. Improved resolution of vibration spectra would result in fewer test failures, and also reduce the force requirements for vibration systems. In the figure, the RMS level of the "improved" vibration criteria is approximately 75% of the "current method" spectrum, therefore 25% less shaker force would be required to produce the improved criteria. Furthermore, in this example, if the test article narrow band resonances fell into the frequency ranges of the valleys in the improved spectrum; i.e., at 115, 240, and 750 Hz, the input acceleration density is a factor of 6 lower than the current method. The RMS response and associated stress levels at each of these resonances would be reduced by a factor of 2.4. In brief, the current method spectrum is a more severe test at all frequencies with the exceptions of the two peak regions at 150 to 200 Hz and 1100 to 1400 Hz.

Significant improvements in control of acoustic tests have been accomplished in recent years, especially with the implementation of digital control for equalization of noise generators. Almost all of the larger payloads are currently being tested in reverberant chambers of different sizes and configurations. A large area of uncertainty exists in the degree of simulation of the actual environment achievable with these tests. As described in Paragraph 2.2.1, correction factors were applied to the test spectrum for Skylab to account for the "chamber efficiency factor". Other programs do not attempt to account for this effect, implying that additional conservatism is introduced into the test program. Additional work is needed to determine if such corrections are needed, and if so, how much correction is required for different chambers and payload configurations.

Further improvements are needed in noise generator/horn capabilities and spectrum control techniques in the low (<50 Hz) and high frequency (>1000 Hz) regions. Since vibration criteria are often based on measurements obtained during acoustic tests, these criteria can only be as accurate as is the capability of duplicating the service environment with a minimum of extrapolation for differences in acoustic levels.

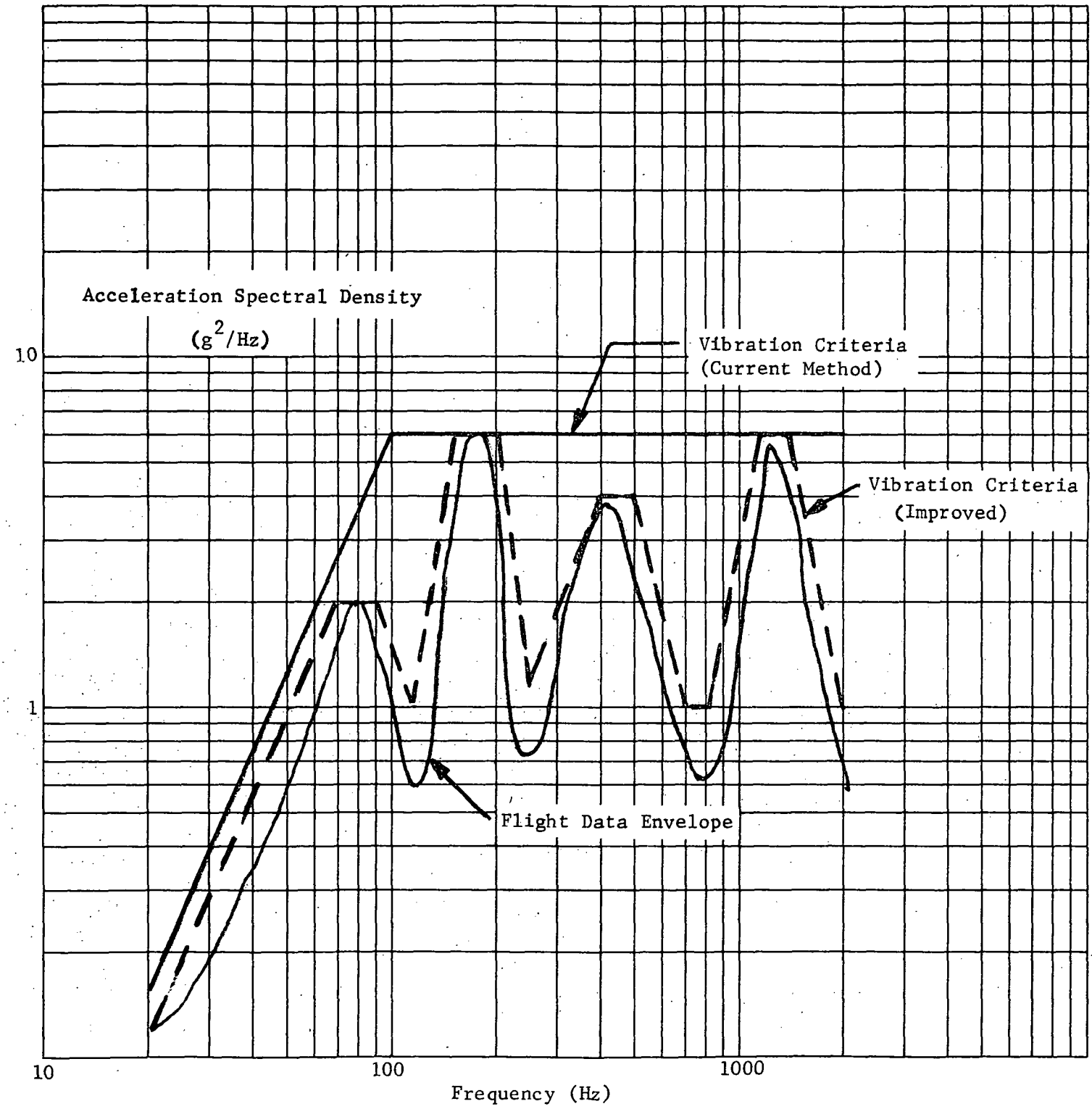

Figure 3-35: Vibration Spectra Comparisons

4.0 SUMMARY AND RECOMMENDATIONS

4.1 Summary

In the first phase of the study information relating to the shuttle missions and physical properties of the candidate payloads was assembled. On the basis of these data, the payloads were classified in terms of mission usage, weight, overall size, etc. Instrumentation requirements for the initial flights were then defined assuming the use of current technology. In order to provide a practical example, a particular payload (LDEF, Mission #4) was selected and a detailed treatment developed. Consideration was paid to the necessary interaction between ground test requirements, dynamic loads analysis and flight instrumentation. By concentrating on a single payload, it was felt that the necessary correlation between the various test and analytical programs would be revealed with more emphasis than a generalized approach would offer. The application of the techniques developed on LDEF to other payloads was then discussed. Potential benefits which could be realized by taking advantage of the latest advances in instrumentation were indicated.

Current methods of data interpretation techniques were addressed in terms of low and mid and high frequency regions, and illustrated with examples drawn from the Skylab and Viking programs. Potential improvements in the current methods were discussed. The emphasis here was on applying more rigorous statistical treatment to the measured data. Methods for testing the assumed statistical properties of the data were reviewed and some of the consequences of basing analysis on incorrect assumptions were considered. Possible sources of error in the data interpretation process were examined, and the relationship discussed between these errors and the test factors necessary to allow for uncertainties in environmental estimates. This phase of the study included a description of the low frequency and mid/high frequency data banks which would be developed from the data obtained in the early flights.

Current methods and potential advances in the field of environmental test methodology were reviewed and examples from Skylab and Viking programs described. An experimental study to investigate the feasibility of multiple-input test techniques was described.

In the final phase of the study, the overall cost savings achievable through improved design/test criteria and test techniques were discussed. The data banks will be used to reduce the uncertainty factors inherent in design and test criteria, which would result in immediate cost savings. Recent analytical

studies in the field of test level optimization for minimum cost were described and some preliminary results shown. Experience on the Viking, Skylab, Titan and Apollo was used to estimate the magnitude of the savings which could have been realized if more accurate test criteria had been available for those programs. Finally, the potential cost benefits associated with improved test methodology were discussed and the main area where such improvements are needed were pointed out.

The current trend of payload contractors is to eliminate as much testing and flight instrumentation as possible because of economic restraints. This approach is highly desirable from an individual payload contractor viewpoint, and for the total shuttle program when one considers the total number of payloads involved. This study was conducted to determine the type of information required from initial payloads and flights necessary to achieve this goal. Consequently, analyses and tests for initial payloads are recommended, even though they might not be required for a specific payload.

4.2 Recommendations

1. Initial payloads must be given comprehensive instrumentation coverage to obtain detailed definition of acoustics, vibration, and interface loads. Recent developments in airborne instrumentation should be utilized to achieve maximum effectiveness.

2. Analytical models of selected initial payloads, coupled with the orbiter, must be developed and verified by modal surveys and flight measurements. In addition, improved analytical techniques are needed such that complete loads cycle analyses of the boost vehicle/payload are not required once the dynamic characteristics of the boost vehicle are known with confidence.

3. Acoustic tests should be performed on initial payloads as early as possible to establish realistic test criteria for components and experiments in order to minimize unrealistic failures and retest requirements. As flight data is acquired, it should be correlated with test results to determine the degree of simulation achieved and whether or not corrections to test levels are required for each technique/facility utilized for these initial payloads, based on vibro-acoustic transfer functions from tests and flights.

4. Permanent data banks should be established from the tests and initial flights and updated as necessary to establish statistical confidence in the data to be used in formulating design and test criteria for future payloads.

5. A more unified design/test specification philosophy is needed if full advantage is to be taken of commonality of components/experiments to be used on different payloads. In addition, the payload community and NASA should become more willing to accept a higher risk of flight failure (at least for multi-mission payloads) if test costs are to be minimized.

6. Additional work is needed to establish a practical testing technique which will provide realistic simulation of vehicle transients in order to eliminate (or minimize) sine sweep testing. The sine sweep approach is considered to be overly conservative in the un-notched regions of the spectrum and difficult to implement at high sweep rates. In addition, implementation of improvements in equalization and control of random vibration spectra should be made, both in the derivation of test criteria and in test performance. Further consideration should be given to the cost effectiveness of a universal test facility, especially with regard to experiments/payloads mounted on standard 3-meter pallets. Flight verification tests performed at such a facility(s) located at the launch site(s) could provide an effective screen for workmanship errors, and reduce costs through minimizing flight acceptance tests on a component level.

5.0 REFERENCES

1. Anon., Integrated Mission Planning - First Two Years of Shuttle Missions, 1979-1980, NASA Technical Memorandum, George C. Marshall Space Flight Center, Alabama, March 1974.

2. Anon., Summarized NASA Payload Descriptions - Automated Payloads, Level A Data, NASA, George C. Marshall Space Flight Center, Alabama, July 1974.

3. Anon., Summarized NASA Payload Descriptions - Sortie Payloads, Level A and Level B Data, NASA, George C. Marshall Space Flight Center, Alabama, July 1974.

4. P. F. Spas, Narrative Technical Description of Current Payload Dynamic Test and Isolation Practices, Task 508, Contract NAS1-12436, McDonnell Douglas Astronautics Company, Western Division, Huntington Beach, California, October 1974.

5. C. V. Stahle and H. R. Gongloff, Final Report - Astronomy Sortie Vibration, Acoustics and Shock Program Planning, Phase 1, G. E. Document No. 74SD4246, Contract NAS5-24022, General Electric, Space Systems Organization, Valley Forge Space Center, Pennsylvania, September 1974.

6. Vibration, Shock and Acoustics Analysis Section, McDonnell Douglas Astronautics Company, Orbital Workshop/ Dynamic Test Article (OWS/DTA) Phase 7 Vibro-Acoustic Test Report, S&E-ASTN-ADD-71, NASA/MSFC, November 1971.

7. Vibration, Shock and Acoustics Analysis Section, MDAC, Orbital Workshop Dynamic Test Article Vibro-Acoustics Test Report, Volume II (Low Frequency Vibration Test), S&E-ASTN-ADD-71, NASA/MSFC, Huntsville, Alabama, November 1971.

8. James W. Fortenberry and Paul Rader, "Fail-Safe Forced Vibration Testing of the Viking 1975 Developmental Spacecraft," - Shock and Vibration Bulletin No. 45, May 1975.

9. R. A. Buck and S. Barrett, Derivation of Revised Random Vibration Criteria for Viking Lander Capsule Components, VER-284, Martin Marietta Corporation, Denver, Colorado, April 1974.

10. Harold W. Bartel and Cecil W. Schneider, A Method for Predicting Acoustically Induced Vibration in Transport Aircraft, AFFDL-TR-74-74, Wright-Patterson Air Force Base, Ohio, September 1974.

11. Application Manual for the S/N Fatigue Life Gauge, Micro-Measurements, Inc., August 1966.

12. Cost, T. B., "Initial Report on Equivalent Damage Measurement by Utilizing S/N Fatigue Gauges," - Shock and Vibration Bulletin No. 39, Part 2, p. 35, February 1969.

13. Kana, D. D. and Vargas, L. M., "Prediction of Payload Vibration Environments by Mechanical Admittance Test Techniques," - AIAA Structures and Structural Dynamics Conference, May 1975.

14. Meyer, W. H. and Pierman, B. D., "Optimizing Subsystem Test Programs", - Proceedings Inst. Env. Sci., April 1974.

15. Roth, P., Detecting Sources of Vibration and Noise Using HP Fourier Analyzers - Application Note 140-1, published by Hewlett-Packard Corporation, January 1971.

16. Day, F. D. and Wada, B. K., "Unique Flight Instrumentation/Data Reduction Techniques Employed on the Viking Dynamic Simulator, " - Shock and Vibration Bulletin No. 45, Part II, February 1975.

17. Bendat, J. S. and Piersol, A. G., Random Data: Analysis and Measurement Procedures, Wiley, N.Y., 1971.

18. Enochson, L. D. and Otnes, R. K., Programming and Analysis for Digital Time Series Data, Shock and Vibration Monograph SVM-3, Shock and Vibration Center, Naval Research Lab, Washington, D.C., October 1968.

19. S. Barrett and B. D. Maytum, "The Development of Sine Vibration Test Requirements for Viking Lander Capsule Components", - Proceedings Inst. Env. Sci., April 1974.

20. W. R. Forlifer, "The Effects of Filter Bandwidth in Spectrum Analysis of Random Vibration", Shock and Vibration Bulletin No. 33, Part II, February 1964.

21. R. Bamford and M. Trubert, A Shock Spectra and Impedance Method to Determine a Bound for Spacecraft Structural Loads, JPL Report No. TM 336694, 1969.

22. Dynamics Analysis Branch, MSFC, Vibration, Shock and Acoustic Specifications for Skylab Components, IN-ASTN-AD-70-1, George C. Marshall Space Flight Center, Alabama, May 1972 (Revised).

23. N. F. Hunter, Jr. and J. V. Otts, "The Measurement of Mechanical Impedance and Its Use in Vibration Testing", Shock and Vibration Bulletin No. 42, Part 1, January 1972.

24. John D.Favour, Malcolm C. Mitchell and Norman L. Olson, "Transient Test Techniques for Mechanical Impedance and Modal Survey Testing", Shock and Vibration Bulletin No. 42, Part 1, January 1972.

25. S. Rubin and F. A. Biehl, Mechanical Impedance Approach to Engine Vibration Transmission Into an Aircraft Fuselage, SAE Pub. No. 670873, 1967.

26. Spectral Dynamics Corporation, The Measurement of Structural Transfer Functions and Mechanical Impedance, Technical Publication M-3 10-74, Spectral Dynamics Corporation, San Diego, California, 1972.

27. John D. Favour and Jay M. Lebrun, "Transient Waveform Control of Electromagnetic Test Equipment", The Shock and Vibration Bulletin No. 40, Part II, December 1969.

28. Piersol, A.C., and Maurer, J.R., Investigation of Statistical Techniques to Select Optimal Test Levels for Spacecraft Vibration Tests, Digitek Corporation, Report 10909801-FC, NASA CR-115778, May 1971.

29. Young, J. P., Cost Optimization of Spacecraft Test Levels, Proceedings Inst. Env. Sci., April 1974.

30. Barrett, R. E., Techniques for Predicting Localized Vibration Environments of Rocket Vehicles, NASA TND-1836, George C. Marshall Space Flight Center, Alabama, October 1963.

6.0 ABBREVIATIONS AND ACRONYMS

AVL	Acoustic/Vibration Laboratory
CF	Coherence function
cg	Center of gravity
cm	Centimeters
dB	Decibels
g	Acceleration due to gravity
GSFC	Goddard Space Flight Center
Hz	Hertz (cycles per second)
in	Inches
IRTCM	Integrated Real Time Contamination Monitor
JPL	Jet Propulsion Laboratory
kg	Kilograms
lb	Pounds
LDEF	Long Duration Exposure Facility
LDTM	Lander Dynamic Test Model
LST	Large Space Telescope
m	Meters
MMC	Martin Marietta Corporation
MSFC	Marshall Space Flight Center
N	Newtons
NASA	National Aeronautics and Space Administration
OWS	Orbital Workshop (Skylab)
PA	Payload Assembly (Skylab)
PD	Procurement document

PSD	Power Spectral Density
psi	Pounds per square inch
PTC	Proof Test Capsule
PTO	Proof Test Orbiter
rms	Root mean square
SAS	Solar Array System
SPL	Sound Pressure Level
VLC	Viking Lander Capsule

APPENDIX A

SHUTTLE PAYLOADS

A-1.0 INTRODUCTION

Appendix A is a summary of information gained as the result of the survey discussed in Section 1.0. Table A-1 and Figures A-1 through A-13 describe payloads which will be carried on the first eleven flights. Data for later payloads are listed in Table A-2 (automated payloads) and Table A-3 (sortie payloads).

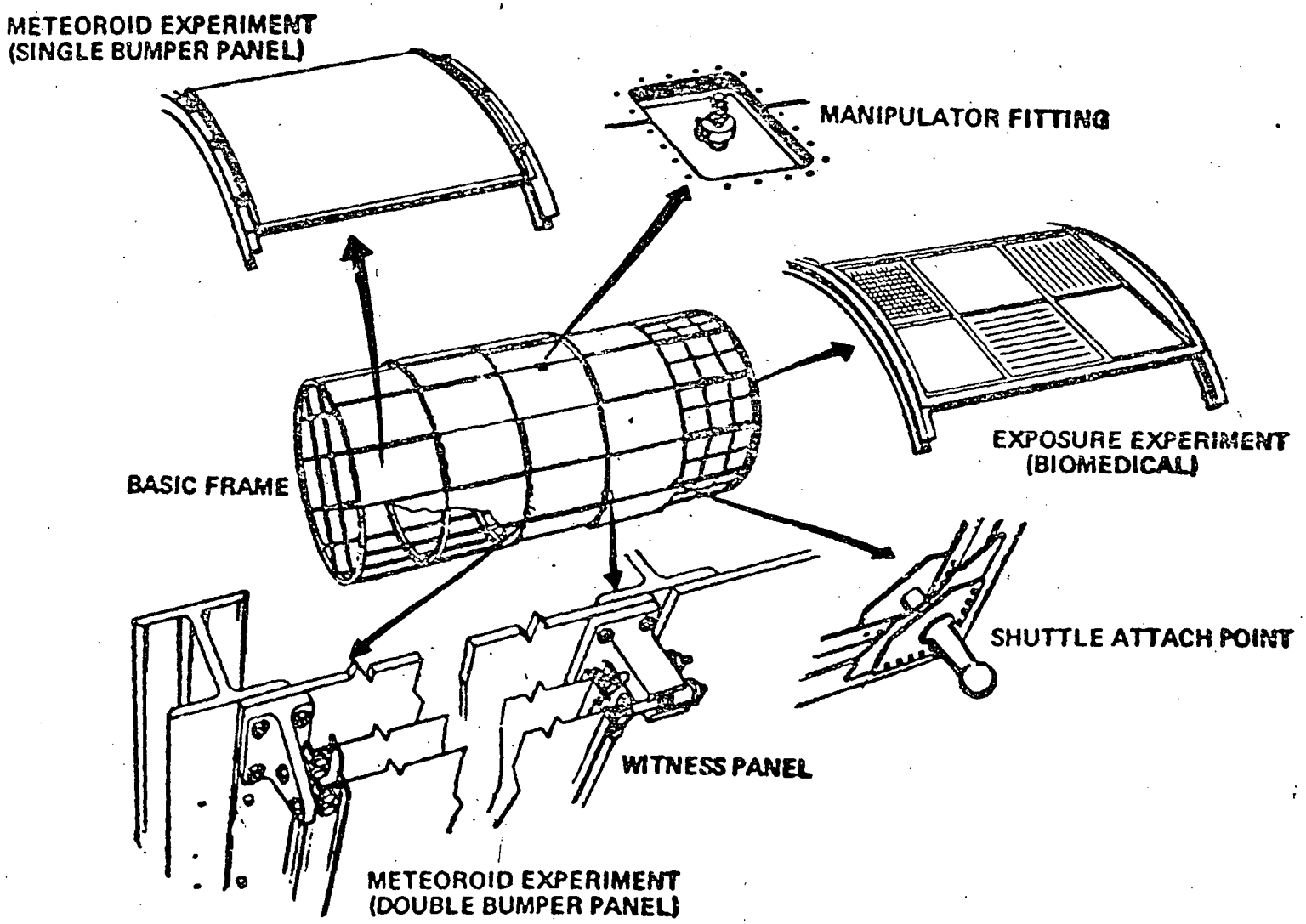

Figure A-1 Long Duration Exposure Facility

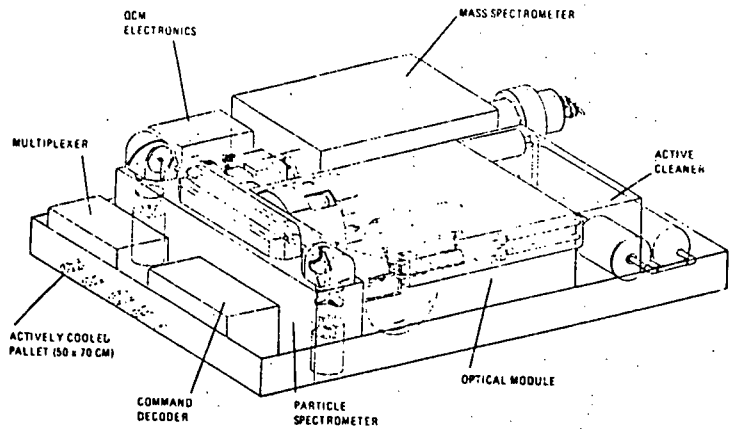

INTEGRATED REAL-TIME CONTAMINATION MONITOR (IRTCM)

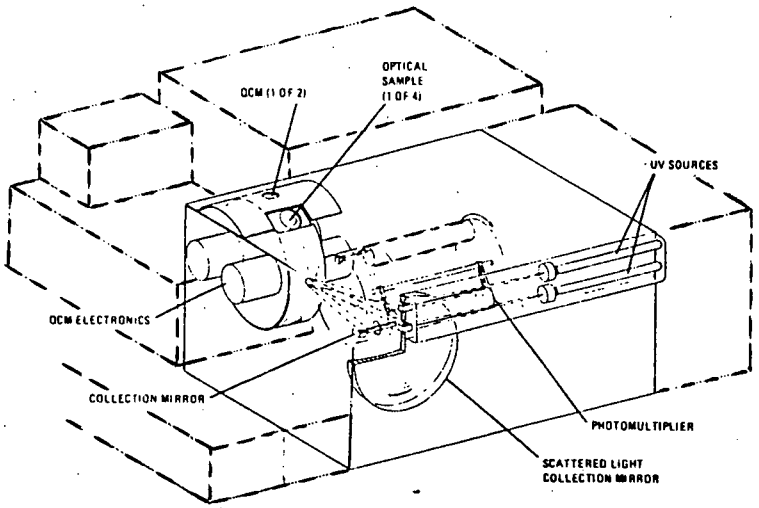

ST246 OPTICAL EFFECTS MODULE

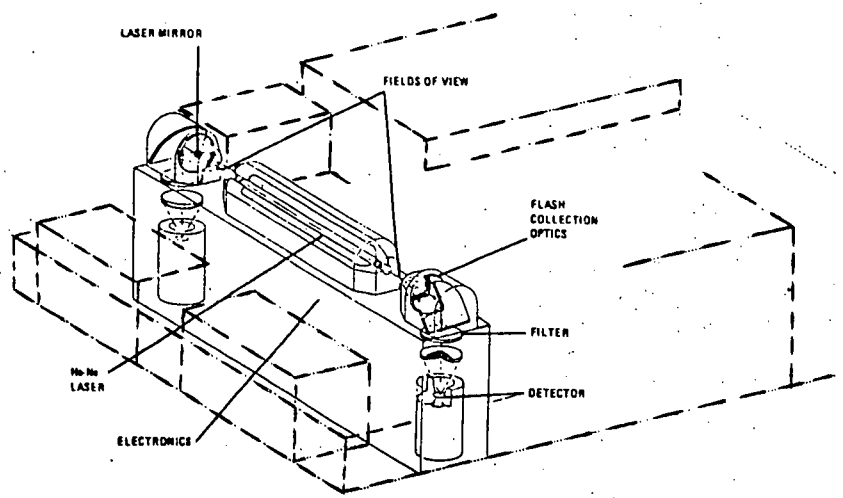

ST247 PARTICLE SPECTROMETER

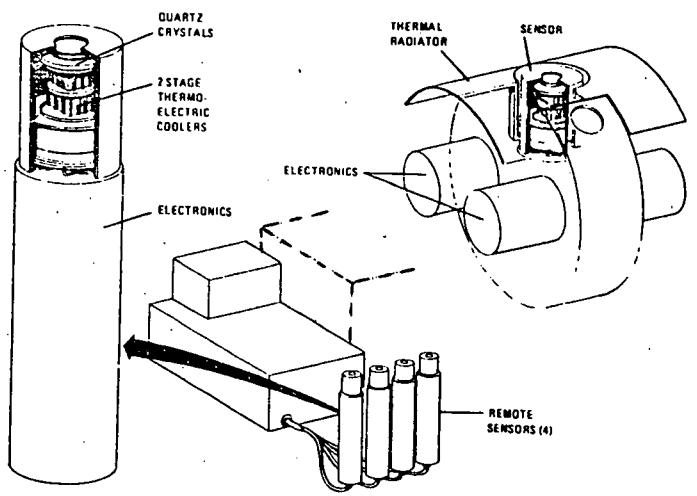

ST249 QUARTZ CRYSTAL MICROBALANCE

NOTE: STOWED AND DEPLOYED CONFIGURATIONS SHOWN, WHERE APPLICABLE.

Figure A-2 Sketches of IRTCM, ST 246, ST 247 and ST 249 Experiments

MISSION #4 - SHUTTLE VERIFICATION
- DEPLOY LDEF
- IRTCM TESTS

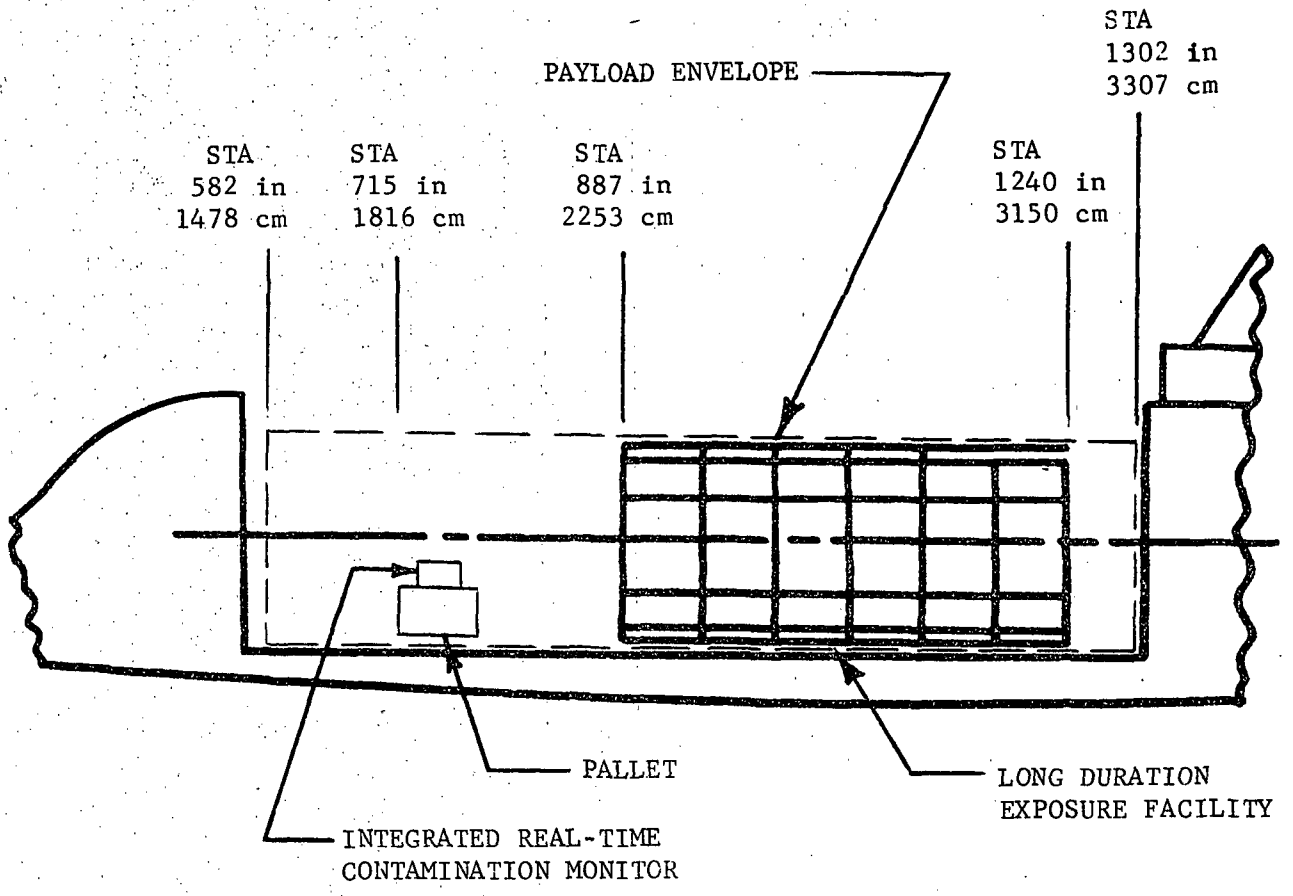

Figure A-3 Payload Configuration - Mission 4

MISSION #5 - SHUTTLE VERIFICATION

- DEPLOY COSMIC BACKGROUND EXPLORER
- CARRY-ON SCIENTIFIC EXPERIMENTS

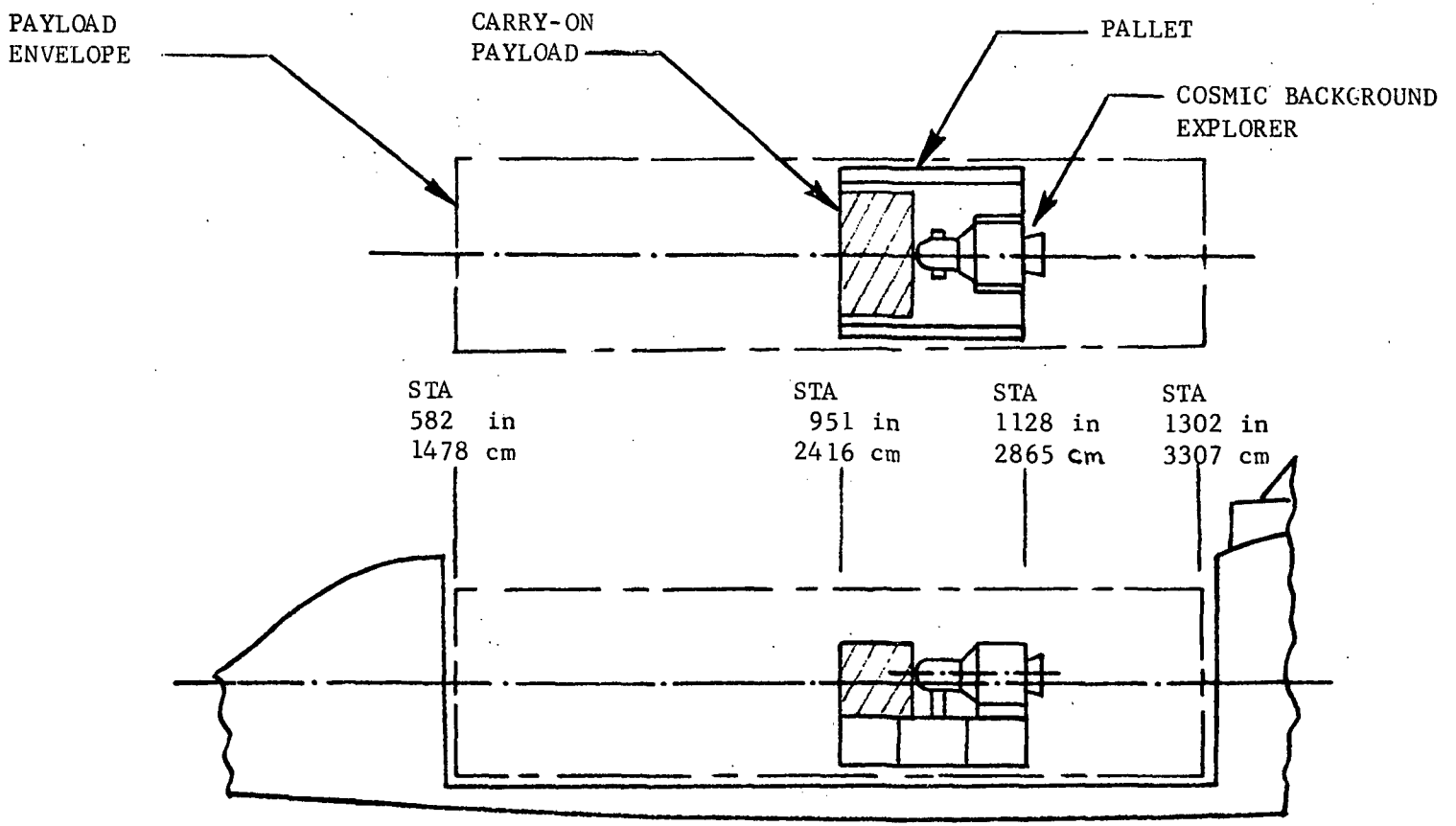

Figure A-4 Payload Configuration - Mission 5

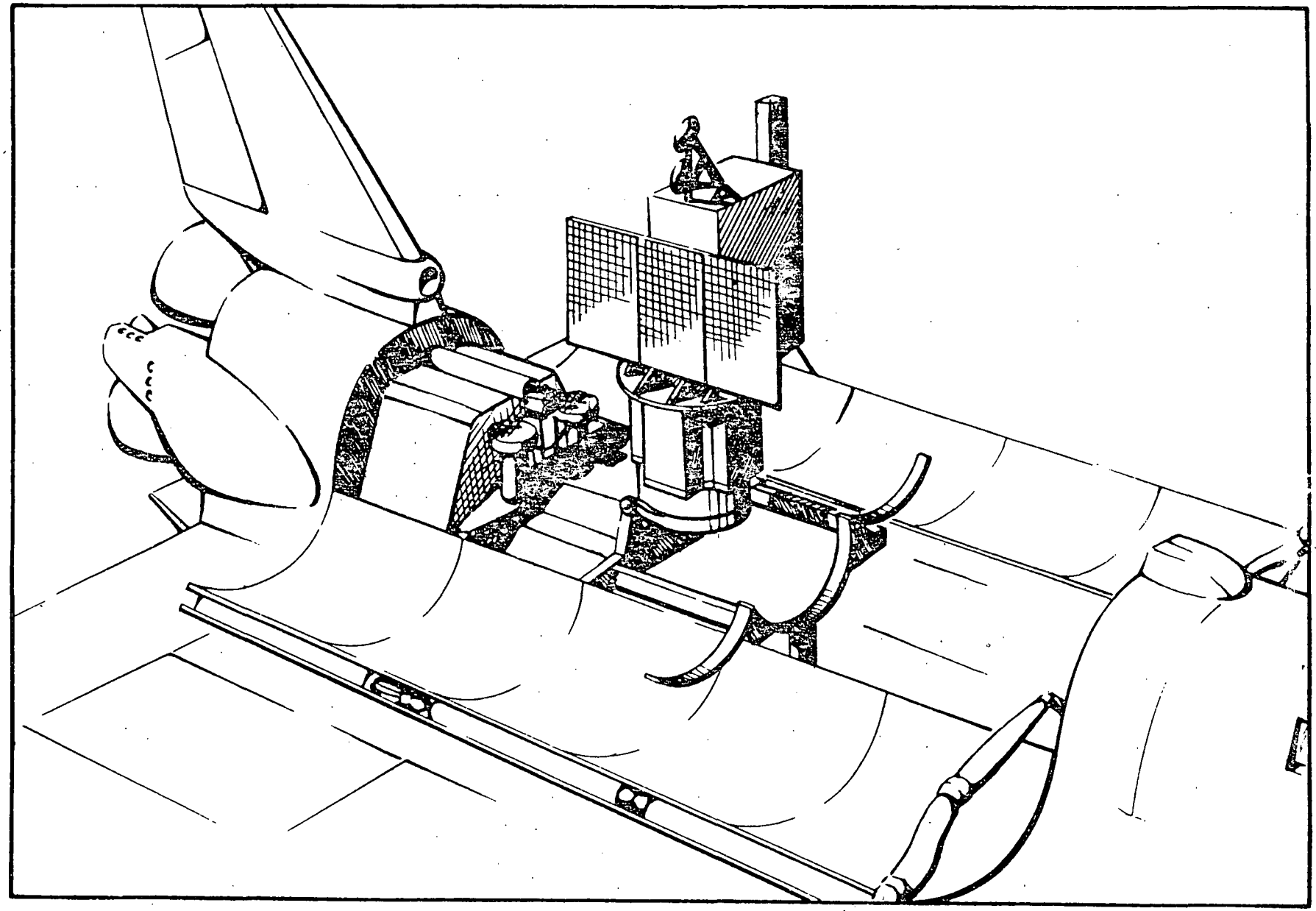

Figure A-5. Earth Observation Satellite - Checkout and Servicing Configuration

MISSION #6 — EOS CHECKOUT FLIGHT

— SPACE PROCESSING EXPERIMENT

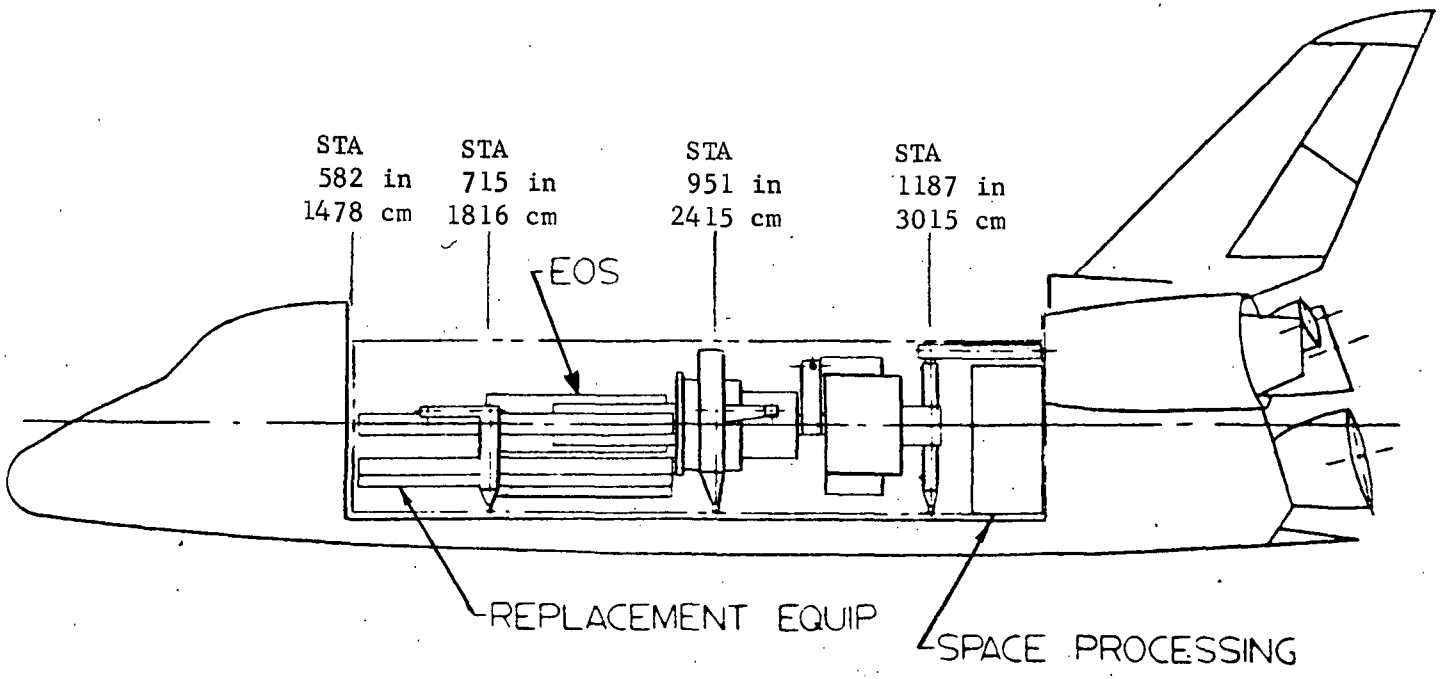

Figure A-6 Payload Configuration - Mission 6

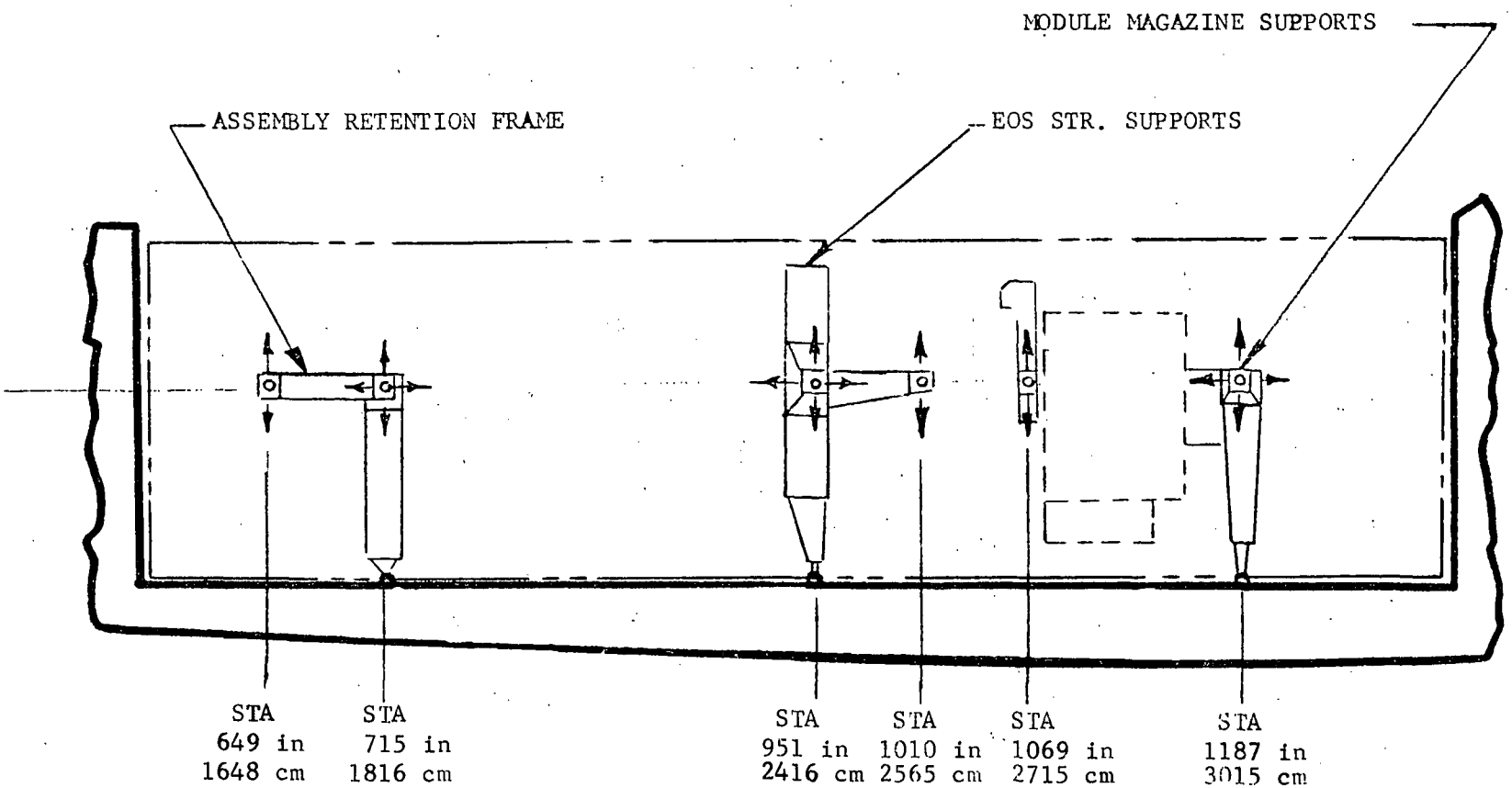

Figure A-7 EOS Structural Supports

MISSION # 7 – SPACELAB # 1 : COMBINED NASA/ESRO

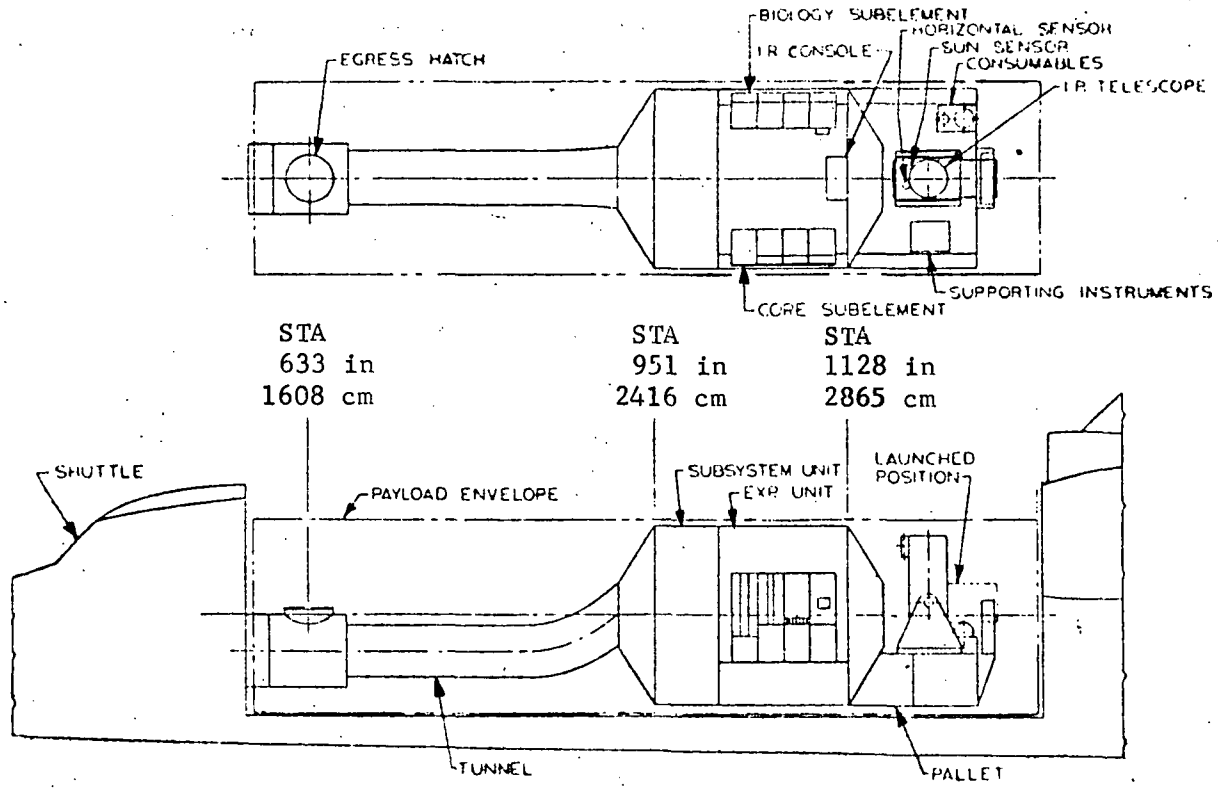

Figure A-8 Payload Configuration - Mission 7

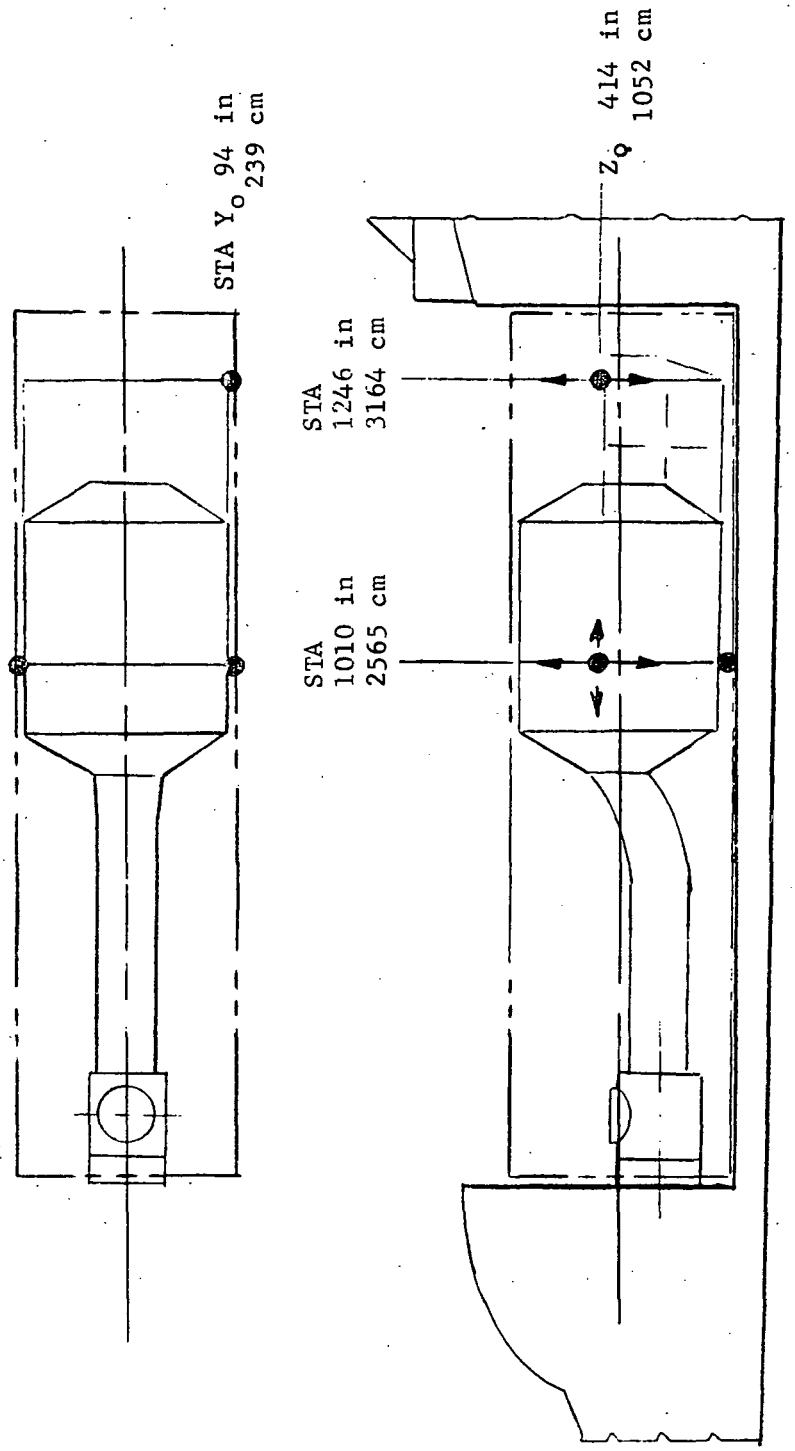

Figure A-9 Payload Structural Supports - Mission 7

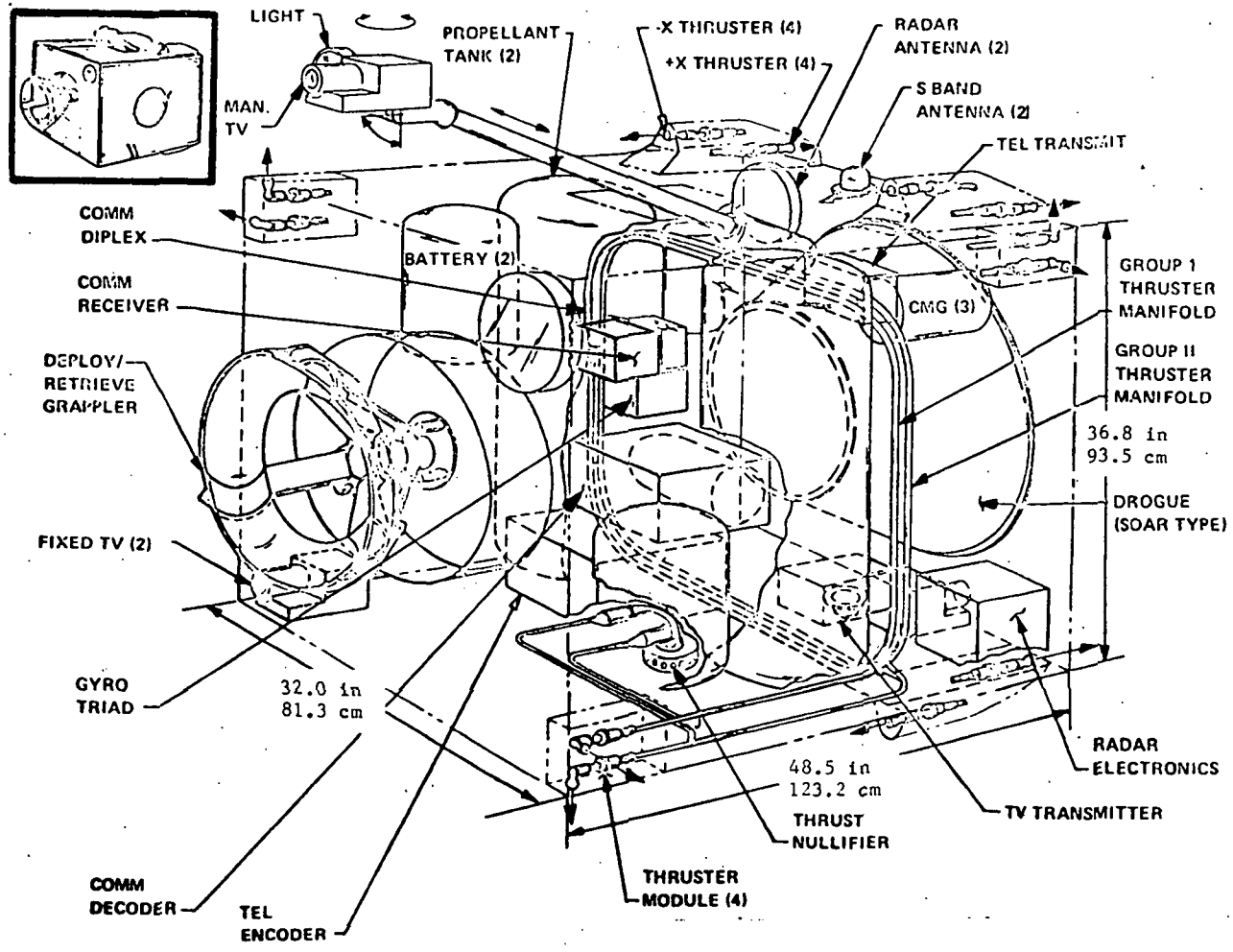

Figure A-10 Experimental Free-Flying Teleoperator Spacecraft

MISSION #8 - DEPLOY BIOMEDICAL EXPERIMENT
SCIENTIFIC SATELLITE #1

- DEPLOY TWO MINILAGEOS.
- CHECKOUT FREE FLYING TELEOPERATOR
- RETRIEVE LONG DURATION EXPOSURE FACILITY

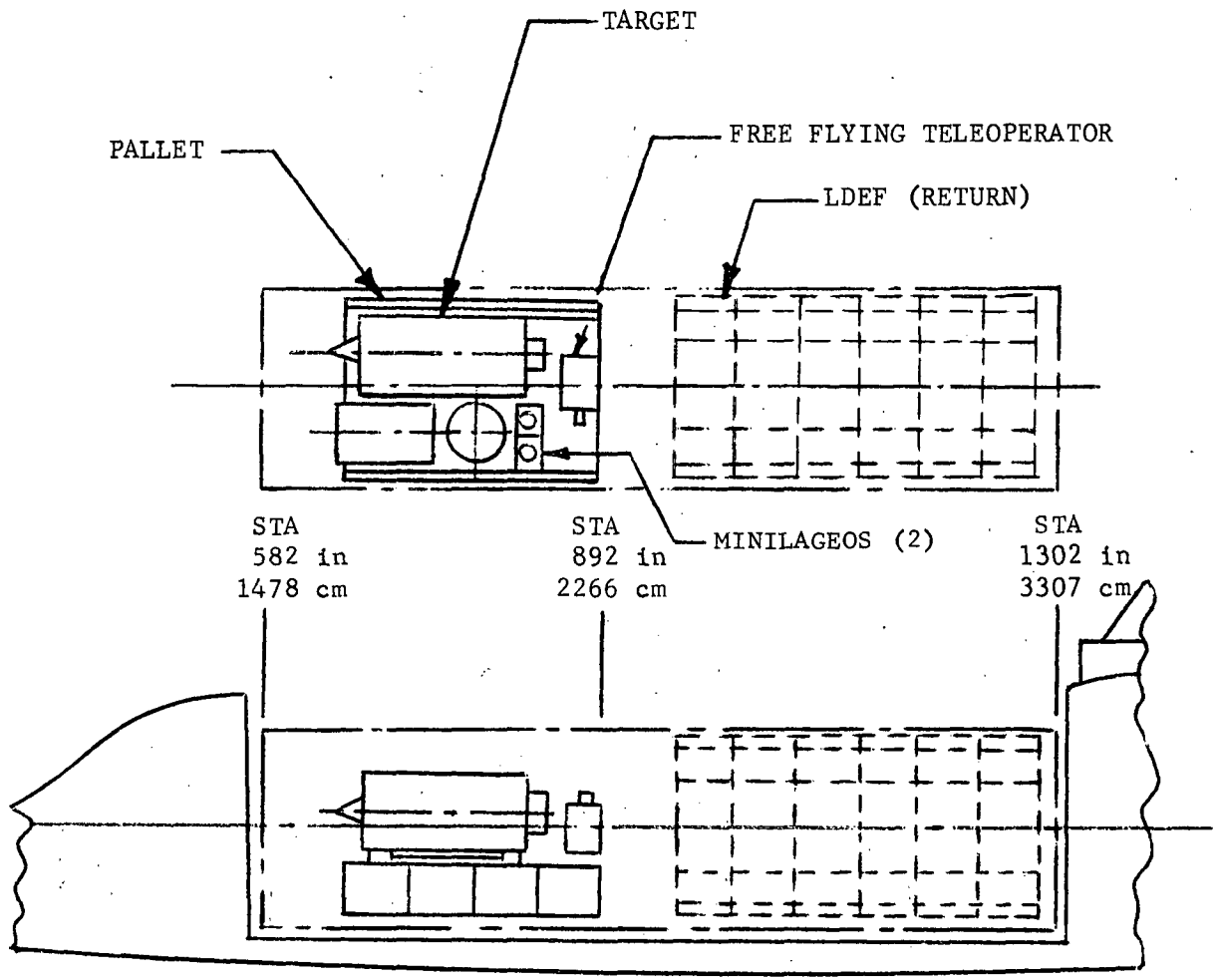

Figure A-11 Payload Configuration - Mission 8

MISSION # 9 – PALLET ONLY: HIGH ENERGY ASTROPHYSICS

– RETRIEVE: SOLAR PHYSICS SATELLITE

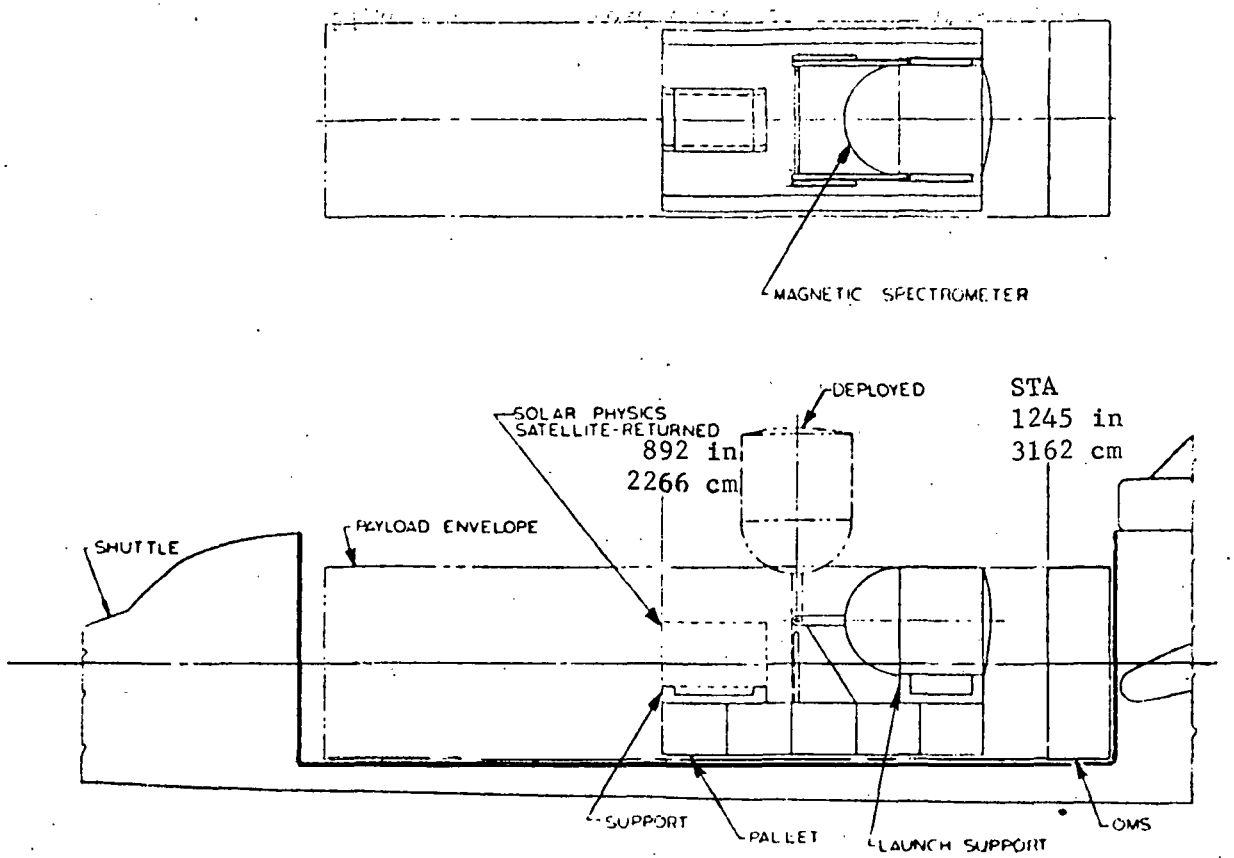

Figure A-12 Payload Configuration - Mission 9

MISSION #11 – SPACELAB # 1: SPACE TECHNOLOGY LAB

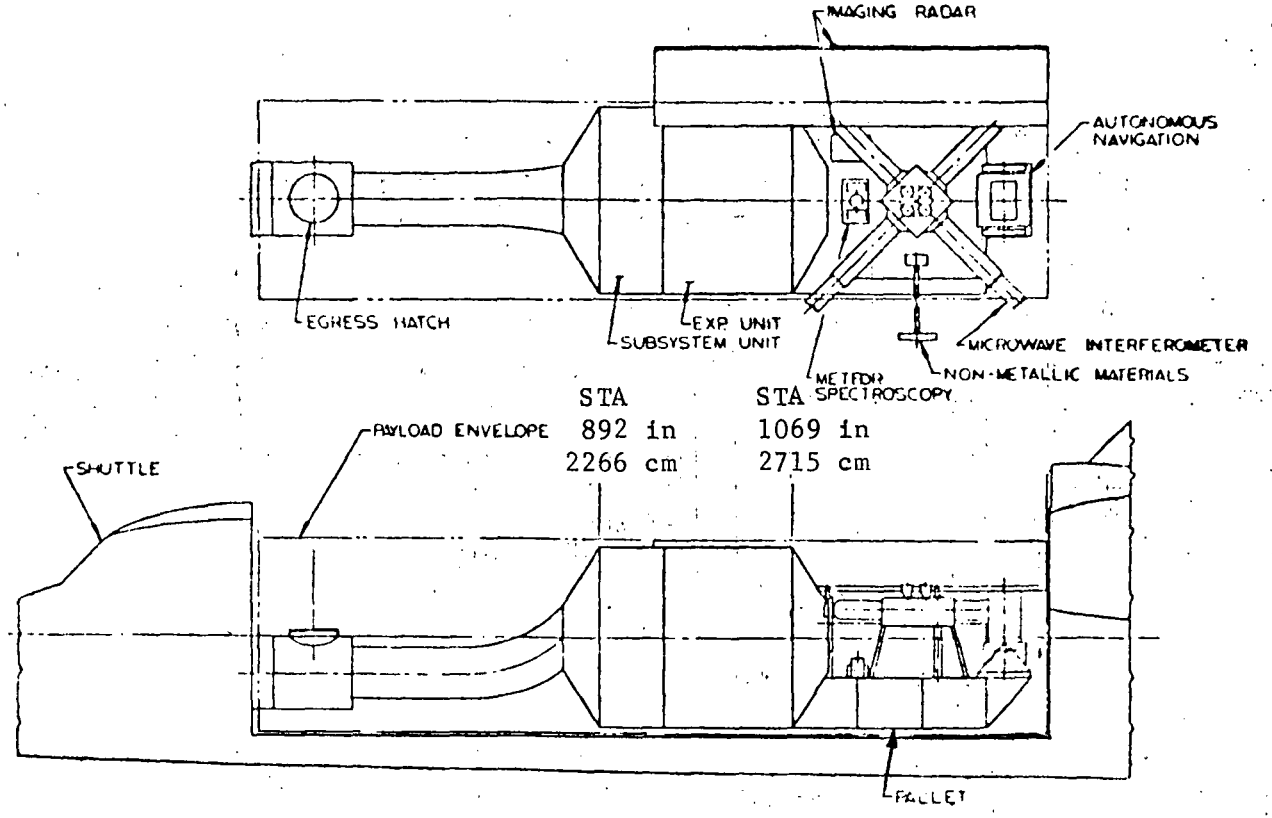

Figure A-13 Payload Configuration - Mission 11

TABLE A-1 PAYLOADS FOR INITIAL FLIGHTS

MISSION NUMBER	PAYLOAD	WEIGHT Kg (lb)		C.G. LOCATION Meters (Feet)						FIGURE REF.
				LAUNCH			LANDING			
		LAUNCH	LANDING	X	Y	Z	X	Y	Z	
1	None									
2	None									
3	None									
4	a) LDEF (ST-01-A)	3856 (8500)	0							A-1
	b) Three IRTCM's (ST-08-S)	159 (351)	159 (351)							A-2
	c) Pallet & Support Structure	421 (928)	421 (928)							A-3
	Total Payload	4436 (9779)	580 (1279)	11.46 (37.6)	0	0	5.24 (17.2)	0	0.34 (1.1)	
5	a) CBE (AS-03-A)	621 (1370)								
	b) Control & Display Plus Cabling	181 (400)	181 (400)							A-4
	c) Carry-On Payload (TBD)	1134 (2500)	1134 (2500)							
	d) Pallet & Support Structure	691 (1523)	691 (1523)							
	Total Payload	2628 (5793)	2006 (4423)	10.7 (35.0)	0	-0.64 (-2.1)	9.78 (32.1)	0	-0.88 (-2.9)	

TABLE A-1 Continued

MISSION NUMBER	PAYLOAD	WEIGHT Kg (lb)		C.G. LOCATION Meters (Feet)						FIGURE REF.
				LAUNCH			LANDING			
		LAUNCH	LANDING	X	Y	Z	X	Y	Z	
6	a) EOS (EO-08-A)	2948 (6500)	2948 (6500)							A-5 A-6 A-7
	b) Control & Display Plus Cabling	204 (450)	204 (450)							
	c) Flight Support System	1588 (3500)	1588 (3500)							
	d) Spares	2722 (6000)	2722 (6000)							
	e) Space Processing	3885 (8564)	3885 (8564)							
	f) Attmt. Structure	408 (900)	408 (900)							
	Total Payload	11755 (25914)	11755 (25914)	12.56 (41.2)	-0.009 (-.03)	-0.274 (-0.9)	12.56 (41.2)	-0.009 (-.03)	-0.274 (-0.9)	
7	a) Spacelab (SP-001 SP-005)	5199 (11462)	5178 (11415)							A-8 A-9
	b) Egress Hatch/ Rescue System	470 (1037)	470 (1037)							
	c) Tunnel	562 (1238)	562 (1238)							

TABLE A-1 Continued

MISSION NUMBER	PAYLOAD	WEIGHT Kg (lb)		C.G. LOCATION Meters (Feet)						FIGURE REF.
				LAUNCH			LANDING			
		LAUNCH	LANDING	X	Y	Z	X	Y	Z	
7 continued	d) Two P/L Specialists	515 (1135)	515 (1135)							
	e) Power Kit	717 (1580)	319 (704)							
	f) Control & Display Plus Cabling	227 (500)	227 (500)							
	g) Special Electronics	515 (1136)	515 (1136)							
	h) Attmt. Structure	161 (354)	161 (354)							
	i) Research Equipt.	2292 (5054)	2292 (5054)							
	Total Payload	10601 (23385)	10189 (22462)	9.63 (31.6)	0.021 (.07)	-0.73 (-2.4)	9.75 (32.0)	0.024 (.08)	-0.64 (-2.1)	
8	a) BESS #1 (LS-02-A)	680 (1500)	0							A-11
	b) Attmt. Structure	394 (869)	394 (869)							
	c) Pallet	724 (1596)	724 (1596)							

TABLE A-1 Continued

MISSION NUMBER	PAYLOAD	WEIGHT Kg (lb)		C.G. LOCATION Meters (Feet)						FIGURE REF.
				LAUNCH			LANDING			
		LAUNCH	LANDING	X	Y	Z	X	Y	Z	
8 continued	d) Spin Table	22.7 (50)	22.7 (50)							
	e) Two Mini-Lageos (OP-03-A)	204 (450)	0							
	f) FFTO + (LS-04-S)	362 (797)	362 (797)							
	g) FFTO Targets	1043 (2300)	1043 (2300)							
	h) Consumables	83 (183)	50 (110)							
	i) LDEF (ST-01-A) - Retrieved	0	3856 (8500)							A-11
	Total Payload	3513 (7745)	6451 (14222)	4.47 (14.67)	-0.046 (-.15)	-0.082 (-.27)	10.1 (33.0)	0.101 (0.33)	0	
9	a) High Energy Astrophysics #1									A-12
	(i) Mag. Spectrometer	3550 (7826)	3550 (7826)							
	(ii) Consumables	288 (634)	288 (634)							

TABLE A-1 Continued

MISSION NUMBER	PAYLOAD	WEIGHT Kg (lb)		C.G. LOCATION Meters (Feet)						FIGURE REF.
				LAUNCH			LANDING			
		LAUNCH	LANDING	X	Y	Z	X	Y	Z	
9 continued	b) Pallet	905 (1995)	905 (1995)							
	c) Control & Display + Cabling + Electronics	680 (1500)	680 (1500)							
	d) P/L Specialist Rescue Equipment	247 (544)	247 (544)							
	e) Power Kit	717 (1580)	319 (704)							
	f) Attmt. Structure	340 (750)	340 (750)							
	g) OMS Kit	1160 (2557)	1160 (2557)							
	h) Solar Physics Satellite - Retrieved	0	1336 (2945)							
	Total Payload	7886 (17386)	8825 (19455)	10.58 (34.7)	0.043 (0.14)	0.082 (0.27)	11.89 (39.0)	0.037 (0.12)	0.037 (0.12)	
10	DOD Mission - TBD									
11	a) Spacelab	5380 (11861)	5359 (11814)							A-13

TABLE A-1 Continued

MISSION NUMBER	PAYLOAD	WEIGHT Kg (Lbs)		C.G. LOCATION Meters (Feet)						FIGURE REF.
				LAUNCH			LANDING			
		LAUNCH	LANDING	X	Y	Z	X	Y	Z	
11 continued	b) Tunnel	508 (1120)	508 (1120)							
	c) Egress Hatch	486 (1011)	486 (1011)							
	d) One P/L Specialist	235 (518)	235 (518)							
	e) Power Kit	717 (1580)	319 (704)							
	f) Control & Display Plus Cabling	499 (1100)	499 (1100)							
	g) Attmt. Structure	454 (1000)	454 (1000)							
	h) Research Equipt.	1898 (4185)	1898 (4185)							
	Total Payload	10149 (22375)	9731 (21452)	9.54 (31.3)	0.09 (0.3)	0.61 (2.0)	9.63 (31.6)	0.098 (0.32)	0.55 (1.8)	

Table A-2 Automated Payloads

AUTOMATED PAYLOADS Source: Summarized NASA Payload Descriptions Automated Payloads Level A Data July 1974	PHYSICAL CHARACTERISTICS						MISSIONS		
	LAUNCH WEIGHT		MAXIMUM DIAMETER		LENGTH		DELIVERY	RETRIEVAL	SERVICE
	Kg	(lbs)	m	(Ft)	m	(Ft)			
ASTRONOMY									
AS-01-A — Large Space Telescope	11340	25005	4.0	13.12	12.9	42.3	3	2	9
AS-02-A — Extra Coronal Lyman Alpha Explorer	595	1312	1.83	6.0	4.06	13.32	6		
AS-03-A — Cosmic Background Explorer	595	1312	1.83	6.0	3.13	10.27	7		
AS-05-A — Advanced Radio Explorer	1199	2644	1.83	6.0	2.46	8.07	4		
AS-07-A — 3m Ambient Temperature IR Telescope	8594	18950	4.57	15.0	12.22	40.1	3	2	6
AS-11-A — 1.5m IR Telescope	6045	13329	4.57	15.0	5.22	17.13	4	3	32
AS-13-A — UV Survey Telescope	T.B.D.		T.B.D.		T.B.D		6	6	
AS-14-A — 1.0m UV-Optical Telescope	4001	8822	4.57	15.0	5.29	17.36	4	3	7
AS-16-A — Large Radio Observatory Array (LROA)	1300	2867	3.34	10.96	5.18	17.0	1		3
AS-17-A — 30m IR Interferometer	3490	7695	4.57	15.0	17.03	55.9	2	2	2
HIGH ENERGY ASTROPHYSICS									
HE-01-A — Large X-Ray Telescope Facility	11869	26171	4.57	15.0	16.0	52.5	1	1	2
HE-03-A — Extended X-Ray Survey	8011	17664	4.57	15.0	5.72	18.8	1	1	2
HE-05-A — High Latitude Cosmic Ray Survey	7062	15572	4.57	15.0	9.15	30.0	1		
HE-07-A — Small High Energy Satellite	594.6	1311	1.83	6.0	2.63	8.63	6		
HE-08-A — Large High Energy Observatory A (Gamma Ray)	8700	19184	4.57	15.0	5.22	17.1	1	1	2
HE-09-A — Large High Energy Observatory B (Magnetic Spectrometer)	6255	13792	4.57	15.0	5.5	18.0	1		
HE-10-A — Large High Energy Observatory C (Nuclear Calorimeter)	5336	11766	4.57	15.0	5.5	18.0	1	1	1
HE-11-A — Large High Energy Observatory D (1.2m X-Ray Telescope)	6771	14930	4.57	15.0	10.22	33.5	2	1	2
HE-12-A — Cosmic Ray Laboratory	10332	22782	4.57	15.0	8.54	28.0	1		4
SOLAR PHYSICS									
SO-02-A — Large Solar Observatory	9825	21664	4.57	15.0	17.7	58.1	1		6
SO-03-A — Solar Maximum Mission	760.8	1678	1.52	5.0	3.19	10.5	6	6	

Table A-2 Continued

AUTOMATED PAYLOADS Source: Summarized NASA Payload Descriptions Automated Payloads Level A Data July 1974	PHYSICAL CHARACTERISTICS						MISSIONS		
	LAUNCH WEIGHT		MAXIMUM DIAMETER		LENGTH		DELIVERY	RETRIEVAL	SERVICE
	Kg	(lbs)	m	(ft)	m	(ft)			
ATMOSPHERIC AND SPACE PHYSICS									
AP-10-A — Upper Atmosphere Explorer	908.8	2004	1.37	4.49	2.36	7.74	4		
AP-02-A — Medium Altitude Explorer	271.8	599	1.37	4.49	1.83	6.0	4		
AP-03-A — High Altitude Explorer	426.6	941	1.22	4.0	1.83	6.0	6		
AP-04-A — Gravity and Relativity Satellite - LEO	600	1323	2.68	8.79	3.58	11.7	2		
AP-05-A — Environmental Perturbation Satellite - Mission A	1488	3281	2.1	6.89	3.7	12.1	2		
AP-06-A — Gravity and Relativity Satellite - Solar	349	770	2.6	8.53	2.1	6.89	2		
AP-07-A — Environmental Perturbation Satellite - Mission B	3946	8701	3.0	9.84	4.6	15.1	2		
AP-08-A — Heliocentric and Interstellar Spacecraft	280	617	3.0	9.84	3.0	9.84	1		
EARTH OBSERVATIONS									
EO-07-A — Advanced Synchronous Meteorological Satellite	1006	2218	4.24	13.9	2.91	9.55	1		
EO-08-A — Earth Observatory Satellite	3475	7662	3.05	10.0	11	36.1	9	6	10
EO-09-A — Synchronous Earth Observatory Satellite	1531	3376	4.3	14.1	5.2	17.1	9		
EO-10-A — Applications Explorer (Special Purpose Satellite)	140.7	310	0.87	2.85	1.06	3.48	16		
EO-12-A — TIROS 'O'	2150	4741	3.05	10.0	4.06	13.3	2	2	
EO-56-A — Environmental Monitoring Satellite	2204	4860	3.05	10.0	3.72	12.2	9		
EO-57-A — Foreign Synchronous Meteorological Satellite	256.8	566	1.91	6.27	3.14	10.3	6		
EO-58-A — Geosynchronous Operational Meteorological Satellite	256.8	566	1.91	6.27	3.14	10.3	9		
EO-59-A — Geosynchronous Earth Resources Satellite	1531	337 6	4.3	14.1	5.2	17.1	4		
EO-61-A — Earth Resources Survey Operational Satellite	732.9	1614	1.52	4.99	3.05	10.0	13		
EO-62-A — Foreign Synchronous Earth Observatory Satellite	1531	3376	4.3	14.1	5.2	17.1	4		

Table A-2 Continued

AUTOMATED PAYLOADS Source: Summarized NASA Payload Descriptions Automated Payloads Level A Data July 1974	PHYSICAL CHARACTERISTICS						MISSIONS		
	LAUNCH WEIGHT		MAXIMUM DIAMETER		LENGTH		DELIVERY	RETRIEVAL	SERVICE
	Kg	(lbs)	m	(ft)	m	(ft)			
EARTH AND OCEAN PHYSICS									
OP-01-A — GEOPAUSE	789	1740	2.0	6.56	2.5	8.2	2		
OP-02-A — Gravity Gadiometer	3277	7226	4.0	13.1	4.6	15.1	1		
OP-03-A — Mini-LAGEOS	204	450	0.5(1)	1.6	N/A	N/A	6		
OP-04-A — GRAVSAT	3086	6805	2 (1)	6.56	2.7(1)	8.9	1		
OP-05-A — Vector Magnetometer Satellite	140.7	310	1.32	4.33	3.97	13.0	9		
OP-06-A — Magnetic Field Monitor Satellite	200.1	441	1.32	4.33	3.97	13.0	3		
OP-07-A — SEASAT - B	940	2073	3.96	13.0	4.57	15.0	1		
OP-51-A — Global Earth & Ocean Monitor System	T.B.D.		T.B.D		T.B.D		9		
SPACE PROCESSING APPLICATIONS									
SP-01-A — Space Processing Free-Flyer	6059	13360	4.27	14.0	3.44	11.3	TBD		
LIFE SCIENCES									
LS-02-A — Biomedical Experiment Scientific Satellite	1814	4000	3.66	12.0	2.90	9.51	24	23	
SPACE TECHNOLOGY									
ST-01-A — Long Duration Exposure Facility	3856	8502	4.32	14.2	9.25	30.3	6	6	

(1) Per Satellite 2 Per Flight

Table A-2 Continued

AUTOMATED PAYLOADS Source: Summarized NASA Payload Descriptions Automated Payloads Level A Data July 1974	PHYSICAL CHARACTERISTICS						MISSIONS		
	LAUNCH WEIGHT		MAXIMUM DIAMETER		LENGTH		DELIVERY	RETRIEVAL	SERVICE
	Kg	(lbs)	m	(ft)	m	(ft)			
PLANETARY									
PL-01-A — Mars Surface Sample Return	4795	10573	4.3	14.1	7.3	24.0	2		
PL-02-A — Mars Satellite Sample Return	8402	18526	4.57	15.0	7.6	24.9	2		
PL-03-A — Pioneer Venus Multiprobe	769	1696	2.54	8.33	2.03	6.66	5		
PL-07-A — Venus Orbital Imaging Radar	3770	8313	3.	9.84	5.6	18.4	2		
PL-08-A — Venus Buoyancy Probe	7429	16381	4.57	15.0	3.5	11.5	2		
PL-09-A — Mercury Orbiter	3125	6891	4.57	15.0	7.6	24.9	2		
PL-10-A — Venus Large Lander	1690	3726	4.57	15.0	5.0	16.4	2		
PL-11-A — Pioneer Saturn/Uranus Flyby	477	1052	2.74	9.0	3.1	10.2	1		
PL-12-A — Mariner Jupiter Orbiter	1600	3528	3.65	12.0	5.8	19.0	2		
PL-13-A — Pioneer Jupiter Probe	477	1052	2.74	9.0	3.1	10.2	2		
PL-14-A — Saturn Orbiter	1286	2836	4.57	15.0	3.0	9.84	2		
PL-15-A — Uranus Probe/Neptune Flyby	815	1797	4.57	15.0	6.4	21.0	2		
PL-16-A — Ganymede Orbiter/Lander	4000	8820	4.57	15.0	7.6	24.9	2		
PL-18-A — Encke Rendezvous	2390	5270	4.57	15.0	6.17	20.2	2		
PL-19-A — Halley Comet Flyby	580	1279	3.0	9.84	3.0	9.84	1		
PL-20-A — Asteroid Rendezvous	2160	4763	3.1	10.2	5.0	16.4	2		
PL-22-A — Pioneer Saturn Probe	477	1052	2.74	9.0	3.1	10.2	1		

Table A-2 Continued

AUTOMATED PAYLOADS Source: Summarized NASA Payload Descriptions Automated Payloads Level A Data July 1974	PHYSICAL CHARACTERISTICS						MISSIONS		
	LAUNCH WEIGHT		MAXIMUM DIAMETER		LENGTH		DELIVERY	RETRIEVAL	SERVICE
	Kg	(lbs)	m	(ft)	m	(ft)			
COMMUNICATIONS/NAVIGATION									
CN-51-A — INTELSAT	1472	3246	2.5	8.2	2.7	8.86	21		
CN-52-A — U.S. DOMSAT 'A'	261.5	577	2.2	7.22	3.2	10.5	7		
CN-53-A — U.S. DOMSAT 'B'	1472	3246	2.5	8.2	2.7	8.86	14		
CN-54-A — Disaster Warning Satellite	582.9	1299	1.4	4.59	5.12	16.8	4		
CN-55-A — Traffic Management Satellite	298.5	658	3.88	12.7	1.58	5.18	11		
CN-56-A — Foreign Communications Satellite A	307.9	679	1.6	5.25	2.36	7.74	4		
CN-58-A — U.S. DOMSAT 'C'	867.7	1913	2.18	7.15	3.69	12.1	6		
CN-59-A — Communications R&D/Prototype Satellite	956.3	2109	3.4	11.2	6.0	19.7	3		
CN-60-A — Foreign Communications Satellite B	331.9	732	2.2	7.22	3.2	10.5	7		
LUNAR									
LU-01-A — Lunar Orbiter	839	1850	2.03	6.66	4.77	15.7	2		
LU-02-A — Lunar Rover	1380	3043	3.23	10.6	4.94	16.2	2		
LU-03-A — Lunar Halo Satellite	1120	2470	2.33	7.64	5.1	16.7	1		
LU-04-A — Lunar Sample Return	2665	5876	3.23	10.6	4.94	16.2	2		

Table A-3 Sortie Payloads

SORTIE PAYLOADS Source: Summarized NASA Payload Descriptions Sortie Payloads Level A Data July 1974 and Level B Data	PHYSICAL CHARACTERISTICS						NUMBERS OF MISSIONS
	LAUNCH WEIGHT		MAXIMUM DIAMETER		ESTIMATED PALLET LENGTH		
	Kg	(lbs)	m	(ft)	m	(ft)	
ASTRONOMY							
AS-01-S — 1.5m Cryogenically-Cooled IR Telescope	3296	7268	2.4	7.87	4.57	15.0	15
AS-03-S — Deep Sky UV Survey Telescope	3774	8322	2.2	7.22	6.0	19.7	8
AS-04-S — 1m Diffraction Limited UV Optical Telescope	1836	4048	3.74	12.3	4.0	13.1	23
AS-05-S — Very Wide Field Galactic Camera	70	154	1.0	3.28	1.0	3.28	2
AS-06-S — Calibration of Astronomical Fluxes	2190	4829			4.1	13.5	2
AS-07-S — Cometary Simulation	19294	42543			13.72	45.0	2
AS-08-S — Multipurpose 0.5m Telescope	554	1222			1.5	4.92	156
AS-09-S — 30m IR Interferometer	2601	5735			16.6(1)	54.5	1
AS-10-S — Adv. XUV Telescope	425.5	938			1	3.28	6
AS-11-S — Polarimetric Experiments	251.5	555			1.52	4.99	1
AS-12-S — Meteoroid Simulation	2289	5047			6.1	20.0	2
AS-13-S — Solar Variation Photometer	20	44.1			0.05	0.16	312
AS-14-S — 1.0m Uncooled IR Telescope	1545	3407			3	9.84	4
AS-15-S — 3.0m Ambient Temperature IR Telescope	5326	11744	3.7	12.1	11(1)	36.1	11
AS-18-S — 1.5 km IR Interferometer	5864	12930			9.15	30.0	4
AS-19-S — Selected Area Deep Sky Survey Telescope	1000	2205			3	9.84	16
AS-20-S — 2.5m Cryogenically cooled IR Telescope	4378	9653			4.6	15.1	3
AS-31-S — Combined AS-01, -03, -04, -05-S	8009	17660			11.8	38.7	19
AS-41-S — Schwartzschild Camera	161.5	356			2.8	9.19	4
AS-42-S — FAR UV Electronographic Schmidt Camera/Spectrograph	160	353			1.38	4.5	6
AS-43-S — UCB Black Brant Payload	291	642			0.5	1.64	5
AS-44-S — XUV Concentrator/Detector	133	293			1	3.28	3
AS-45-S — Proportional Counter Array	62	137			1.6	5.25	5
AS-46-S — Wisconsin UV Photometry Experiment	98.1	216			1	3.28	8
AS-47-S — Attached Far IR Spectrometer.	170	375			1	3.28	3

Table A-3 Continued

SORTIE PAYLOADS Source: Summarized NASA Payload Descriptions Sortie Payloads Level A Data July 1974 & Level B Data	PHYSICAL CHARACTERISTICS						NUMBERS OF MISSIONS
	LAUNCH WEIGHT		MAXIMUM DIAMETER		ESTIMATED PALLET LENGTH		
	Kg	(lbs)	m	(ft)	m	(ft)	
AS-48-S — Aries/Shuttle UV Telescope	461.5	1018			3	9.84	15
AS-49-S — First UCB Black Brant Payload	273	602			0.5	1.64	1
AS-50-S — Combined UV/XUV Measurements (AS-04-S, 10-S)	2971	6551			5	16.4	3
AS-51-S — Combined IR Payload (AS-01-S, 15-S)	9186	20255			15.6(1)	51.2	4
AS-54-S — Combined UV Payload (AS-03-S, 04-S)	7017	15472			10	32.8	5
AS-61-S — Attached Far IR Photometer (Wide FOV)	145	320			1	3.28	2
AS-62-S — Cosmic Background Anisotropy	220	485			1	3.28	2
AS-01-R — LST Revisit	4400	9702			4	13.1	9
HIGH ENERGY ASTROPHYSICS							
HE-11-S — X-ray Angular Structure	5872	12948	4.27	14.0	6.1	20.0	6
HE-12-S — High Inclination Cosmic Ray Survey	5190	11444			9.15	30.0	5
HE-13-S — X-ray/Gamma Ray Pallet	5034	11100			7	23.0	5
HE-14-S — Gamma Ray Pallet	4687	10335			5	16.4	6
HE-15-S — Magnetic Spectrometer	4003	8827	4.58	15.0	4.6	15.1	3
HE-16-S — High Energy Gamma-Ray Survey	6152	13566			4	13.1	3
HE-17-S — High Energy Cosmic Ray Study	2000	4410			1	3.28	4
HE-18-S — Gamma-ray Photometric Studies	6740	14862			2	6.56	5
HE-19-S — Low Energy X-ray Telescope	1814	4000			3.5	11.5	5
HE-20-S — High Resolution X-ray Telescope	4335	9559			3	9.84	2
HE-03-R — Extended X-ray Survey Revisit	4400	9702			4	13.1	2
HE-11-R — Large High Energy Observatory D Revisit	4400	9702			4	13.1	5

(1) Payload Length Pallet Not Required

Table A-3 Continued

SORTIE PAYLOADS Source: Summarized NASA Payload Descriptions Sortie Payloads Level A Data & Level B Data July 1974	PHYSICAL CHARACTERISTICS						NUMBERS OF MISSIONS
	LAUNCH WEIGHT		MAXIMUM DIAMETER		ESTIMATED PALLET LENGTH		
	Kg	(lbs)	m	(ft)	m	(ft)	
SOLAR PHYSICS							
SO-01-S — Dedicated Solar Sortie Mission (DSSM)	5619	12390	1.47	4.82	13.7	44.9	25
SO-11-S — Solar Fine Pointing Payload	3519	7759	1.47	4.82	8.8	28.9	5
SO-12-S — ATM Spacelab	11336	24996			6	19.7	TBD
ATMOSPHERIC AND SPACE PHYSICS							
AP-06-S — Atmospheric, Magnetospheric, and Plasmas in Space (AMPS)	5381	11865	4.0	13.1	7.6	24.9	30
EARTH OBSERVATIONS							
EO-01-S — Zero-G Cloud Physics Laboratory	796.9	1757	3.05	10.0	0	0	11
EO-05-S — Shuttle Imaging Microwave System (SIMS)	7432	16388	18	59.1	18(1)	59.1	18
EO-06-S — Scanning Spectroradiometer	520	1147	0.91	2.98	2.13	6.99	17
EO-07-S — Active Optical Scatterometer	442.6	976			2	6.56	16
EARTH AND OCEAN PHYSICS							
OP-02-S — Multifrequency Radar Land Imagery	1470	3241	0.45	1.48	0.6	1.97	19
OP-03-S — Multifrequency Dual Polarized Microwave Radiometry	633.2	1396	2.12	6.96	3	9.84	9
OP-04-S — Microwave Scatterometer	387.6	855	0.5	1.64	1.1	3.61	8
OP-05-S — Multispectral Scanning Imagery	1470	3241	0.7	2.30	0.6	1.97	19
OP-06-S — Combined Laser Experiment	343.2	757	4.6	15.1	0.6	1.97	17

(1) Length of Stowed Antenna

Table A-3 Continued

SORTIE PAYLOADS Source: Summarized NASA Payload Descriptions Sortie Payloads Level A Data July 1974 & Level B Data	PHYSICAL CHARACTERISTICS						NUMBERS OF MISSIONS
	LAUNCH WEIGHT		MAXIMUM DIAMETER		ESTIMATED PALLET LENGTH		
	Kg	(lbs)	m	(ft)	m	(ft)	
SPACE PROCESSING APPLICATIONS							
SP-01-S — SPA No. 1 - Biological (Manned) (B+C)	2547	5616	4.1	13.5	1.3	4.27	3
SP-02-S — SPA No. 2 - Furnace (Manned) (F+C)	3524	7770			2.45	8.04	2
SP-03-S — SPA No. 3 - Levitation (Manned) (L+C)	4104	9049			2.45	8.04	2
SP-04-S — SPA No. 4 - General Purpose (Manned) (G+C)	2325	5127			1.30	4.27	12
SP-05-S — SPA No. 5 - Dedicated (Manned) (B+F+L+G+C)	7085	15622			3.68	12.1	9
SP-12-S — SPA No. 12 - Automated Furnace (FP+CP)	3187	7027			2.45	8.04	3
SP-13-S — SPA No. 13 - Automated Levitation (LP+CP)	3801	8381			2.45	8.04	2
SP-14-S — SPA No. 14 - Manned and Automated (B+G+C+FP+LP)	6365	14035	4.1	13.5	2.45	8.04	10
SP-15-S — SPA No. 15 - Automated Furnace/Levitation (FP+LP+CP)	4907	10820	4.1	13.5	2.45	8.04	10
SP-16-S — SPA No. 16 - Biological/General (Manned) (B+G+C)	3119	6877			1.3	4.27	11
SP-19-S — SPA No. 19 - Biological and Automated (B+C+FP+LP)	5793	12774			2.45	8.04	9
SP-21-S — SPA No. 21 - Minimum Biological (B+C)	926	2042			N/A		TBD
SP-22-S — SPA No. 22 - Minimum Furnace (Manned) (F+C)	829	1828			N/A		TBD
SP-23-S — SPA No. 23 - Minimum General (G+C)	748	1649			N/A		TBD
SP-24-S — SPA No. 24 - Minimum Levitation (Manned) (L+C)	930	2051			N/A		TBD
LIFE SCIENCES							
LS-04-S — Free Flying Teleoperator	344.8	760			1.53	5.02	12
LS-09-S — Life Sciences Shuttle Laboratory	2846	6275	4.1	13.5	N/A		28
LS-10-S — Life Sciences Carry-on Laboratories	261	576	1.52	4.99	N/A		24

Table A-3 Continued

SORTIE PAYLOADS Source: Summarized NASA Payload Descriptions Sortie Payloads Level A Data July 1974 & Level B Data	PHYSICAL CHARACTERISTICS						NUMBERS OF MISSIONS
	LAUNCH WEIGHT		MAXIMUM DIAMETER		ESTIMATED PALLET LENGTH		
	Kg	(lbs)	m	(ft)	m	(ft)	
SPACE TECHNOLOGY							
ST-04-S — Wall-less Chemistry + Molecular Beam (Facil. No. 1)	643	1418			5	16.4	23
ST-05-S — Superfluid He + Particle/Drop Positioning (Facil. No. 2)	439.7	970			0	0	23
ST-06-S — Fluid Physics + Heat Transfer (Facil. No. 3)	621.6	1371			0	0	21
ST-07-S — Neutral Beam Physics (Facil. No. 4)	58.5	129			5	16.4	9
ST-08-S — Integrated Real Time Contamination Monitor	52.7	116	0.71	2.33	N/A	-	TBD
ST-09-S — Controlled Contamination Release	62.7	138			0.7	2.30	3
ST-11-S — Laser Information/Data Transmission	54.4	120			5	16.4	3
ST-12-S — Entry Technology	4	8.82			N/A	-	12
ST-13-S — Wake Shield Investigation	450	992			5	16.4	4
ST-21-S — ATL P/L No. 2 (Module + Pallet)	1353	2983			6	19.7	7
ST-22-S — ATL P/L No. 3 (Module + Pallet)	2330	5138	3.3	10.8	6	19.7	7
ST-23-S — ATL P/L No. 5 (Pallet Only)	3228	7118	4.57	15.0	15	49.2	9
COMMUNICATIONS AND NAVIGATION							
CN-04-S — Terrestrial Sources of Noise + Interference	289.1	637	3.05	10.0	1.6	5.25	8
CN-05-S — Laser Communication Experimentation	388.6	857	1.53	5.02	1.8	5.91	6
CN-06-S — Communication Relay Tests	677.8	1495			3	9.84	5
CN-07-S — Large Reflector Deployment	1922	4238			15(1)	49.2	4
CN-08-S — Open Traveling Wave Tube	120.6	266			0.5	1.64	3
CN-11-S — Stars & Pads Experimentation	111.6	246			1	3.28	TBD
CN-12-S — Interferometric Navigation & Surveillance Techniques	188.9	417			0.5	1.64	6
CN-13-S — Shuttle Navigation Via Geosynchronous Satellite	60	132			0	0	6

(1) Using Modified Design, Folding of Ribs Could Reduce Length of Pallet By 50%.

APPENDIX B

DYNAMICS PROGRAM FOR THE LDEF PAYLOAD

TABLE OF CONTENTS

B-1.0 INTRODUCTION

The primary objective of Mission #4 of the Shuttle Program is to demonstrate the Shuttle's capability to launch and deploy a satellite. The Long Duration Exposure Facility (LDEF) was selected by Space Shuttle Program Office as the initial satellite to be deployed. Other objectives of the flight include monitoring the environment in and around the Shuttle using three Integrated Real Time Contamination Monitors (IRTCM's), which detect the presence of contaminants and determine the amount and rate of their disposition. The payload also includes a 5 foot standard pallet, provided so that additional carry-on experiments can be considered at a later date. More detailed information can be found in Reference B-1 and is shown in Figures B-1.1 through B-1.4.

This appendix presents a recommended approach to a dynamics program for the LDEF payload, and is intended to serve as an example for payloads on initial flights. We recognize that variations to the approach will be required for other payloads depending on each payload configuration and mission requirement. Further, it should be recognized that the approach described is not necessarily that which would be recommended if the LDEF were the only payload under consideration, but is aimed at obtaining information for application to future payloads in order to reduce overall program costs.

Examples of analytical techniques are presented, a recommended test program outlined, the flight measurement program defined, data interpretation techniques described, and the interrelationship and correlation of these factors discussed. The dynamics program is shown in block diagram form in Figure B-1.5.

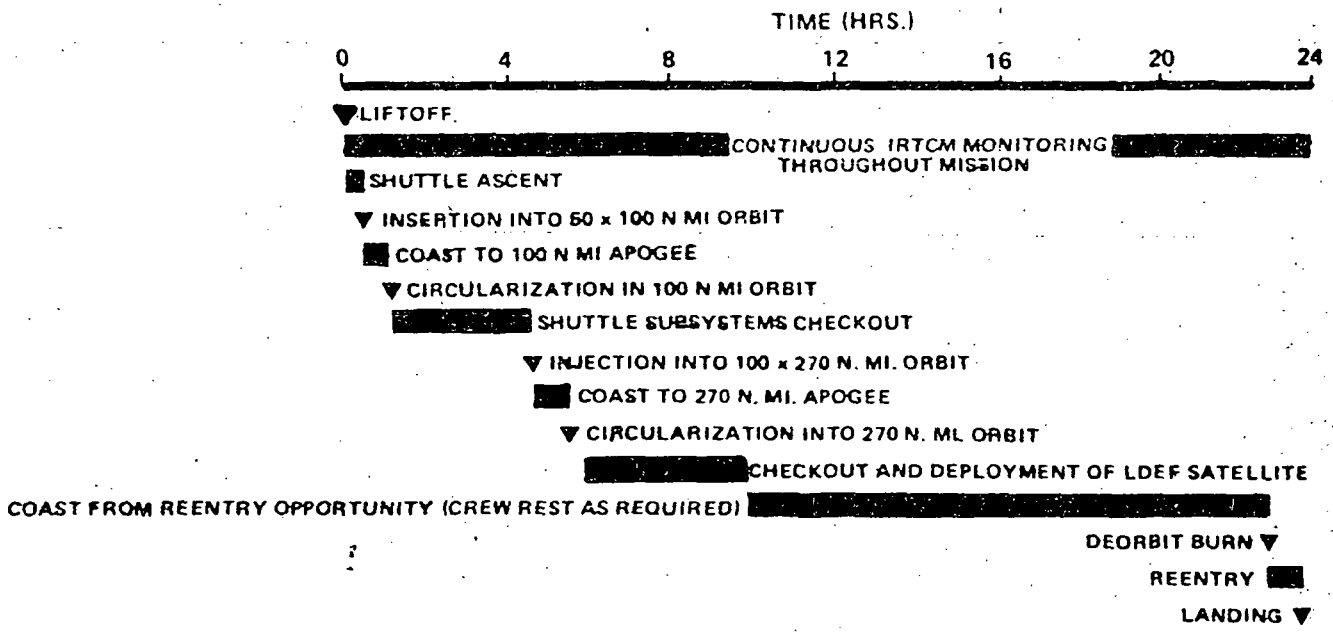

Figure B-1.1: Mission 4 Sequence of Events

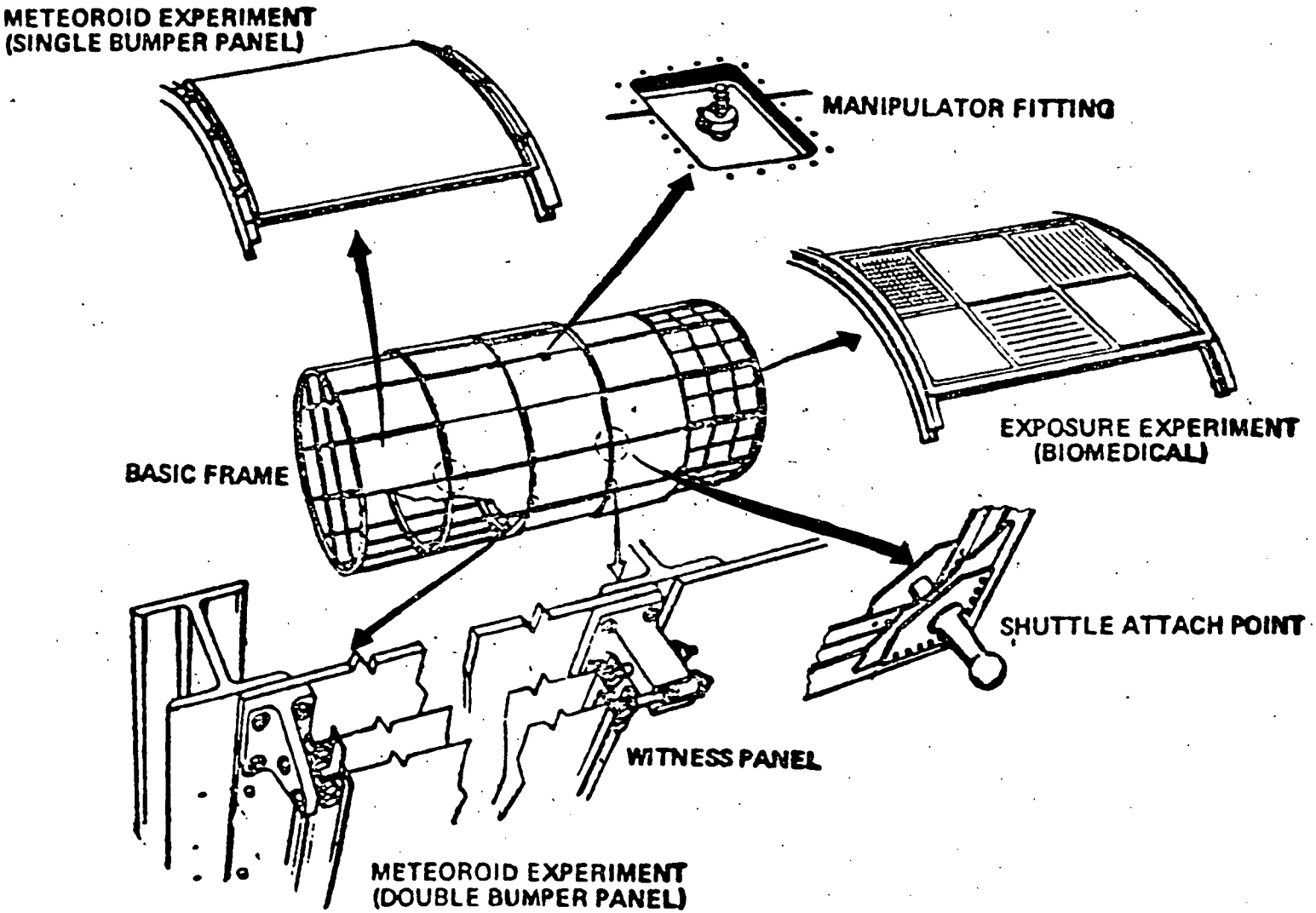

Figure B-1.2 Long Duration Exposure Facility.

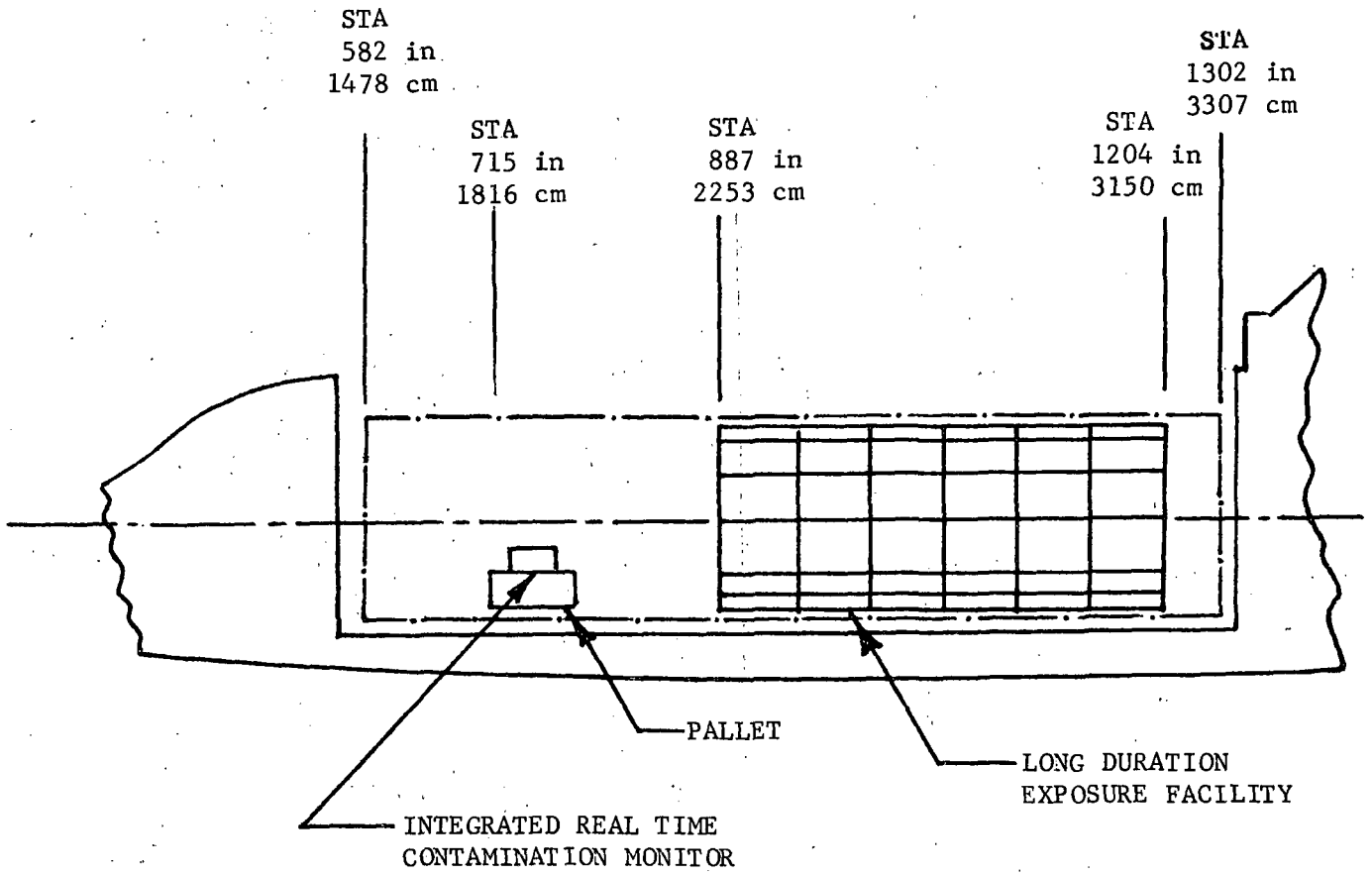

Figure B-1.3: Shuttle Payload Bay, Mission 4 Configuration

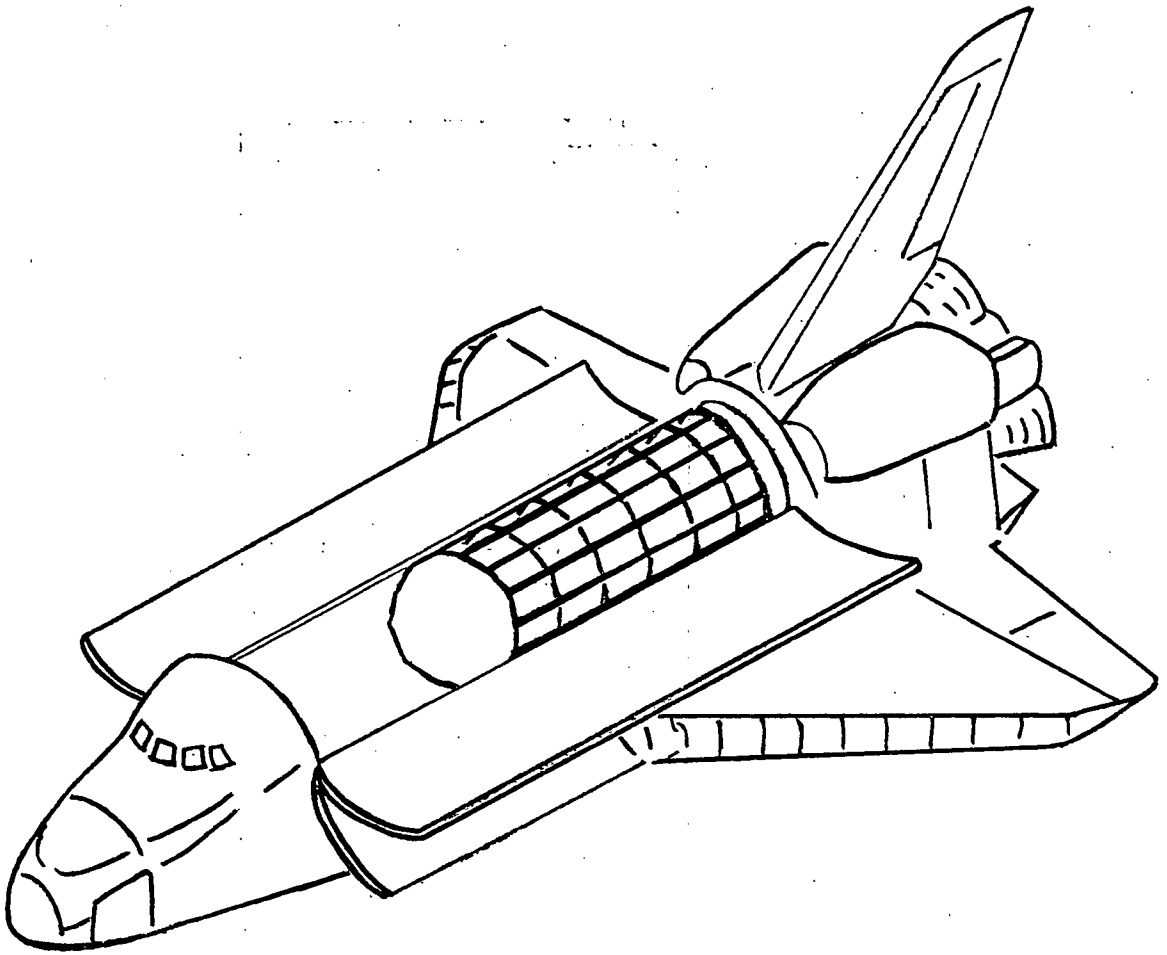

Figure B-1.4 LDEF/Orbiter Configuration

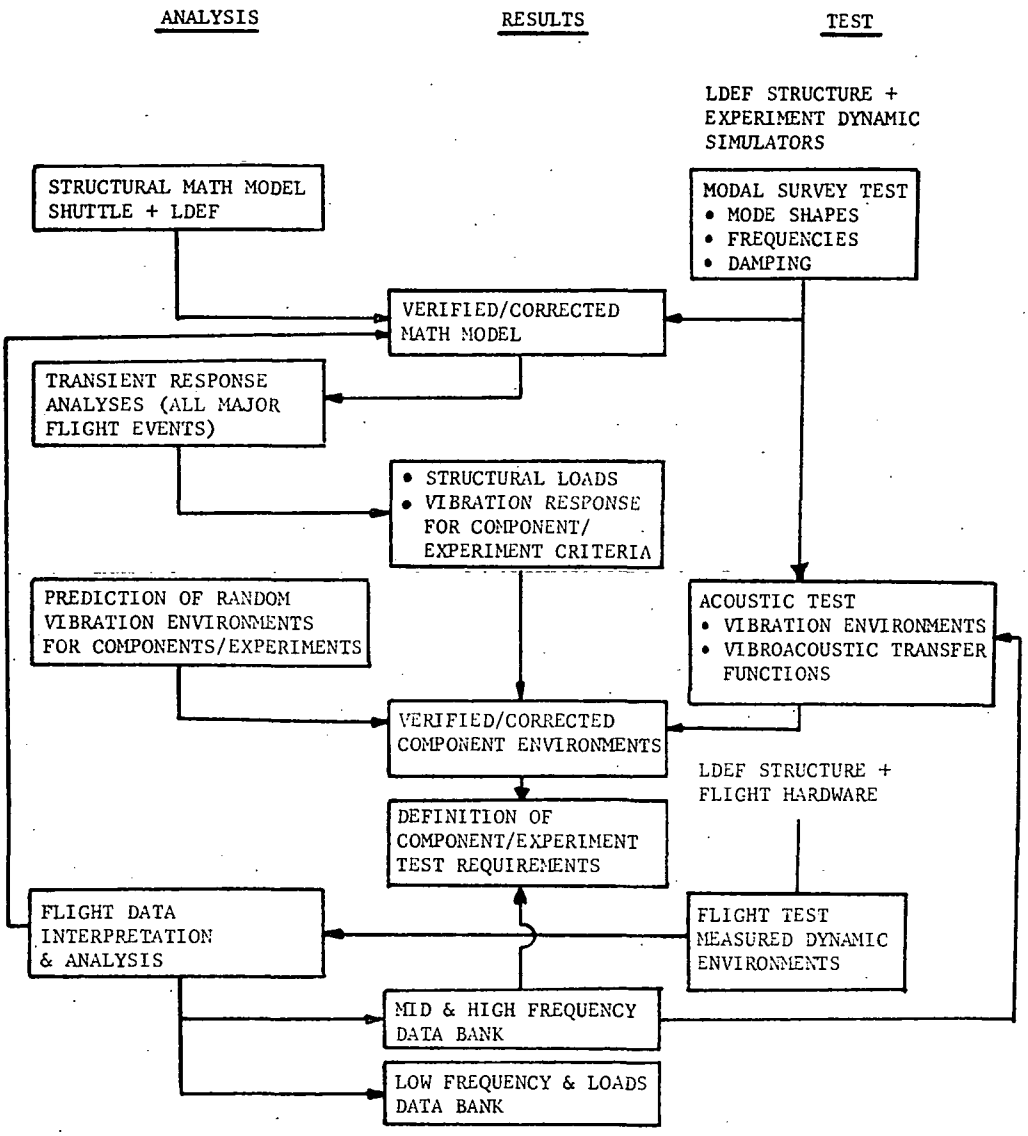

Figure B-1.5 - Dynamics Program for LDEF

B-2.0 ANALYSIS

B-2.1 INTRODUCTION AND OBJECTIVES

The "state of the art" analytical techniques are a resultant of the single booster/single payload concept. For each payload and booster combination, complete finite element models are derived and coupled for the response analysis.

With the advent of the Shuttle Program, a new concept will begin. Standard reusable launch vehicles will deliver and, in some cases, retrieve payloads covering a wide range of structural size, stiffness and weight. It will be required to minimize costs at all stages in the development of these payloads. With standard boosters and data from previous flights, analytical efforts for future flights can be reduced.

As an example of the "state of the art" techniques and methods, the Long Duration Exposure Facility (LDEF) was modeled and taken through the major phases of analysis.

The LDEF was designed to be launched by the Shuttle launch vehicle and gather scientific data for an extended period of time in earth orbit. It is currently planned as one of the first few Shuttle development flights as described in Reference B-1.

The objectives of this section are:

1. To present simplified finite element models for both the LDEF and Shuttle Orbiter,

2. To discuss the test correlation techniques and considerations for the LDEF model,

3. To present the model coupling techniques and results, and

4. To present the coupled model loads analysis techniques and results.

B-2.2 DISCUSSION OF GROUND RULES AND ASSUMPTIONS

Detailed information about the configuration and design of the LDEF are not finalized at this time; in fact, many configurations have been proposed. As a result, many assumptions had to be made in order to form a meaningful, yet simple, model of a coupled LDEF and Shuttle Orbiter. Information was gathered from existing Shuttle payload data (in particular Ref. B-1) and additional data was received from the Technical Monitor. This general information is shown pictorially in Figures B-1.1 through B-1.4. With these sets of data, a simplified LDEF model was generated.

As is shown in Figure B-1.2, a large portion of the experiment packages are located on the circumference of the structure in trays of varying sizes. Since no definite weight or mass distribution was known at the time of this analysis, imaginary beams were assumed to span the rings of the LDEF structure to carry the bulk of the experiment package weight. This is probably the largest deviation from the actual structural design. The result was an open framework structure, as pictured in Figures B-2.1 and B-2.2 with most of the experiment weight concentrated along the centerline.

Somewhat more information was available concerning the interface between the Shuttle Orbiter and the LDEF. The total number of interface points and their general locations were known. From this data the interface load carrying directions were chosen to result in a statically determinate LDEF/Orbiter interface for convenience.

B-2.3 DESCRIPTION OF THE MODELS

B-2.3.1 LONG DURATION EXPOSURE FACILITY

Physical Description - The LDEF model is essentially a 30 foot long cylinder, 14 feet in diameter, constructed of aluminum "I" beams. The length of the structure is divided into 6 bays by 7 rings, also constructed of aluminum "I" beams, as shown in Figures B-2.1 and B-2.2, along with the coordinate system used for the analysis.

As a convenience for the computer analysis the experiment package weight was assumed to lie in the centerline of the LDEF structure. To facilitate this weight, imaginary beams were assumed to span the rings. These beams were physically put into the model with the section properties of the "I" beams of the actual structure (Figures B-2.3 and B-2.4).

The mass distribution was assumed in order to give a composite center of gravity (c.g.) near the c.g. given in Reference B-1. To accomplish this, 60% (or 3000 lb) of the experiment package weight was assumed to be symmetric about the center "ring". Then to shift the center of gravity, the remaining 40% (2000 lb) was located 73.28 inches from the forward end of the LDEF (see Figures B-2.5 and B-2.6).

Stiffness Model - It is not the intent of this report to detail the finite element programs used to generate the stiffness or mass matrices for models, but rather to illustrate the analytical techniques. Generally, the LDEF model was derived using a finite element program that generates a stiffness matrix along with a consistent mass matrix. Each element in the model considered axial, torsional, and bending degrees of freedom (d.o.f.).

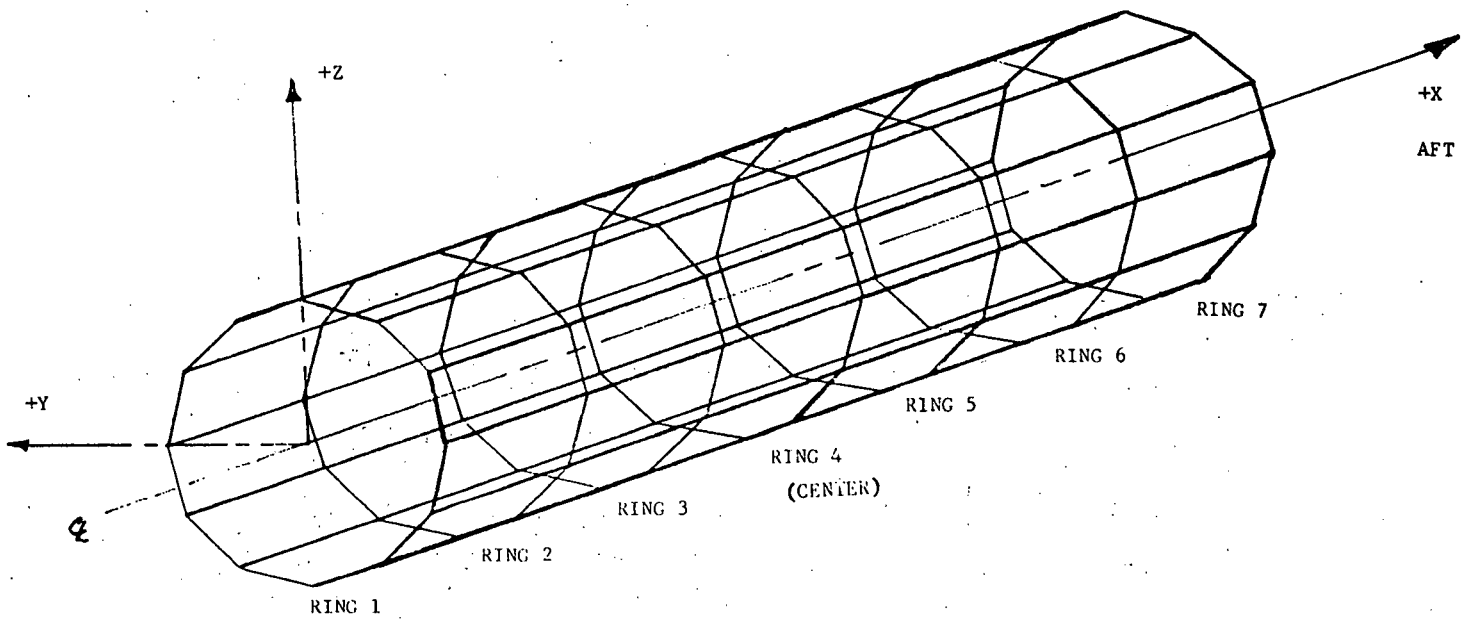

Figure B-2.1: LDEF Structure (Assumed Beams Not Shown)

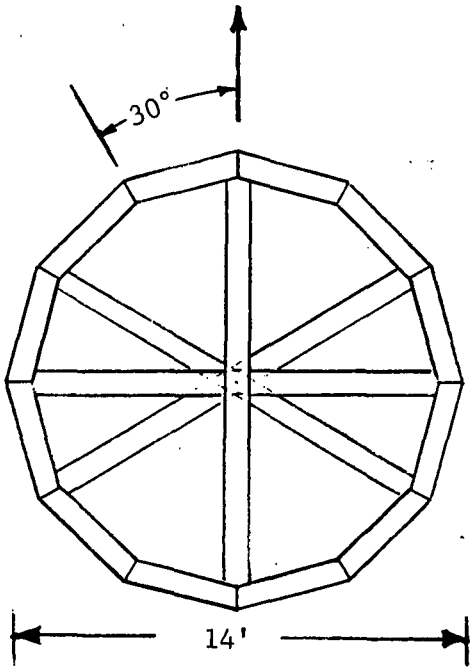

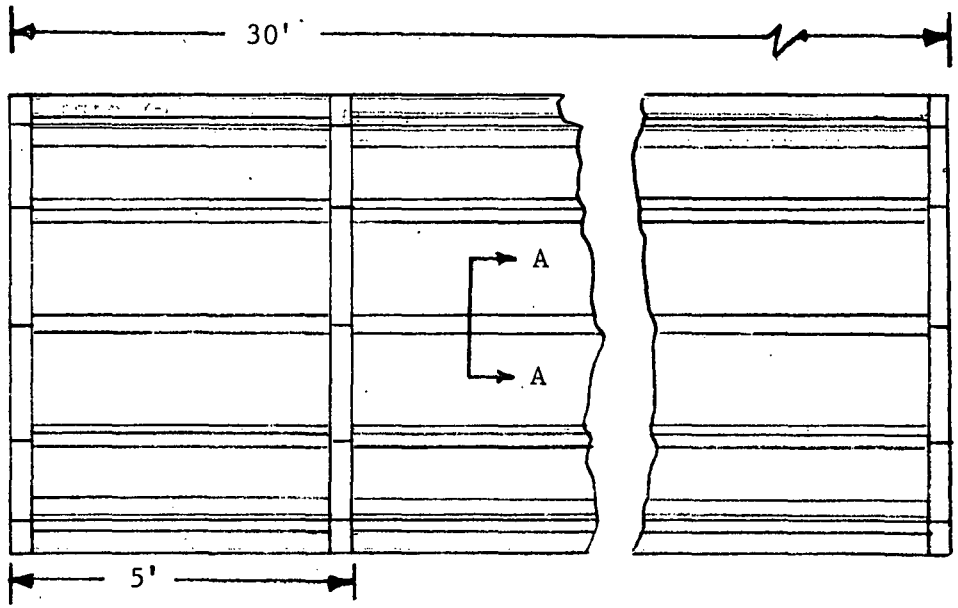

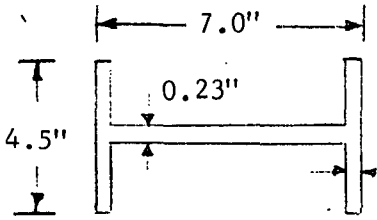

AREA = 4.86 IN^2

SECTION (A-A)

TYP.

MATERIAL: Aluminum

WEIGHTS: Structure - 4200 lb
Package - 5000 lb

Figure B-2.2: LDEF Structural Detail

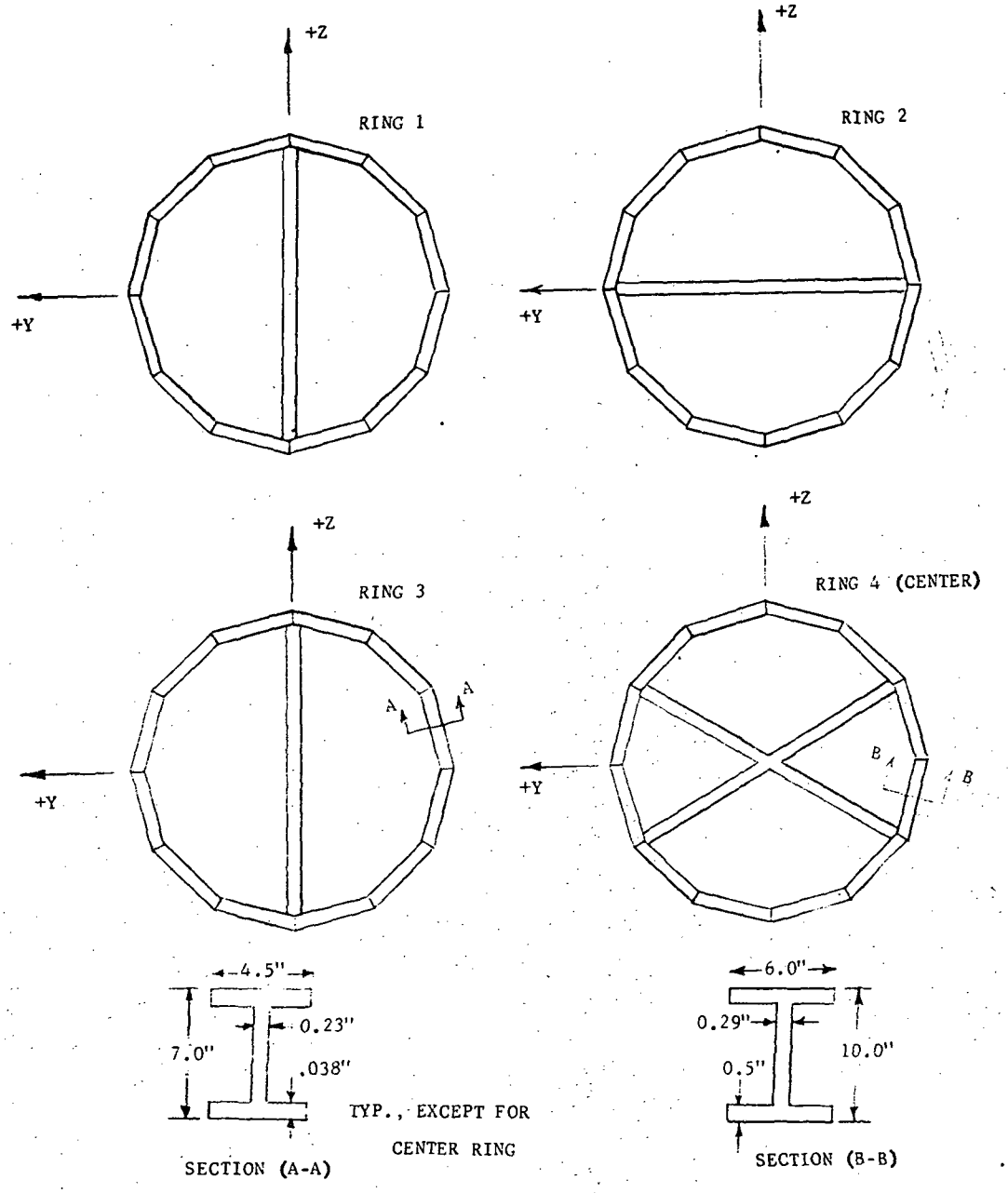

Figure B-2.3 : LDEF Ring Structure

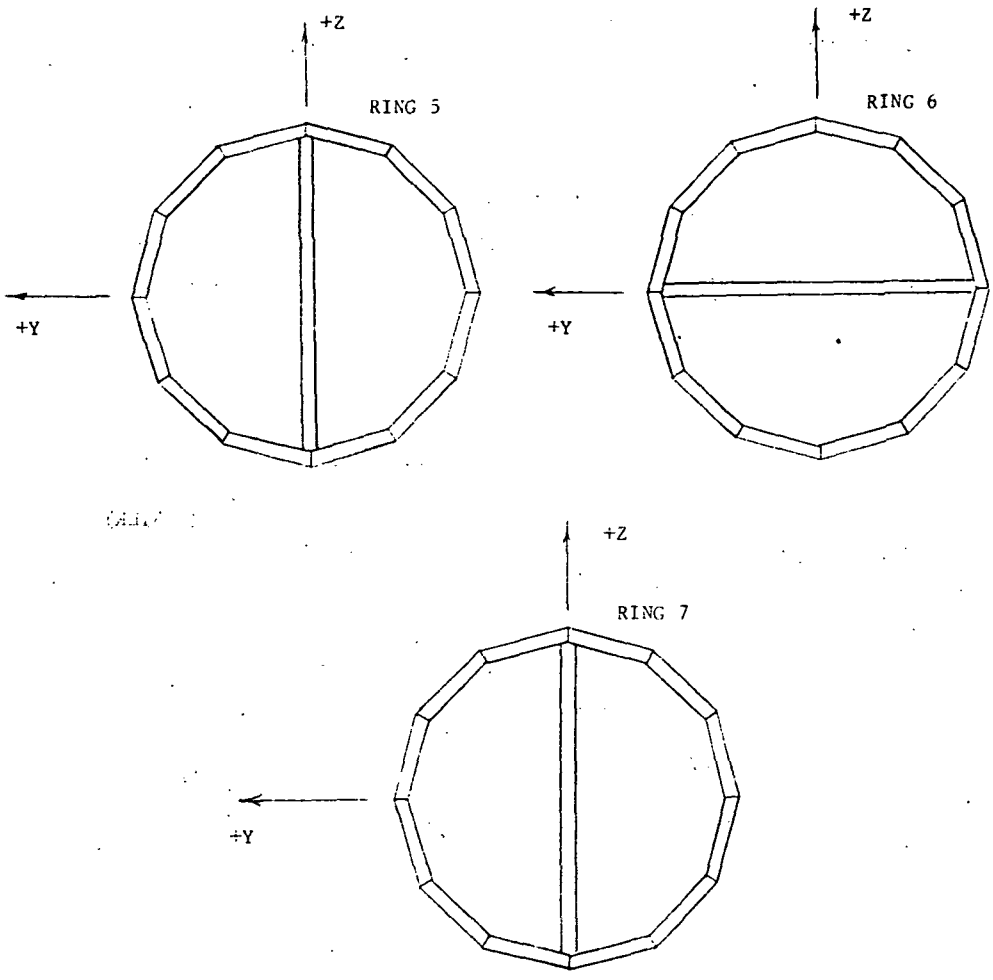

Figure B-2.4 : LDEF Ring Structure

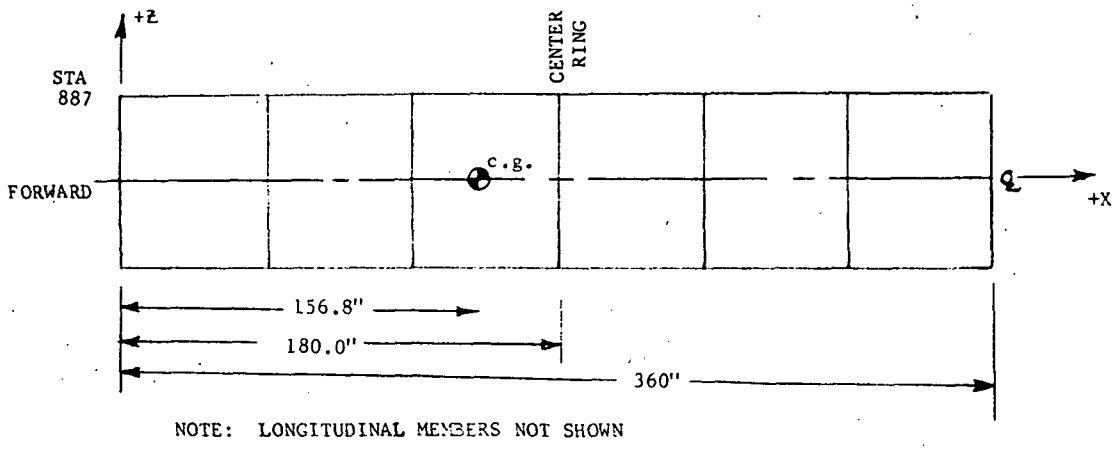

Figure B-2.5 : LDEF Center of Gravity

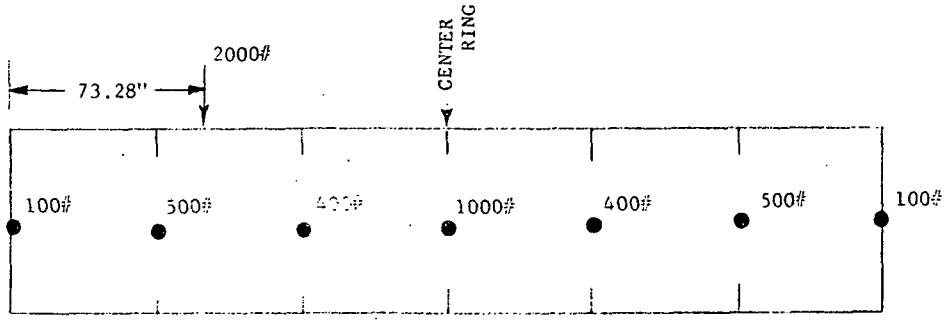

Figure B-2.6: Schematic of LDEF Experiment Weight Distribution

To minimize the computer effort, the complete model was not generated at once. The structure was broken down into structural components consisting of half-bays. A finite element model (f.e.m.) was generated for each structural component. Sequentially, each component was discretely coupled to the adjoining component and undesired degrees of freedom were collapsed out. This process was continued until the forward half of the LDEF model was complete.

Since the model is symmetric about the center ring, the forward half was then transformed to generate the aft half of the complete model. Figure B-2.7 shows the complete LDEF model.

In Figure B-2.7, node points 7, 14, 15 and 16 constitute the LDEF/Orbiter interface. This interface will be detailed below.

Mass Model - As was stated above, the finite element program used for the LDEF structure generated a consistent mass matrix for the elements used. This resulted in a reasonably accurate mass matrix for the LDEF basic structure with the assumed beams.

The experiment package mass was then discretely added to the degrees of freedom on the assumed beams according to the schematic shown in Figure B-2.6. The exception was the 2000 lb to be applied 73.28 inches from the forward end to correct the center of gravity.

Referring to Figure B-2.7, this 2000 lb was split into two 1000 lb imaginary packages and placed on two panels between rings 2 and 3. These panels are bounded by node points 3, 4, 9, 10 and 5, 6, 11 and 12 respectively. The imaginary packages were assumed to have a radius of gyration of 10.0 inches for convenience. Figure B-2.8 shows more detail on the geometry of the panel. (Note: the d.o.f. for the panel points were rotated to a local coordinate system).

To apply the mass, a method of "mass smearing" was utilized and is described below:

The desired end result is to write the motion of the d.o.f. associated with the concentrated mass in terms of those associated with the four panel points, or

$$\{q\} = [T]\ \{q'\} \qquad (1)$$

Where $\{q\}$ = d.o.f. for mass

$[T]$ = transformation matrix

$\{q'\}$ = d.o.f. for the panel points.

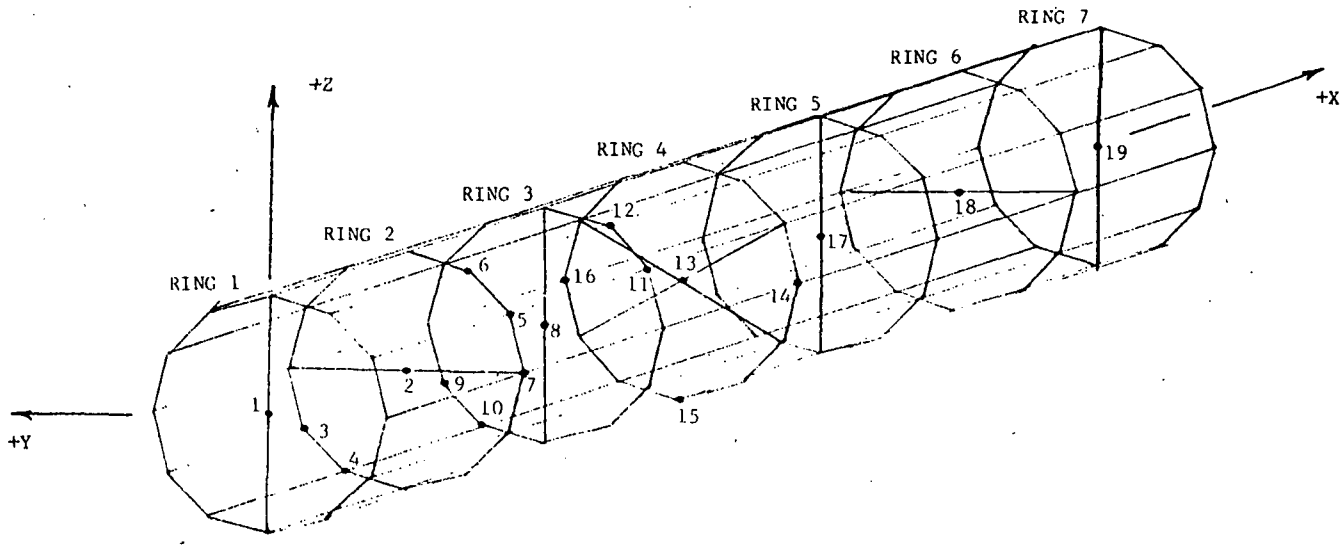

IDENT NODE	DEGREE OF FREEDOM X	Y	Z	TX	TY	TZ	NODE LOCATION X	Y	Z	COMMENT
1	1	2	3	-0	-0	-0	0.	0.	0.	RING 1 CNTR
2	4	5	6	-0	-0	-0	60.0000	0.	0.	RING 2 CNTR
3	7	8	9	-0	-0	-0	60.0000	72.7500	-42.0000	RING 2
4	10	11	12	-0	-0	-0	60.0000	42.0000	-72.7500	RING 2
5	13	14	15	-0	-0	-0	60.0000	-72.7500	42.0000	RING 2
6	16	17	18	-0	-0	-0	60.0000	-42.0000	72.7500	RING 2
7	-0	-0	19	-0	-0	-0	60.0000	-84.0000	0.	RING 2 I/F
8	20	21	22	-0	-0	-0	120.0000	0.	0.	RING 3 CNTR
9	23	24	25	-0	-0	-0	120.0000	72.7500	-42.0000	RING 3
10	26	27	28	-0	-0	-0	120.0000	42.0000	-72.7500	RING 3
11	29	30	31	-0	-0	-0	120.0000	-72.7500	42.0000	RING 3
12	32	33	34	-0	-0	-0	120.0000	-42.0000	72.7500	RING 3
13	35	36	37	-0	-0	-0	180.0000	0.	0.	RING 4 CNTR
14	38	-0	39	-0	-0	-0	180.0000	-84.0000	0.	RING 4 I/F
15	-0	40	-0	-0	-0	-0	180.0000	0.	-84.0000	RING 4 I/F
16	41	-0	42	-0	-0	-0	180.0000	84.0000	0.	RING 4 I/F
17	43	44	45	-0	-0	-0	240.0000	0.	0.	RING 5 CNTR
18	46	47	48	-0	-0	-0	300.0000	0.	0.	RING 6 CNTR
19	49	50	51	-0	-0	-0	360.0000	0.	0.	RING 7 CNTR

Figure B-2.7 : LDEF Finite Element Model

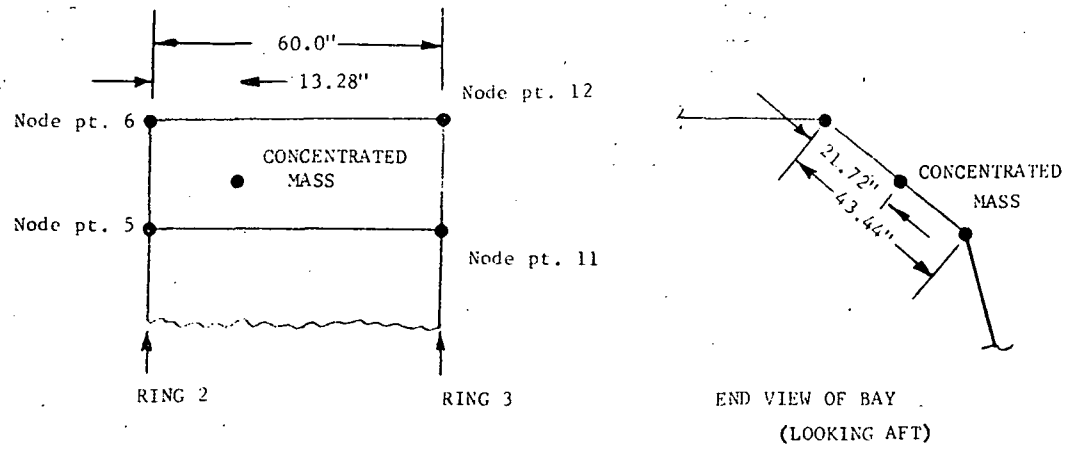

Free Body Diagram:

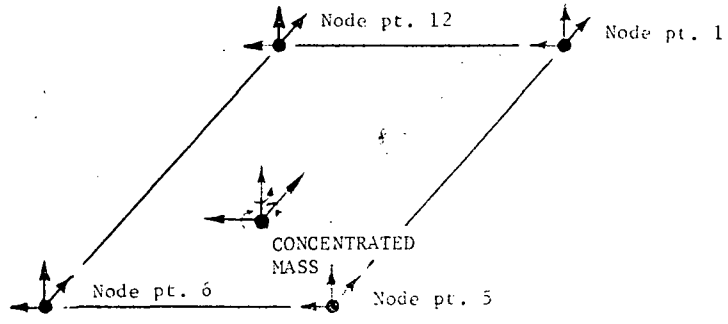

Figure B-2.8: Concentrated Mass Details

The derivation starts by assuming the concentrated mass and panel points are a rigid body,

$$\{q'\} = [RBT] \{q\} \quad (2)$$

Where $[RBT]$ = a rigid body transformation

Multiplying both sides of (2) by $[RBT]^T$,

$$[RBT]^T \{q'\} = [RBT]^T [RBT] \{q\} \quad (3)$$

Note here that $[RBT]^T [RBT]$ is a symmetric matrix and can be inverted, thus

$$\left([RBT]^T [RBT]\right)^{-1} [RBT]^T \{q'\} = \{q\} \quad (4)$$

or

$$\{q\} = [T] q' \quad (5)$$

Where $[T] = \left([RBT]^T [RBT]\right)^{-1} [RBT]^T$

Now that $[T]$ has been generated, it can be used to "blow-up" the 6x6 mass matrix associated with the concentrated packages,

$$[M'] = [T]^T [M][T] \quad (6)$$

Where $[M']$ = (12x12) new mass matrix

$[M]$ = old (6x6) mass matrix

Once the mass matrix was "blown-up" to a (12x12), it was then discretely added to the mass of the 4 panel points.

Test Correlation - The next major step in the analytical effort is to verify the analytical model. This is necessary to demonstrate the reliability in math models for predicting the low frequency environments.

In order to fulfill at least part of this objective, a modal analysis was performed on the LDEF model grounded at the LDEF/Orbiter interface. The mass and stiffness models described above constitute 51 d.o.f. Mode shapes for 48 d.o.f. were generated (the six interface d.o.f. were grounded). Figures B-2.9 through B-2.10 show the mode shapes for the first mode and are representative for the structure. Note that the radial members shown in the plots are imaginary and were inserted to clarify the plots. Table B-2.1 gives a complete list of the frequencies for the grounded LDEF model.

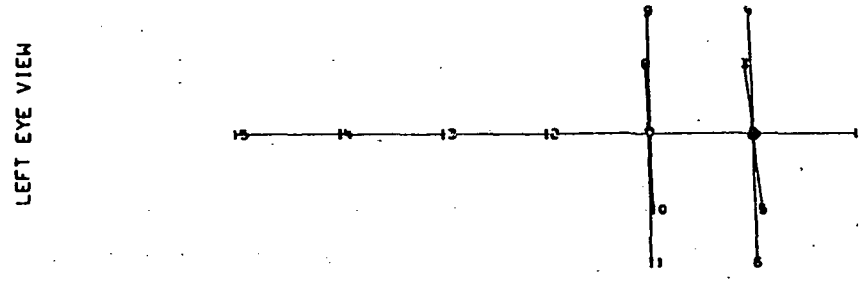

LDEF MODEL (GROUNDED) — UNDEFLECTED MODEL

CENTER OF EYES LOCATION
X = 1.80000000E+02
Y =-1.53100000E+03
Z = 0.
RUN NO. = LDEFPT

VIEW POINT LOCATION
X = 1.80000000E+02
Y = 0.
Z = 0.
DATE = 18JA75

ROLL ANGLE = -0. DEG
CONE ANGLE = 20.0DEG
EYE TO EYE = 3.0 IN

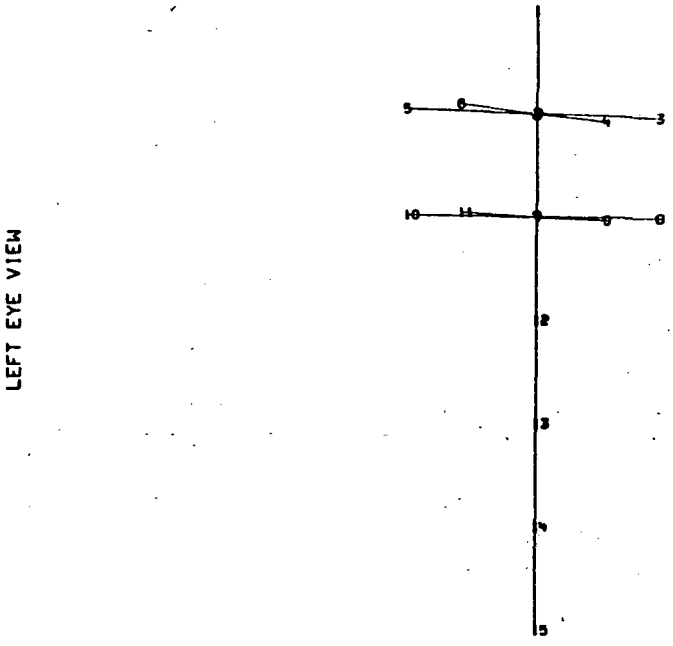

LDEF MODEL (GROUNDED) — UNDEFLECTED MODEL

CENTER OF EYES LOCATION
X = 1.80000000E+02
Y = 0.
Z = 1.53100000E+03
RUN NO. = LDEFPT

VIEW POINT LOCATION
X = 1.80000000E+02
Y = 0.
Z = 0.
DATE = 18JA75

ROLL ANGLE = -0. DEG
CONE ANGLE = 20.0DEG
EYE TO EYE = 3.0 IN

Figure B-2.9: LDEF Undeflected Mode Shape

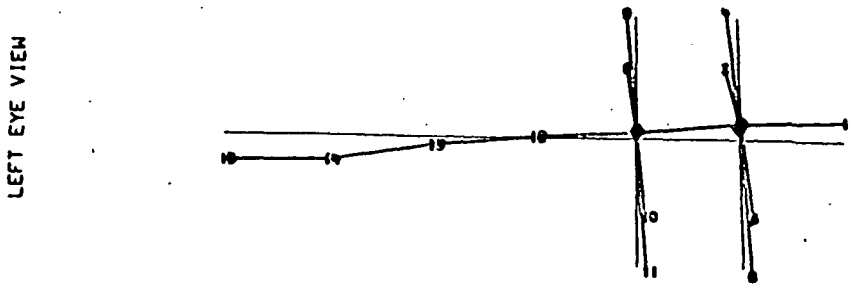

LDEF MODEL (GROUNDED) MF = 44.9, MODE(1) = 3.18 HZ

CENTER OF EYES LOCATION	VIEW POINT LOCATION	ROLL ANGLE = -0. DEG
X = 1.80000000E+02	X = 1.80000000E+02	CONE ANGLE = 20.0DEG
Y =-1.53100000E+03	Y = 0.	EYE TO EYE = 3.0 IN
Z = 0.	Z = 0.	
RUN NO. = LDEFPT	DATE = 18JA75	

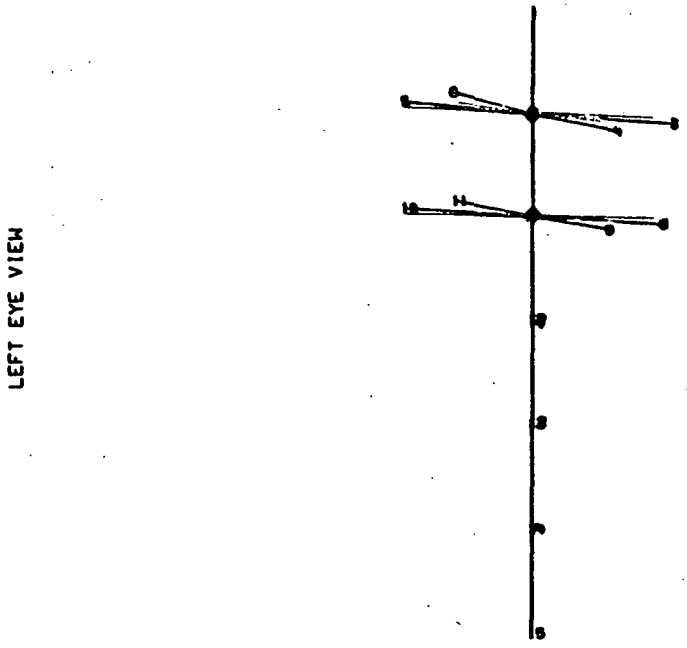

LDEF MODEL (GROUNDED) MF = 44.9, MODE(1) = 3.18 HZ

CENTER OF EYES LOCATION	VIEW POINT LOCATION	ROLL ANGLE = -0. DEG
X = 1.80000000E+02	X = 1.80000000E+02	CONE ANGLE = 20.0DEG
Y = 0.	Y = 0.	EYE TO EYE = 3.0 IN
Z = 1.53100000E+03	Z = 0.	
RUN NO. = LDEFPT	DATE = 18JA75	

Figure B-2.10: Mode No. 1 For LDEF

Table B-2.1: LDEF Grounded Modal Frequencies

Mode No.	f(Hz)	Mode No.	f(Hz)
1	3.18	24	26.06
2	5.40	25	27.93
3	5.80	26	29.66
4	5.99	27	31.52
5	6.14	28	35.97
6	6.81	29	39.46
7	8.18	30	44.61
8	8.67	31	45.02
9	9.36	32	49.66
10	10.75	33	57.16
11	11.48	34	67.91
12	13.56	35	74.57
13	14.34	36	85.97
14	14.42	37	136.9
15	14.64	38	270.6
16	15.41	39	285.0
17	16.15	40	346.0
18	17.41	41	350.4
19	17.83	42	363.2
20	20.92	43	412.3
21	21.79	44	427.2
22	24.74	45	547.5
23	25.48		

In order to correct the math model certain types of information are necessary. Exact frequencies for the major modes are important. Actual mode shapes, damping and effective mass are also important, for they can reveal the true response of the structure to the low frequency environments.

There are numerous ways of correcting the math model to reflect the test results. For simple cases it may be adequate to merely scale the frequencies and assume no change in the mode shape. More detailed correction can be done by actually changing stiffness and mass terms for the model.

For this report however, no test data was available. Therefore the assumption was made herein that the final model, with mass and stiffness as described above, has been test correlated and is correct.

B-2.3.2 SHUTTLE ORBITER

It is not the intent of this report to detail the development of the Shuttle Orbiter model. The overall assumption is that the model for the launch vehicle is correctly derived and test-correlated. However a brief description is necessary to understand the analysis that follows in this report.

The Orbiter model was developed in its original form from only NASTRAN data. The stiffness properties were sufficient but some minor assumptions were necessary to complete the mass data. For instance, it was necessary to assume a radius of gyration to determine a mass moment of inertia. Figures B-2.11 through B-2.13 show the original and final Orbiter models. Note that all degrees of freedom not necessary to couple to the LDEF or force the model were collapsed out.

Node points 4, 5, and 6, shown in Figure B-2.13, are the interface points between the Orbiter and the External Tank, and node points 2 and 3 are the interface points between the Orbiter and the LDEF. This interface will be described in more detail in the following section.

B-2.4 MODEL COUPLING

There are two basic methods of coupling finite element models practiced today. One is commonly called "inertial" or "modal" coupling and the other, "discrete" coupling. Briefly, the "inertial" technique involves coupling the models through the mass matrices. The latter involves discretely adding, in the appropriate d.o.f., the mass and stiffness to form the coupled model. The LDEF/Orbiter model was generated using the discrete coupling technique.

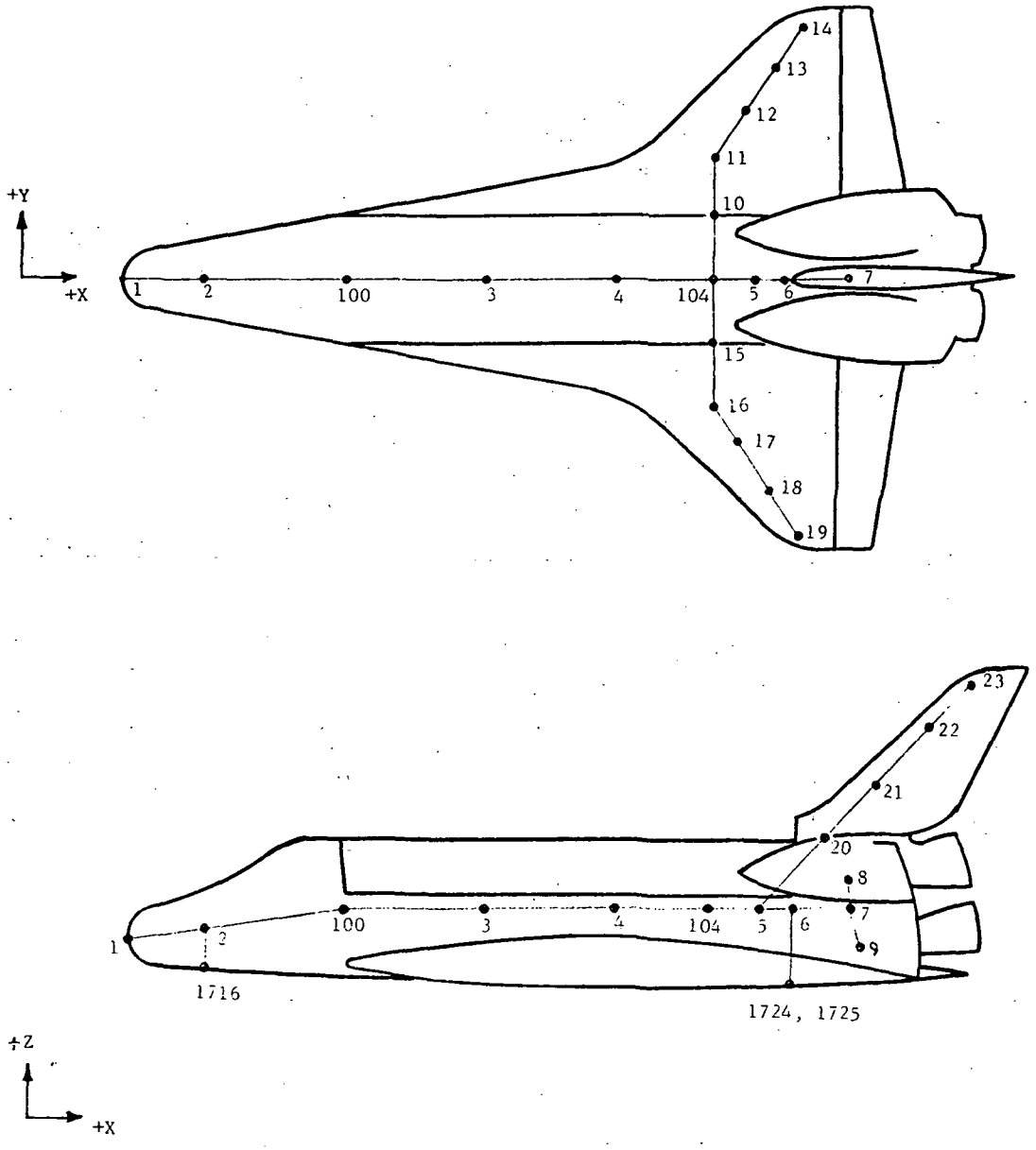

Figure B-2.11 : Orbiter Original Model

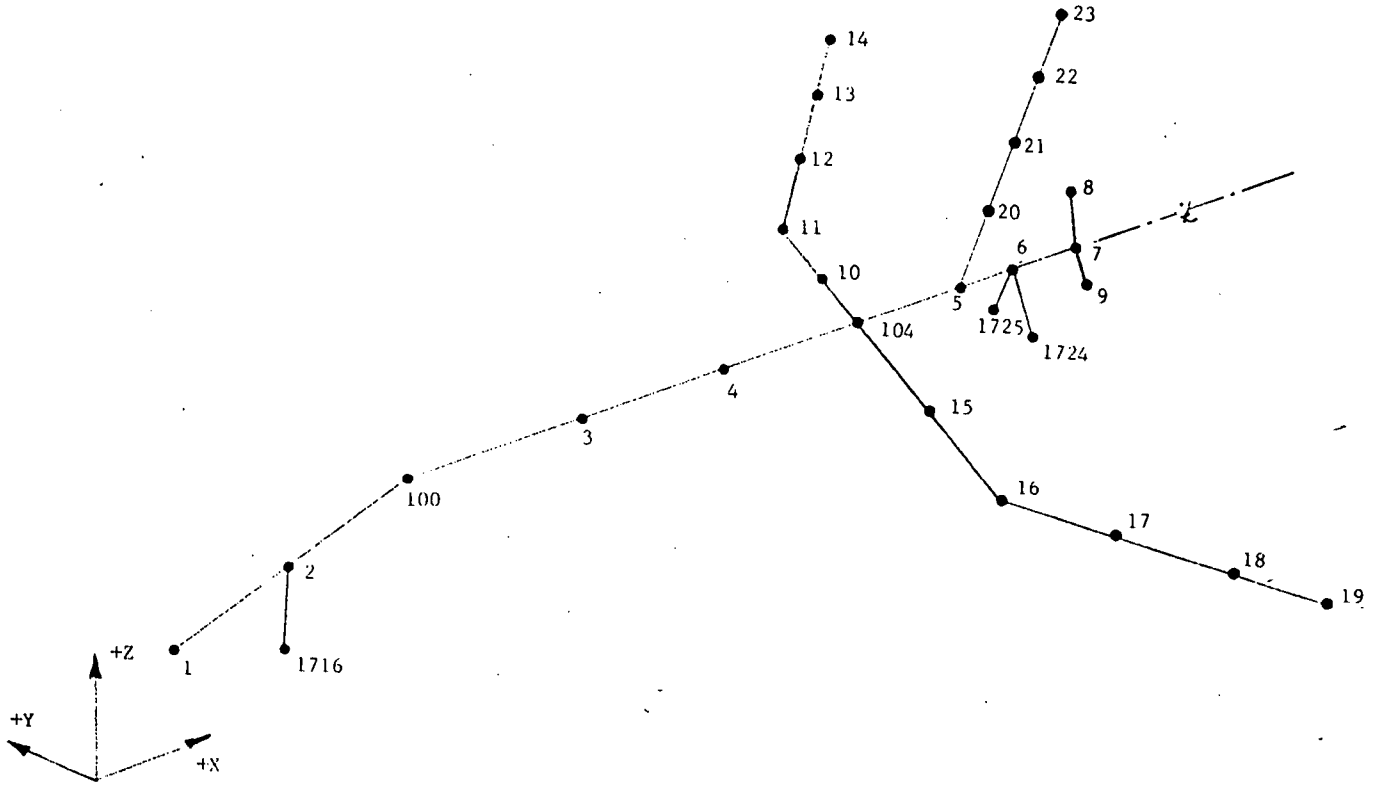

Figure B-2.12 : Orbiter Original Model

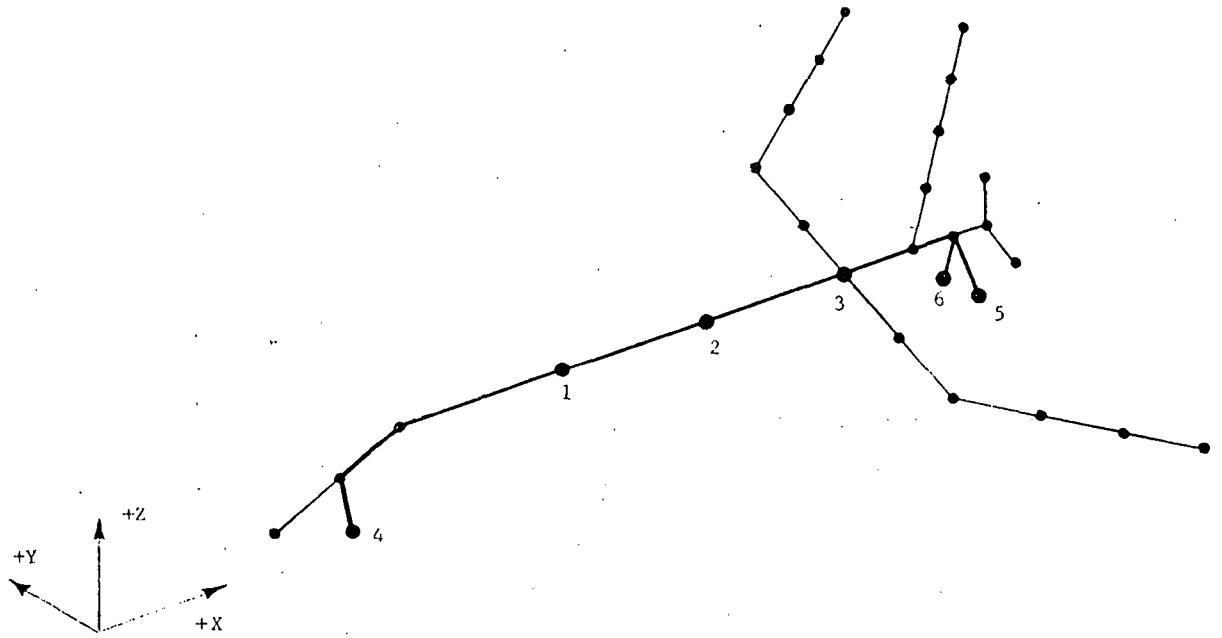

IDENT NODE	DEGREE OF FREEDOM X	Y	Z	TX	TY	TZ	NODE LOCATION X	Y	Z	COMMENT
1	1	2	3	4	5	6	1579.0000	0.	337.1900	FUSE. PT 4
2	7	8	9	10	11	12	1796.0000	0.	335.2900	FUSE. PT 5
3	13	14	15	16	17	18	1944.0000	0.	334.0000	FUSE. PT 6
4	19	20	21	-0	-0	-0	1133.0000	0.	221.3000	ORB I/F 1716
5	22	23	24	-0	-0	-0	2058.0000	101.2900	195.2600	ORB I/F 1724
6	25	26	27	-0	-0	-0	2058.0000	-101.2900	195.2600	ORB I/F 1725

Figure B-2.13 : Reduced Orbiter Model

Normally, this technique applies to two bodies whose interface points occupy the same or adjacent geometric location. This was not true however for the LDEF and Orbiter models as they have been described.

Referring to Figure B-2.7, it can be seen that the LDEF interface reaction points lie on two Y-Z planes which are normal to the X axis and are 120 inches apart. It can also be seen by referring to Figure B-2.13, that the Orbiter/LDEF interface points consist of 2 points on the stick model that are 148 inches apart on the X axis.

Therefore, in order to couple the two models discretely, the assumption was made that the interface between the two models was rigid. This allowed the LDEF interface d.o.f. to be constained down to the appropriate Orbiter points and added.

One other discrepancy should be noted. The coordinate axis system for the Orbiter model from the NASTRAN data was rotated approximately 0.009 degrees with respect to the LDEF analysis coordinate system. This rotation was assumed to be negligible and therefore ignored.

The final coupled LDEF/Orbiter model is condensed in a Degree of Freedom Table, Table B-2.2. A drawing of the coupled bodies is not included because of the confusion which could be caused by showing two stick models coincident on the same axis. Instead a "GMC" matrix was calculated for the coupled modes. With the "GMC" matrix, the participation factor or contribution of each d.o.f. is shown for each mode. Table B-2.3 shows the participation of the of the first degree of freedom to every mode as a representative example. It is a manner of showing in what modes degree of freedom 1 is active.

This coupled finite element model was then uncoupled in a modal solution program, resulting in 72 mode shapes including 6 rigid body modes. Table B-2.4 gives a list of the frequencies for the coupled modes.

B-2.5 RESPONSE ANALYSIS AND RESULTS

The final step in the analytical effort is the prediction of the payload's response to the launch and boost environment. The lift-off event was selected to illustrate the technique.

B-2.5.1 LIFTOFF FORCING FUNCTIONS

For this analysis, information was obtained on the Orbiter/External Tank interface loads for the liftoff event. This information consisted of copies of the loads time history plots for these interface points, and were applied at node points 19, 20 and 21 in Table B-2.2.

Table B-2.2: Degree of Freedom Table, Coupled LDEF/Orbiter Model

Ident. Mode	X	Y	Z	TX	TY	TZ	X	Y	Z	COMMENT
1	1	2	3	-0	-0	-0	1616.00	0.	335.29	Ring 1 CNTR
2	4	5	6	-0	-0	-0	1676.00	0.	335.29	Ring 2 CNTR
3	7	8	9	-0	-0	-0	1676.00	72.75	293.29	Ring 2
4	10	11	12	-0	-0	-0	1676.00	42.00	262.54	Ring 2
5	13	14	15	-0	-0	-0	1676.00	-72.75	377.29	Ring 2
6	16	17	18	-0	-0	-0	1676.00	-42.00	408.04	Ring 2
7	19	20	21	-0	-0	-C	1736.00	0.	335.29	Ring 3 CNTR
8	22	23	24	-0	-0	-0	1736.00	72.75	293.29	Ring 3
9	25	26	27	-0	-0	-0	1736.00	42.00	262.54	Ring 3
10	28	29	30	-0	-0	-0	1736.00	-72.75	377.29	Ring 3
11	31	32	33	-0	-0	-0	1736.00	-42.00	408.04	Ring 3
12	34	35	36	-0	-0	-0	1796.00	0.	335.29	Ring 4 CNTR
13	37	38	39	-0	-0	-0	1856.00	0.	335.29	Ring 5 CNTR
14	40	41	42	-0	-0	-0	1916.00	0.	335.29	Ring 6 CNTR
15	43	44	45	-0	-0	-0	1976.00	0.	335.29	Ring 7 CNTR
16	46	47	48	49	50	51	1579.00	0.	337.19	FUSE. PT 4
17	52	53	54	55	56	57	1796.00	0.	335.29	FUSE. PT 5
18	58	59	60	61	62	63	1944.00	0.	334.00	FUSE. PT 6
19	64	65	66	-0	-0	-0	1133.00	0.	221.30	ORB I/F 1716
20	67	68	69	-0	-0	-0	2058.00	101.29	195.26	ORB I/F 1724
21	70	71	72	-0	-0	-0	2058.00	-101.29	195.26	ORB I/F 1725

Table B-2.3: Modal Contributions for Degree of Freedom No. 1, Coupled LDEF/Orbiter

Mode No.	Contribution %	MODE No.	Contribution %
1	0.00	37	0.02
2	0.07	38	0.50
3	0.00	39	0.49
4	0.00	40	17.02
5	0.00	41	44.90
6	0.00	42	17.50
7	0.00	43	2.24
8	0.00	44	0.01
9	0.00	45	0.00
10	0.00	46	0.06
11	0.00	47	0.63
12	0.00	48	0.00
13	0.00	49	0.49
14	0.00	50	0.04
15	0.00	51	0.01
16	0.00	52	0.00
17	0.00	53	0.00
18	0.00	56	0.05
19	0.00	55	0.00
20	0.00	56	0.00
21	0.00	57	0.00
22	0.00	58	0.24
23	1.16	59	0.72
24	0.00	60	0.00
25	0.09	61	0.00
26	0.00	62	0.00
27	0.03	63	0.00
28	0.00	64	0.00
29	0.10	65	0.00
30	0.00	66	0.00
31	0.00	67	0.00
32	0.00	68	0.00
33	0.00	69	0.00
34	0.00	70	0.00
35	7.81	71	0.00
36	5.76	72	0.00

Table B-2.4: Coupled LDEF/Orbiter Frequencies

Mode No.	f (Hz)	Mode No.	f (Hz)
1	0.00	37	22.04
2	0.00	38	22.24
3	0.00	39	24.73
4	0.00	40	25.44
5	0.00	41	26.06
6	0.00	42	27.58
7	3.14	43	28.16
8	3.51	44	30.02
9	4.21	45	31.30
10	5.44	46	31.44
11	5.84	47	31.75
12	5.99	48	34.63
13	6.15	49	36.02
14	6.43	50	36.92
15	6.86	51	39.37
16	8.14	52	40.12
17	8.70	53	43.87
18	9.38	54	44.64
19	10.06	55	45.06
20	10.75	56	49.48
21	10.90	57	49.78
22	11.53	58	52.88
23	13.64	59	58.30
24	14.34	60	67.99
25	14.42	61	74.67
26	14.62	62	86.68
27	15.41	63	139.2
28	15.67	64	270.8
29	16.15	65	285.1
30	16.49	66	346.2
31	17.42	67	350.4
32	17.83	68	363.5
33	18.02	69	412.3
34	19.33	70	427.3
35	20.90	71	547.5
36	21.69	72	2526.

Figure B-2.14 shows one of the actual loads time histories used in the analysis. These loads include effects of 3 Orbiter engines, External Tank side load representing vortex shedding, and a "y" direction wind load corresponding to a 2 second gust at 34.4 knots. Each engine thrust is 417,000 lb at sea level (peak 458,000 lb). The time scale shown in the figures starts after liftoff but prior to SRM fire.

B-2.5.2 ANALYTICAL TECHNIQUES AND RESULTS

The technique used to calculate the responses of the coupled model should demonstrate the current "state of the art" in payload analysis.

Generally the technique involves driving the coupled model in the modal domain, then using the modal responses to obtain the discrete responses.

Considering the coupled equations of motion,

$$[M]\{\ddot{q}\} + [C]\{\dot{q}\} + [K]\{q\} = \{F\} \qquad (7)$$

Where $[M]$ = coupled mass matrix

$[C]$ = coupled damping matrix

$[K]$ = coupled stiffness matrix

$\{q\}$ = discrete d.o.f.

$\{F\}$ = external forces

This set of equations can be uncoupled by substituting:

$$\{q\} = [\phi]\{\xi\} \qquad (8)$$

Where $[\phi]$ = modes matrix

$\{\xi\}$ = model d.o.f.

and assuming linearity,

$$\{\dot{q}\} = [\phi]\{\dot{\xi}\} \qquad (9)$$

$$\{\ddot{q}\} = [\phi]\{\ddot{\xi}\} \qquad (10)$$

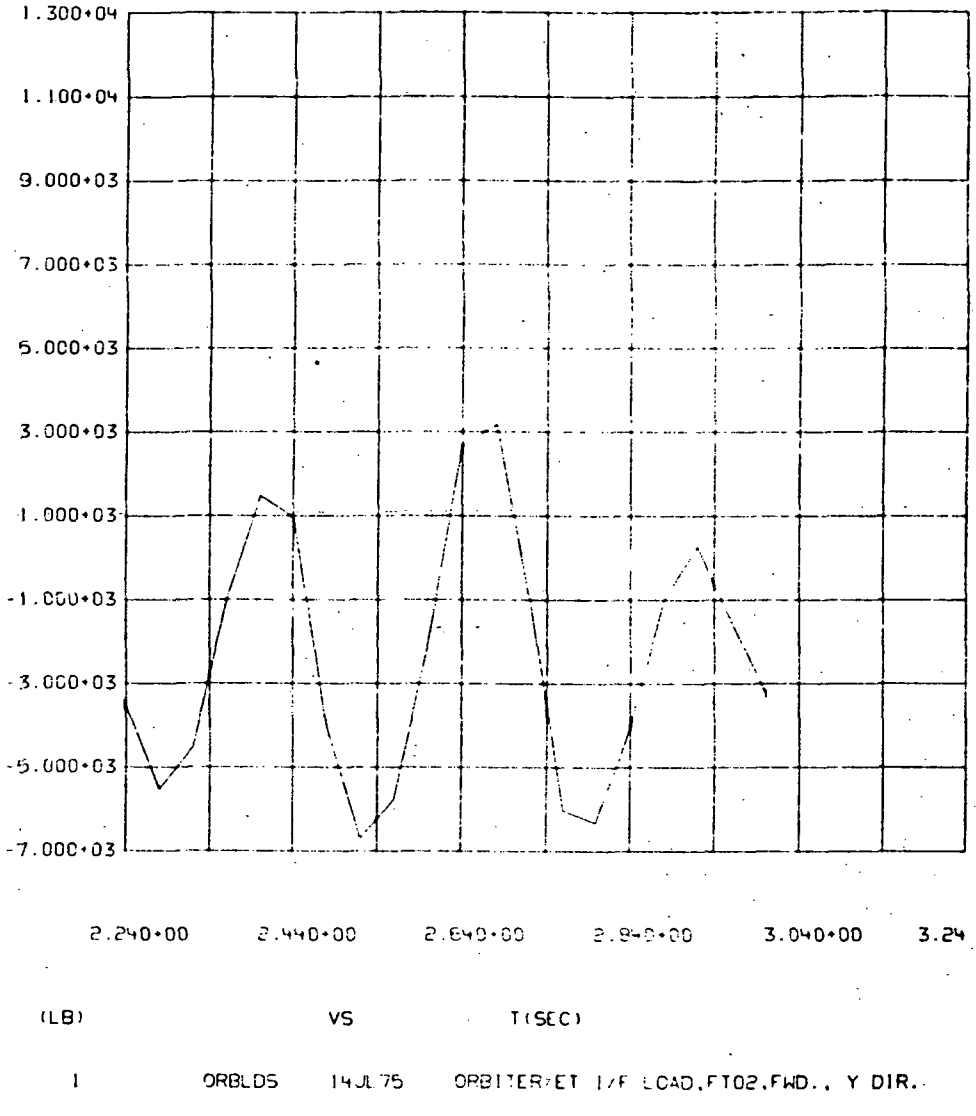

Figure B-2.14a: Load Applied at Node Point 19

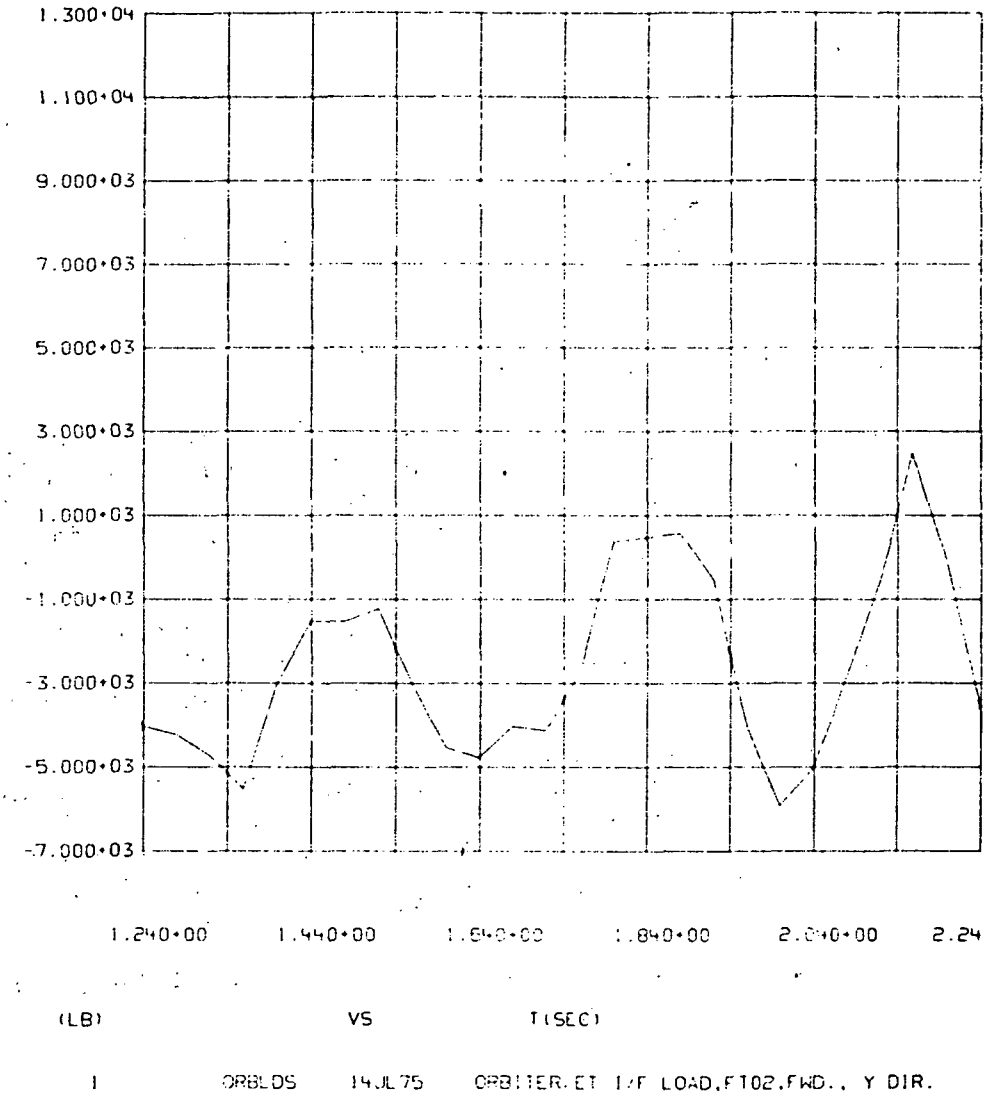

Figure B-2.14b Load Applied at Node Point 19

therefore (7) becomes

$$[M][\phi]\{\ddot{\xi}\} + [C][\phi]\{\dot{\xi}\} + [K][\phi]\{\xi\} = \{F\} \qquad (11)$$

Then pre-multiplying by $[\phi]^T$ yields,

$$[\phi]^T[M][\phi]\{\ddot{\xi}\} + [\phi]^T[C][\phi]\{\dot{\xi}\} + [\phi]^T[K][\phi]\{\xi\} = [\phi]^T\{F\} \qquad (12)$$

Our modes are normalized such that

$$[\phi]^T[M][\phi] = [I] \quad \text{(generalized mass)} \qquad (13)$$

and (12) becomes

$$[I]\{\ddot{\xi}\} + [2\zeta\omega]\{\dot{\xi}\} + [\omega^2]\{\xi\} = [\phi]^T\{F\} \qquad (14)$$

where $[2\zeta\omega]$ = generalized damping

$[\omega^2]$ = generalized stiffness

Equation (14) represents the uncoupled set of equations of motion of the model in the modal domain. The column vector, $\{F\}$ represents the set of interface loads described above as a function of time. They also include 417,000 pounds constant thrust forces for the engines to balance the loads. This equation was solved in the time domain for modal accelerations as a function of time, then substituted into equation (10) for the discrete responses. This technique can also be used to calculate internal loads, by substituting a loads coefficient matrix for the modes in equation (10).

Examples of the time responses are shown in Figures B-2.15 and B-2.16. Only the three orthogonal directions for the first 2 node points are shown as representative. In most applications, the frequency content of the response is also meaningful. To meet this end, Fourier Spectra of the responses were calculated and shown in Figures B-2.17 through B-2.19 for the first node point.

In summary, the maximum and minimum peak responses for all the coupled degrees of freedom are shown in Table B-2.5.

B-2.6 CONCLUDING DISCUSSION

The assumptions made in generating the models caused some discrepancies in the true structure vs these math models. With better mass data one can derive a math model for the LDEF with completely different structural characteristics. For this reason, the results presented herein should not be taken as the final set. The results do, however, typify the major analytical efforts practiced in the "state of the art".

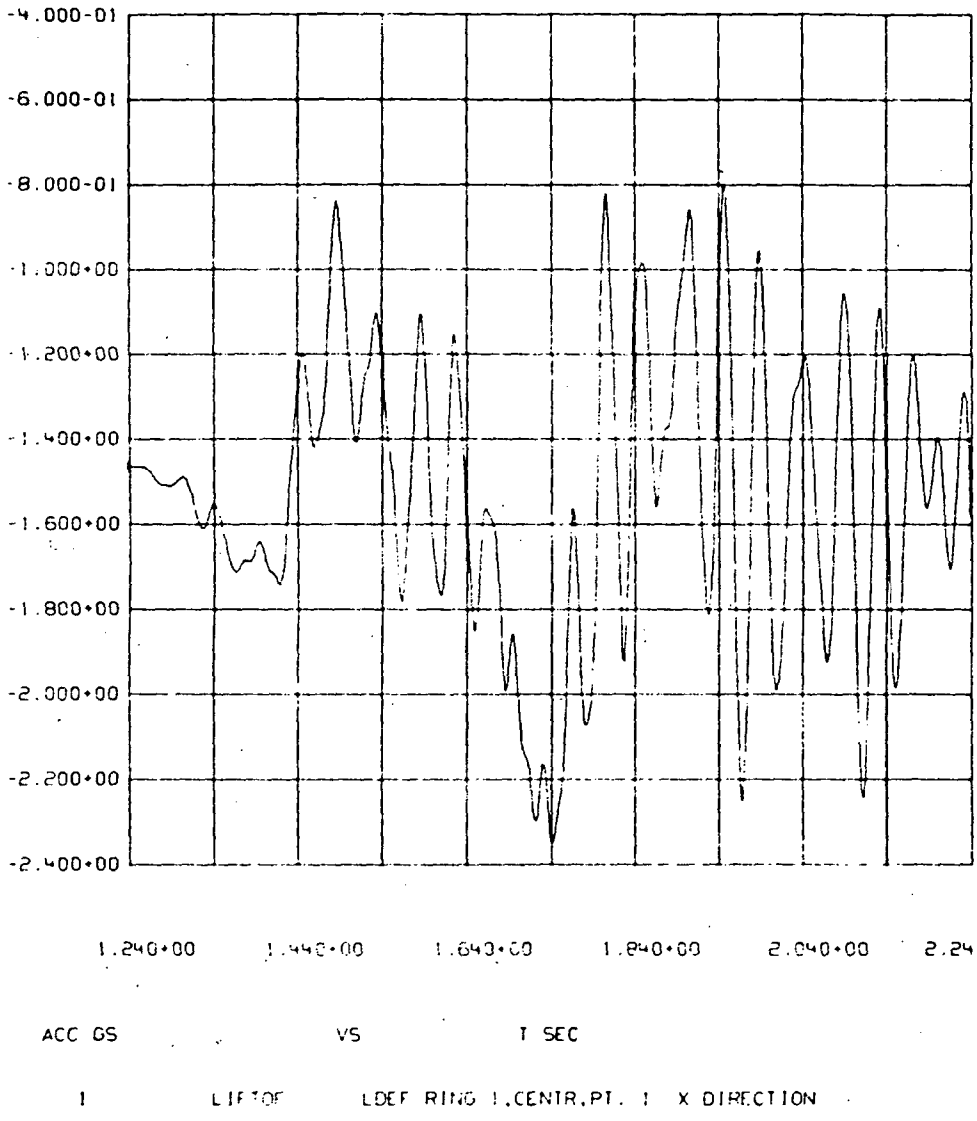

Figure B-2.15: Acceleration Time History at LDEF Ring 1 Center, Point 1X

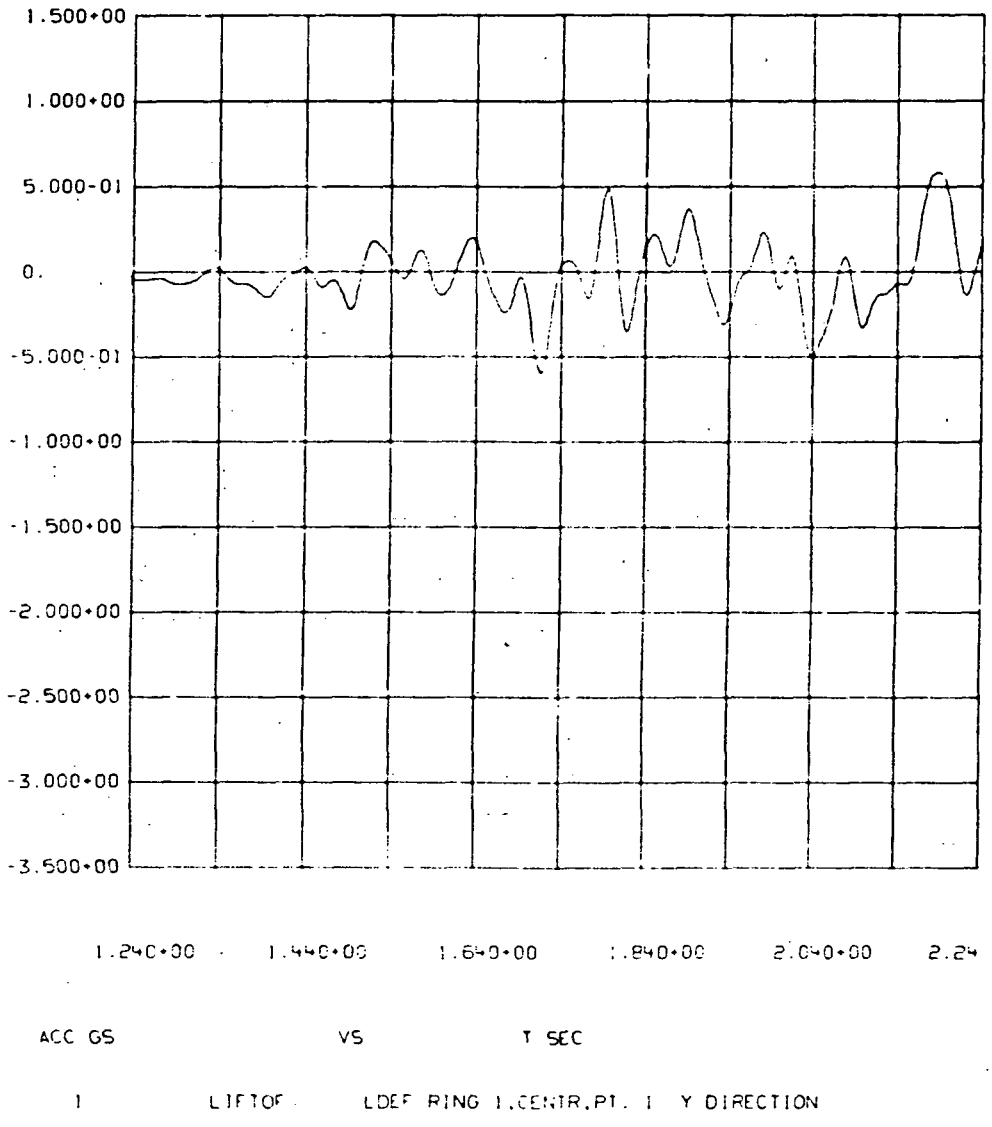

Figure B-2.16: Acceleration Time History at LDEF Ring 1 Center, Point 1Y

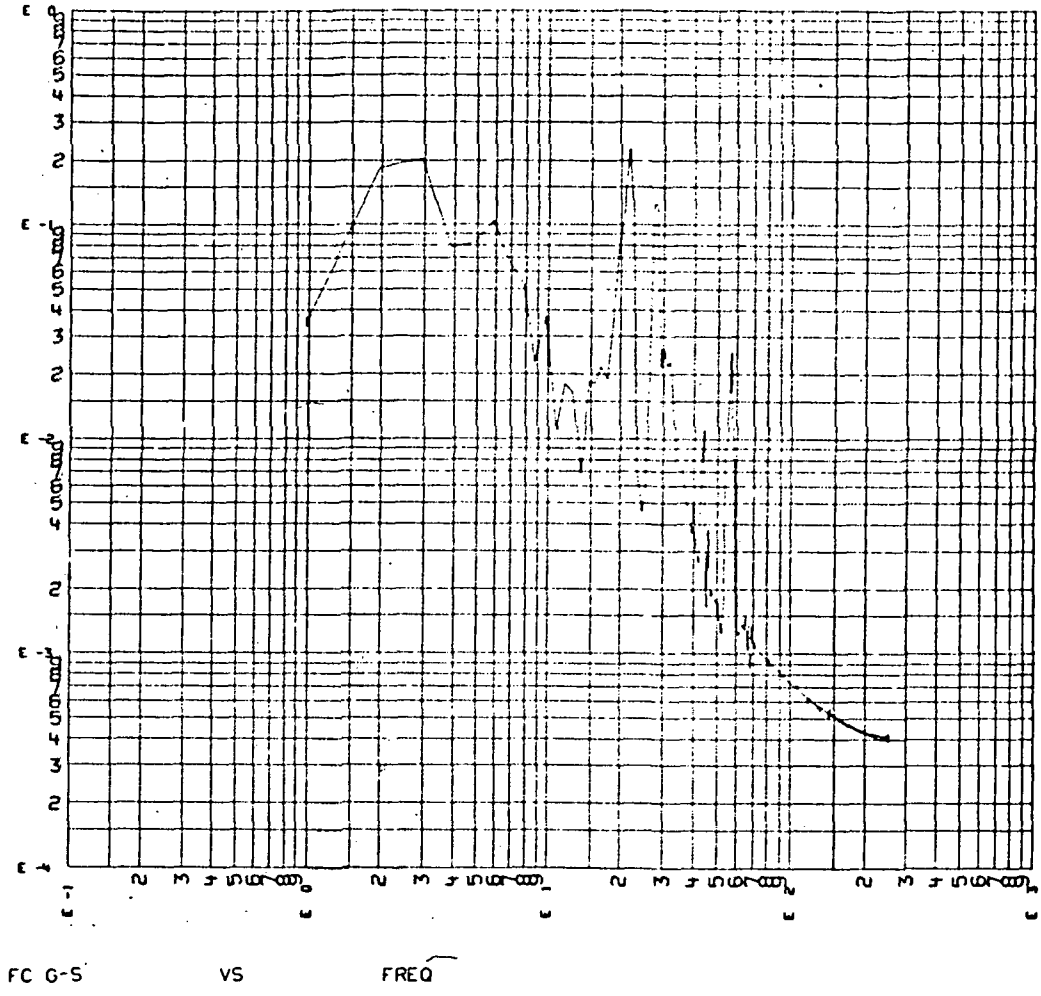

Figure B-2.17: Fourier Spectrum for LDEF, Point 1X

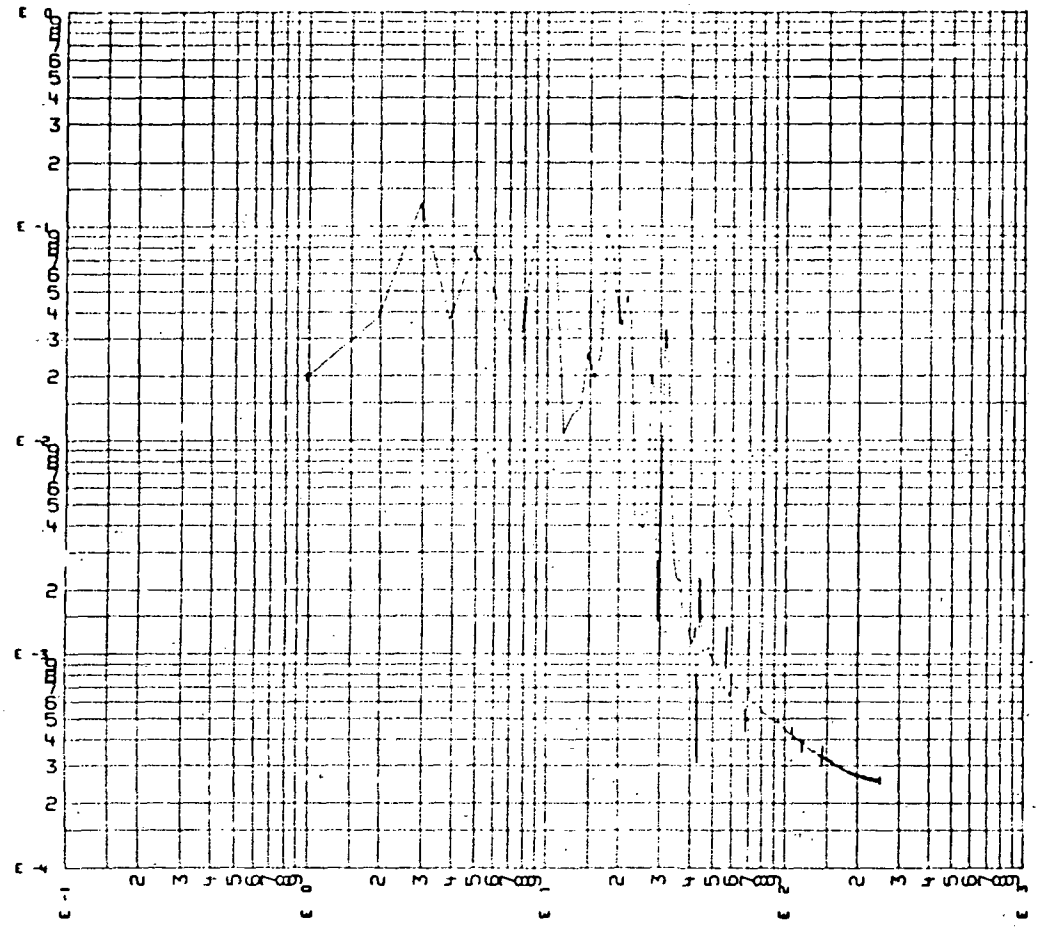

Figure B-2.18: Fourier Spectrum for LDEF, Point 1Y

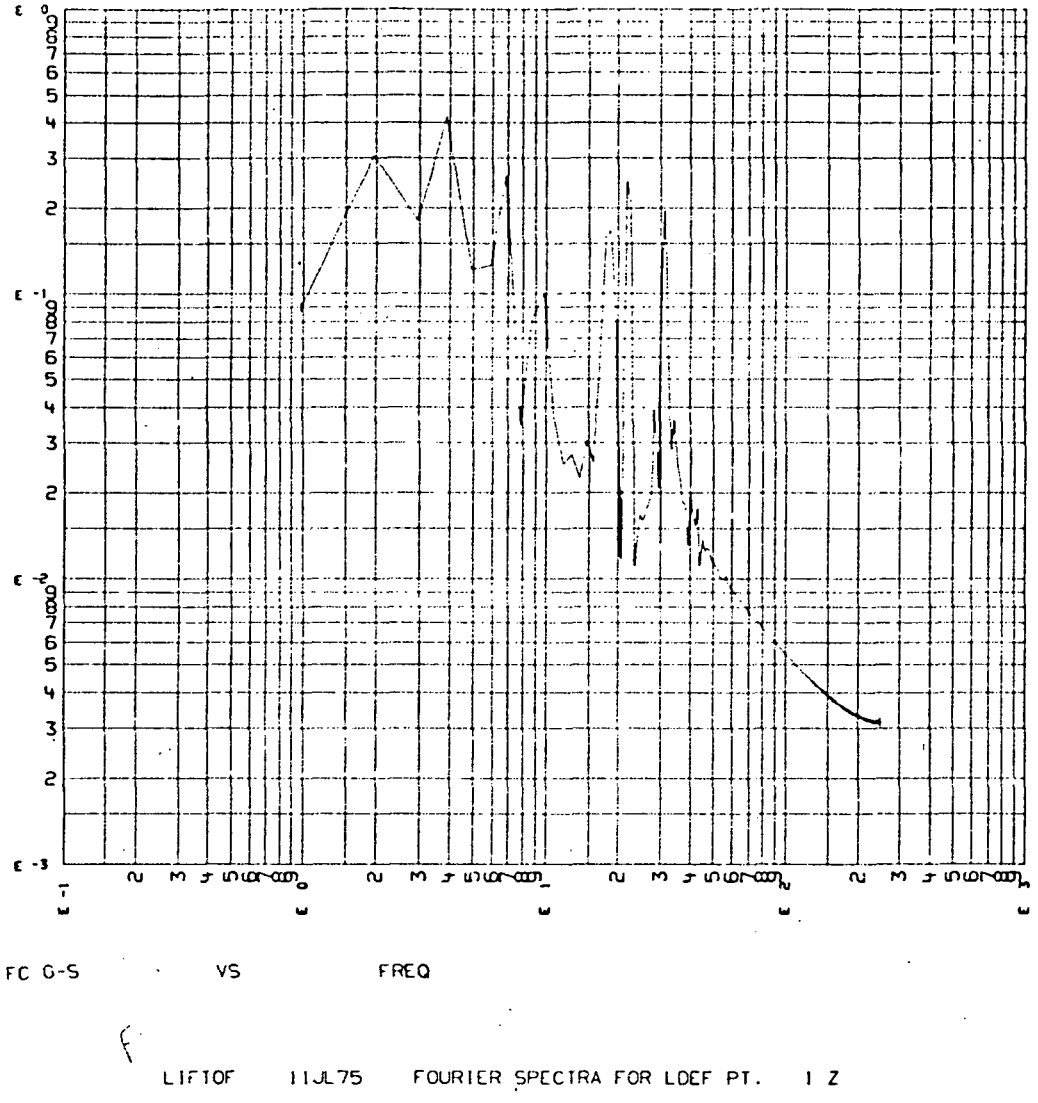

Figure B-2.19: Fourier Spectrum for LDEF, Point 1Z

Table-B-2.5: Maximum and Minimum Responses During Liftoff

D.O.F.	TIME OF MAX (SEC)	MAX (g)	TIME OF MIN (SEC)	MIN (g)
1	2.36	-0.73	1.74	-2.35
2	2.82	1.35	2.87	-3.04
3	2.26	1.48	2.18	-1.54
4	2.38	-1.09	1.73	-2.30
5	2.80	1.10	2.89	-1.29
6	2.78	2.37	2.15	-2.74
7	2.36	-1.09	1.72	-2.22
8	2.17	1.32	2.25	-1.38
9	2.79	1.50	2.87	-1.50
10	1.90	-0.91	1.77	-2.28
11	2.95	1.42	2.87	-1.33
12	2.79	1.50	2.87	-1.50
13	2.37	-0.84	1.74	-2.45
14	2.85	0.80	2.15	-1.15
15	2.77	0.94	2.91	-0.98
16	2.37	-0.73	1.73	-2.57
17	2.89	1.02	2.96	-1.23
18	2.77	0.94	2.91	-0.99
19	2.39	-0.90	1.74	-2.34
20	2.99	2.22	2.90	-2.01
21	1.96	1.41	2.16	-1.50
22	2.36	-1.09	1.72	-2.22
23	2.17	0.91	2.25	-0.81
24	2.74	1.35	2.85	-1.52
25	1.90	-0.91	1.77	-2.27
26	2.16	0.98	2.88	-0.94
27	2.74	1.35	2.85	-1.52
28	2.37	-0.84	1.74	-2.44
29	2.85	0.76	3.00	-0.91
30	2.76	1.33	2.43	-1.39
31	2.37	-0.73	1.73	-2.57
32	1.79	0.90	2.17	-1.08

(Continued)

Table B-2.5: (Continued)

D.O.F.	TIME OF MAX (SEC)	MAX (g)	TIME OF MIN (SEC)	MIN (g)
33	2.76	1.33	2.43	-1.39
34	2.39	-1.01	1.74	-2.31
35	2.76	0.77	2.86	-0.60
36	1.99	1.36	2.13	-1.35
37	2.39	-0.89	1.74	-2.34
38	2.79	1.16	2.87	-1.60
39	1.96	1.57	2.17	-1.60
40	2.39	-1.09	1.74	-2.30
41	2.78	0.88	2.91	-1.28
42	1.73	2.65	2.14	-3.60
43	2.41	-0.81	1.74	-2.38
44	2.99	4.53	2.94	-4.08
45	2.26	2.50	2.18	-2.01
46	2.38	-1.07	1.72	-2.29
47	2.78	0.60	2.84	-0.69
48	2.02	0.92	2.10	-0.99
49	2.98	.003	2.83	- .005
50	1.89	.005	1.79	- .005
51	2.76	.003	2.87	- .003
52	1.49	-1.11	1.73	-2.22
53	2.77	0.72	2.88	-0.63
54	2.26	0.81	2.15	-0.96
55	3.00	.006	2.84	- .004
56	2.02	.003	1.81	- .003
57	2.82	.003	2.78	- .004
58	1.48	-1.11	1.73	-2.21
59	2.74	0.45	2.89	-0.57
60	1.97	0.69	2.15	-0.81
61	2.93	.002	2.90	- .003
62	1.96	.004	1.88	- .004
63	2.80	.003	2.76	- .004

Prior to the first few Shuttle missions, the phases described herein, i.e., math model test correlation, etc., should be repeated to evaluate the unknown dynamic characteristics of the Shuttle system. With the increased confidence and reliability gathered from the flight data and math models, the analytical efforts for the remaining Shuttle flights can be sharply decreased.

B-3.0 TEST PROGRAM

This section describes the system level dynamic tests recommended for the LDEF payload. Static tests for verification of structural integrity and the component/experiment test programs are not addressed.

Based on an evaluation of the type of structure and configuration of the LDEF payload, we feel that qualification and/or acceptance tests on a system level are not required. Two system level development type tests (a modal survey and an acoustic test) are recommended using primary structure as flight-type hardware, and dynamic simulators for components and experiments.

B-3.1 MODAL SURVEY TEST

This test is needed to obatin data for verification/correction of the structural math model of the LDEF, for coupling with the Space Shuttle model to determine structural loads and low frequency vibration produced by transient events such as engine ignition, shutdown, landing shock, gusts, etc. Mode shapes, frequencies, and damping should be determined over the frequency range for which confidence exists in the results of the math model.

B-3.2 ACOUSTIC TEST

Prior to the qualification test program for experiments and components, an acoustic test of the LDEF primary structure and dynamic simulators for components should be conducted to obtain data to define the random vibration criteria for components/experiments and verify the structural integrity of bracketry and secondary structure. It is desirable to use the complete LDEF structure for this test. However, if this configuration presents a serious problem from an acoustic facility capability standpoint, a test utilizing one or two bays of the LDEF structure could provide meaningful results. During this test, measurements at mounting locations should be obtained for the entire range of component/experiment weights. Ideally, multiple runs should be conducted with changes to the component/experiment weights made between runs so that the local mounting point stiffness remains invariant. Obviously, the microphone and accelerometer flight measurement locations defined in Section B-4.0 should be duplicated as far as is practical in order to obtain data for comparison with flight and evaluate the test versus flight vibroacoustic transfer functions. These data can then be utilized to assess the degree of simulation provided by the acoustic test, and form the basis for altering the test environment (if necessary) for future payloads.

If a structural test article is available for this test, consideration should be given to utilizing it as a test bed for qualifying experiments/components acoustically instead of using shakers, potentially saving the cost of design and fabrication of some test fixtures.

B-4.0 FLIGHT MEASUREMENT PROGRAM

B-4.1 INTRODUCTION

The flight measurement program has been developed for the LDEF as part of an overall "state of the art" instrumentation requirements study. Consideration is being paid to ground test requirements and dynamic loads analysis as well as flight test requirements. It is felt that, by concentrating on a single payload for detailed treatment, the correlations and necessary feedback between the test and analytical programs will be revealed with more emphasis than a generalized approach. The techniques developed on LDEF/IRTCM will then be applicable to other payloads.

B-4.2 OBJECTIVES OF FLIGHT MEASUREMENT PROGRAM

The flight measurement program is intended to obtain data on the acoustic environment inside the payload bay during the boost phase, acoustically induced random vibration and quasi-sinusoidal low-frequency transients. Instrumentation will also be located in other regions of the Booster, as defined by Rockwell International personnel, so that good coverage will be obtained both external and internal to the payload bay.

Figure B-1.1 shows a breakdown of Mission 4 into the dynamically significant phases. This sequence of events was used as a basis for planning the usage of dynamic instrumentation.

B-4.3 ASSUMPTIONS

A number of assumptions had to be made regarding the detailed geometry of the payload, since this is not yet defined. For the most part, these reflected the preliminary information given in the description of Mission 4 in Reference B-1. Additional information on structural member sizes was provided by the Contract Technical Monitor.

Figures B-4.1 and B-4.2 show the structural configurations used in this study, with the axis convention and member numbering scheme indicated.

According to Reference B-1, the LDEF experiments will be mounted on "a wide variety and number of trays on the circumferential surface. The trays, which vary in size from 0.13 x 0.49 ft. to 4.0 x 6.0 ft. will each hold a completely self-contained experiment, or, if needed, several adjacent trays may contain the individual elements of a single experiment. Shelves in the LDEF bay have also been designed for the mounting of experiments."

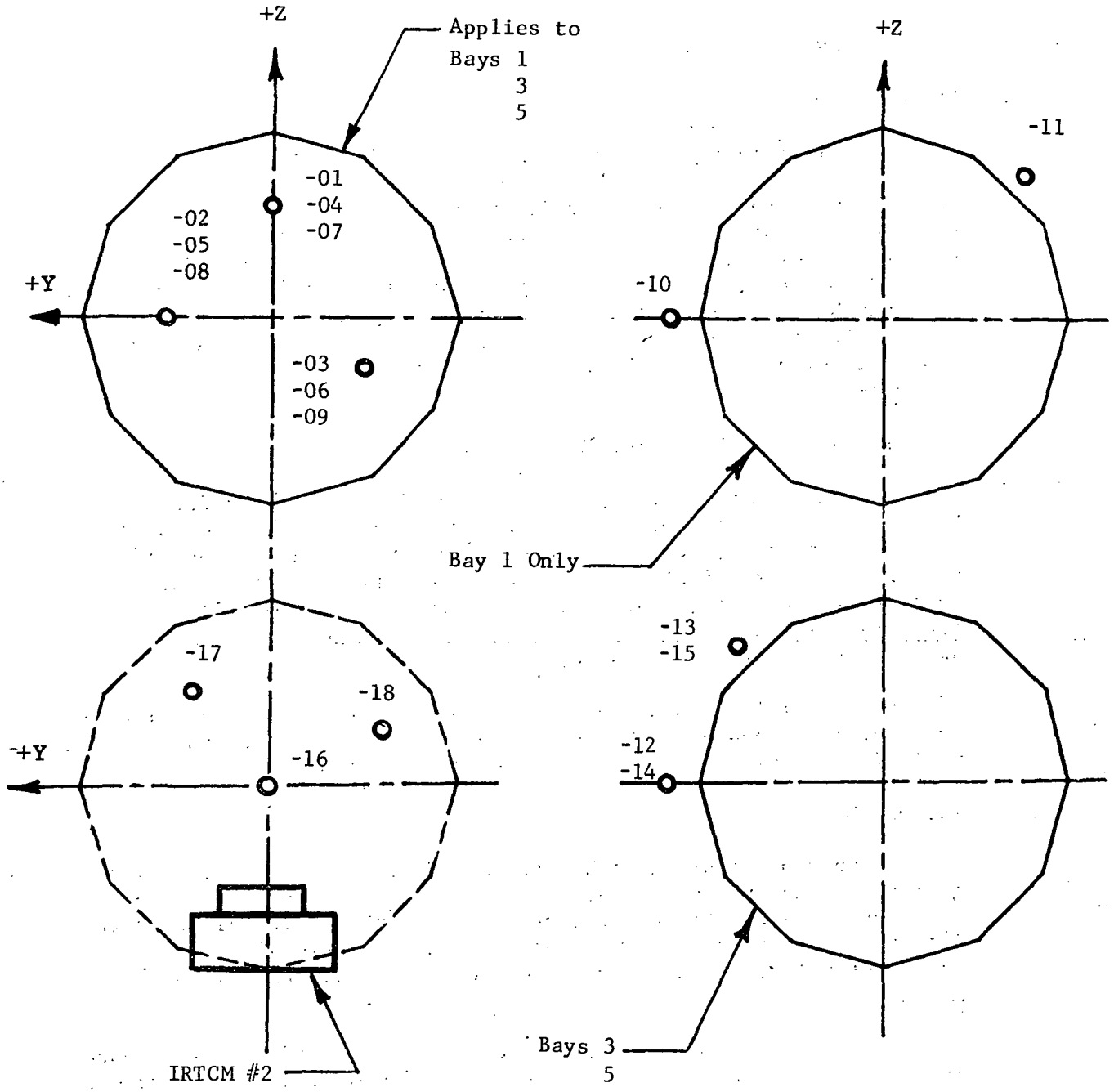

Figure B-4.1 Microphone Locations

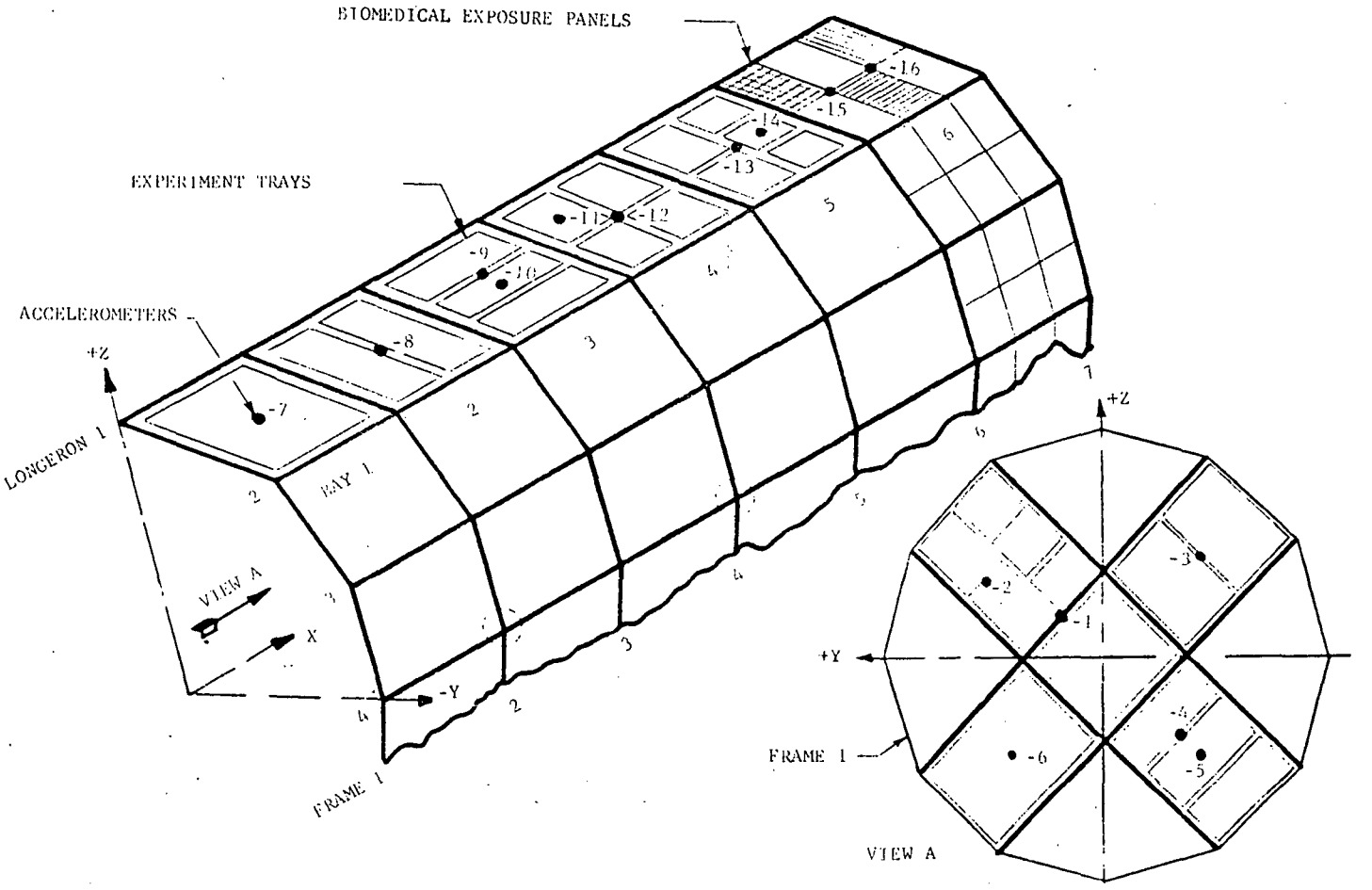

Figure B-4.2 : Locations of High Frequency Accelerometers (HFA-XX)

For the purposes of this study it was assumed that experiment trays are mounted in each of the four forward bays, between Longerons #1 and 2 and on the shelf or bulkhead covering Frame #1. A range of tray sizes was selected, varying from 29 x 14 inches to 43 x 60 inches.

It was assumed that there would be no limitation on onboard recording and multiplexing capability. Furthermore, it was assumed that up to 14 telemetry channels would be available, with a usable frequency range of 2 to 2000 Hz.

It is required to obtain dynamic data on the LDEF during re-entry and landing. However, the problem arises on how to physically acquire the data, since the LDEF will be deployed into orbit, breaking all mechanical and electrical connections, and then retrieved during the next mission.

Two possibilities are being considered:

1. Have automatic or manual reconnection to the Orbiter instrumentation system;

2. Have the LDEF mounted instrumentation and signal conditioning equipment, together with a power supply, completely self-contained with the LDEF; this could be reactivated at the start of re-entry by a timer or pressure sensitive switch.

B-4.4 INSTRUMENTATION REQUIREMENTS

B-4.4.1 TYPES OF TRANSDUCERS

For low-frequency dynamic loads measurements both strain gages and low-frequency accelerometers will be used. High-frequency accelerometers will be installed for measuring acoustically and mechanically induced random vibration. Acoustic environments will be measured with microphones.

B-4.4.2 SIGNAL CONDITIONING EQUIPMENT

For maximum utilization of the transducers, it is planned to use charge amplifiers having gain ranges which can be changed if necessary during the actual mission, so that, for instance, the same low-frequency accelerometer can be used for measuring both vibration and landing shock. The actuation of the gain changes will be related to the mission sequence of events, using an automatic timing system or achieved by remote control from the ground. In addition, the charge amplifiers will be capable of providing multiple outputs covering different frequency and gain ranges. The input signal generated by an accelerometer or strain gage can thus be used to give optimum frequency and dynamic range overlap.

B-4.4.3 DATA RECORDING EQUIPMENT

Magnetic tape recording equipment will be required having the capability for recording 154 multiplexed channels of data. A frequency range of 0 HZ to 3 KHz is required.

B-4.4.4 TELEMETERING REQUIREMENTS

It is assumed that 14 telemetry channels are available. These will be assigned to instrumentation which would be used for diagnostic purposes in the event of a mission failure. Candidate assignments are:

a) Two external microphones (ME-15 and ME-16 in Table B-4.1);

b) Three dual-range accelerometers at payload support points on center frame (DRA-08, -10 and -12 in Table B-4.1);

c) Three dual-range accelerometers at the center of the Frame 1 bulkhead (DRA-13, -14 and -15).

The final allocation of instrumentation to be telemetered in real time will require close coordination with Rockwell International, who will be providing the same kind of coverage on the Orbiter.

B-4.5 INSTRUMENTATION LIST

Table B-4.1 lists the proposed flight instrumentation by type, location, and frequency and dynamic range requirements. The locations are also shown in the figures, as indicated in the last column of the table.

B-4.6 CONCLUDING DISCUSSION

A preliminary flight measurement program has been developed for the LDEF/IRTCM payload. In the absence of firm design data, it was necessary to make many assumptions regarding detailed geometry and mass distribution. Three different kinds of instrumentation were specified: acoustic microphones, accelerometers and strain gages. The rationale associated with the requirements called out for the different kinds of instrumentation will be discussed separately.

B-4.6.1 ACOUSTIC MICROPHONES

The microphone locations were the easiest to select, being relatively independent of the details of the payload geometry. The basic requirement is to measure the acoustic field within the payload bay, both inside and outside the LEDF, and in the part of the payload bay forward of the LDEF which is occupied by the 5-ft pallet and one of the IRTCMs. Locations were selected so as to minimize the possibility of measuring standing wave patterns. In addition, the angular locations of the microphones and their distances from the LDEF centerline were selected to avoid radial symmetry.

Table B-4.1 Instrumentation List

TRANSDUCER TYPE	IDENT NO.	GENERAL LOCATION	APPROX. STATION X ins	X cm	Y ins	Y cm	Z ins	Z cm	SENSING AXIS	FREQ RANGE (Hz)	DYNAMIC RANGE	REFER TO FIG. NO.
Acoustic Microphones	MI-01	Internal	919	2334	0	0	60	152.4	Not Applic.	10-3K	100-150dB	B-4.1
	MI-02	Bay 1	919	2334	50	127	0	0				
	MI-03		919	2334	-34.6	-87.9	-20	-50.8				
	MI-04	Ditto,	1035	2629	0	0	60	152.4				
	MI-05	Bay 3	1035	2629	50	127	0	0				
	MI-06		1035	2629	-34.6	-87.9	-20	-50.8				
	MI-07	Ditto	1156	2936	0	0	60	152.4				
	MI-08	Bay 5	1156	2936	50	127	0	0				
	MI-09		1156	2936	-34.6	-87.9	-20	-50.8				
	ME-10	External,	919	2334	100	254	0	0			110-160dB	
	ME-11	Bay 1	919	2334	-70.7	-179.6	70.7	-179.6				
	ME-12	Ditto,	1035	2629	100	254	0	0				
	ME-13	Bay 3	1035	2629	70.7	179.6	70.7	179.6				

NOTES

X, Y, Z directions defined in Figure B-4.2

Table B-4.1 Instrumentation List

TRANSDUCER TYPE	IDENT NO.	GENERAL LOCATION	APPROX. STATION X ins	X cm	Y ins	Y cm	Z ins	Z cm	SENSING AXIS	FREQ RANGE (Hz)	DYNAMIC RANGE	REFER TO FIG. NO.
Acoustic Microphones	ME-14	Ditto,	1156	2936	100	25.4	0	0	Not	10-3K	110-160dB	B-4.1
	ME-15	Bay 5	1156	2936	70.7	179.6	70.7	179.6	Applic.			
	ME-16	In region of	744.5	1891	0	0	0	0				
	ME-17	IRTCM #2,	744.5	1891	42.4	107.7	30	76.2				
	ME-18	fwd. of LDEF	744.5	1891	-52	132	30	76.2				
Dual Range Accels.	DRA-01	On payload Support fitting, Frame 2 at	947	2405	-84	213.4	0	0	X	2-2K	Note 1.	B-4.5
	DRA-02	Longeron 4	947	2405	-84	213.4	0	0	Z			
	DRA-03	Ditto Frame 4 at Longeron 4	1067	2710	-84	213.4	0	0	X			
	DRA-04		1067	2710	-84	213.4	0	0	Z			
	DRA-05	Ditto Frame 4 at Longeron 7	1067	2710	0	0	-84	-213.4	Y			

NOTES

1. ±10g for low-frequency vibration, ± 30g for high frequency vibration

Table B-4.1 Instrumentation List

TRANSDUCER TYPE	IDENT NO.	GENERAL LOCATION	APPROX. STATION X ins	X cm	Y ins	Y cm	Z ins	Z cm	SENSING AXIS	FREQ RANGE (Hz)	DYNAMIC RANGE	REFER TO FIG. NO.
Dual Range Accels.	DRA-06	Ditto Frame 4 at	1067	2710	84	213.4	0	0	X	2-2K	Note 1	B-4.5
	DRA-07	Longeron 10	1067	2710	84	213.4			Z			
	DRA-08	Frame 1,	887	2253	0	0			X			
	DRA-09	Center	887	2253					Y			
	DRA-10		887	2253					Z			
	DRA-11	Frame 2	947	2405					X			
	DRA-12	Center	947	2405					Y			
	DRA-13		947	2405					Z			
	DRA-14	Frame 3 Center	1007	2558					X			
	DRA-15	Frame 4,	1067	2710					X			
	DRA-16	Center	1067	2710					Y			
	DRA-17		1067	2710					Z			

NOTES

Table B-4.1 Instrumentation List

TRANSDUCER TYPE	IDENT NO.	GENERAL LOCATION	APPROX. STATION X ins	X cm	Y ins	Y cm	Z ins	Z cm	SENSING AXIS	FREQ RANGE (Hz)	DYNAMIC RANGE	REFER TO FIG. NO.
Dual Range Accels.	DRA-18	Frame 7,	1247	3167	0	0	0	0	X	2-2K	Note 1	B-4.6
	DRA-19	Center	1247	3167	0	0	0	0	Y	↓	↓	↓
	DRA-20		1247	3167	0	0	0	0	Z			
	DRA-21	Frame 2	947	2405	-42	-106.7	72.75	184.8	X			
	DRA-22	at	947	2405	↓	↓	↓	↓	Y			
	DRA-23	Longeron 2	947	2405					Z			
	DRA-24	Frame 3	1007	2558					X			
	DRA-25	at	↓	↓					Y			
	DRA-26	Longeron 2							Z			
	DRA-27	Frame 3			-72.75	-184.8	42	106.7	X			
	DRA-28	at			↓	↓	↓	↓	Y			
	DRA-29	Longeron 3	↓	↓					Z	↓	↓	↓

NOTES

Table B-4.1 Instrumentation List

TRANSDUCER TYPE	IDENT NO.	GENERAL LOCATION	APPROX. STATION X ins	X cm	Y ins	Y cm	Z ins	Z cm	SENSING AXIS	FREQ RANGE (Hz)	DYNAMIC RANGE	REFER TO FIG. NO.
Dual Range Accels.	DRA-30	Frame 5	1127	2862.6	-42	106.7	72.75	184.8	X	2-2K	Note 1	B-4.6
	DRA-31	at	1127	1127					Y			
	DRA-32	Longeron 2	1127	1127					Z			
	DRA-33	Frame 6	1187	3015					X			
	DRA-34	at	1187	3015					Y			
	DRA-35	Longeron 2	1187	3015					Z			
	DRA-36	Frame 7	1247	3167					X			
	DRA-37	at	1247	3167					Y			
	DRA-38	Longeron 2	1247	3167					Z			
	DRA-49	On IRTCM	715	1816	24	61	-72.75	-184.8	X			B-4.3
	DRA-50	Pallet	715	1816	24	61			Y			
	DRA-51	Support Points	715	1816	-24	-61			X			
	DRA-52		715	1816	-24	-61			Y			
	DRA-53		745	1892	-24	-61			Y			
	DRA-54		774	1966	0	0	-94	-238.8	Z			

NOTES

Table B-4.1 Instrumentation List

TRANSDUCER TYPE	IDENT NO.	GENERAL LOCATION	APPROX. STATION X ins	X cm	Y ins	Y cm	Z ins	Z cm	SENSING AXIS	FREQ RANGE (Hz)	DYNAMIC RANGE	REFER TO FIG. NO.
High Freq. Accels.	HFA-01	Frame 1	887	2253	15.6	39.6	15.6	39.6	X	2-2K	± 40g	B-4.2
	HFA-02	Bulkhead, +Y, +Z quadrant			45.6	115.8	30	76.2				
	HFA-03	Ditto -Y, +Z quadrant			-36	-91.4	36	-91.4				
	HFA-04	Ditto			-22.8	-57.9	-22.8	-57.9				
	HFA-05	-Y, -Z quadrant			-36	-91.4	-36	-91.4				
	HFA-06	Ditto +Y, -Z quadrant			36	91.4	-36	-91.4				
	HFA-07	On experiment tray between Longeron 1 & 2 in Bay 1	917	2329	-21	53.3	78.4	199.1	Note 2			

NOTES 2. Accels on experiment trays mounted so that sensitive axis is normal to plane of tray.

Table B-4.1 Instrumentation List

TRANSDUCER TYPE	IDENT NO.	GENERAL LOCATION	APPROX. STATION X ins	X cm	Y ins	Y cm	Z ins	Z cm	SENSING AXIS	FREQ RANGE (Hz)	DYNAMIC RANGE	REFER TO FIG. NO.
High Freq. Accels	HFA-08	On experiment tray, between Longerons 1 & 2 Bay 2	977	2482	-21	-53.3	78.4	199.1	Note 2	2-2K	±40g	B-4.2
	HFA-09	Ditto	1037	2634	-21	-53.3	78.4	199.1				
	HFA-10	Bay 3	1037	2634	-14	-35.6	80.3	204				
	HFA-11	Ditto	1082	2748	-11.5	-29.2	81.2	206.2				
	HFA-12	Bay 4	1097	2786	-21	-53.3	78.4	199.1				
	HFA-13	Ditto	1157	2939	-21	-53.3	78.4	199.1				
	HFA-14	Bay 5	1172	2977	-21	-53.3	78.4	199.1				
	HFA-15	On Biomedical Exposure Panels,	1207	3066	-21	-53.3	78.4	199.1				
	HFA-16	Bay 6, between Longerons 1 & 2	1227	3116	-21	-53.3	78.4	199.1				

NOTES

Table B-4.1 Instrumentation List

TRANSDUCER TYPE	IDENT NO.	GENERAL LOCATION	APPROX. STATION X ins	X cm	Y ins	Y cm	Z ins	Z cm	SENSING AXIS	FREQ RANGE (Hz)	DYNAMIC RANGE	REFER TO FIG. NO.
High Freq. Accels.	HFA-17	On pallet, adjacent to IRTCM Mounting Feet	731	1856.7	-10	-25.4	-72.75	-184.8	X	2-2K	±40g	B-4.3
	HFA-18		731	1856.7	-10	-25.4	-72.75	-184.8	Y			
	HFA-19		731	1856.7	-10	-25.4	-72.75	-184.8	Z			
	HFA-20		759	1927.9	10	25.4	↓	↓	X			↓
	HFA-21		759	1927.9	10	25.4			Y			
	HFA-22		759	1927.9	10	25.4			Z			
	HFA-23	On fwd. bulkhead, adjacent to IRTCM Mounting Feet	563	1430	TBD	TBD	TBD	TBD	X			B-4.4
	HFA-24		↓	↓	↓	↓	↓	↓	Y			↓
	HFA-25								Z			
	HFA-26								X			
	HFA-27								Y			
	HFA-28								Z			
	HFA-29	On aft bulkhead, adjacent to IRTCM Mounting Feet	1308	3322	↓	↓	↓	↓	X	↓	↓	↓
	HFA-30		↓	↓					Y			
	HFA-31								Z			
	HFA-32								X			
	HFA-33								Y			
	HFA-34								Z			

NOTES

Table B-4.1 Instrumentation List

TRANSDUCER TYPE	IDENT NO.	GENERAL LOCATION	APPROX. STATION X ins	X cm	Y ins	Y cm	Z ins	Z cm	SENSING AXIS	FREQ RANGE (Hz)	DYNAMIC RANGE	REFER TO FIG. NO.
Strain Gages	S-01	Payload support fitting, Frame 4 at Longeron 4	1067	2710	-84	-213.4	0	0	Fitting longitudinal	0-50	Note 3	B-4.8
	S-02				-84	-213.4						
	S-03				-84	-213.4						
	S-04				-84	-213.4						
	S-05	Ditto			84	213.4						
	S-06	Frame 4 at			84	213.4						
	S-07	Longeron 10			84	213.4						
	S-08											
	S-09	Ditto			0	0	-84	-213.4				
	S-10	Frame 4 at			0	0	-84	-213.4				
	S-11	Longeron 7			0	0	-84	-213.4				
	S-12				0	0	-84	-213.4				
	S-13	Ditto	947	2405	-84	-213.4	0	0				
	S-14	Frame 2 at Longeron 4	947	2405	-84	-213.4	0	0				

NOTES

3. Dynamic range for strain gages will be selected following completion of loads analysis.

A total of 18 microphones were called out, nine of which are located inside, and nine outside the LDEF. The nine internal microphones are distributed equally among Bays 1, 3 and 5. Three of the external microphones are in the forward payload bay, to allow the acoustic environment in the region of the IRTCM to be defined. The remaining six microphones are outside the LDEF, in positions corresponding to Bays 1, 3 and 5 (two microphones per bay) to provide correlation with their internal counterparts. The data from the microphones will be used to calculate acoustic/vibration transfer functions for the payload, and to support the study of the effects of different payload sizes on the internal acoustic environment.

B-4.6.2 ACCELEROMETERS

The assumed experiment tray geometry is shown in Figure B-4.2. High-frequency accelerometers were called out for the trays in sufficient numbers to allow the calculation of acoustic/vibration transfer functions, for a range of tray sizes and mass loading conditions. This set of data will provide good coverage for the class of low density payload elements which will commonly occur on the Shuttle program.

The pallet on which the IRTCM is mounted is also instrumented with high-frequency accelerometers, shown in Figure B-4.3. However, since this type of pallet will be used for many other small payloads, its transmissibility characteristics should be thoroughly investigated during ground testing prior to its first use. Instrumentation will be installed on the two IRTCMs mounted on the forward and aft bulkheads of the payload bay, indicated in Figure B-4.4.

Accelerometers were also assigned for measuring the low-frequency overall payload inputs during ascent transients and the major component low-frequency in flight environments. The locations, shown in Figures B-4.5 and B-4.6 were chosen, based on an analytical model of the LDEF, with the majority of the experiments assumed to be attached to support structure mounted on the seven primary structure rings. It is desirable to measure the high-frequency environment at the same locations. Also, at the payload support points, it will be required to measure the landing shock environment. Instrumentation at these points will completely define the input. Information on shock levels transmitted from the fittings into the payload itself can readily be gained from ground testing. In order to achieve coverage with the minimum number of transducers, it is proposed to use a dual-range accelerometer system, shown in block diagram form in Figure B-4.7. Multiple input/output amplifiers are available (for example, the Columbia 5600 series or the Endevco 2640 series charge amplifiers) to facilitate such an arrangement.

The acceleration data will be used to compare with the pre-flight analysis and to apply to the flight data bank for the next series of payloads.

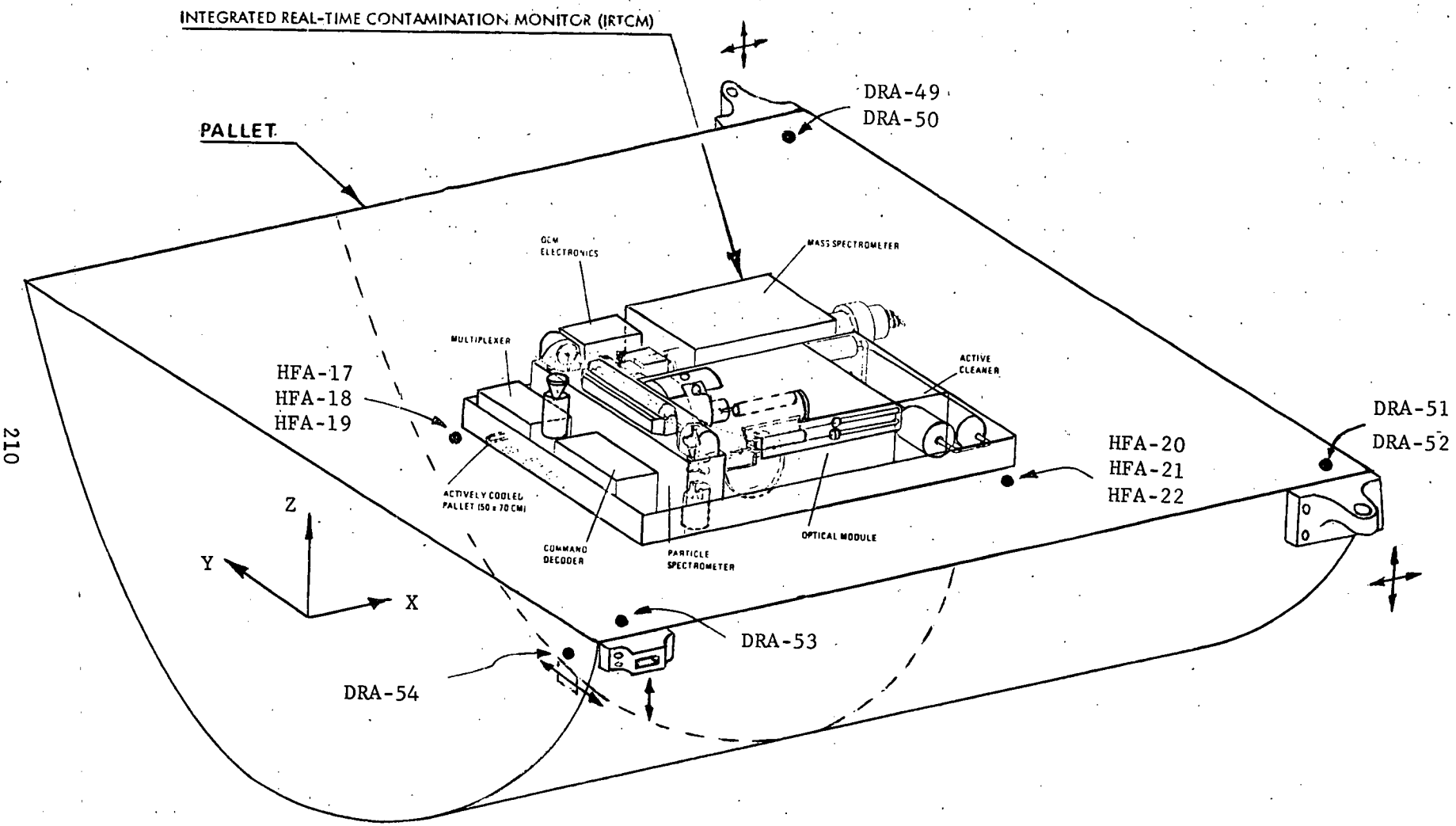

Figure B-4.3 Locations of Accelerometers on Pallet and IRTCM

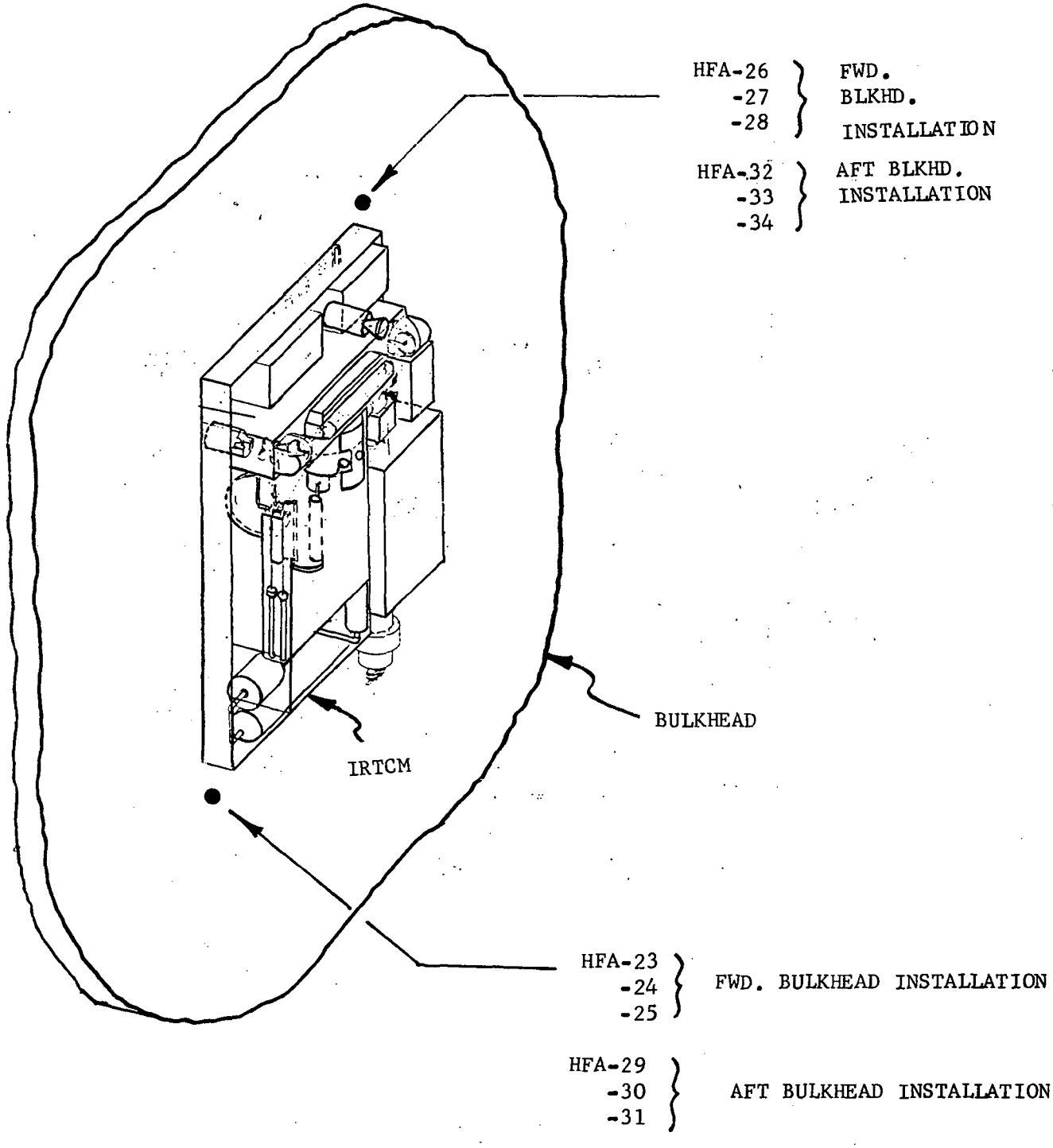

Figure B-4.4: Locations of Accelerometers on Bulkhead-Mounted IRTCM's

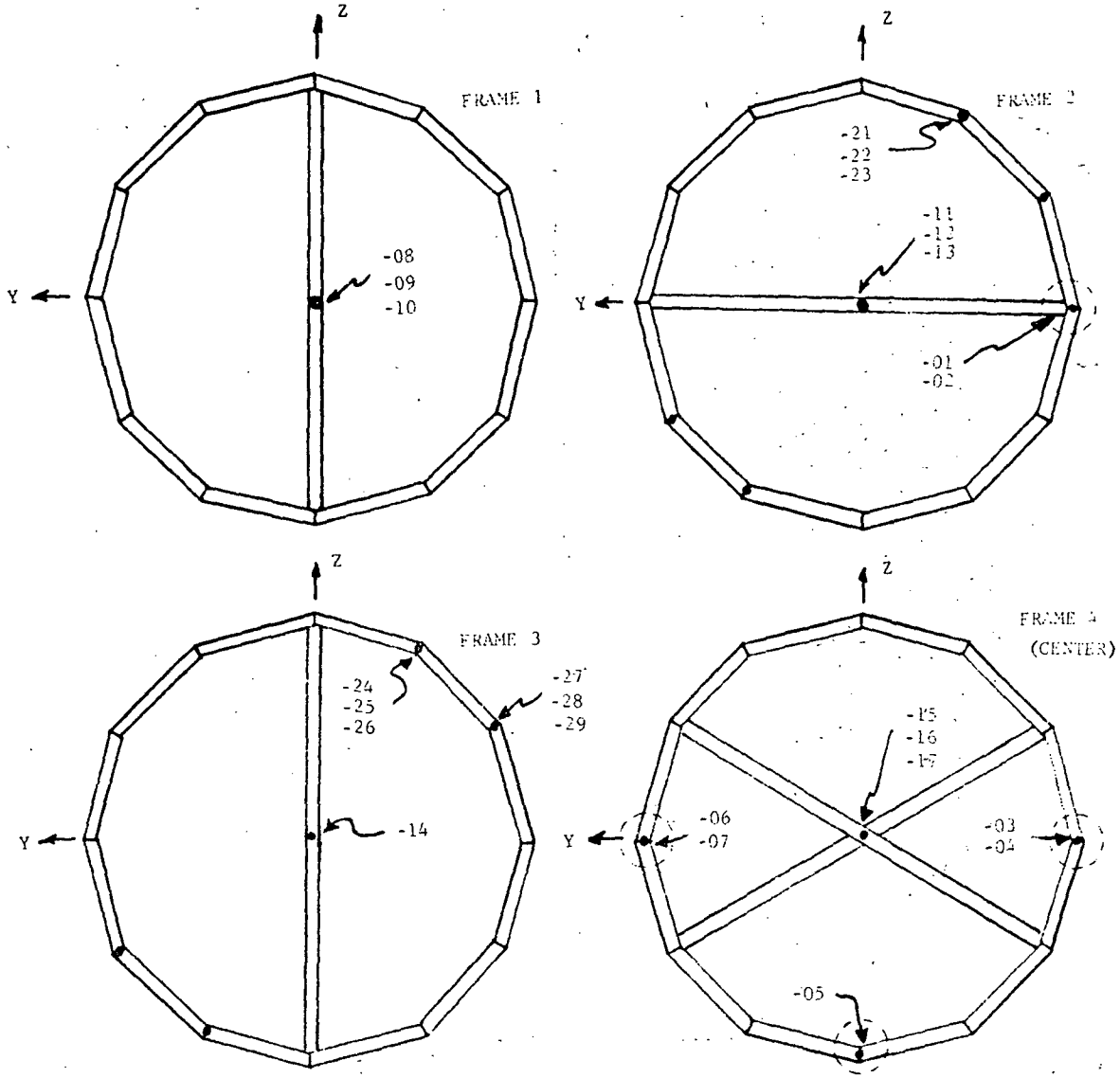

Figure B-4.5: Locations of Dual Range Accelerometers (DRA-XX)

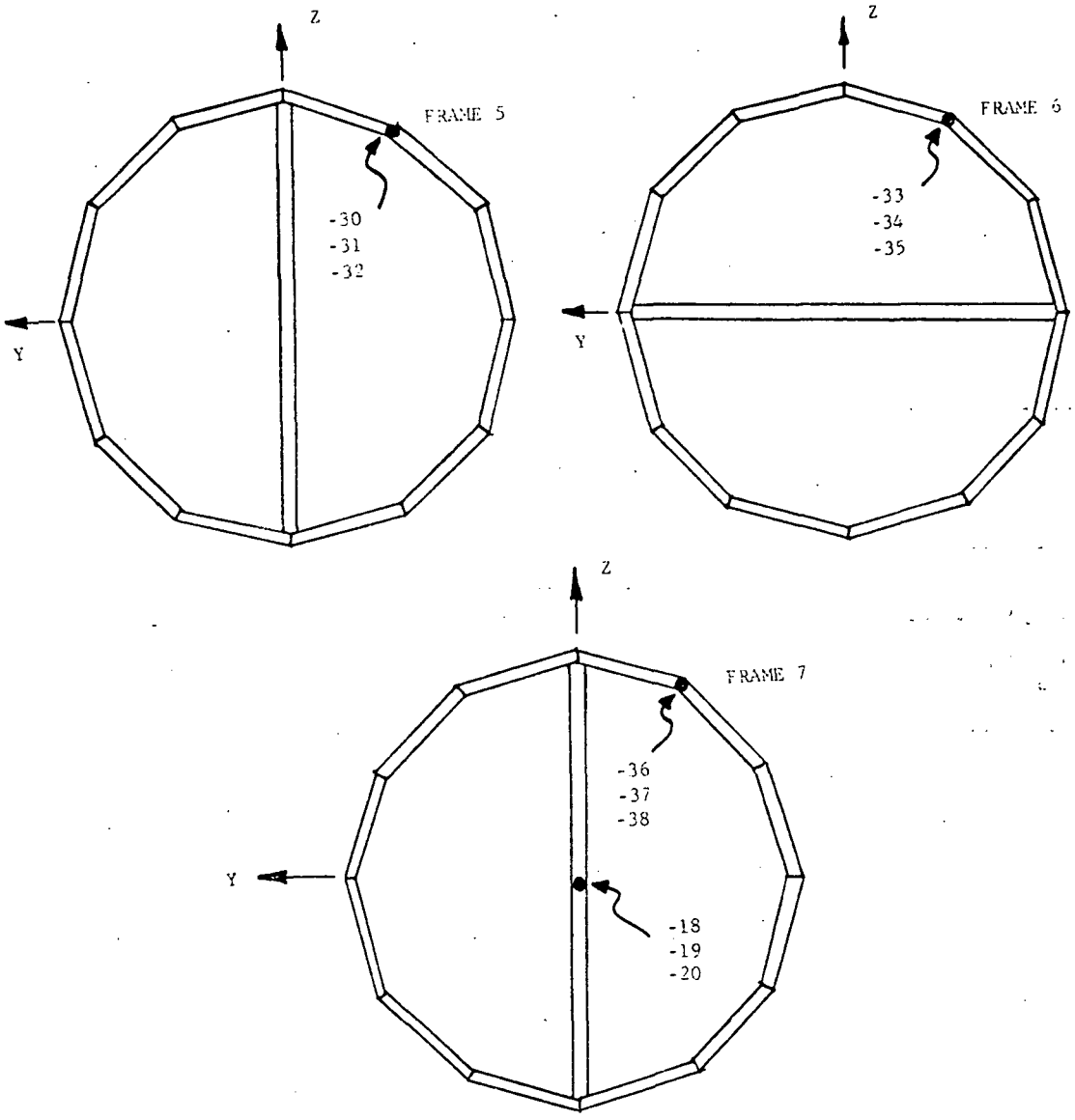

Figure B-4.6: Locations of Dual Range Accelerometers (DRA-XX)

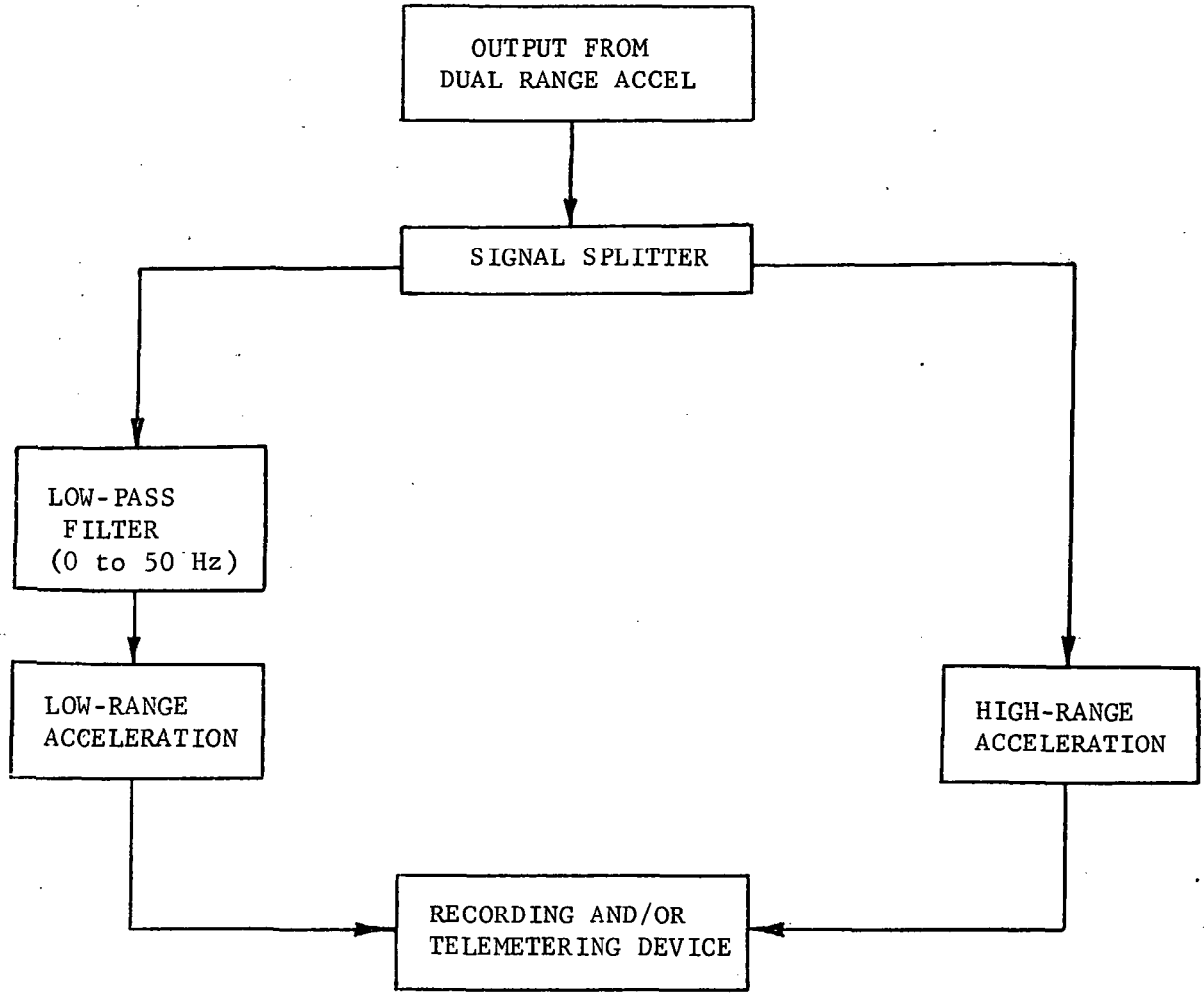

Figure B-4.7 : Dual Range Instrumentation Scheme

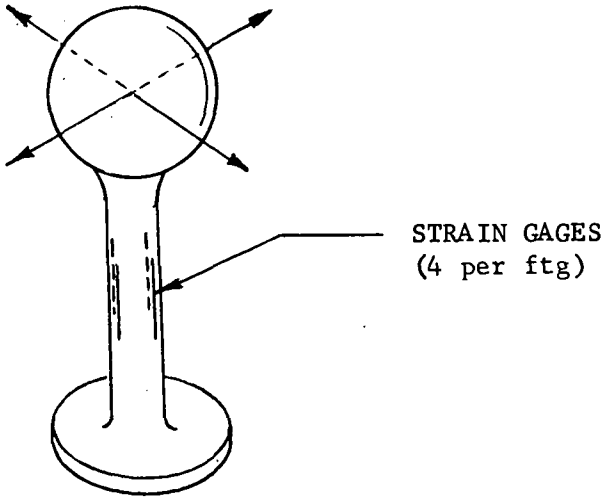

TYPE I FITTING

TYPE II FITTING

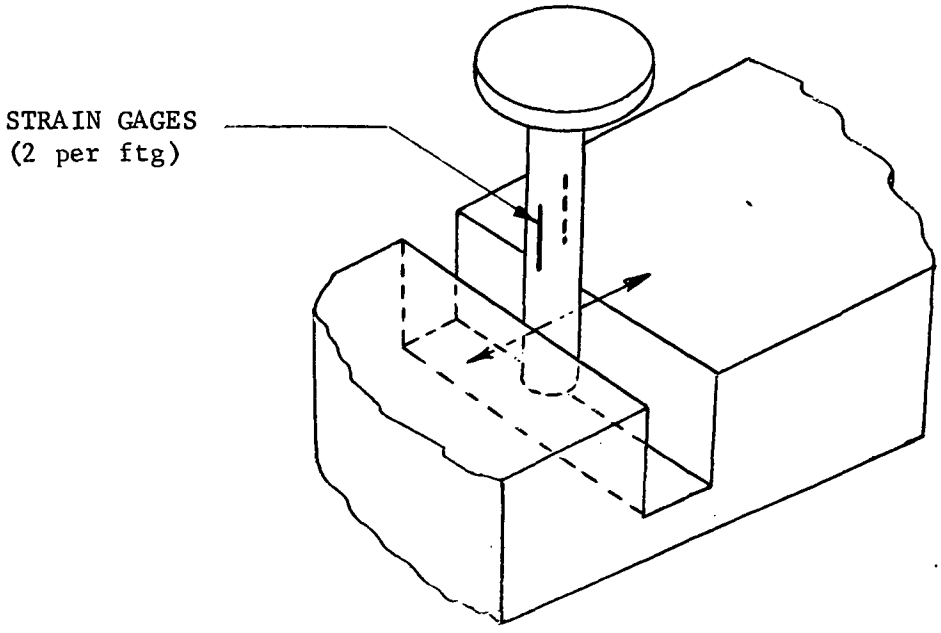

Figure B-4.8: Payload Support Fittings, Showing Strain Gages

B-4.6.3 STRAIN GAGES

It is proposed to use strain gages only on the payload support fittings. Two different fitting types are used on the LDEF as shown schematically in Figure B-4.8. One type takes loads along two axes; the second takes loads along a single axis, consisting essentially of a rigid member sliding in a slotted plate. Type 1 fittings would use four strain gages each, while Type 2 would use two gages. LDEF has three Type 1 and one Type 2 fittings, for a total of 14 strain gages.

B-5.0 REFERENCES

B-1: Anon. , Integrated Mission Planning - First Two Years of Shuttle Mission, 1979-1980, NASA Tech. Memo, George C. Marshall Space Flight Center, Alabama, March 1974 .